Hydrogen enrichment of biogas through reforming & its utilization in compression ignition engine under dual fuel mode

A Thesis

Submitted in Fulfilment of the Requirements for the award of the degree of

DOCTOR OF PHILOSOPHY

By:

PALI ROSHA

(Regd. No. 901514002)

School of Energy and Environment

Thapar Institute of Engineering and Technology
Patiala- 147004, India
October, 2019

DECLARATION

This is to declare that the research work which is being presented in this thesis entitled "**Hydrogen enrichment of biogas through reforming & its utilization in compression ignition engine under dual fuel mode**" in fulfilment of requirement of the degree of 'Doctor of Philosophy' in School of Energy and Environment, Thapar Institute of Engineering and Technology, Patiala, India, is an authentic record of my own research work carried out under the supervision of Dr. Amit Dhir (Associate Professor, School of Energy and Environment, TIET, Patiala, India) and Prof. S.K. Mohapatra (Senior Professor, Department of Mechanical Engineering, TIET, Patiala, India). Documents embodied in this thesis, from other researchers' works are duly listed in the reference section.

The matter presented in this thesis has not been submitted, in part or full, to any other institute in India or Abroad for the award of any degree.

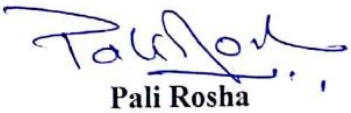

Pali Rosha

(Regd. No. 901514002)

CERTIFICATE

It is certified that the thesis entitled "**Hydrogen enrichment of biogas through reforming & its utilization in compression ignition engine under dual fuel mode**" which has been submitted by Mr. Pali Rosha in the fulfilment of the requirements for the award of the degree of '**Doctor of Philosophy**' in School of Energy and Environment, Thapar Institute of Engineering and Technology, Patiala, India, is a record of the candidate's own independent and original research work carried out by him under our supervision and guidance. The matter embodied in this thesis has not been submitted, in part or full, to any other institute for the award of any degree in other University or Institute.

7/5/19

Dr. Amit Dhir
Associate Professor & Head,
School of Energy and Environment,
TIET, Patiala, India.

7/5/19

Prof. S.K. Mohapatra
Senior Professor,
Department of Mechanical Engineering,
TIET, Patiala, India.

ACKNOWLEDGEMENT

First and foremost, I would like to express my sincere gratitude to my supervisors ***Dr. Amit Dhir****, Associate Professor & Head, School of Energy and Environment, TIET, Patiala, and* ***Prof. S.K. Mohapatra****, Senior Professor, Department of Mechanical Engineering, TIET, Patiala, India for their continuous support in my Ph.D. study and related research. I appreciate all their contributions of time, ideas, motivation, knowledge and funding to make my Ph.D. experience productive and stimulating.*

I express my heartfelt gratitude to ***Dr. Prakash Gopalan****, Director, TIET, Patiala, for providing the opportunity to work in this esteemed organization. Without the precious support it would not be possible to conduct this research. I feel special gratitude towards* ***Dr. Rafat Siddique****, Dean, Research and Sponsored Projects, TIET, Patiala for his valuable guidance and support during my research work.*

I gratefully acknowledge the funding sources that made my Ph.D. work possible. A very special gratitude goes out to ***Ministry of New& Renewable energy (MNRE), Govt. of India*** *for providing financial support to carry out study through the Research & Development Project bearing sanction number* ***103/223/2014-NT****.*

I have had the pleasure of association with the members of Doctoral Committee, ***Prof. N. Tejo Prakash, Dr. Amjad Ali*** *and* ***Dr. Anita Rajor*** *with whom I have had many fruitful discussions, academic and otherwise. Their encouragement is greatly acknowledged.*

I would like to thank ***Mr. Gurpreet Singh, Mr. Mohammad Suhail****,* ***Mr. Bharat Singh Negi****,* ***Mr. Sukhbir Singh*** *and* ***Mr. Parminder Singh*** *for their constant support and kind help throughout my research work. This research work would have not come to a successful completion without the help I received from SAI Labs, TIET, Patiala; SAIF, PU, Chandigarh and MRC, MNIT, Jaipur.*

An experimental research programme generally poses a lot of hurdles at various stages. In my daily work I have been blessed with friendly and cheerful lab mates who have made this adventure at Enviro-energy research lab at TIET, Patiala truly a time I will never forget.

The outcome of my research work is due to fruitful technical discussion, never-ending support and motivation of my colleagues, ***Mr. Rahil Changotra****,* ***Dr. Himadri Rajput****,* ***Mr. Sanjoy Gorai****,* ***Ms. Prabhdeep Kaur****,* ***Ms. Ina Thakur*** *and* ***Mr. Himanshu Sharma****.*

I am very much indebted to my ***grandfather*** *for always showering his blessings from above. I would like to thank my family for all their love and encouragement. For my parents, who have raised me with love and supported me in all my pursuits. I am also grateful to my other family members and friends who have supported me along the way.*

Above all, I owe it all to the Almighty God for granting me the wisdom, health and strength to undertake this research task and enabling me to its completion.

Pali Rosha

ABSTRACT

Today's worldwide energy sectors are mainly focused on power generation by using unsustainable fossil fuels. However, from long-term perspective, power must be produced from renewable resources because of unpredictability and shortage of worldwide fossil fuel reserves. Gaseous fuel induction in compression ignition engine has picked up much attention over the most recent few years, particularly when it is produced from renewable resources. Catalytic reforming has been considered as an effective technique to produce H_2-enriched biogas (HEB) from the various feedstocks. The reforming techniques which proven their potential for HEB production have been comprised of steam reforming (SR), dry reforming (DR) and partial oxidation (PO). Among these, only SR has been commercialized for the H_2 production, and another (DR and PO) have their own drawbacks which limit their implementation in industries. The combined DR and PO which is so-called dry oxidative reforming (DOR), has an approach to overcome issues occurred in DR technique.

In the present study, HEB production has been accomplished with commercially available Ni and synthesized catalysts under DR and DOR processes at temperature ranges from 650 to 900°C, with a CH_4/CO_2 ratio of 1.5:1. Moreover, attention has been focused to elucidate the influence of catalyst performance on the reactant (CH_4 and CO_2) conversion and product (H_2 and CO) yield, as well as, on the H_2/CO ratio of the DR and DOR processes. Box-Behnken design (BBD) has been used to optimize the DOR process parameters for HEB production by integrating response surface methodology (RSM) in the presence of Ni nanoparticle. The effect of the CH_4/CO_2 (1-2) and O_2/CH_4 (0.1-0.3) ratios on the catalytic performance of DOR has been assessed in the temperature range of 800 to 900°C. The empirical regression models have been developed to identify the influential and most significant parameters. Various Ni based novel catalysts have been synthesized at laboratory scale with wet impregnation method using metal oxides viz., CeO_2, Al_2O_3, TiO_2, and ZnO. The textural and structural properties of synthesized catalysts have been assessed by XRD (X-ray diffraction), BET (Brunauer–Emmett–Teller), FESEM (Field emission scanning electron microscopy) and TPR (Temperature programmed reduction). The carbon deposition in wt.% over the spent catalysts has been determined using CHNS Elemental Analyzer.

Influence of reaction temperature was strong on H_2/CO ratio in both reforming processes, whereas, weight hour space velocity (WHSV) showed variation in products yields. In DR, Ni

showed better performance at high temperature and low WHSV. Highest CH_4 conversion and H_2 selectivity of 77.1 and 36.7%, respectively, were observed at 900°C temperature and 20,000 NmL g^{-1} h^{-1} WHSV, whereas, increased WHSV to 40,000 NmL g^{-1} h^{-1}, 21.6 and 26.3% decrement in CH_4 conversion and H_2 selectivity was observed. DOR employed at 0.17 O_2/CH_4 ratio with high reaction temperature (≥850°C) showed improved performance in terms of reactant conversion and H_2 yield. At 900°C, CH_4 conversion and H_2 selectivity of 80.8 and 35.9 %, respectively, were obtained at 0.17 O_2/CH_4 ratios in DOR. Carbon deposition of 0.40 wt % was examined under dry reforming at 900°C, whereas, negligible carbon deposition (0.003 wt.%) was observed in case of DOR after 2h of continuous reaction stream. More than 95% value of determination coefficients by analysis of variance proved that the developed regression models were highly satisfactory. Experimentally, maximum H_2 enrichment of 38.7% with 82.9 and 90.8% of CH_4 and CO_2 conversions, respectively, were achieved at optimal reaction conditions of 900°C, 1.5 of CH_4/CO_2 ratio and 0.10 ratio of O_2/CH_4.

The H_2-TPR results revealed that 11 wt. % Ni impregnation on TiO_2 support makes the catalyst with strong metal-support interaction which moderates the metal sintering. Also, the addition of CeO_2 effectively improved the CH_4 and CO_2 conversions as well as H_2 enrichment. At 850°C, 11 wt. % Ni/TiO_2 catalyst leads to 70.5% CH_4 conversion with 32.0% H_2 enrichment, whereas, $Ni_{0.11}/Ce_{0.20}$ (Al_2O_3-TiO_2) yielded high CH_4 conversion (84.9%) with 40.6% of H_2 enrichment. No significant change in the activity of the catalyst was observed with 22.6 wt. % of carbon deposited on the $Ni_{0.11}/Ce_{0.20}$ (Al_2O_3-TiO_2) catalyst, after 18h of continuous reforming. Moreover, under DOR biogas, the stoichiometric H_2/CO ratio (1.2) was observed at 0.47 O_2/CH_4 ratios with negligible carbon deposition. Thus, $Ni_{0.11}/Ce_{0.20}$ (Al_2O_3-TiO_2) catalyst exhibited better activity and selectivity with high catalyst stability at 850°C. Further, in order to reduce carbon deposition on the catalyst bed, dry oxidative reforming was carried out at 650°C with varying proportions of O_2/CH_4 ratio which resulted in significantly higher CH_4 conversion with low catalyst deactivation. The effect of Zn loading (10 and 20 wt. %) on the catalytic activity was assessed in terms of reactant (CH_4 and CO_2) conversion, product (H_2 and CO) yield and H_2/CO ratio. At 650°C, CH_4 conversion and H_2 selectivity achieved were 18.1 and 4.3%, respectively, whereas, at 900°C, enhanced CH_4 conversion (78.5%) and H_2 (29.8%) selectivity were achieved with $Ni_{0.1}/CeO_2$ catalyst. It was also observed that Ni supported on mixed support exhibited higher reactant conversions when compared to Ni supported with ceria. At 900°C, $Ni_{0.10}$/ ($Zn_{0.1}$-$Ce_{0.9}$)

catalyst showed higher CH_4 and CO_2 conversion of 83.1 and 97.0%, respectively, with 40.3% of H_2 enrichment.

HEB (gaseous fuel) has also been utilized in a CI engine under dual fuel mode with diesel and B20 as pilot fuels. Palm oil was used for biodiesel production, and B20 biodiesel blend was used to achieve diesel substitution. Experimentation was carried out on the 3.5 kW CI engine test rig by varying brake mean effective pressure (bmep) between 0 and 3.5 bar, as well as, HEB (0.1 to 0.5 kg/h). HEB induction effects on various engine characteristics (combustion, performance, and emission) were studied at rated engine speed (1500 rpm). Results revealed that the ignition delay period and peak cylinder pressure increased with increasing HEB proportion (0.1 to 0.5 kg/h) in comparison to diesel and B20 mode. The heating value of HEB (57.0 MJ/Kg) is higher when compared to diesel (42.0 MJ/Kg) and (41.2 MJ/kg), which led to improved brake thermal efficiency in dual fuel modes. The emission results showed that with an increase of HEB rates, the NOx emission mildly decreases, but smoke opacity and hydrocarbon emissions majorly reduce. The influence of compression ratio (16:1, 17:1 and 18:1) on various engine characteristics by fuelling diesel and B20 along with HEB under dual fuel mode in compression ignition engine was also investigated. Experimental observations revealed that ignition delay (ID) period decreased persistently, whereas the peak cylinder pressures and brake thermal efficiency increased with increasing CR (16:1 to 18:1) under HEB-Diesel and HEB-B20 dual fuel modes. The hydrocarbon, carbon monoxide and smoke emissions decrease continuously, while, the increase of oxide of nitrogen with increasing CR (16:1 to 18:1) was observed. Thus, the HEB induction may be a feasible technological solution to overcome the issue of low BTE and high hydrocarbon emissions in biogas operated CI engines.

Keywords:

Hydrogen production; dry reforming; Nickel nanoparticle; catalyst; methane; carbon dioxide; biogas; compression ignition; diesel; biodiesel; combustion; performance; emission.

Dedicated to my grand father

LIST OF FIGURES

LIST OF TABLES

CONTENTS

NOMENCLATURE

DR	Dry Reforming
DOR	Dry Oxidative Reforming
MFC	Mass Flow Controller
H_2	Hydrogen
N_2	Nitrogen
CH_4	Methane
CO_2	Carbon Dioxide
O_2	Oxygen
CO	Carbon Monoxide
RWGS	Reverse Water Gas Shift
SEC	Specific Energy Consumption
RSM	Response Surface Methodology
CI	Compression ignition
PID	Proportional integral derivative
CV	Calorific value of fuel
LPM	Liter per minute
LPH	Liter per hour
Rpm	Revolution per minute
DI	Direct injection
bTDC	Before top dead centre
VCR	Variable compression ratio
IP	Injection pressure
ID	Ignition delay
PCP	Peak cylinder pressure
SOI	Start of injection
NHRR	Net heat release rate
CHR	Cumulative heat release
CP	Cylinder pressure
HC	Hydrocarbon
BSEC	Brake specific energy consumption
BSFC	Brake specific fuel consumption
NOx	Oxide of nitrogen

BTE	Brake thermal efficiency
Ppm	Parts per million
HSU	Hartridge smoke unit
BP	Brake power
kW	Kilowatt
B20	20% biodiesel blended with 80% diesel
POME	Palm oil methyl ester

Chapter-1

INTRODUCTION

With increasing total populace, domestic economies and expectations for everyday comfort, the interest in conventional non-renewable energy sources increasing worldwide. Fossil fuels (coal, oil and natural gas) have been a central driver of the social, economic and technological development of the country which influences human welfare. In recent years, excessive use of fossil fuels for power or energy generation has resulted in their depletion and environmental degradation (Escobar et al., 2009; Chanphavong et al., 2018). The compression ignition (CI) engines are the primary consumer of fossil fuels, and their combustion in CI engines emits toxic and harmful emissions which lead to deteriorating air quality. Keeping in view of these environmental issues and depleting fossil fuels, it is imperative to shift toward renewable energy resources that could replace hydrocarbon fossil fuels. The worldwide research endeavors have been committed towards the development of clean and energy productive fuels which are renewable (Khin et al., 2004; Patel et al., 2015). The so-called renewable resources for power or energy generation have been proposed in the last few decades, including sun, water, wind and biomass (Jiang et al., 2018). Inspite of this, the transition of these resources has slowed down due to the non-availability of wind and solar power, round the clock (Li et al., 2018). Therefore, to address this situation, it is fundamental to move towards a renewable resource independent of meteorological conditions.

Recently, research efforts are being focused on renewable gaseous fuels for power or energy generation (Pecharaply et al., 2007; Kumar et al., 2014; Che Mat et al., 2018). In this situation, Hydrogen (H_2) is envisioned as a clean and appealing energy carrier in the 21st century (Miyamoto et al., 2009). H_2 is energy effective and eco-friendly fuel in light of its high calorific value (120 MJ/kg) and carbon neutral gaseous fuel that prompts to produce zero carbon based emissions during combustion (Waheed et al., 2013). With the increasing demand of H_2 and the depletion of fossil fuels, renewable resources for H_2 production have gained attention. H_2 from renewable sources, such as biogas, seems to be a promising route in view of its sustainability and accessibility (Lin et al., 2012). India has officially upgraded the

capability of biogas plants by 31.8% from 2014 to 2015 (Cacua et al., 2016). Biogas primarily consists of methane (CH_4), carbon dioxide (CO_2), and traces of hydrogen (H_2), carbon monoxide (CO), hydrogen sulfide (H_2S) and oxygen (O_2) (Italiano et al., 2016). Biogas is relatively cheaper and readily available fuel gas, its conversion to energy efficient product like H_2-enriched biogas (HEB) has gained attention because of the worldwide availability of biogas (Gustavsson et al., 1995). Moreover, both CH_4 and CO_2 are the attractive renewable carbon source; thus, exploitation of biogas to produce H_2-enriched gas stream not just uses the two noteworthy greenhouse gases (CH_4 and CO_2) but can be used for power or energy generation by direct combustion in the dual fuel CI engine. Because of the main concern related to the utilization of biogas directly in CI engines, especially due to carbon-based emissions and reduce efficiency, a technique i.e. dry reforming (DR) of biogas has been suggested by the various researcher to produce H_2-enriched gaseous fuel (Ruckenstein et al., 1995; Boyano et al., 2011). DR technique has not been implemented industrially due to huge energy requirement and carbon deposition. From energy consumption aspect and H_2 economy, aforesaid goals must be accomplished at lower temperatures than conventional DR. Along these lines, to achieve a high H_2 yield/selectivity with least carbon deposition; development of appropriate catalysts is the need of the hour.

1.1. Motivation

Over the past decade, global climate variations affected by several environmental issues such as the rising greenhouse gases concentration (including CO_2) into the atmosphere, has gained wide attention. Global warming at present turns into a key environmental issue caused by the increase in atmospheric greenhouse gases (GHGs) levels. In particular, carbon dioxide (CO_2) is perceived as one of the major GHG identified by the International Panel on Climate Change. The other GHGs are nitrous oxide (N_2O), methane (CH_4), sulfur hexafluoride (SF), hydrofluorocarbons (HFCs) and perfluorocarbons (PECs). These gases are associated with the environment, economic development, and energy consumption. Major outcomes brought about climate change by unnatural warming, re-balancing of eco-systems, rising sea-levels, and so on. Whereas, human activities getting more conspicuousness for the enhancement of atmospheric GHG concentrations. It's promoting changes in temperature that are occurring much quicker than normal environmental conditions. When considering the major sources of the CO_2 emissions; industries with smoke stacks account for a surprisingly large part of the

environmental change issue. In fact, India is already the fourth largest greenhouse gas emitter of the world which is expected to reach the top position in the near future (IEA, 2015).

Today's worldwide energy sectors are mainly focused on power generation by using unsustainable fossil fuels. However, in the long-term perspective, power must be produced from renewable resources due to the unpredictability and shortage of worldwide fossil fuel reserves. Fossil fuels, at present, constitute about 80% of the total energy share with almost 50% of it being associated with the transportation sector, which is mainly based on the diesel engine (Escobar et al., 2009; Gupta et al., 2015). It would be interesting to know that, more than 6.5 million diesel engines exist at present in the Indian farming sector for various activities (Patel et al., 2016). Non-renewable fossil fuels will probably be the principle resources of essential energy throughout the coming decades. However, energy-driven consumption of petroleum derivatives has promoted a fast increment in CO_2 emissions, upstanding the overall carbon cycle and coming about to a planetary warming impact. No doubt, the dwindling fossil-fuel reserve, and the environmental pollutants are the well-known pressing issues that need to be addressed today. Therefore, to address these aforesaid dilemmas, it is imperative to shift towards an eco-friendly fuel to power CI engines. The mitigation of greenhouse gas emissions from the environment is the key motivation for the utilization of renewable fuels in CI engine. The worldwide share of renewable energy is about 9% and will rise up to 12% by 2040 (NEAA, 2003).The worldwide automotive fuel consumption in the automotive sector is shown in Fig. 1.1.

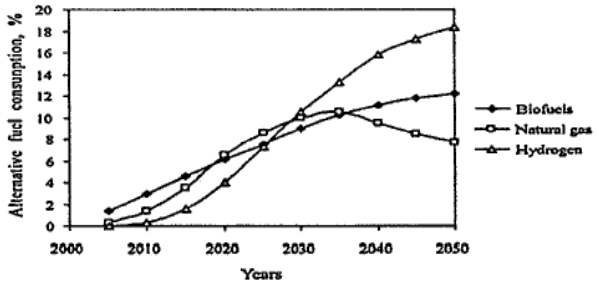

Fig.1.1. Projection of worldwide automotive fuel consumption (Patel et al., 2016)

Worldwide research at present is entirely focused on appropriate technology as well as an alternative fuel that would be used in these existing diesel engines with no or fewer noxious pollutants. Use of sophisticated electronic controllers in the CI diesel engine enables reduced emission and better fuel efficiency in comparison to the previous counterpart (US, DOE,

2003). However, the positive effects of this technology are overshadowed by its high price tag; hence, can't be commercially employed. In the last few decades, various alternative fuels have been proposed, targeting at cleaner and sustainable energy sources in order to counteract the consequences of the emissions from the CI engines. These include vegetable oil, alcohols, biofuels, compressed natural gas (CNG), natural gas (NG), liquefied petroleum gas (LPG), syngas, methane (CH_4), biogas, hydrogen (H_2), etc for the replacement of diesel fuels used in CI engine (Bohacik et al., 1996; Ramesohl et al., 2006). Studies are being focussed on the usage of gaseous fuels like natural gas for CI engines worldwide, because of their better mixing characteristics with air. H_2 is also one of the commonly known clean energy resources; but, the discovery of environment-friendly technique to produce H_2 at a lower price is the challenging task.

1.2. Hydrogen/Syngas production

H_2 is currently being produced by various techniques; for example, steam reforming, pyrolysis and gasification using water and biomass as sources (Hauserman et al., 1994; Lucredio et al., 2006; Mohamedali et al., 2018). However, all these aforesaid techniques require a huge amount of energy during operation, and also emit carbon dioxide (CO_2) which is the main contributor to climate change. Extensive research has been explored previously on several catalytic reforming processes for production of H_2-enriched biogas or syngas. These include steam reforming (SR) (Boyano et al., 2011; Ji et al., 2018); dry reforming (DR) (Ruckenstein et al., 1995; Broadford et al., 1996), partial oxidation (PO) (Ruckenstein et al., 1999; Larimi et al., 2012), etc. All reforming techniques differ in their oxidant used, product ratio (H_2/CO), energy requirements and kinetics of the reaction. Among these, only SR has been commercialized for the production of syngas and hydrogen (H_2), since it offers highest H_2/CO ratio (3:1) related to the other reforming processes (Chen et al., 2010). Additionally, DR process suffers from two main obstacles; rapid catalyst deactivation and huge energy requirement which lead to high operational cost (Hu et al., 2004).

Consequently, in order to make energy-efficient process, another technology, i.e., PO has been investigated as another technique for H_2-enriched biogas production. In contrast, from the energy point of view, PO has the capability to obtain high CH_4 conversion with excellent H_2 selectivity at high space velocities (Avila-Neto et al., 2009; Jimmy et al., 2017). Despite fast reaction kinetics and favorable thermodynamics, PO has not yet reached the

commercialization stage due to certain challenges e.g. slight decrease in CO selectivity leads to complete combustion, which ends up in high local temperature on the catalyst surface causing catalyst deactivation due to solid-solid reactions (sintering) and carbon deposition on the catalyst surface (Jing et al., 2006).

1.3. Reforming catalysts

Ni based catalyst is generally used in catalytic reforming because it offers high effectiveness at elevated temperatures (Fidalgo et al., 2010). Moreover, Co based catalysts have also been employed since it provides higher coking resistance and stability over a higher reaction temperature. Sousa et al., (2012) performed a comparative study on the deactivation behavior of Co and Ni catalyst in DR reactions. It was revealed that the catalyst stability due to Co and Ni species formed graphitic and amorphous carbon. Noble metals catalysts have not gained much attention due to their limited availability and higher cost; therefore, these are economically competitive when compared to Ni and Co (Ranjbar et al., 2012). However, the noble metal (Rh, Ru, Ir, and Pd) catalysts have less cooking resistance in comparison to Ni based catalysts (Gadalla et al., 1989). Hu et al., (2002) suggested that the high dispersion of metal (noble/non-noble) species on various (Al_2O_3/CeO_2/ZrO_2/TiO_2) oxides could reduce the coke formation.

1.4. Catalyst support

Catalyst support firmly influences the catalytic activity by providing a large surface area to metal scattering. In DR reactions, catalyst support plays a key role in reducing the coke formation and enhancing the catalyst activity. Meanwhile, various supports have already been explored by researchers, including Al_2O_3 (Bekeketidou et al., 2012), SiO_2 (Frontera et al., 2013), MgO (Danilova et al., 2014), TiO_2 (Shinde et al., 2014), and CeO_2 (Derk et al., 2013) in the reforming process because of their thermal stability and surface area. Seo et al., (2013) prepared TiO_2 supported catalyst over Ni and tested for dry reforming of CH_4 at a reaction temperature of 800°C. It was observed that the activity and stability of Ni/TiO_2 catalyst became more when compared to bare Ni. Similarly, Kim et al., (2015) examined the effect of water gas shift reaction (RWGS) at 900°C by adding Ce to Ni/TiO_2 catalyst and attained improvement in catalytic performance. It is evident that reducible supports like TiO_2 and CeO_2 provide better activity and suppress coke formation when compared to the non-reducible supports like Al_2O_3 and SiO_2 (Kurungot et al., 2004; Laosiripoana et al., 2005).

1.5. Alternative gaseous fuels

Renewable energy holds a key solution to the crisis of fossil fuels depletion and environmental degradation. The prominence of renewable gaseous fuels is increasing worldwide so as to lessen harmful tailpipe emissions, improve engine performance and reduced dependence on fossil fuels. In this way, research has been focussed on alternative fuels aiming to address the issues related to automobile sector. This section explores the utility of three gaseous fuels namely H_2, biogas, and syngas in CI engine as an alternative fuel under dual fuel mode. The properties of the diesel, H_2, biogas, and carbon monoxide are shown in Table.1.1 (Saravanan et al., 2007; Shirk et al., 2008; Antunes et al., 2008; Bora et al., 2014; Hernandez et al., 2016; Rinaldini et al., 2017).

Table.1.1. Properties of the diesel and certain gaseous fuels like H_2, biogas and CO

Properties	**Diesel**	**Hydrogen**	**Biogas**	**Carbon monoxide**
Chemical composition	$C_{12}H_{26}$	H_2	CH_4 : 60-70%; CO_2 : 30-40%; CO : 0.18%; H_2 : 0.18% (volume)	CO
Calorific value (MJ/Kg)	42.36	119.98	20-25	10.1
Density (kg/m^3)	840	0.081	1.2	1.249
Maximum flame speed (m/s)	0.38	2.92	0.25	0.19
Octane number	-	130	120	-
Cetane number	40-45	-	-	-
Auto- ignition temperature (°C)	254-285	585	700	605
Stoichiometric A/F ratio (mass)	14.5	34.3	6	2.45
Minimum energy required for ignition (MJ)	0.06	0.02	-	0.40
Energy density (MJ/Nm^3)	2.82	2.87	-	3.79
Flame temperature in air (K)	-	2328	-	2394
Diffusivity in air (cm^2/s)	-	0.63	0.111	0.208
Quenching gap in air (cm)	-	0.064	-	3.15
Flammability limits (% by Vol.)	0.7-5	4-75	7.5-14	12.5-74

1.5.1. Hydrogen

H_2 as an energy carrier is counted as a very peculiar long-period renewable fuel because of its eco-friendly nature and distinctive properties from the conventional fuel (Midilli et al., 2008; Kannah et al., 2019). Major concerns related to the combustion of H_2 in the air are its unique characteristics like high flame speed, high energy density/unit mass, wide flammability range, low ignition energy, high diffusivity, etc (Petkov et al., 1989; Nandor et al., 2018). H_2 based dual fuel CI engines suffer an obstacle of premature ignition due to low ignition energy of H_2, which is one of the challenges related to its usage in CI engine. In 1820, the practical attempt was done by Rev. W. Cecil on an H_2-operated engine, in which H_2 gas was used to produce force (Das et al., 1990). Further, over 1000 vehicles were converted to H_2 in Germany and England in 1930 (Hoffmann et at., 1981). Various studies have been documented with regard to the technical viability and challenges posed by the utilization of H_2 as a fuel in CI engine in the later 20^{th} century (Haragopala et al., 1983; Naber et al., 1998). In 2007, a national H_2 energy roadmap was formulated by MNRE (Ministry of New and Renewable Energy), which targeted around one million H_2fuelled vehicles in India by 2020 (National hydrogen energy road map, 2006).

1.5.2. Biogas

In a scientific world, when the safety and viability of energy alternatives are being debated, it is pertinent to consider one of the dominant renewable energy alternatives, particularly biogas. Biogas is a cheaper, cleaner and potentially renewable fuel produced by fermentation or anaerobic digestion of organic matters like non-edible seed cakes, cow dung, food waste, animal waste, agricultural waste, sewage sludge, municipal waste, etc (Jingura et al., 2009). In addition, the energy recovery of biogas from biomass is extremely rewarding and a viable alternative option to replace conventional fossil fuels. Biogas is primarily methane (CH_4) and carbon dioxide (CO_2) with small traces of carbon monoxide (CO), hydrogen (H_2), oxygen (O_2) and hydrogen sulfide (H_2S). The energy content of biogas mainly depends on the concentration of CH_4. Biogas with a high percentage of CH_4 could be marked as good quality gas, which has high heating value and produces blue flame after burning in the air. The presence of diluents like CO_2 in biogas lowers its energy content, which significantly reduces the fuel quality in terms of combustion. The origin of the biogas plant traced back to 1859 in Bombay. In 1898, the United Kingdom used anaerobic digestion to convert sewage into biogas which was then used to light street lamps. In 2002, biogas used in the urban transport

sector of Sweden alone has successfully reduced greenhouse gases by 9000 t/y (IEA Bioenergy task 37). Moreover, a huge potential for biogas generation has been available throughout India. In fact, India has already enhanced the biogas plants capacity by 42.3% from 2002 to 2012 (Lohan et al., 2015). During 2014-15, around 20,700 lakh cubic meter of biogas was produced within the country, which is equal to 5% LPG consumed (Mandal et al., 1999). Even, rural households have been using biogas for heating and cooking purpose. Biogas is a renewable fuel which is easy availability and makes a good substitute for conventional diesel. Moreover, it is also used in dual fuel CI engines owing to its high anti-knock properties when compared to conventional diesel fuel. It also requires an additional ignition source to initiate the ignition, as in the case of H_2 fuel (Lounici et al., 2014).

1.5.3. Syngas

Syngas is an important energy source and is that form of energy, which is not present naturally. It is a mixture of H_2 and CO, and is produced from biogas not only reduces the amount of greenhouse gas emissions but in fact, it recycles and increases the usability of these gases by producing H_2-rich energy product (Karim et al., 2003). Efforts to utilize biomass energy must be concentrating on those applications that have favorable prospects of market development, for example, generation of power using syngas produced from biogas through dual fuel CI engines route. Syngas can also be produced by plenty of sources that contain carbon, including coal, natural gas, gasification, or virtually any hydrocarbon feedstock, by reaction with oxygen or steam (Spath et al., 2003). Syngas can be used in dual fuel CI engines, and this option is more attractive because CI engines are more widely used in off-road applications, owing to their fuel efficiency and robustness. Although, use of syngas in a dual fuel CI engine has provided additional advantages, such as the reduction of CO_2 emissions, but, it won't burn directly in CI engines due to its high self-ignition temperature. So, it can be used as a secondary fuel in dual fuel CI engines in a similar way as other gaseous fuels.

1.6. Biodiesel

Biodiesel as an alternative renewable fuel picking up popularity as it is a clean oxygenated fuel derived via transesterification of vegetable oil/animal fat (Iranmanesh et al., 2008; Marwaha et al., 2018).It is only alternative fuel which offers convenience of use in CI engine without any engine modification. Biodiesel is derived for complete similarity with customary

diesel and can be mixed with diesel to improve the proficiency of the engine with no problems. Biodiesel has been considered as a fuel that adds to energy sustainability, and can be used in CI engines either in pure form or by blending with conventional diesel (Mahla et al., 2018). It is more eco-friendly and non-toxic fuel when compared to ordinary diesel; moreover, its high lubricant properties improve engine performance as well (Chauhan et al., 2016). Biodiesel as a fuel helps decreasing the contamination, additionally diminishes health hazards and gives the general public A CLEANER AND GREENER TOMORROW.

1.7. Dual fuel concept

Injection of gaseous fuel in CI engine is not a new technology; it has been investigated by many researchers with widespread success (Miyamoto et al., 2009; Barik et al., 2014). Usually, gaseous fuel is mixed with the intake air during the suction stroke of dual fuel CI engine, either through manifold injection or through direct injection into the cylinder (Kumar et al., 2014). Depending upon the availability of fuels, dual fuel CI engines can be switched to either dual fuel mode or single fuel mode. In dual fuel mode, a certain amount of pilot fuel must be sprayed as an ignition source due to high auto-ignition temperature of the gaseous fuel. Usually, the quantity of diesel fuel (pilot fuel) required for adequate ignition is around 10 to 20 % of the quantity required for single fuel mode operation (Mitzlaff et al., 1988). The main objective of a dual fuel technology is to reduce the consumption of conventional fossil fuels with increased substitution by alternative renewable fuels, which are economically viable and environmental friendly (Karim et al., 1980). There are several issues associated with the performance of dual fuel CI engines. For example, at lower load, the dual fuel engine operation tends to exhibit poor thermal efficiency, lower fuel utilization, prolonged ignition delay and higher emissions which are attributed to low ignition ability of gaseous fuels (Gunea et al., 1998). Moreover, the performance of dual fuel CI engine largely depends on the combustion behaviour, engine operating conditions, and design parameters; such as speed, load, pilot fuel injection timing, compression ratio, inlet manifold condition, pilot fuel mass, the composition of gaseous fuel, etc (Karim et al., 2003; Hekkert et al., 2005).

1.8. Aim of proposed work

The major objective of the present study is to produce HEB through DR and DOR processes, using commercial and lab synthesized catalysts. Moreover, study explores utilization of HEB in CI engine under dual fuel mode with diesel and biodiesel as pilot fuels. In this direction,

systematic experimental investigations have been carried out in a tubular type fixed-bed down flow catalytic reforming reactor. Efforts have been made to maximize H_2 content in biogas using commercial and laboratory synthesized catalysts. Wet impregnation method was employed for catalyst synthesis using different support's viz., TiO_2, Al_2O_3, CeO_2, and ZnO. Characterization of synthesized catalysts has been done with various techniques in order to assess their different structural and physicochemical properties, as well as to develop a relationship between these properties with the activity/selectivity of the reforming catalyst.

Produced HEB was further utilized in a dual fuel CI engine using diesel and biodiesel as pilot fuels. Palm oil was used for biodiesel production, and B20 biodiesel blend was prepared with conventional diesel. Engine study was carried out in a single cylinder, four stroke, DI, water cooled, constant speed, variable compression ratio CI engine with rated power (3.5 kW). Fumigation technique was employed for injecting HEB into the air manifold of the engine cylinder. The dual fuel engine was run in brake mean effective pressure ranges between 0 and 3.5 bar. Various engine characteristics comprise of combustion, performance and emission have been investigated. Moreover, the noise level of the dual fuel CI engine has been assessed under single and dual fuel modes. The combustion, performance and emission characteristics of engine fuelled with HEB were compared with neat diesel and B20 fuel.

1.9. Objectives of research work

The main objectives of study include:

- Dry oxidative reforming of biogas to produce hydrogen enriched biogas by commercially available Ni based catalyst.
- Synthesis of catalyst supported on appropriate supports to improve its activity and selectivity.
- Assessment of engine performance in terms of combustion, performance, noise and emission characteristics with different proportion of hydrogen enriched biogas-diesel and hydrogen enriched biogas-biodiesel under dual fuel operation.

Chapter-2

LITERATURE REVIEW

This chapter initially presents the review of literature related to catalytic reforming techniques, followed by their reaction thermodynamics. Emphasis is also given to the various emissions emanating from CI engines. This chapter also elaborates the influence of gaseous fuels (like H_2, biogas, syngas) injection to CI diesel engine under dual fuel mode with diesel/biodiesel as a pilot fuel. Various engine characteristics such as combustion, performance, and emission of the dual fuel CI engine using gaseous fuels as a secondary fuel have been analyzed and compared with CI engine working under single fuel mode. Findings of some experimental studies have been detailed in the discussion for selective important parameters as case studies.

2.1. Catalytic reforming techniques

Catalytic reforming has been considered as an effective technique to produce hydrogen (H_2)/syngas from the various feedstocks. This section focuses on the dry and dry oxidative reforming processes.

2.1.1. Dry reforming

DR refers to a process in which a mixture of H_2 and CO, which is so-called syngas, is produced by converting CH_4 and CO_2 molecules. DR reforming process was first studied by Fisher et al. in 1928 over the presence of non-noble (Ni, Co) metal catalysts and revealed that catalyst deactivation occurred due to severe carbon formation. The relationship between reactant composition and carbon formation was developed to moderate catalyst deactivation (Reitmeier et al., 1948). Further, the catalyst synthesis method (i.e. co-precipitation) for DR reforming reaction was first proposed by Rostrup-Nielsen in 1964 followed to Patent in 1974. Various metal oxides such as aluminum (Al), magnesium (Mg), and nickel (Ni) were employed during catalyst synthesis. It was identified that Al and Mg formed spinel framework, whereas some Mg on the catalyst surface led to counteract carbon formation. Different metals loaded onto the catalyst have distinctive abilities for the DR reaction.

Pakhare et al., (2014) reviewed various noble (Rh, Pt, Ir, Ru) and non-noble (Ni, Fe, Co) metals catalysts in the DR of CH_4. Noble metals offer higher coke resistance, but their high cost made it unviable choice for commercial use in industrial applications (Mesrar et al., 2018). It was reported that non-noble catalysts exhibited higher catalytic activity, but their tendency to coke formation makes it unsuitable for long-term operations. Thus, research endeavors are now being focused towards the catalyst development which leads to enhance catalytic activity, reducing coke formation and long team stability. Also, the bimetallic (Ni-Mo, Ni-Ce, Ni-Zr) and monometallic (Ni) catalysts performed well for DR when compared to noble metals. However, the pore textural properties of bimetallic catalyst have been improved due to the formation of the combined metal cluster (Xu et al., 2009).

Moreover, carbon formation is also a noteworthy issue in DR which can be reduced by adding alkali/alkaline earth metal by increasing the basicity of the catalyst (Crisafulli et al., 1999; Suelves et al., 2005). Also, priorities of catalyst for dry reforming reactions include limited coke formation, with high H_2 yield (Hu et al., 2004). From energy consumption aspect and H_2 economy, aforesaid goals must be accomplished at lower temperatures than conventional DR. Noteworthy, reducing the reforming temperature comparatively reduces the catalyst activity. The catalytic activity in DR has been reported to enhance in the presence of metal oxides, in terms of reactants conversion and products yield (Arbag et al., 2018). Various supports have been explored by researchers, including Al_2O_3 (Bekeketidou et al., 2012), SiO_2 (Frontera et al., 2013), MgO (Danilova et al., 2014), TiO_2 (Shinde et al., 2014), and CeO_2 (Derk et al., 2013) in the DR process because of their thermal stability and surface area. CeO_2 support is renowned for the exchange of lattice oxygen during the reversible reaction which results in the reduction of carbon deposition on the catalyst surface (Laosiripojana et al., 2008). However, CeO_2 loses oxygen stockpiling capacity at higher reaction temperature on account of its vulnerable to sintering. TiO_2 provides lower oxygen storage capacity in comparison to CeO_2, but has higher resistance to sintering, particularly at a higher temperature, consequently giving more thermally stable catalyst (Rezaei et al., 2006). Zinc oxide (ZnO) has a high melting point (1975°C), which enables a relatively large surface area at a higher temperature range. Studies reported that ZnO addition had positive outcomes in increasing the activity and stability of reforming catalysts (Rajbongshi et al., 2014; Moradi et al., 2014; Shao et al., 2017). Chen et al., (2011) reported that the ZnO loading prevents initial activity loss, decreases CO selectivity and enhances the stability of the catalyst. Moreover, the metallic phase of Ni-based catalysts is greatly influenced by Zn

content, which limits coke formation and enhances catalyst stability (Anjaneyulu et al., 2016). At temperature of 400°C, the dry reforming reactions were performed with mixed (ZnO-Al_2O_3) support Ni catalysts and reported that the Ni catalyst with higher Zn content exhibited better activity when compared to Al_2O_3 support (Sokolov et al., 2017). Similarly, Park et al., (2018) investigated the effect of Zn (promoter) on the performance of Co/ZrO_2 catalyst and revealed that the alloy (Co-Zn) prevents the oxidation of metal which lead to enhanced catalyst stability. Movasati et al., (2017) stated that Zn provides higher coking resistance with stronger metal-support interaction. At higher temperature, ZnO supported catalysts exhibited better activity with long term stability (Nataj et al., 2019). Goula et al., (2017) reported the benefit of CeO_2 support towards the development of mixed support catalysts for DR. According to Rezaei et al., (2009), the Ce promoted Ni catalysts exhibited better redox properties with incredible resistance to carbon formation. Ocsachoque et al., (2011) studied CeO_2 promoted mono (Ni) and bimetallic (Ni-Rh) catalysts with Al_2O_3 (support), and reported that Ce addition enhanced catalyst activity and stability, and additionally diminished the carbon deposition when compared to unpromoted catalyst. Bereketidou et al., (2012) explored the impact of Ce on the performance of Ni/Al_2O_3 catalyst in the DR reactions, and reported that Ce addition not only expands the catalyst activity but also suppressed coke formation. Similarly, Laosiripojana et al., (2008) reported that increase in Ce content diminishes the stability of catalyst at elevated temperatures. Noteworthy, as the Ce catalyst ages, its activity decreases to some extent due to sintering at high temperature and consequently, deactivate at high temperature, thereby need of developing a more stable catalyst which can withstand at an elevated temperature for the longer time period (Hori et al., 1998). In this context, doping of another rare earth element in Ce may be advantageous to stabilize Ce against sintering.

2.1.2. Dry oxidative reforming

In DOR, additional oxygen (O_2) is supplied along with CH_4 and CO_2 to initiate oxidative reactions and gasifying the carbon deposited on the catalyst surface during the reaction (Sepehria et al., 2017; Al-Fatesh et al., 2018). This strategy provides additional advantages; such as increased reactant (CH_4 and CO_2) conversion at a lower temperature ranges, reduced the formation of a hot spot, enhanced catalyst stability and deactivation resistance (Chen et al., 2010). In 1992, the DOR (i.e. combined dry and partial oxidation reforming) was first studied by Vernon et al., (1192) in which transition metals (Ru, Rh, Ni, Pt, Pd, Ir) supported

on inert oxides were used to produce syngas. It was inferred that 1 % Ir/Al_2O_3 catalyst exhibited higher product (H_2 and CO) yield with negligible carbon deposition. Further, it also tailored CH_4:CO_2:O_2 ratios in order to achieve a thermoneutral reaction. The H_2/CO ratio and selectivity could be tailored by changing the reactants composition to make it suitable for different applications. Souza et al., (2003) stated that DOR not only increases CH_4 conversion, also enhances catalyst stability. At lower temperature ranges, the CH_4 combustion is a predominant reaction in DOR, followed by reforming of the remaining CH_4 by CO_2 and the reactant H_2O. The catalyst stability increases noticeably with the addition of O_2 in the feed, which further reduces the coke formation on the catalyst surface. Hadian et al., (2013) performed experiments by injecting O_2 over various Ni loading catalysts on $MgAl_2O_4$. It was reported that Ni (7 wt. %) significantly improved CH_4 conversion with almost zero carbon deposition. The heat transfer between exothermic and endothermic reactions is facilitated by DOR process. Therefore, syngas/H_2 production is safer when compared to partial oxidation alone, in light of the fact that the danger of explosion because of hot spots is eliminated by the injection of CO_2. Nematollahi et al., (2011) tested noble (Rh and Ru) metals in the DOR reaction up to 50 h of continuous reactant flow and observed higher CH_4 conversion with negligible carbon deposition over the catalyst surface. Asencios et al., 2013 reported higher conversion rates and product selectivity over MgO-ZrO_2 supported catalysts at 0.16 O_2/CH_4 ratios. Higher O_2 contents in reactant feed exhibited large decrement in CO_2 conversion values, whereas, H_2O production was found to be higher due to the dominant CH_4 combustion reaction.

2.2. Thermodynamic of reforming reactions

DR is a highly endothermic reaction (Eq.2.1) and produces syngas with unity H_2/CO molar ratio. DR reaction requires huge energy requirement to attain reaction equilibrium, because of the high stability and dissociation energy of reactants (CH_4 and CO_2). Also, syngas production is greatly influenced by the simultaneous occurrence of reverse water gas shift (RWGS) reaction (Eq.2.2) that consumes H_2 in the reforming and produces more CO; hence, H_2/CO becomes less than unity. The carbon formation in DR reactions is primarily associated with the reactions: CH_4 cracking, Eq.2.3; Boudouard reaction, Eq.2.4, as reported by Lashof et al., (1990).

$$CH_4 + CO_2 \rightarrow 2H_2 + 2CO \qquad \Delta H = 247 \text{ kJ/mol} \qquad (2.1)$$

$$CO_2 + H_2 \leftrightarrow CO + H_2O \qquad \Delta H = 41 \text{ kJ/mol} \qquad (2.2)$$

$$CH_4 \rightarrow C + 2H_2 \qquad \Delta H = 75 \text{ kJ/mol} \qquad (2.3)$$

$$2CO \rightarrow C + CO_2 \qquad \Delta H = -171 \text{ kJ/mol} \qquad (2.4)$$

The reaction mechanism involved in the DR process described in detail by Solymosi et al., (1992). The CH_4 activation proceeds via sequentially follow the steps of reactions 2.5-2.8, and at the last part of the chain, carbon.

$$CH_4 \rightarrow CH_{3(x)} + H_{(x)} \qquad (2.5)$$

$$CH_{3(x)} \rightarrow CH_{2(x)} + H_{(x)} \qquad (2.6)$$

$$CH_{2(x)} \rightarrow CH_{(x)} + H_{(x)} \qquad (2.7)$$

$$CH_{(x)} \rightarrow C_{(x)} + H_{(x)} \qquad (2.8)$$

As, the CH_4 cracking alone on the catalyst metal surface is very limited but this process is upgraded by adsorbed O molecules produced via CO_2 activation, Eq. (2.9).

$$CO_2 \rightarrow CO_{(x)} + O_{(x)} \qquad (2.9)$$

$$CO_{(x)} \rightarrow C_{(x)} + O_{(x)} \qquad (2.10)$$

In the case when both CH_4 and CO_2 exist, their self-decomposition is improved via the reactions, 2.11-2.13. The CH_4 cracking is encouraged by adsorbed O, whereas the CO_2 dissociation by adsorbed H_2 and perhaps by other CH, residues. Also, the formation of undesired product (H_2O) is compensated with CO_2 for subsequent reactions with C formed by Eq. 2.3.

$$CO_2 + H_{(x)} \rightarrow CO_{(x)} + OH_{(x)} \qquad (2.11)$$

$$CH_4 + O_{(x)} \rightarrow CH_{3(x)} + OH_{(x)} \quad (2.12)$$

$$CH_{(n)} + O_{(x)} \rightarrow CO + n\,H_{(x)} \quad (2.13)$$

$$2OH_{(x)} \rightarrow H_2O + O_{(x)} \quad (2.14)$$

DOR is a network of multi-reactions. The main reactions involved in DOR process represented in reactions 2.15-2.18; moreover, reactions (2.1)-(2.4) are also associated with DOR process. Both CO_2 and O_2 (Eq. 2.15) acted as oxidants in the DOR process, O_2 led to complete conversion due to more stability of CO_2 species. The CH_4 dissociation follows the same steps as discussed earlier, while, part of CH_4 is consumed by either partial (Eq. 2.16) or complete (Eq. 2.17) oxidation of CH_4.

$$(1.5x)CH_4 + (x)CO_2 + (0.25x)\,O_2 \rightarrow (2.5x)CO + (3x)H_2 \quad (2.15)$$

$$CH_4 + \frac{1}{2}O_2 \leftrightarrow CO + 2H_2 \qquad \Delta H = -36 \text{ kJ/mol} \quad (2.16)$$

$$CH_4 + 2O_2 \leftrightarrow CO_2 + 2H_2O \qquad \Delta H = -802 \text{ kJ/mol} \quad (2.17)$$

$$CH_4 + H_2O \leftrightarrow CO + 3H_2 \qquad \Delta H = 206 \text{ kJ/mol} \quad (2.18)$$

2.3. Compression ignition engine emissions

CI engines mainly utilized in transportation, agriculture, power generation, generator sets, marine, military, etc (Faiz et al., 1996; Hiroyuki et al., 2011). These are the building squares of a country's economy, particularly for developing countries, like India. However, these engines are under attack nowadays because of the consistent increment in harmful pollutants. The main pollutants incorporate unburned hydrocarbon (HC), oxides of nitrogen (NO_X), particulate matter (PM) and carbon monoxide (CO) (Dhariwal et al., 1997; Akash Deep et al., 2017).

2.3.1. Hydrocarbon (HC)

Hydrocarbons (HC) emissions generate on account of incomplete fuel combustion inside engine cylinder. It is sorted as cyclic hydrocarbons, olefins (alkenes), paraffin (alkanes) and acetylenes (alkynes) (Hiroyuki et al., 2011).In CI engines, the HC emissions in the tailpipe rely on fuel type, untidy injection, injector needle bounce, nozzle cavity volume, and irregular operating conditions. At temperature (≥600°C), the HC emissions continuously react in the exhaust under O_2 availability. HC emissions from the tailpipe are bringing down when compared to HC leaving the engine cylinder. Noteworthy, it forms in engine exhaust, and in the fuel system, engine crankcase, and from environmental venting of vapors amid fuel dispensing and distribution (Faiz et al., 1996). Crankcase HC emissions, evaporative losses of HC emissions and tailpipe HC emissions have, 20-35, 15-25, and 50–60%, respectively of total HC emissions (Dhariwal et al., 1997).

2.3.2. Oxides of Nitrogen (NOx)

NOx formation pathways are fuel NOx, thermal NOx and prompt NOx (Subramanian et al., 2011; Ahmad et al., 2016). In CI engines (thermal NOx) heavily depends on the O_2 availability, volumetric efficiency, gas temperature and pressure (in-cylinder), combustion duration, and the reaction residence time of the charge (Kadota et al., 2002). Ordinarily, it is formed when consumed gas temperatures are at a maximum i.e. between the start of combustion (SOC) and shortly after peak pressure. It is accepted that at combustion temperature (≥800°C) the di-atomic N_2 changes into an exceedingly reactive monoatomic (Basha et al., 2011; Reşitoğlu et al., 2015). Thereafter, this N_2 (monoatomic) reacts with in-cylinder O_2 and form NOx (Iranmanesh et al., 2011).

2.3.3. Particulate Matter (PM)

PM emissions comprise predominantly of soot, an inorganic fraction (IF), and soluble organic fraction (SOF) (Maricq et al., 2007). It is derived from the agglomeration of partly burned fuel, fuel oil ash content, and cylinder lube oil. Over 50% of the total PM emissions are soot that is black smoke. At low air/fuel ratios (AFR), soot is produced in the temperature and pressure range of 1327 to 1527°C and 50 to 100 bar, respectively (Stanmore et al., 2001). SOF comprises heavy HCs condensed/adsorbed on the soot. In lean mixture conditions, always regions around the injected fuel spray at AFR (≤ 1). Indeed, even without simple correlations that can foresee the PM production quantitatively overall, it tends to be expressed

that the O_2 availability and the in-cylinder gas temperature are the primary variables affecting the PM formation (Sharma et al., 2005).

2.3.4. Carbon Monoxide (CO)

CI engines are lean combustion engines in which AFR ratio (λ>1) used during fuel combustion (Kim et al., 2016). In CI engines, CO formation is insignificant and mainly results from the incomplete combustion where the oxidation process does not happen completely. Its concentration largely depends on AFR, and it is most elevated where the excess-air factor (k) is less than unity i.e. rich mixture (Raubet al., 1999). In the rich mixtures, because of air inadequacy and reactant concentration, all the carbon can't convert to CO_2 and thus CO formation (Kampa et al., 2008). However, a fraction of CO is also emitted over lean conditions on account of chemical kinetic effects (Walsh et al., 2001).

2.4. Emission regulations and standards

The emission standards limit implemented in India over the few years for HD engines are tabulated in Table 2.1.

Table 2.1 Emission standards for heavy- duty engines
(https://www.dieselnet.com/standards/eu/hd.php)

Stage	Year	Test	CO	HC	CH_4	NOx	PM	PN	NH_3
			g/kWh						
	1996	ECE R49	11.20	2.4		14.4	-		
India 2000	2000	ECE R49	4.50	1.1		8	0.36		
BS II	2005	ECE R49	4.00	1.1		7	0.15		
BS III	2010	ESC	2.10	0.66		5	0.1		
		ETC	5.45	0.78		5	0.16		
BS IV	2010	ESC	1.50	0.46		3.5	0.02		
		ETC	4.00	0.55		3.5	0.03		
BS V	N.A.	ESC	1.50	0.46		2	0.02		
		ETC	4.00	0.55	1.1	2	0.03		
BS VI	2020	WHSC(CI)	1.50	0.13		0.4	0.01	8.0×10^{11}	10
		WHTC(CI)	4.00	0.16		0.46	0.01	6.0×10^{11}	10
		WHTC(PI)	4.00	0.16	0.5	0.46	0.01	6.0×10^{11}	10

In India, emission regulations came into action in 1989 under the central motor vehicle rule (CMVR) No.15 for non-transport vehicle. Following this, emission regulations were introduced for gasoline light-duty vehicles in 1991, and thereafter, in 1992 for diesel vehicles. India stage-I norms were introduced from April 2000 and since this year. India has adopted and been following the European emission and fuel regulations for four-wheeled light duty and heavy-duty vehicles. India is now following Bharat Stage IV norms with 50 ppm sulphur content in diesel. This number has gone down to 10 ppm sulphur with the updated BS VI diesel fuel which has introduced for NCT of Delhi from April 1, 2018. Prior it was proposed to launch BS V norms in April 2019 and BS VI norms in April 2023. In early 2016, the Government of India leapfrogged BS V norms and straightaway move to BS-VI norms as the former ones were only a slight improvement over BS IV norms in terms of emissions. It is expected that BS VI fuel will be implemented all over the country from April 2020. Table 2.2 displays the sulfur limits enforced by government all over the country.

Table 2.2 Implementation of fuel sulfur content reductions in India (https://www.transportpolicy.net/standard/india-fuels-diesel-and-gasoline)

Date	Diesel	Gasoline
1995	10,000 ppm (nationwide)	-
1996	5,000 ppm (Delhi + selected cities)	-
1998	2,500 ppm (Delhi)	-
1999	500 ppm (BS II, Delhi, limited supply)	-
2000	2,500 ppm (nationwide)	-
2001	500 ppm (BS II, selected cities)	-
2005	500 ppm (BS II, nationwide)	500 ppm (BS II, nationwide)
	350 ppm (BS III, selected cities)	150 ppm (BS III, selected cities)
2010	350 ppm (BS III, nationwide)	150 ppm (BS III, nationwide)
	50 ppm (BS IV, selected cities)	50 ppm (BS IV, selected cities)
2017	50 ppm (BS IV, nationwide)	50 ppm (BS IV, nationwide)
2020	10 ppm (BS VI, nationwide)	10 ppm (BS VI, nationwide)

2.5. Gaseous fuel as an alternative fuel

Gaseous fuels have been emerging as attractive alternative energy resources to replace diesel fuel either partially or completely in CI engine. The influence of gaseous fuels (like H_2, biogas, syngas) induction in dual fuel CI engine with diesel/biodiesel as a pilot fuel has been described as follows:

2.5.1. Hydrogen as a gaseous fuel

H_2 injection under dual fuel mode was recommended as the best method to improve emissions, as well as to enhance performance of CI engines (Homan et al., 1979; Haragopala et al., 1983). Many studies focussed on the evaluation of the performance of H_2-diesel dual fuel CI engine (Naber et al., 1988; Kumar et al., 2003; Hamdan et al., 2016). Likewise, Kumar et al., (2003) observed a small quantity of H_2 as a secondary fuel with diesel/Jatropha oil as pilot fuel in CI engine lead to larger combustion rate due to high flame speed and wide flammability limits of H_2. As a result, BTE was increased by 7.6% when compared to pure 'Jatropha oil' with an H_2 mass share of 7% under full load condition (Kumar et al., 2003). Recently, Hamdan et al., (2016) utilized H_2 supplement in a CI engine with Jojoba methyl ester as a pilot fuel and reported a major improvement in thermal efficiency whereas, reduces SFC, which can be a potential supplement to cut back the dependence of conventional fuels.

Due to high auto-ignition temperature (576°C), the use of H_2 in CI engines necessitates some ignition facilitator. Researchers have been working on different techniques to overcome this major barrier like Homan et al., (1979) used glow plug as a source of ignition for H_2 and found quicker engine operation with combustion taking place during the injection period. In spite of increasing the CR to 29, IMEP hasn't changed because the injector pressure ranging from 8.3-9.8 MPa was not enough to cause flow in the orifice to the sonic that resulted in a high fraction of H_2 entering into the cylinder after TDC.

H_2 has higher flammability limits when compared to biogas and syngas; hence, a wide variety of power output of a dual fuel CI engine may be possible by varying in the excess air ratio of the mixture. Whereas, high flame speed and heating value of H_2 changes the combustion behaviour of the mixture when injecting H_2 as a secondary fuel in CI engine. Generally, H_2 based dual fuel CI engines showed quicker combustion rate and the rapid rise in pressure with the increasing proportion of H_2 in the mixture (Naber et al., 1988). H_2 assisted CI engines suffer from major hurdle of limited H_2 injection and beyond this, H_2

create several issues such as high in-cylinder peak pressure, auto-ignition of premixed H_2-air charge and too advanced combustion (Haragopala et al., 1983). Lata et al., (2011) reported a steady rise in pressure rate (0.24 bar/°CA) with 50% H_2 volume share at 80% load, which is due to the different thermodynamic properties of H_2 and air, along with the varying intake pressure. Similarly, Wong et al., (1990) investigated the influence of H_2 as a sole fuel in a modified low heat rejection CI engine and reported a rapid rise in pressure rate during compression of H_2-air charge, the self-burning temperature of H_2-air charge is large enough when compared to other hydrocarbon fuels.

The in-cylinder pressure is regarded as an important parameter used to predict combustion behaviour inside the cylinder. Moreover, at medium and high, the in-cylinder pressure increased consequently with rising H_2 energy share whereas at low loads, it follows a reverse trend (Masood et al., 2007; Edwin et al., 2008). The reduction of in-cylinder pressure at low load was due to the deterioration in premixed charge combustion. It was reported that the in-cylinder pressure declined by 11.2% with increasing H_2 (21.4 to 49.6 LPM) at lower load (Santoso et al., 2013). Moreover, these trends are in contrast at high and medium loads due to a high H_2 burning velocity, which leads to complete and rapid fuel combustion. It was revealed that the maximum cylinder pressure increased in the ranges between 1.1 to 11.2% with H_2 addition when compared to diesel (Yilmaz et al., 2017). Study explored the induction of H_2 in CI engine and reported rise in-cylinder peak pressure up to 3% H_2 induction, beyond which in-cylinder peak pressure reduced. Moreover, the apparent rise in peak heat release rate could be observed with a higher rate of H_2. This may be due to the synergic effect of the diffusion and fast turbulence of diesel and H_2 that enhance the peak heat release rate.

The maximum H_2 energy share in a dual fuel CI engine has been restricted by an onset of knocking, which has been found be the main hurdle that plague the successful utilization of H_2 as a fuel in CI engine (Abdelaal et al., 2016). Further, the H_2 content in a CI was enhanced by using two different strategies; (a) retardation in pilot fuel injection timing, (b) use water as an additive. It was experimentally evaluated that the low-temperature combustion strategies would play a dominant role in improving the H_2 energy share in CI dual fuel engine (Liew et al., 2010). Among both strategies, water injection dual fuel mode offered significant rise of 36.0% H_2 energy (Chintala et al., 2015). Additionally, by varying compression ratios of the dual fuel CI engine resulted in significant enhancement in H_2 energy. It has been reported that

thermal efficiency improved with the increase in H_2 energy share, but the efficiency declined significantly with reduction in compression ratios (Chintala et al., 2015).

Normally, the thermal efficiency of any dual fuel CI engine largely depends upon specific heat and compression ratio. With the rise of the specific heat and compression ratio, the thermal efficiency increases consequently. Many studies reported results on various H_2 substitution rates as a future fuel for CI engines without compromising brake torque, thermal efficiency and power output (Nagaki et al., 1999; Selim et al., 2004; McWilliam et al., 2008 Boretti et al., 2011). In this vein, a wide range of experiments was performed by varying H_2 flow rates from 0 to 50 LPM with a step of 10 LPM. With an increase in H_2 induction to 30 LPM, knocking starts with consequent loss in efficiency and power. This is attributed of incomplete combustion caused by less quantity of air availability as higher rates of H_2 replaced the intake air and therefore led to power loss (Mathur et al., 1993). As the availability of oxygen inside the combustion chamber is reduced with H_2 addition, BTE reduced at 7.5% H_2 energy share, but increasing the H_2 energy share would increase the combustion efficiency due its better combustion characteristics (Ghazal et al., 2013).

Similarly, the variable energy shares of H_2 (8.39, 8.73 and 10.1%) used in the experiments conducted by Geo and Nagarajan (2008) revealed improved BTE with H_2 injection almost at all flow rates when compared to the absence of H_2. Although BTE was enhanced to 29.3% from 27.9% with 8.73% H_2 energy share at full load condition, but the increase were still less than the diesel alone (Geo et al., 2008). Varde et al., (1983) indicated that, at low H_2 aspirating rates, the BTE either declined or remained constant relative to the diesel operation. Since the stoichiometric A/F ratio of H_2 is 2.3 times larger than the diesel. Low rates of H_2 showed a high value of lambda; therefore high combustion temperature is needed to burn the H_2 mixed charge. Further, higher peak cylinder pressure was measured at full rated load relative to 6% H_2 energy share. An et al., (2013) reported that, at low load conditions, a small amount of H_2 like 3% (vol. basis) increased the ITE by 34.7% with 1600 rpm rated speed. On the other side, at 2400 and 3200 rpm, no change in ITE was observed under same loading conditions; which might be due to the higher burning velocity of H_2. Since H_2 carries 1.17% more energy than diesel; therefore achieving same power output requires a lower quantity of H_2 to displace diesel under same loading conditions. This could be postulated that H_2 addition improves brake power/brake thermal efficiency under all load conditions (Yadav et al., 2014). At low load, H_2 couldn't burn properly, thus resulting in

poor thermal efficiency. Moreover, BSFC decreased consequently due to high energy rate of H_2 when compared to diesel (Debnath et al., 2012).

Gaseous fuel in dual fuel CI engine would not self-ignite spontaneously, which may lead to knocking, overheating of cylinder walls, high peak pressure and rate of pressure rise (Kumar et al., 2015). Gopal et al., (1982) represented the combustion process of a H_2-diesel dual fuel CI engine at variable loading conditions and reported that at lower diesel flow rate; there was an instantaneous drop in BTE, a problem of knocking and abrupt change in the peak pressure rise rate with H_2 induction. Further, Mathur et al., (1992) found the optimum full load energy of 38% with H_2 and at given energy substitution rate, there was negligible loss in thermal efficiency and power with no knocking. Afterward, rapid reduction in thermal efficiency and BMEP occurred with serious engine knocking, which was explained on the basis of differences in cetane ratio, stoichiometric ratio and combustion characteristics of the fuel-air mixture.

BTE has been reported to improve with change in the injection timing of the dual fuel CI engine. For instance, Saravanan et al., (2007) reported, at injection timing of 5° and 15° ATDC (After Top Dead Centre) with duration of 90° CA, the BTE escalated by 24.5 and 34.1% respectively, when compared to diesel. This kind of behaviour may be because of enhanced combustion caused by the better mixing of H_2 and air. It was identified the optimal conditions for maximum brake power output i.e. at 0.20 and 0.25 equivalence ratios, for 17°CA BTDC and 12°CA BTDC injection timing, respectively. Even, the advancement in injection timing leads to high peak cylinder pressures, and therefore, more NOx emission was observed (Roy et al., 2010). For instance, Ikegami et al., (1980) reported that terribly early injection lower the quantity of fuel delivery and the mixture may fail to ignite within the normal phase during the combustion stroke, hence, inviting a misfiring. These aforesaid handicaps could be overcome by a specially fabricated high-pressure injector, which has high resistance to resist in-cylinder pressure and temperature.

A considerable amount of literature has stated that stoichiometric ratio of H_2-air mixture become weaker at intermediate loads, which results in lowering the flame speed but with increasing load, the mixture would be shifted towards stoichiometric condition; hence give comparable peak heat release rate. Heat release rate curve for a CI engine could be classified as; premixed combustion phase, diffusion combustion phase and after burning phase, as depicted in Fig. 2.1.The large portion of the heat release might occur during premixed and

diffusion combustion phase (Ferguson et al., 1986). Chintala et al., (2014) also stated the similar analogy for CI diesel engine; in all three phases the total heat release would be ended at 90° CA-ATDC. Although, both after-burning and diffusion combustion phases decreases by increasing energy share of premixed charge. On the contrary, Karagoz et al., (2015) described the negative effect caused by these advance faces of combustion, just like on thermal efficiency and reported that maximum reduction in BTE of 10.9% at 40% load with H_2-diesel fuel mode was observed when compared to diesel.

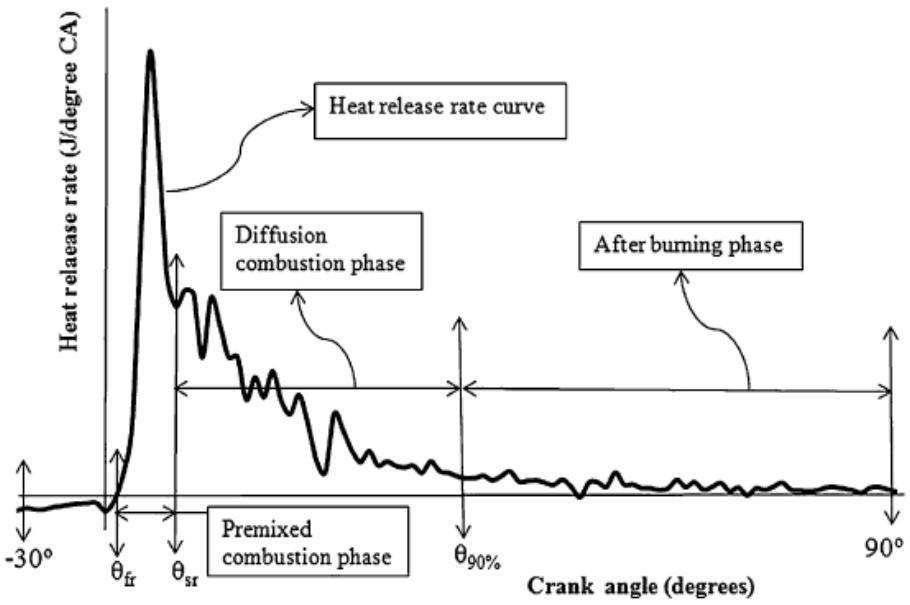

Fig. 2.1. Classification of combustion process in CI engine (Ferguson., 1986)

In a H_2-diesel dual fuel CI engine, an abrupt change in the ignition delay period could lead to increase the energy losses and a portion of H_2 didn't burn in the cylinder, which kept escaping from the tailpipe, thus deterioration the thermal efficiency (Talibi et al., 2014). However, Lilik et al., (2010) reported a fluctuation in the ID period with increasing H_2- fraction in CI engine. There are several explanations corresponding to an initial increase in ID which might be because of decreases in O_2 partial pressure with rising fraction of H_2 as a fuel and due to reduction in the in-cylinder charge (H_2-air) temperature owing to high overall specific heat (Lata et al., 2011).

Since H_2 fuel is considered as an eco-friendly fuel, therefore, its combustion in CI engine would not emit carbon-based pollutants. Heywood stated that the HC and CO formations in CI diesel engine are primarily due to incomplete combustion of fuel, which might be further controlled by proper fuel/air ratio inside the combustion chamber (Heywood et al., 1988).

Notable, fuel-rich mixture promotes CO emission formation, which tends to rise constantly corresponding to equivalence ratio. The emissions of CO and HC originate from the boundary layers and crevices, which are too cold to allow for complete combustion of fuel. In general, adding the H_2 to CI engine would provide high H_2 to carbon ratio of the combined charge that contributes the inner cylinder to reduce CO and also the more homogeneous mixture of fuel enables complete combustion (Sandalci et al., 2014). Furthermore, increasing the amount of H_2 increased the NOx emissions because H_2 causes the generation of radicals, which promote NOx formation. Also, the impact of a small match between the peak cylinder pressure and increased heat release rate is responsible for producing NOx emissions (Wong et al., 1999).

Miyamoto et al., (2011) stated that H_2 addition with a late injection of diesel fuel results in a reduction of combustion temperature; hence reduction in NOx emission. The injection of small amount of H_2 (2%) has a negative impact in terms of brake power and efficiency but has the positive impact in terms of emissions. For example, at 40% load condition, the NOx emission reduced with a lower substitution rate of H_2 (<8%), and later on increased at higher loads. The reduced in-cylinder heat transfer losses were reported in the H_2-fuelled mode because of better air-fuel mixing with reduced heterogeneity of fuels, thereby reducing peak gas temperatures and subsequent reduction in NOx emissions (Antunes et al., 2009). Carbon based emissions showed a reduced trend under most of the engine operating conditions due to the "carbon free" H_2 fuel. The CO_2 and CO emissions decreased consecutively with an increase in H_2 fraction due to the absence of carbon in the fuel changed with H_2 (Birtas et al., 2011). Zhou et al., (2014) reported 34.9 and 39.0% advancement in combustion phase for 30 and 40% H_2 addition, respectively. It can be observed that all emissions were under control but smoke and NOx levels increase with H_2 addition owing to outweighing peak in-cylinder pressure at full load condition. The effect of H_2 enrichment on the emission characteristics of CI engine at full rated load and found that the CO and smoke emissions were improved, but HC emission increased with increasing H_2 percentage (Kose et al., 2013; Karagoz et al.,2016).

Few scattered studies explored the measurement of the unburned H_2 emissions of dual fuel CI engines. In this aspect, it focused on the H_2 emissions emitted from a H_2-diesel dual fuel engine (Gatts et al., 2010) and reported that unburned H_2 emission increased but its combustion efficiency decreased linearly with H_2 addition up to a threshold value. However,

improvement in combustion efficiency and reduction in H_2 emissions was observed with increasing engine load (Abu-Jrai et al., 2007).

As the heat content of H_2 is 2.82 times higher than diesel fuel, and the faster burning rate of H_2 leads to increase the in-cylinder temperature earlier during the power stroke in dual fuel CI engine with H_2 combustion when compared to diesel. Shirk et al., (2008) recorded higher EGT with 5% H_2 substitution along with biodiesel blended (B20) pilot fuel, which was slightly higher than diesel. Higher EGT could be due to a higher heating value of the H_2 (120 MJ/kg). The other reason may be due to high flame temperature and rapid combustion with H_2 indication under dual fuel mode.

In order to reduce the fossil fuel consumption and emission levels, another alternative technique homogeneous charge compression ignition (HCCI) engine concept was explored. In this engine, a premixed homogeneous air-fuel mixture is injected into the cylinder. Diesel fuel alone is not appropriate for HCCI engine operation because of its high propensity and low volatility (Kong et al., 2002). Szwaja et al., (2009) analyzed the results of H_2 combustion by using HCCI engine and disclosed that H_2-air combustion under HCCI mode generated extremely high knocking; which could be overcome by adopting lean combustion. When compared to diesel fuel, around 40% higher peak cylinder pressure was measured in the H_2 HCCI mode and this quick pressure rise suggests that a considerably higher heat release rate (Antunes et al., 2008). A negligible effect on HC and CO emissions was observed, whereas some H_2 in the exhaust could be seen due to injection of H_2 under non-optimized conditions. Interestingly, lesser NOx levels were observed in an H_2-HCCI mode in comparison to the diesel engine.

Although, direct H_2 injection into the cylinder has some advantages like high volumetric efficiency, high engine power output but it requires especially designed injectors that should be durable against high temperature and pressure in the cylinder. Indeed, some modification must be required to install these injectors on the cylinder head. An effort has been done by Saravanan and Nagarajan using the aforesaid injector to inject H_2 into the intake manifold, whereas diesel was used to initiate the H_2 combustion. H_2 was fed at a constant flow rate (5.51 min^{-1}) throughout load spectrum. At 75% of rated load, NOx emission was increased because of improvement in the fuel combustion zone with H_2 induction that also leads to higher BTE (Saravanan et al., 2009).

Findings of various studies revealed that the utilization of H_2 as an energy carrier to existing CI engine under dual fuel mode is a promising option to enhance the performance and improve the emissions characteristics. The injection of small amount of H_2 to a CI engine can reduce the heterogeneity of a diesel fuel spray, which offers better circumstances throughout the combustion process. However, the implementation of H_2 as a fuel largely depends upon its availability, competitive price, and its safe storage system.

2.5.2. Biogas as a gaseous fuel

The long-term utility of a biogas-diesel dual fuel CI engine has been tested by Tippayawong et al., in 1993 and reported negligible effects on power output and efficiency up to the first 2000 h run of dual fuel CI engine. Thereafter, a little quantity of carbon deposition inside the combustion chamber was observed. The energy conversion efficiency under dual fuel mode was significantly less, which may be due to the large replacement of pilot fuel by gaseous fuel (Duc et al., 2007).

Gaseous fuel, which complies with the requirements of the standards, could be used in dual fuel CI engines; while biogas produced by anaerobic digestion contains an excessively high concentration of water vapour and H_2S, and therefore, doesn't meet the standards of engine fuels. A part from that, the extent of CO_2 in biogas is higher, which reduces its energy content. Many studies have been reported in the past evaluating the effect of CO_2 concentration in biogas. Makareviciene et al., (2013) revealed that increasing the CO_2 percentage in biogas decreases the fuel quality in term of combustion, thereby increasing fuel consumption. CO_2 behaves as an inert gas that subsequently increased the specific heat of the intake charge, and causes a reduction in the flame propagation speed (Bedoya et al., 2009). Generally, biogas-diesel dual fuel engine offers low BTE and high BSFC due to the presence of CO_2. Bari et al., (1996) reported an increase in BSFC for CO_2 percentage above 30% (Vol. basis) in the biogas. This may be due to the effect of diluents like CO_2 in the combustion chamber, which lower local gas temperature by absorbing heat energy from the combustion and affecting the burning speed of the biogas-air charge. It means increasing proportion of CO_2 in biogas decreases BTE because of low mean combustion temperature. Nathan et al., (2010) explained that CO_2 content in biogas up to 40 % did not affect the performance of dual fuel CI engine, but beyond that, CO_2 may affect the ignition delay period due to dissociation into O_2 and CO. Kovacs et al., (2010) stated that, the CO_2 content in the tailpipe emissions depends largely on the CO_2 presence in the biogas itself. Cacua and Villalba figure

out that CO_2 emission of the trigeneration system under biogas-diesel dual fuel mode was successfully decreased by 24.9 % when compared to single generation mode (Cacua et al., 2016).

It has also been reported that by using O_2 enriched air in a biogas-diesel dual fuel CI engine attenuates the effect of diluents (CO_2) in decreasing the burning velocity, ignition delay timing of CH_4 and adiabatic flame temperature (Rajkumari et al., 2010). Moreover, Cacua et al., (2012) examined the effect of O_2 enriched air on the engine characteristics of a dual fuel CI engine and revealed that CH_4 emission and ignition delay time were belittled with 27% O_2 enriched air while the BTE was inflated. These changes are attributed to the decreases in the temperature of the overall gas-air mixture and low burning velocities of biogas relating to CH_4. Luijten et al., (2011) also inferred that BTE is hardly affected at higher loads, but largely depends on the CH_4/CO_2 ratios in biogas composition.

Methane (CH_4) is the main component in biogas composition (up to 65%), and its high octane rating exhibits a greater resistance to knock and makes it appropriate for engines which have typically higher CRs. Moreover, the increase in CH_4 content of biogas resulted in higher BTE due to higher heat release rate, as reported (Crookes et al., 2006; Jiang et al., 1989). The lower carbon content in CH_4 compared to petroleum diesel fuel simultaneously decreases the tailpipe exhaust emissions (Henham et al., 1998). Apart from that, replacement of pilot fuel with biodiesel (Crookes et al., 2006), increasing compression ratios (Jiang et al., 1989), using EGR technology to preheat the inlet charge (Yoon et al., 2011), are the different strategies for increasing BTE.

The combustion process under dual fuel mode is more complex than the single mode. In fact, the use of any gaseous fuel having high auto-ignition temperature will acts as a heat sink within the combustion period of dual fuel CI engine. As a result, an uneven increases in the specific heat capacity of the working fluid due to induction of biogas, further decreases the combustion temperature (Pattanaik et al., 2013). Moreover, biogas charged dual fuel CI engine permits the co-combustion of a premixed diluted mixture involving low in-cylinder temperature and increased homogeneity in charge which results in low smoke/NOx emissions. Numerous studies available in literature are dedicated to dual fuel CI engines have proven that the successful use of said engines is possible within the wide range of loads. Recent findings of Kalsi et al. (2010) revealed that the CI engines could be run with the maximum biogas energy shares at a part and high loads. At higher loads, the in-cylinder

pressure in dual fuel mode is higher when compared to the conventional diesel mode. This behaviour may be due to the consequence of the higher heat release rate. On the other hand, at low engine loads, the lower BTE and higher BSFC are usually caused by incomplete combustion of biogas-air mixture due to over lean mixture and lower temperature. Further, improvement in BSFC and BTE is shown in Fig.15 and 16 under dual-fuel combustion at 80 % loads (Yoon et al., 2011). Previous studies revealed several strategies for improvement of dual fuel operation at part load viz. use of low substitution levels (AbdAlla et al., 2004), preheating of inducted air–fuel mixtures (Poonia et al., 1999; AbdAlla et al., 2001), changes in the initial charge pressure and temperature with EGR (Wong et al.. 1996; Selim et al., 2003) and modification of the pilot fuel injection system (Sahoo et al.. 2003; Nwafor et al., 2007).

Ignition delay is a critical parameter that affects the combustion of any gaseous fuel as longer ignition delay periods results in unacceptable pressure rise that ends up in knock drawback. For gaseous fuels, a prolonged ignition delay was observed with the increase of their percentage levels in the mixture. Barik et al., (2014) carried out a series of experiments on the utilization of biogas as a secondary fuel in the single cylinder, direct injection CI engine at flow rates (0.3, 0.6, 0.9 and 1.2 kg/h), and at variable engine loads. The findings illustrate that the biogas-air mixture undergoes prolonged ignition delay under biogas-diesel dual fuel combustion in comparison to single fuel. The longer ignition delay with a biogas-operated engine was explained through the established fact of O_2 deficiency, which may cause incomplete combustion and subsequently decrease fuel energy conversion (Yoon et al., 2011).

The comparative study has been conducted by Bora et al., in 2014 on the effect of compression ratios on various engine characteristics of a biogas-diesel dual fuel engine. Generally, the peak cylinder pressure is lower under dual fuel mode when compared to diesel for all compression ratios. These findings confirmed that with an increase in compression ratio, peak cylinder pressure of a biogas dual fuel engine increased. However, the ignition delay decreased as the compression ratio increased. This prolonged ignition delay of biogas dual fuel engine is due to the larger amount of biogas fuel accumulated in the first & second stroke of the engine, and reduction of mixture charge temperature, when compared to neat diesel operated CI engine. It may be noted that greater rise of temperature with higher compression ratio during compression stroke leads to better combustion of fuels; hence

higher NOx and lower HC/CO emissions were found. As a consequence, the volumetric efficiency might drop, while the improvement in BTE with regards to compression ratio (Bora et al., 2016). This significant improvement in BTE of a biogas-diesel dual fuel CI engine could be due to the sufficient time for pilot fuel to make a homogeneous mixture with biogas and air. Generally, there is an optimal injection timing for every hydrocarbon fuel for a particular CI engine beyond which thermal efficiency does not increase either with retarding or advancing injection timing (Barik et al., 2015). Similarly, Barik et al., (2017) found a significant increment in CO emissions by varying injection timing in biogas-biodiesel duel fuel mode than that of biodiesel mode. This may be attributed to the existence of flame rich zone and the incomplete oxidation of biogas under dual fuel mode.

NOx formation is largely dependent on the oxygen availability, combustion temperature and retention time for reaction (Kalsi et al, 2017). The findings of various researchers confirmed the significant reduction in NOx and smoke emissions throughout load spectrum using biogas as a secondary fuel with diesel/biodiesel as pilot fuel in CI engine (Barik et al., 2013; Ramesha et al., 2015). On the contrary, the HC and CO emissions were found to be higher with increasing biogas energy shares. This enhancement was affected from the dilution of premixed charge with CO_2 that results in incomplete oxidation; therefore a suitable technology needs to be developed to overcome this issue. Bora et al., (2015) published data on biogas-biodiesel/diesel dual fuel engine, and it was revealed that the EGT of biogas dual fuel mode was higher than that of diesel mode. The attainable reason of higher EGT with biogas dual fuel mode can be the late combustion of biogas fuel, which tends to shorten the length for extraction of power. On the contrary, the combustion of emulsified fuel tends to lower the EGT owning to the cooling impact of micro-explosion.

Hence, the use of biogas in existing diesel engine under dual fuel mode offers both environmental and economic benefits. It's been also reported that dual fuel engine needs higher fuel energy for producing same power output when compared to diesel mode. The emission parameters were observed to reduce considerably with biogas addition to CI engine working under dual fuel mode.

2.5.3. Syngas as a gaseous fuel

The renewable fuels having a composition of CH_4, CO and H_2 are particularly interesting as the depletion of fossil fuels has become a major issue worldwide. The work of Hernandez et

al., (2016) highlighted the effect of CH_4, CO, and H_2 separately, when the petroleum diesel fuel is partially replaced with aforementioned gases. It has been reported that the replacement of diesel fuel with said gases may deteriorate the thermal efficiency because of the shift of combustion caused by higher premixed ratios and unburned gaseous fuel, which escape from the combustion chamber. The injection of syngas in dual fuel CI engine not only provide lesser fuel consumption but in addition, enhances the combustion quality as described by Rinaldini et al., (2017).

However, the volumetric composition of H_2 and CO in syngas largely depends on the source and the production technique. Sahoo et al., (2012) tested three different compositions of H_2 and CO in syngas as a dual fuel in CI engine. The combustion of syngas with H_2 and CO proportion of 100:0 resulted in the 72.3% replacement of diesel fuel in dual fuel mode. At low and higher loads, decrement in diesel substitution rate was found due to the insufficient O_2 availability, which leads to incomplete combustion of syngas. On the other hand, the volumetric efficiency reduced for all the combinations of syngas throughout the load spectrum due to the displacement of sucked air by syngas. NOx emissions reduction was observed with increase in CO concentration in syngas, which was attributed to the lower adiabatic flame temperature of CO enriched syngas. However, increase in unburned HC and CO emissions were reported with rise in CO proportion present in syngas.

In addition, Sahoo et al., (2011) tried to investigate theoretically the performance limits of a syngas-diesel dual fuel CI engine by using availability analysis. An increase in destruction availability was observed on lower loads at all H_2 enrichment levels in syngas due to reduced heat transfer availability losses and poor fuel combustion. At the higher load conditions beyond 40%, a reduction in destroyed availability was noticed, attributed to the higher combustion pressure and temperature. There is strong evidence in the literature that the H_2 and CO_2 content affected the dual fuel CI engine performance and emission characteristics. Syngas enriched with H_2 showed better thermal efficiency and higher combustion flame temperature, which enhance the heat release rate and in-cylinder pressure that subsequently increased NOx emissions. However, the decrease in NOx emission was observed for the CO_2 rich syngas dual fuel mixtures when compared to diesel fuel alone. This was attributed to the relatively higher specific heat capacity; and the lower in-cylinder combustion temperature for the syngas enriched with CO_2 operated under dual fuel mode when compared to neat diesel fuel (Azimov et al., 2011).

Another recent investigation demonstrated the effect of various CH_4-CO_2-H_2 and CH_4-CO_2 mixtures, diesel injected by two flow rates (Talibi et al., 2017). The authors reported that the increase in heat release rate for the CH_4-CO_2-H_2 dual fuel mixtures was considerably lower in comparison to diesel fuel only. This could be due to the presence of CO_2 proportion in mixture impending combustion through lower flame temperature. Lower CO_2 emissions were observed relative to $0.6CH_4$- $0.4CO_2$ mixture, still equivalent to CO_2 emission from $0.8CH_4$- $0.2CO_2$ when compared to diesel alone. It has been underlined the desirability to scrub the biogas post production in order to reduce CO_2 emissions. The CO_2 enhancement in mixtures considerably decrease in-cylinder flame temperature which significantly reduces NOx emissions, but at the same time higher CO, PM and HC emissions owing to the reason of reduction in thermal oxidation.

2.6. Biodiesel in CI engine

Biodiesel as an alternative renewable fuel picking up popularity as it is a clean oxygenated fuel derived via transesterification of vegetable oil/animal fat (Farrukh et al., 2018; Marwaha et al., 2018). Biodiesel has been considered as a fuel that adds to energy sustainability, and can be used in CI engines either in pure form or by blending with conventional diesel (Mahla at al., 2018; Kumar et al., 2019). It is more eco-friendly and non-toxic fuel when compared to ordinary diesel; moreover, its high lubricant properties improve engine performance as well (Chauhan et al., 2016). Muralidharan et al., (2011) utilized biodiesel blends in CI engine and expressed that brake thermal efficiency (BTE) is directly proportional, but the brake specific fuel consumption (BSFC) were inversely proportional to engine load. Further, the bounded oxygen (O_2) in biodiesel provides better fuel burning and also reduces exhaust gas contaminations. Several studies revealed that biodiesel-diesel blends reduce PM, smoke opacity, HC and CO emissions, but NOx formation increases due to enhancing in-cylinder combustion temperature (Pramanik et al., 2003; Xue et al., 2011; Gautam et al., 2018). Similarly, Schumacher et al., (1996) found optimal biodiesel blend (B20) in emission aspect and stated that retardation in fuel injection reduces NOx formation to some extent; however, PM, HC, CO pollutants remained constant. This reduction in harmful emissions is often accompanied by a tradeoff in power, torque, and SFC. Ramadhas et al., (2005) tested B20 in urban bus fleets and identified higher fuel consumption (2-5%) when compared to neat diesel.

CI engine design parameters such as compression ratio (CR), injection timing, and injection pressure (IP) cause countable effects towards the combustion of any hydrocarbon fuel. In this context, innovative research has just been done to examine the impacts of fuel IP and engine CR by performing Jatropha biodiesel (Jindal et al., 2019). It was reported that the IP (250 bar) and CR (18:1) enhance BSFC and BTE by 10.0 and 8.9%, respectively. The extensive research has been done on biodiesel utilization in CI engine over the recent few decades, while, mostly done at fixed CR (Devan et al., 2009; Sukumar et al., 2010). But, few scattered studies explored the utilization of biodiesel by varying engine CR. In this perspective, Sharma et al., (2015) reported that ignition delay (ID) period decreases and peak cylinder pressure (PCP) increase with biodiesel at higher CR (18.5:1). It was stated that the ID period reduces by 13.9 % with the rise in CR from 14:1 to 18:1 (ELKassaby et al., 2013). Moreover, the improvement in biodiesel combustion properties was also stated with rising in CRs. It was stated that 20 % biodiesel in conventional diesel leads to improve performance characteristics of CI engine (Balat et al., 2010). Kumar et al. (2015) compared neat diesel with B20 palm biodiesel and found improvement in engine performance parameters, as well as harmful emissions reduced. Deepanraj et al., (2011) findings demonstrated that with increasing palm biodiesel percentage in diesel, the specific fuel consumption (SFC) and NOx emissions increase, while, the reduction in HC and CO emissions was observed.

2.7. Research gaps

After review of the literature on renewable fuels research, it has been observed that renewable fuels offered tremendous advantages, yet they are currently a controversial area of science. While researchers have paid substantial attention to greenhouse gas emissions, the new study says, they have focused little on how the production and utilization of renewable fuels affects biodiversity and human health. The R&D gaps and priorities can be identified as following:

- Fossil fuels play a vital role to satisfy the world energy demand, but due to increasing population and improved living standard, there will be shortage of conventional energy resources which needs to be addressed by renewable ones.
- Comparatively poor low-temperature flow properties are a characteristic of biodiesel that limits its application.

- Biogas as a fuel in CI engine offers low calorific value because of the presence of large proportion of CO_2 which also leads to climate change, therefore reforming of biogas for energy enrichment may be explored as an attractive option for CI engine.
- Current commercial processes for syngas and H_2 production largely depends on fossil fuels, so alternative processes need to be developed that do not depend on fossil hydrocarbon resources.
- Major challenge associated with running an engine on pure H_2 is premature ignition and flashback due to its very low ignition energy.
- Indeed, maximized yield of H_2 by steam reforming was obtained with high CO_2 content, so further studies are required in this direction to reduce CO_2 content.
- Although, the CO_2 content in dry reforming is less, but it's highly endothermic nature leads to high energy demand, so need of the hour is to examine energy efficient processes.
- Moreover, literature studies indicate that the dry reforming reactions are inevitably accompanied by carbon deposition, thus, development of catalyst that minimizes carbon deposition is a key research priority.
- The noble catalysts (Rh, Ru and Pt) have been used for dry reforming by various researcher but these noble metals are expensive and of limited availability, and are therefore, in practice, not suitable for the process at an industrial level.
- Ni based catalysts are foremost utilized in the reforming processes with limitation of less stability for reaction with O_2 and CO_2 as oxidants, so additional studies need to apply in evaluating the effect of the catalyst support and addition of promoters elements over coke formation.
- Majority of researchers indicated that NOx and HC emissions increased while using pure H_2 as a fuel in CI engine and it is imperative to find optimal H_2 usage in conjunction with diesel/biodiesel in order to obtain the nominal peak pressure and reduced emissions.
- Few scattered reports exist on the running of a commercial diesel engine under dual fuel mode: diesel/biodiesel along with hydrogen enriched biogas, so present study is focussed with the intention of improving the thermal efficiency and reducing emissions with little or no modification in the CI engine.

Chapter-3

MATERIALS AND METHODOLOGY

In this chapter, the details of materials used in the catalyst synthesis as well as biodiesel production have been presented in the initial section, and various approaches/techniques used for their characterization and synthesis have been elucidated subsequently. The description of the reforming reactor, the exit gases effluent assessing system, and the catalytic reforming procedure has been detailed separately. It also provides the details of engine test rig used for conducting experiments under single and dual fuel modes; thereafter, the procedure adopted along with details of equipment used for experimentation has been elaborated paragraphically.

3.1. Chemicals and Materials

Commercial nickel (Ni) nanoparticle (particle size: 20nm; surface area: 55m^2/g) purchased from Loba Chemie, Mumbai, India. Titanium dioxide [TiO_2] and cerium oxide [CeO_2] were procured from Sigma-Aldrich. Nickel nitrate hexahydrate [Ni $(NO_3)_2.6H_2O$], aluminum nitrate nonahydrate [Al $(NO_3)_3.9H_2O$], zinc nitrate hexahydrate [Zn $(NO_3)_2.6H_2O$] and cerium nitrate hexahydrate [Ce $(NO_3)_3.6H_2O$] salt precursors were supplied by Loba Chemie, Mumbai, India. Ethanol and methanol (Merck, 99.5%); potassium hydroxide (KOH) of analytical grade was provided by Loba Chemie, Mumbai, India.

The liquid fuels used in this study were: palm oil and diesel; palm oil was used for biodiesel production, and both were procured locally. Moreover, the used ultrapure gases consist of CH_4 (99.999%), CO_2 (99.999%), O_2 (99.999%), H_2 (99.999%) and N_2 (99.999%) were provided by Ankur gases, Jaipur-India.

3.2. Catalyst preparation

Various Ni based catalysts were prepared using wet-impregnation method (Perego et al., 1997) at laboratory scale. The different oxides supports used comprised of TiO_2, CeO_2, Al_2O_3

and ZnO of catalyst preparation. The preparation procedure for all the catalysts was identical, with either varying the salt precursors.

3.2.1. Preparation of Ni/TiO_2 catalysts

Before impregnation, the bare TiO_2 was first kept into muffle furnace for 3h at 800°C in order to eliminate surface impurities. Thereafter, 2 g of TiO_2 support was dissolved in an aqueous solution of C_2H_5OH (60 mL) under vigorous stirring in the 150 mL beaker. Homogeneous solutions of CH_3OH (60 mL) and Ni $(NO_3)_2.6H_2O$salt were prepared separately into other vessels, with different Ni concentrations viz., 7, 11, 15, and 19 wt. % of TiO_2 support. The specific solution of CH_3OH and Ni $(NO_3)_2.6H_2O$ was subsequently poured dropwise into the existing solution of TiO_2 and C_2H_5OH in the 150 mL beaker, followed by continuous stirring (800 rpm) at room temperature for 24h. The resulted slurry was dried in an air-tight oven (110 °C) for 24 h and subsequently calcined at 550°C for 4h. Similarly, TiO_2 supported catalysts with different Ni contents were prepared and labeled as $Ni_{0.07}/TiO_2$, $Ni_{0.11}/TiO_2$, $Ni_{0.15}/TiO_2$ and $Ni_{0.19}/TiO_2$.

3.2.2. Preparation of Ni/Ce (Al_2O_3-TiO_2) catalysts

Ni/Ce (Al_2O_3-TiO_2) catalysts were prepared by sequential impregnation method. The sole TiO_2 was thermally treated in the same manner as discussed in section 3.2.1. Al_2O_3-TiO_2 mixed support was prepared by impregnated alumina into the TiO_2 support. First, the aqueous solution of CH_3OH (60 mL) and Al $(NO_3)_3.9H_2O$ were mixed dropwise to the slurry of CH_3OH (60 mL) and TiO_2 in such as manner so that equal mass ratio of alumina and titania is obtained. The rest of the procedure was identical as that follows for Ni/TiO_2 catalyst. Simultaneously, the different CeO_2 decorated (Al_2O_3-TiO_2) mixed supports were prepared with different Ce contents (10 to 30 wt. % of mixed support) using Ce $(NO_3)_3.6H_2O$ salt precursor. Finally, Ni (11 wt. %) was impregnated into obtained Ce (Al_2O_3-TiO_2) mixed support using Ni $(NO_3)_2.6H_2O$ as Ni precursor. Finally, the obtained catalysts were designated as $Ni_{0.11}$/ $Ce_{0.10}$ (Al_2O_3-TiO_2), $Ni_{0.11}$/ $Ce_{0.20}$ (Al_2O_3-TiO_2) and $Ni_{0.11}$/ $Ce_{0.30}$ (Al_2O_3-TiO_2).

3.2.3. Preparation of 10 wt. % Ni/CeO_2 catalyst

The Ni/CeO_2 was prepared at fixed Ni content i.e. 10 wt. %. Initially, CeO_2 support was calcined in the muffle furnace at 500°C for 3h to eliminate surface impurities. After that, the CeO_2 was impregnated with an aqueous solution of Ni $(NO_3)_2.6H_2O$ with the appropriate

amount to obtain 10 wt. % Ni loading. Various aqueous solutions of support/salt and solvent (C_2H_5OH) were prepared in the same manner as that for Ni/ TiO_2 catalyst, discussed in the section 3.2.2.

3.2.4. Preparation of Ni/(ZnO-CeO_2) catalysts

Ni-based catalysts supported on mixed (Zn-Ce) supports were prepared using wet impregnation technique with different proportions of ZnO-CeO_2 (10:90; 20:80) and were designated as $Ni_{0.10}$/ ($Zn_{0.1}$-$Ce_{0.9}$) and $Ni_{0.10}$/ ($Zn_{0.2}$-$Ce_{0.8}$). Firstly, CeO_2 was thermally treated same as in case of $Ni_{0.1}/CeO_2$ catalyst, thereafter, the CeO_2 was impregnated with an aqueous solution of Zn $(NO_3)_2.6H_2O$ with appropriate concentration to obtain different Zn loading (10 and 20 wt. %). The obtained (Zn-Ce) supports were used subsequently and impregnated with Ni $(NO_3)_2.6H_2O$ to get 10 wt. % Ni.

3.3. Characterization

The different structural and physicochemical properties of all metal supported catalysts were assessed to develop a link between these properties with the activity/selectivity of the reforming catalyst. Further, the characterization of palm oil methyl ester (POME) was done in order to determine various chemical and physical properties.

3.3.1. Catalyst characterization

The XRD patterns were identified by X-ray diffractometer (Rigaku Ultima IV Advance, Cu-Kα radiation) in the 2θ range between 20-100°.The average Ni particle sizes corresponding to the reflection peak intensity (111) in the XRD spectra's were determined using Scherrer equation (Eq.3.1).The surface areas (BET) were analyzed using N_2 adsorption/desorption isotherms at liquid nitrogen temperature, with a Quantachrome Nova 1200 instrument. FESEM (Field emission scanning electron microscopy) images of catalysts were captured with a JEOL JSM-6701F, whereas, TPR (Temperature programmed reduction) analysis of each catalyst was performed in a semiautomatic Micromeritics 2900 apparatus equipped with a TCD under flowing 5% H_2/He mixture at 30 ml min^{-1} flow rate with 50mg of sample. Finally, the carbon deposition in wt. % over the spent catalysts was assessed using CHNS Elemental Analyzer (Flash 2000 HT by Thermo Scientific) by treating sample at 960°C.

$$L=\frac{0.9\lambda}{\beta Cos\theta} \tag{3.1}$$

Where L is the crystallite width (nm), λ is incident radiation wavelength (nm), β is full width at half maximum intensity (radians), and θ is Bragg angle (degree).

3.3.2. Characterization of biodiesel

The ASTM standard test methods were employed to determine various physico-chemical properties of POME, with their respective test given in parentheses, such as density (D1298), cetane number (D976), kinematic viscosity (D 445), flash point (D 93), fire point (D93), calorific value (D240), cloud point (D2500), pour point (D97), and acid value (D664).

3.4. Reforming reactor

Biogas reforming tests with or without O_2 were performed in a down-flow fixed bed reactor. Schematic layout and actual image of the reforming reactor are shown in Fig. 3.1. The reactor has an inner diameter (1.0 cm) and length (70 cm), and is placed vertically in a tubular electric furnace. The power rating of the reactor is 4.5 kW with a maximum attainable temperature of 1100°C. For high-temperature stability, an alloy (Inconel 620) was used as the reactor material. CH_4, CO_2 and O_2 were used as the reactant gases; moreover, H_2 for catalyst reduction, and N_2 used as a carrier gas to prevent the oxidation of catalyst during the attainment of desired temperatures. The reaction temperatures were monitored and controlled by a PID based control panel coupled with the reforming unit. A calibrated thermocouple (K type) was inserted directly inside the thermo-well of the reactor for monitoring the bed temperature. Catalyst was sandwiched in a middle of the quartz wool to carry out the reaction in a packed bed reactor. The flow rates of reactant gas mixtures were controlled through mass flow controllers (Alicat make). Exit gases effluent passes through the condenser and gas-fluid separator before being analyzed by the gas analyzer. Continuous gas flow analyzer was employed to analyze product gases, with their measurement range given in parentheses, such as CO (0-100%), CO_2 (0-50%), CH_4 (0-100%), and H_2 (0-100%).

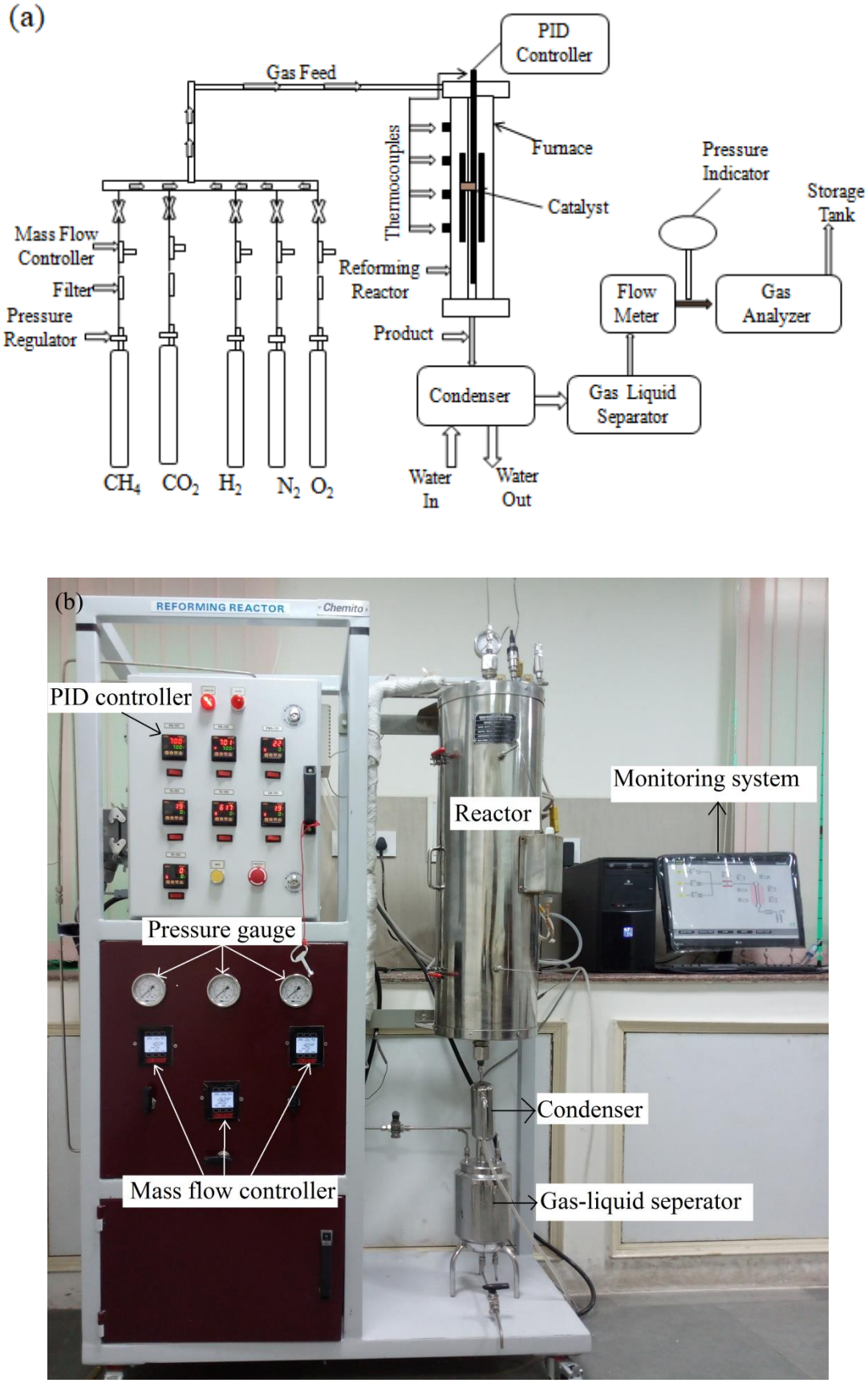

Fig. 3.1 Biogas reforming reactor (a) Schematic layout; (b) Actual image

3.5. Catalytic reforming

Catalytic activity over biogas reforming was tested in the temperature range between 650 and 900°C at 1 bar. For DR reactions, synthetic biogas was prepared with a fixed molar ratio of CH_4:CO_2 = 1.5:1 and fed to the reforming reactor. Prior to reaction, a fixed amount of catalyst (150 mg) was loaded in the middle of the quartz wool packed reactor, and then it was subsequently heated to the pre-defined temperature at the ramp rate of 10°C min^{-1} in 30 $NmLmin^{-1}$ flow of N_2. Once the desired reaction temperature reached, a dwell of 40 min was held before feeding the reactants to obtain the steady state condition inside the reactor. Then, the catalyst was activated by reduction with pure H_2 flow in the temperature ranges obtained by H_2-TPR analysis. Performance data was recorded after 2h on-stream, and the catalytic stability was assessed for 18h at fixed temperature over the catalysts where higher H_2 enrichment was obtained.

Biogas reforming was carried out in the two phases; initially done with pure Ni nanoparticle followed by lab synthesized catalysts. Preliminary experimental tests were carried out to evaluate the effective conditions (process temperature and feed rate) to maximize H_2 enrichment in the biogas under DR. The DR reactions are highly endothermic, as discussed earlier. Therefore, high temperature (700-900°C) ranges were adopted in the biogas DR in order to study the effects of reaction temperature on reactant (CH_4 and CO_2) conversions and product (H_2 and CO) yields; by using fixed catalyst amount (150 mg) and WHSV (20,000 NmL g^{-1} h^{-1}). Then, by varying WHSV ranges (20,000- 60,000 $NmLg^{-1}$ h^{-1}), the impact of WHSV on the catalytic performance with respect to CH_4conversions and product (H_2 and CO) yield was also examined; on the temperature offering maximum H_2 enrichment in biogas. WHSV (40,000 $NmLg^{-1}$ h^{-1}) was chosen for the DOR; since DOR doesn't perform well at low space velocities, observation obtained from reported literature (Enger et al., 2008). Thereafter, DOR was carried out subsequently by adding extra O_2 in the proportion between 0-0.37 as for CH_4 volumetrically; moreover, the reaction temperature was kept in the ranges 650 and 900 °C. DR of biogas was also done with various Ni-based catalysts supported on different supports (viz., Al_2O_3/CeO_2/TiO_2/ZnO). DR reactions were started initially with a temperature of 650 °C; thereafter, the reaction temperature was increased stepwise until the H_2/CO ratio reached to stoichiometric (i.e. H_2/CO = 1) or to the nearly constant value (≤1). After the completion of DR with lab-synthesized catalysts, the most active and stable catalyst was chosen to investigate the effect of O_2 addition in DOR at

650°C. The additional O_2 was inducted in the ratio between 0-0.57 with respect to CH_4 on volumetric basis.

The different performance parameters for the reforming process were determined, as mentioned in Eqs. (3.2) to (3.7).

$$CH_{4\ conversion}\ (\%) = \frac{CH_{4\ (in)} - CH_{4\ (out)}}{CH_{4\ (in)}} \times 100 \tag{3.2}$$

$$CO_{2\ conversion}\ (\%) = \frac{CO_{2\ (in)} - CO_{2\ (out)}}{CO_{2\ (in)}} \times 100 \tag{3.3}$$

$$H_{2\ yield}\ (\%) = \frac{H_{2\ (out)}}{2\ CH_{4\ (in)}} \times 100 \tag{3.4}$$

$$CO_{\ yield}\ (\%) = \frac{CO_{\ (out)}}{CH_{4\ (in)} + CO_{2\ (in)}} \times 100 \tag{3.5}$$

$$H_{2\ selectivity}\ (\%) = \frac{H_{2\ (out)}}{2\ (CH_{4\ (in)} - CH_{4\ (out)})} \times 100 \tag{3.6}$$

$$CO_{\ selectivity}\ (\%) = \frac{CO_{\ (out)}}{(CH_{4\ (in)} - CH_{4\ (out)}) + (CO_{2\ (in)} - CO_{2\ (out)})} \times 100 \tag{3.7}$$

Weight hour space velocity (WHSV), in units of NmL g^{-1} h^{-1} and specific energy consumption (SEC), in kJ/NmL of H_2, were calculated using equations 3.8 and 3.9, respectively.

$$WHSV\ \left(NmL\ g^{-1}\ h^{-1}\right) = \frac{Feed\ rate\ (NmL/h)}{Mass\ of\ catalyst\ (g)} \tag{3.8}$$

$$SEC\ (kJ/NmL\text{-}H_2) = \frac{Energy\ required\ (kJ/min)}{H_2\ produced\ (NmL/min)} \tag{3.9}$$

3.6. Response surface Methodology (RSM) and Box-Benkhen Design (BBD)

The optimization of HEB was statistically performed by RSM with Box–Behnken factorial design technique using Minitab 17 software. The set of experiments was built using a 15 run, three-level, three-factor Box–Behnken factorial design and randomly performed to elucidate the effect of each independent variable on the dependent variables. The independent variables considered for this study are the reaction temperature, X_1; the CH_4/CO_2 ratio, X_2; and the O_2/CH_4 ratio, X_3. These independent variables were studied at different levels (-1, 0 and 1). Moreover, reactant (CH_4 and CO_2) conversions, product (H_2 and CO) yields, selectivities of H_2 and CO, H_2/CO ratio, and SEC were selected as the responses. The maximum temperature

of 900°C was chosen for being the highest CH_4 conversion, as reported in previous reports (Nakagawa et al., 2001; Nematollahi et al., 2012). The minimum temperature level of 800°C was chosen to neglect the influence of side reactions, such as Boudouard (Eq. 2.4) and methane decomposition (Eq. 2.3) reactions (Yan et al., 2003; Sajjadi et al., 2015). The various CH_4/CO_2 ratios were chosen considering different CH_4 and CO_2 proportion in biogas composition, whereas, different O_2/CH_4 ratios to evaluate the effect of DOR process on H_2-enriched biogas production were used. The list of ranges and levels of the independent variables with coded and actual values of each prominent parameter are tabulated in Table 3.1.

Table 3.1 Selected reaction parameters and their levels for analysis

Independent Variables	Symbol	Unit	Range and levels		
			-1	0	1
Reaction Temp.	X_1	(°C)	800	850	900
CH_4/CO_2	X_2	--	1.0	1.5	2.0
O_2/CH_4	X_3	--	0.10	0.20	0.30

After experimentation, an empirical model was generated using analysis of variances (ANOVA) at 95% confidence level. This model was examined through second-order quadratic equation, using Eq. (3.10).

$$Y = \beta_0 + \beta_1 X_1 + \beta_2 X_2 + \beta_2 X_3 + \beta_{12} X_1 X_2 + \beta_{13} X_1 X_3 + \beta_{23} X_2 X_3 + \beta_{11} X_1^2 + \beta_{22} X_2^2 + \beta_{33} X_3^2 \quad (3.10)$$

Where Y is the predicted response, β_0 is the intercept constant, β_1, β_2 and β_3 are the linear coefficients, β_{12}, β_{13} and β_{23} are intersection coefficients, and β_{11}, β_{22} and β_{33} are the squared coefficients.

3.7. Biodiesel production

The palm-based biodiesel was produced in the batch type reactor of capacity 1 L. The equipments connected to the reactor were: mechanical stirrer, condenser, PID controller and the round heating coil, as seen in Fig.3.2.

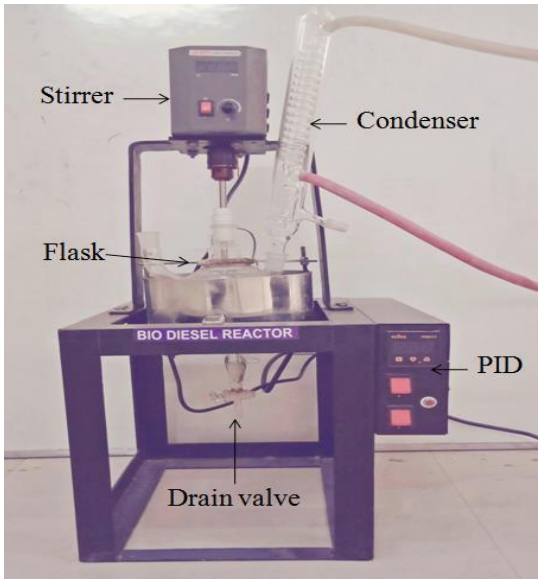

Fig. 3.2. Reactor for biodiesel production

The free fatty acid (FFA) content of palm oil has been reported in Table 3.2 (Alkabbashi et al., 2009), and it was found to be less than unity. Consequently, the single step alkaline transesterification process was chosen for biodiesel production. The reaction parameters adopted for the transesterification process were: reaction temperature (60 °C), stirring speed (250 rpm), methanol to oil molar ratio (10:1), potassium hydroxide (KOH) concentration (1.4 wt. %) and reaction time (60 min), as per reported literature (Alkabbashi et al., 2009). Palm oil was kept initially into an air-tight oven (100 °C) for 24 h in order to remove moisture content. Subsequently, 500 ml sample of moisture free oil was taken and poured into the round bottom flask of biodiesel reactor. A homogeneous solution of CH_3OH and KOH were prepared separately into another vessel. After initiating the reaction, when the oil temperature reaches to 60 °C, the solution of CH_3OH and KOH was poured into the reactor flask and the reaction mixture was stirred by continuously heating upto 60 min. Thereafter, the obtained product was allowed to settle in the separating funnel until two distinct liquid layers formed, palm oil methyl ester (POME) and denser glycerol were seen subsequently. The POME was separated, and washed several times with distilled water until the pH value reached between 6.5 and 7. The excess CH_3OH and H_2O present in POME were removed by means of rotary evaporator. Finally, the dried POME was taken into a bottle, and the different properties were determined as per ASTM standards.

Table 3.2 Palm oil fatty acid composition (Alkabbashi et al., 2009)

Fatty acid name	Structure	wt. %
Oleic	18:1	36.9
Myristic	14:0	1.23
Stearic	18:0	4.22
Palmitic	16:0	48
Palmitoleic	16:1	0.05
Linoleic	18:2	9.1
Arachidic	20:0	0.3
Linolenic	18:3	0.25

3.8. Engine test rig

The engine test rig used in the present investigation was: Kirloskar TV 1, single cylinder, 4-stroke, direct injection (DI), water cooled, constant speed (1500 rpm) and variable compression ratio (VCR) dual fuel CI engine with rated power output (3.5 kW). The schematically representation of the engine test rig used is represented in Fig.3.3. Depending upon the availability of fuels, it can be switched to either dual fuel mode or single fuel mode (Diesel). Fumigation technique was employed for injecting gaseous fuel (HEB) into the air manifold of the engine cylinder. The equipments coupled to the engine test rig were: eddy current dynamometer, electrical tachometer, load sensor, and switches. The engine was loaded accordingly at variable rates using eddy current dynamometer with the help of electromagnetic force. Moreover, the cylinder block arrangement was used to change compression ratio (CR) of the engine cylinder. Calibrated digital thermocouples (K type) were used to monitor temperatures of engine oil, exhaust, and intake air. HEB was kept in a high-pressure cylinder of 47 L capacity. A two-stage pressure regulator was used to reduce high (200 bar) pressure to 1.5 bar.HEB mass stream rate was controlled by means of mass flow controller (Alicat make), while Diesel flow rate estimation using calibrated burette (vol.) and stopwatch. In HEB pipeline the gas filter and non-return value were mounted in series, and the hose of pipe was connected to the intake air manifold of the engine cylinder. The HEB passes through the mass flow controller and flame trap before being injected into the engine cylinder. The geometry specifications of CI engine test rig are tabulated in Table 3.3.

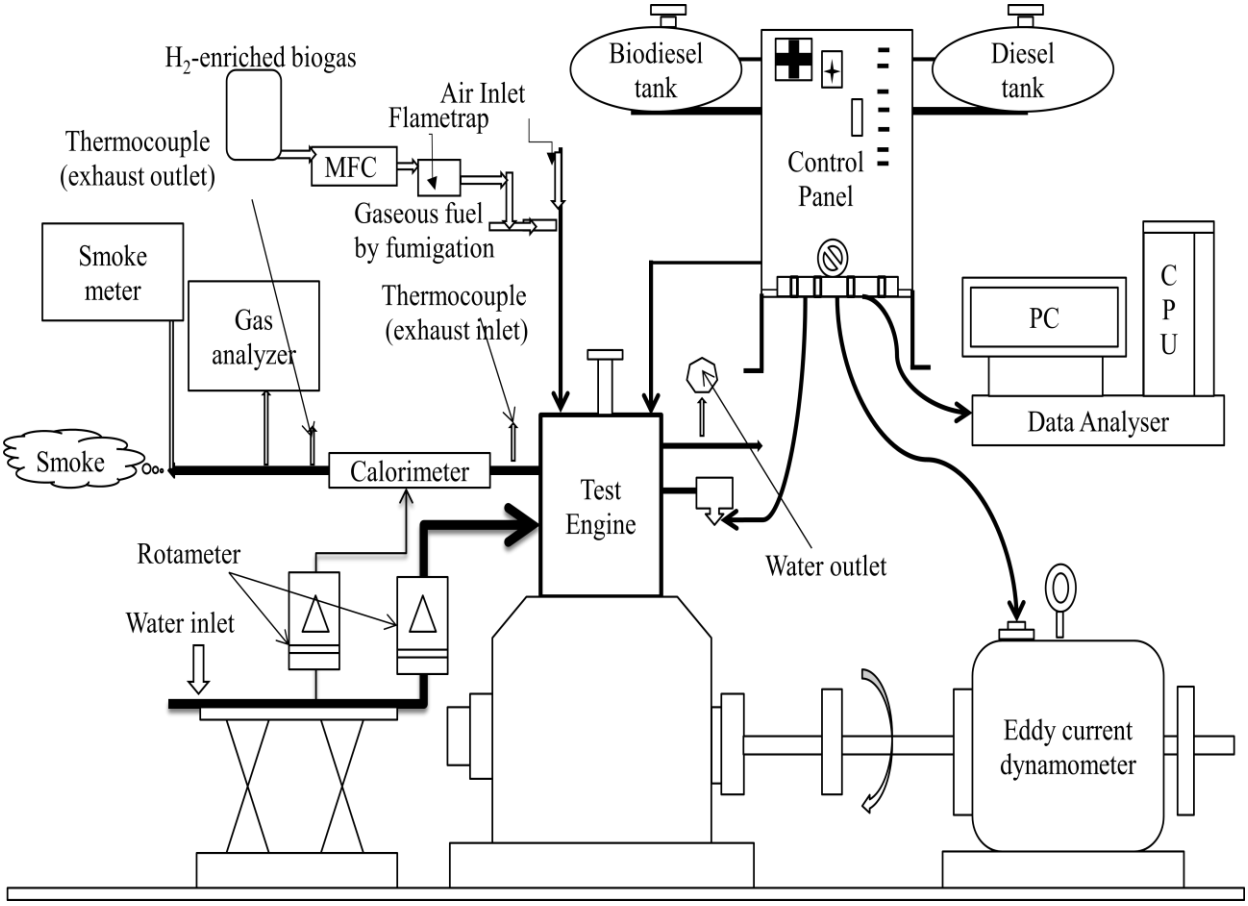

Fig. 3.3. Schematic layout of the CI engine test rig

Table 3.3 Technical specifications of CI engine test rig

Parameter	Description
Type	3.5 kW Single cylinder, DI, VCR engine
Make and model	Kirloskar TV 1
Rated speed (rpm)	1500
Stroke length, (mm)	110
Bore (mm)	87.5
Swept volume (cc)	661
Method of cooling	Water cooled
Compression ratio	12:1-18:1
Injection pressure (kg/cm^2)	200
Injection timing (bTDC)	23°
Air box	Mild steel fabricated with U-tube manometer and orifice meter

3.9. Experimental procedure

Experimental study was carried out by varying brake mean effective pressure (bmep) in the range between 0 and 3.5 bar, at rated engine speed (1500 rpm). Before experimentation, the engine was regulated as per the catalogue values. Using respective rotameters, the water flow rate for engine was kept at 250 LPH and 150 LPH for calorimeter. Engine was started initially with pure diesel at no load conditions and warmed up continuously till the oil and cooling water temperatures reach to nearly constant value, which took almost 25-30 minutes. The combustion analysis was examined based on the average of 100 consecutive cycles, with sampling rate of 1°CA. Before being analyzed the tailpipe emissions of engine, the gas analyzer was calibrated using standard gases in order to ensure accuracy of measure values. Meanwhile, the smoke meter readable was adjusted at zero before recording of each measurement. The performance and emission characteristics have been evaluated, along with detail analysis of combustion characteristics. The combustion analysis comprises ignition delay (ID), peak cylinder pressure (PCP), cylinder pressure (CP), and net heat release rate (NHRR). Moreover, the engine performance parameters viz., brake thermal efficiency (BTE), brake specific fuel consumption (BSFC), brake specific energy consumption (BSEC) and exhaust gas temperature (EGT) were also studied. Subsequently, the comparison of different emissions with respect to single and dual fuel modes was made in terms hydrocarbon emission (HC), oxides of nitrogen (NOx), carbon monoxide (CO) and smoke opacity. AVL 437c was used for the measurement of smoke opacity and for tailpipe emissions (AVL 444 digas analyzer). The noise level was measured by Testo 816. The general specifications of the gas analyzer and smoke meter are tabulated in Table 3.4 and 3.5, respectively. The AVL 437c measures the opacity of contaminated air in particular of CI exhaust emissions. A measuring chamber of a defined measuring length and non-reflective surface is filled homogeneously with exhaust gas. The light attenuation caused by the exhaust gas particles trapped between a light source and a receiver ("opacity" in %) is measured. The specific absorption of the exhaust gas ("k", in m^{-1}) is calculated based on the opacity. The calculation is based on the Beer-Lambert law.

Preliminary test runs were carried out at engine CR of 17:1 and 17:5 with pure diesel. Therefore, 17:1 CR was chosen for pure diesel in order to generate baseline data for comparison with B20 at different CRs. The higher CRs (16:1 to 18:1) close to standard CR were adopted in order to examine the effect of VCR. The comparison of results was made between pure diesel at 17:1 CR and B20 over CRs of 16:1, 17:1 and 18:1. Further, the engine

was also operated on dual fuel modes and performed different sets of experiments subsequently. It is also inferred from the previous literature that the gaseous fuels combusted well at higher CR engines (Karim et al., 1980). Consequently, the standard CR (17:5) was taken to obtain high in-cylinder pressure and temperature; moreover, for the comparative analysis of single and dual fuel modes. Initially, study was done initially with diesel (single fuel mode), and then, HEB was injected in the ranges between 0.1 and 0.5 kg/h. Thereafter, the most effective HEB flow rate was chosen to investigate the effect of variable compression ratio (16:1, 17:1 and 18:1) on the different engine characteristics including combustion, performance and emissions. Moreover, the same set of experimentation was replicated for B20 fuel, as like in diesel under duel fuel mode.

Various engine performance parameters with respect to single and dual fuel modes were determined, using Eqs. (3.11) to (3.14).

$$BTE_{diesel}(\%) = \frac{BP \times 3600}{m_{diesel} \times LCV} \times 100 \tag{3.11}$$

$$BTE_{dual}(\%) = \frac{BP \times 3600}{(m_{HEB} \times LCV_{HEB}) + (m_{diesel} \times LCV_{diesel})} \times 100 \tag{3.12}$$

$$BSFC_{diesel}(kg/kW\,h) = \frac{m_{diesel}}{BP} \tag{3.13}$$

$$BSEC_{dual}(MJ/kW\,h) = \frac{(m_{HEB} \times LCV_{HEB}) + (m_{diesel} \times LCV_{diesel})}{BP} \times 100 \tag{3.14}$$

Where BP is the brake power (kW), m_{diesel} and m_{HEB} are mass flow rate (kg/h) of diesel and HEB, respectively, and LCV is lower caloric value of respective fuels (KJ/kg).

Table 3.4 Specifications of AVL 444 digas exhaust gas analyzer

Parameter	Measuring range	Resolution	Accuracy
CO	0-10 vol. %	0.01 vol. %	± 0.1 vol. %
CO_2	0-20 vol. %	0.1 vol. %	± 0.3 vol. %
HC	0-20,000 ppm	1ppm	± 10 ppm
O_2	0-22 vol. %	0.01 vol. %	± 0.2 vol. %
NOx	0-5000 ppm	1ppm	± 20 ppm

Table 3.5 Specifications of AVL 437c smoke meter

Particular	Specification
Measuring range	0-100 %
Accuracy and reproducibility	± 1% full scale reading
Measurement chamber	0.430 m ± 0.005 m of effective length
Light source	Halogen bulb 12 V/ 5W
Detector	Selenium photocell diameter 45 mm Max. sensitivity in light
Maximum Smoke	Temperature at entrance (210° C)

3.10. Experiment repeatability

To ensure the repeatability and consistency of results, each set experiment was replicated thrice, and their average value was taken into consideration for calculating performance parameters.

3.11. Uncertainty analysis

It was carried out for the measured and calculated parameters of the current investigation, using sequential perturbation approach (Moffat, 1982). The results of this analysis with respect to different parameters are tabulated in Table 3.6.

Overall uncertainty=

$$\sqrt{\begin{aligned}&(\text{Fuel flow rate})^2 + (\text{Flow properties})^2 + (\text{CO})^2 + (\text{CO}_2)^2 + (\text{NO}_x)^2 + (\text{HC})^2 \\ &+(\text{Smoke opacity})^2 + (\text{Engine load})^2 + (\text{Temperature indicator})^2\end{aligned}}$$

$= \pm 1.84$

Table 3.6 Uncertainty of measured and calculated parameters

Measurement	Units	Uncertainty %age
HC	ppm	±0.2
CO	vol. %	± 0.1
NOx	ppm	±0.5
CO_2	vol. %	± 0.2
Fuel properties	-	± 1.0
Smoke opacity	vol. %	± 1.0
Engine load	-	± 0.2
Fuel flow rate	mL	± 1.0
Temperature indicator	°C	± 0.15

Chapter-4

RESULTS AND DISCUSSION

Dry reforming has potential to produce energy efficient gaseous fuel i.e. H_2-enriched biogas. When biogas is being utilized for H_2-enriched biogas production, it offers viable technology for the utilization of two main undesired greenhouse gases. Following to the materials and methodologies adopted, this chapter initially presents the outcomes of biogas reforming reactions with pure Ni nanopowder. Thereafter, the catalytic reforming outcomes in terms of different performance parameters following by characterization of various synthesized catalysts results have been discussed. It also provides the experimental observations of the utilization of HEB in CI engine under dual fuel mode.

4.1. Dry reforming of biogas with pure Ni nanoparticle

Preliminary experimental tests were carried out to evaluate the effective conditions (process temperature and feed rate) to maximize H_2 enrichment in the biogas under dry reforming.

4.1.1. Effect of reaction temperature reactant conversion and product yield

The effect of reaction temperature on the CH_4 and CO_2 conversions was studied at the temperature range of 700-900°C, as shown in Fig. 4.1 (a). CH_4 and CO_2 conversions increased with temperature initially at a slow pace up to 800°C, beyond which the conversions rose quickly and attained the maximum value of 77.1 and 94.8% for CH_4 and CO_2, respectively, at 900°C. As, the dry reforming is an endothermic reaction (Eq.4.1) so higher conversions are favored at elevated temperatures. CO_2 conversions were found to be higher when compared to CH_4 conversions throughout the temperature range. This may be attributed to the preferable dissociation of CO_2 and CH_4 decomposition over the catalyst (Kodama et al., 2003). H_2 and CO yield increased with temperature, as seen in Fig. 4.1(b). At 800°C, the difference between H_2 and CO yields increased, which may be due to the occurrence of reverse water gas shift (RWGS) reaction (Eq.2.2) that consumes H_2 in the reforming and produce more CO (Barelli et al., 2014). Further, at 900°C, the effect of RWGS reaction has been minimized, which is in agreement with reported literature (Djinovic

et al., 2012). H_2/CO ratio remained less than unity throughout the dry reforming, as shown in Fig. 4.1(c). Interestingly, the H_2/CO ratio decreased with increased temperature up to 800°C which was due to the reduction in H_2 yield in comparison to CO. Thereafter, the H_2/CO ratio increased and approaches to unity at 900°C. This enhanced H_2/CO ratio at a higher temperature might be due to the predominant CH_4 cracking reaction, especially at 900°C, which favored the production of more H_2 (Eq. 2.3).

$$0.6\,CH_4 + 0.4\,CO_2 \rightarrow 0.8\,H_2 + 0.8\,CO + 0.2\,CH_4 \quad \Delta H = 98.9\ \text{kJ/mol} \qquad (4.1)$$

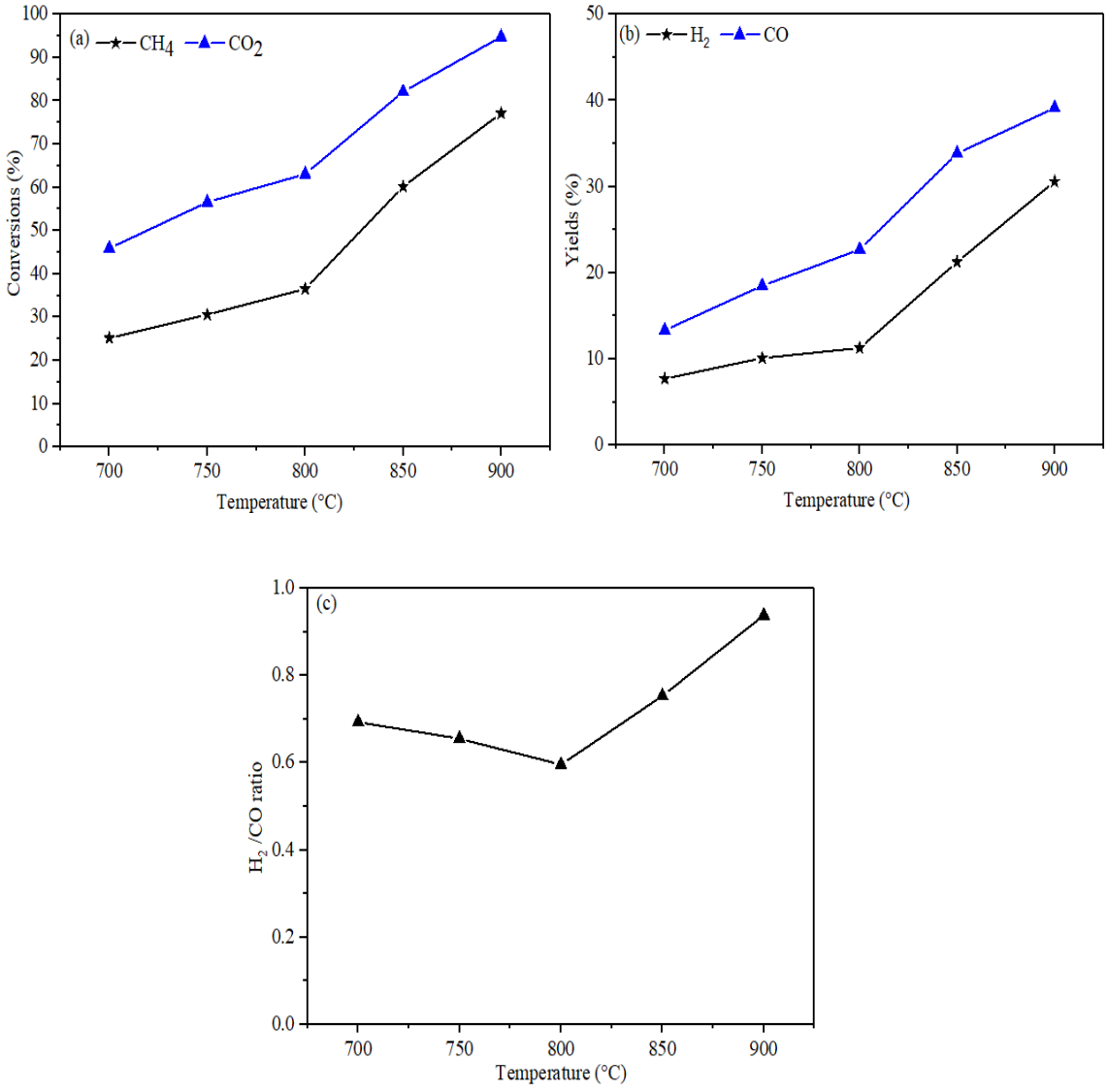

Fig.4.1. Effect of reaction temperatures on (a) CH_4 and CO_2 conversions; (b) H_2 and CO yields; (c) H_2/CO ratio in the dry conditions at WHSV of 20,000 NmL g^{-1} h^{-1}

4.1.2. Effect of WHSV on CH_4 conversion, CO and H_2 yields

Previous results ascertained that the dry reforming reactions performed well at higher temperature ranges; consequently, 900 °C temperature was chosen to study the influence of WHSV, because H_2 yield of 30.6% was obtained in HEB at 900°C. WHSV was varied from 20,000 to 60,000 NmL g^{-1} h^{-1} to access its impact on catalytic performance regarding CH_4 conversion and products (H_2 and CO) yields. Higher CH_4 conversions and product yields were obtained with WHSV of 20,000 NmL g^{-1} h^{-1} (Fig. 4.2), which is may be due to the higher residence time of reactants inside the reactor vessel. CH_4 conversion and products yields were consequently decreased as the WHSV was increased from 20,000 to 60,000 NmL g^{-1} h^{-1}. This suggests that higher WHSV decreases selectivity of H_2 and CO.

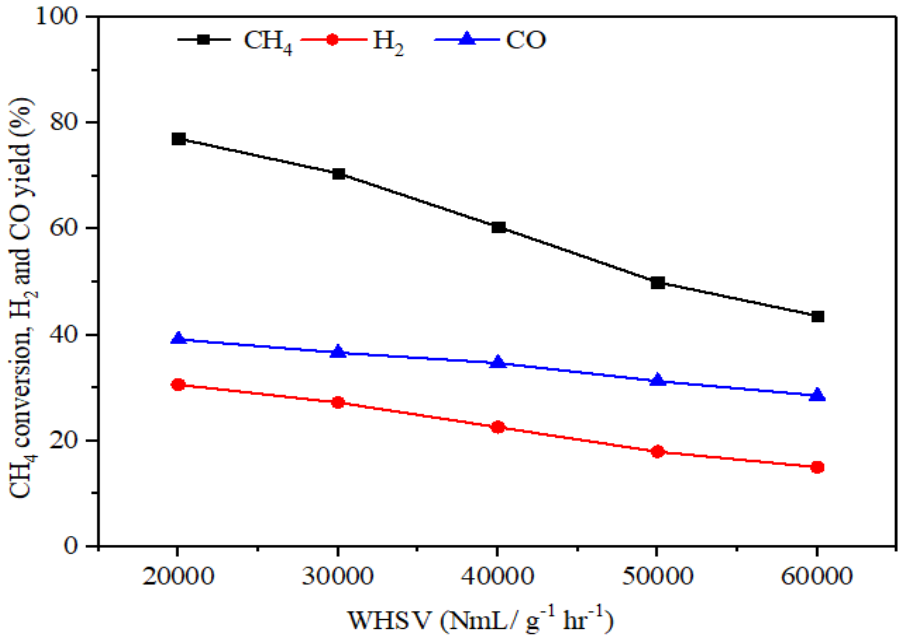

Fig.4.2. Effect of WHSV on CH_4 conversion, CO and H_2 yields

4.2. Dry oxidative reforming of biogas with pure Ni nanoparticle

It has been observed that biogas dry reforming reactions favoured at high temperature and low WHSV. High operating temperatures make the reforming process highly energy intensive, so O_2 was introduced during the reforming to initiate exothermic reactions to reduce the energy requirement in the reforming process.

4.2.1. Effect on CH_4 and CO_2 conversions

Fig.4.3 (a) & (b) portray the reaction temperature effects on CH_4 and CO_2 conversions, respectively, at WHSV (40,000NmL g^{-1} h^{-1}), under dry oxidative reforming. CH_4 conversion increased with the increase of temperature up to 750°C and thereafter, a steady decreased was observed at 800°C. This decrement in CH_4 conversion was due to the reverse partial oxidation reaction (Eq. 2.16), since the exothermicity of above reaction decreased with rising temperature, the equilibrium shifted to the left (Chen et al.,2015). At higher temperature (>800°C), CH_4conversion significantly improved because, in dry oxidative reforming, dry CO_2 reforming become predominated reaction (Eq. 4.1) at elevated temperature, hence, CH_4conversion remained high (Enger et al, 2008). Meanwhile, the CH_4 conversion enhanced and reached a maximum of 80.8% at 900°C when O_2/CH_4 ratio of 0.17 was used, implying that the O_2 has a positive effect on the conversion. At higher temperature (≥800°C), with O_2/CH_4 ratio (>0.17) reduced CH_4 conversion, because higher O_2/CH_4 ratio leads to complete combustion of CH_4 (Eq. 2.17), and results to CO_2formation thus reducing H_2 yield. These observations are in confirmation of the thermodynamic simulation study which reported the optimal O_2/CH_4 ratio between 0.10-0.20 at a given temperature ranges (Amin et al., 2007). On the contrary, CO_2 conversion decreased under all O_2/CH_4 ratios because of complete or partial combustion of CH_4 by reacting with O_2 (Yang at al., 2018).

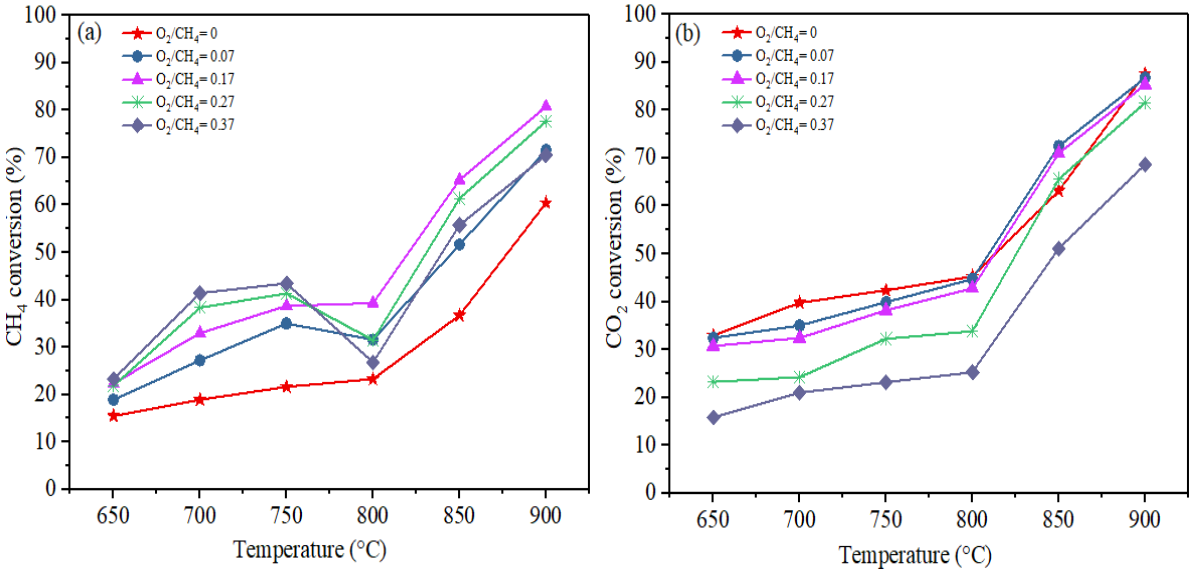

Fig.4.3. Effect of reaction temperature and O_2/CH_4 ratio on (a) CH_4 conversions; (b) CO_2 conversions in dry oxidative reforming

Moreover, combustion of CH_4 formed an additional amount of CO_2 which increased the CO_2 in the exit gas. Likewise, at 700°C and O_2/CH_4 of 0.37, the CO_2 formation increased to 31.6% from 25.9% when compared to 0.07 O_2/CH_4. The results revealed that the dry oxidative reforming has substantial effects on both reactant conversions, and the findings are in good agreement with the reported work (Ruckenstein et al., 2001).

4.2.2. Effect on H_2 and CO yields

Fig.4.4 (a) & (b) show the yields of H_2 and CO during the reforming with or without oxygen additions at the temperature ranging from 650 to 900°C. Again, the H_2 yield follows the same trend as that of CH_4 conversion with respect to reaction temperature. At 800°C, H_2 yield decreased and then suddenly increased at higher temperatures because of the decrement and increment in CH_4 conversions, as discussed earlier. Compared to O_2 free reforming (i.e. $O_2/CH_4 = 0$), the presence of O_2 consequently increased the H_2 yield and attained a maximum value of 29.9% with O_2/CH_4 ratio of 0.17 at 900°C. Moreover, H_2 yield decreased with the increase of O_2/CH_4 ratio value greater than 0.17, especially at a higher temperature (≥800°C). This effect was attributed to the reason that at a high ratio of O_2/CH_4 both RWGS reaction (Eq. 2.2) and CO_2 reforming (Eq.4.1) are endothermic (Mattos at al., 2003). Increase in temperature favored above reactions, but, the RWGS reaction rate increased due to the increase in CO_2 and a decrease in CH_4 at higher temperature.

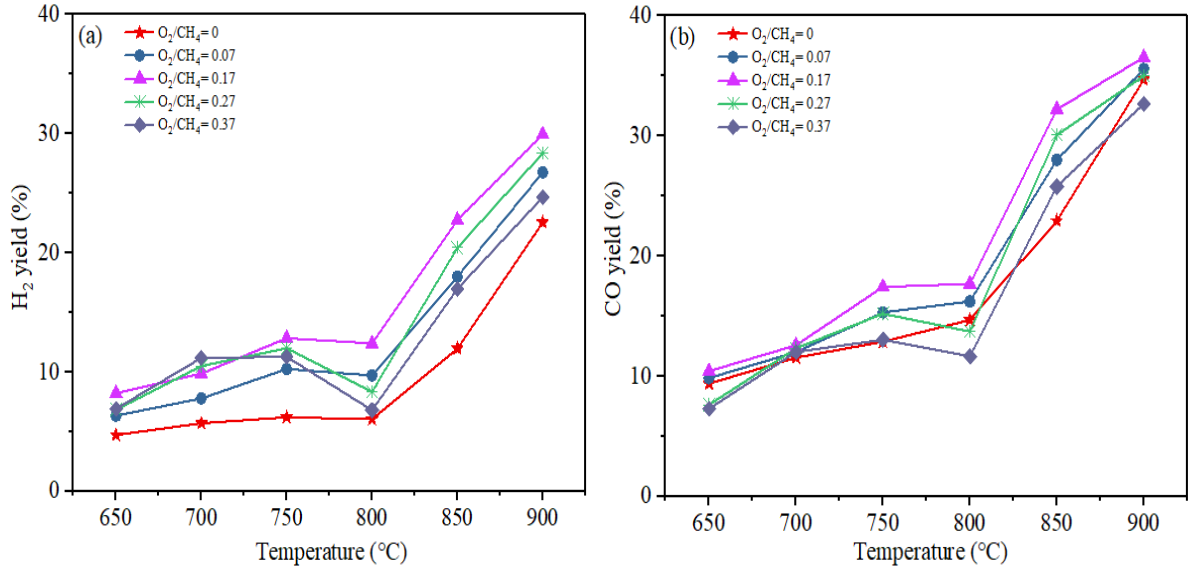

Fig.4.4. Effect of reaction temperature and O_2/CH_4 ratio on (a) H_2 yield; (b) CO yield in dry oxidative reforming at WHSV 40,000 NmL g^{-1} $h^{-1}$and 0.17 O_2/CH_4

These results indicate that the larger O_2/CH_4 ratio is not favorable for H_2 enrichment, due to the increase in CO_2 formation. On the contrary, CO yield increased with increasing temperature, but it remains altered with respect to temperature and O_2/CH_4 ratio. This effect was attributed to additional CO_2 formation while inducting O_2 into gas mixture during reforming. Interestingly, at 900°C, higher CO yield values when compared to H_2 yields are the clear indication of dry reforming because H_2/CO ratio value remained less than unity, as mentioned in Eq. 4.1.

4.2.3. Effect on H_2/CO ratio

Fig.4.5 illustrates the effect of adding a different proportion of O_2 on H_2/CO product ratio. It has been observed that adding O_2 results higher H_2/CO ratio throughout the temperature ranges when compared to O_2 free reforming. More than unity value of H_2/CO ratio was achieved using O_2/CH_4 ≤0.27 at 650 and 700°C, which further decreased with increasing temperature due to the predominance of endothermic at higher temperature (Nematollahi et al., 2012).The H_2/CO ratio value approaches to minimal with increasing temperature (up to 800°C), thereafter, increased to 0.98 with O_2/CH_4 ratio of 0.17 at 900°C. This result confirmed that, at 800°C, H_2/CO ratio was influenced by RWGS reaction (Eq. 2.2), as also reported in the literature (Souza et al., 2003). At higher temperatures (≥800°C), H_2/CO ratio value was less than unity under all O_2/CH_4 ratios confirmed dry reforming (Eq. 4.1) is predominant at higher temperature.

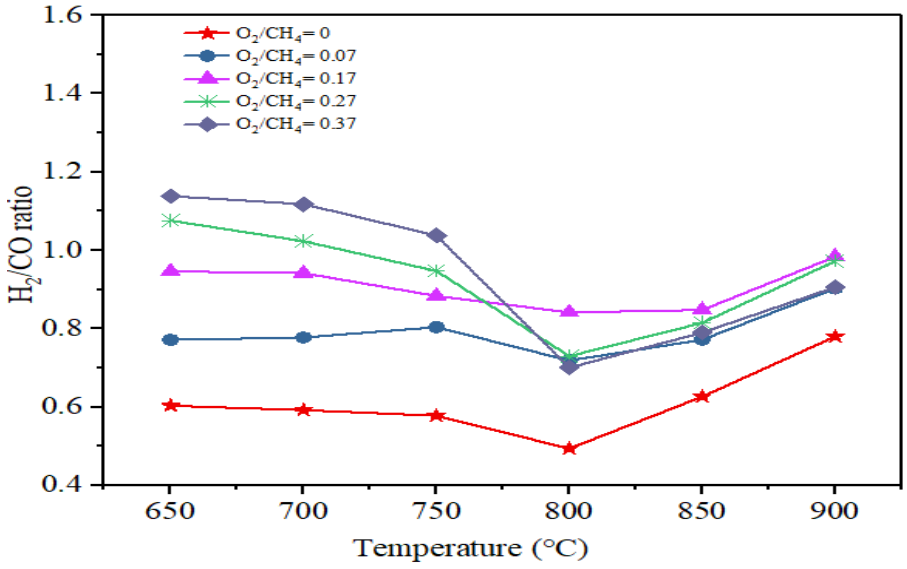

Fig.4.5. Effect of reaction temperature and O_2/CH_4 ratio on H_2/CO ratio in dry oxidative reforming at WHSV 40,000 NmL g^{-1} $h^{-1}$and 0.17 O_2/CH_4

4.2.4. Concentration of reagents and products

Variations in the product selectivity were observed by varying the reaction temperature while keeping the molar ratio of reactants constant. The concentration of reagents and products profile as shown in Fig. 4.6 indicate that, the H_2 enrichment of 35.9% was achieved at 900°C with WHSV and O_2/CH_4 of 40,000 NmL g^{-1} h^{-1} and 0.17, respectively. At all temperature ranges, the H_2 production remained lower than CO due to lower apparent activation energy barrier for CO formation than that for H_2 and it becomes 0.98 H_2/CO ratio at 900°C (Bradford et al., 1996). This plot also confirmed that CH_4 combustion occurred to a larger extent at lower temperature ranges, which prompts high CO_2 formation, bringing about a high concentration of CO_2 in exit gas.

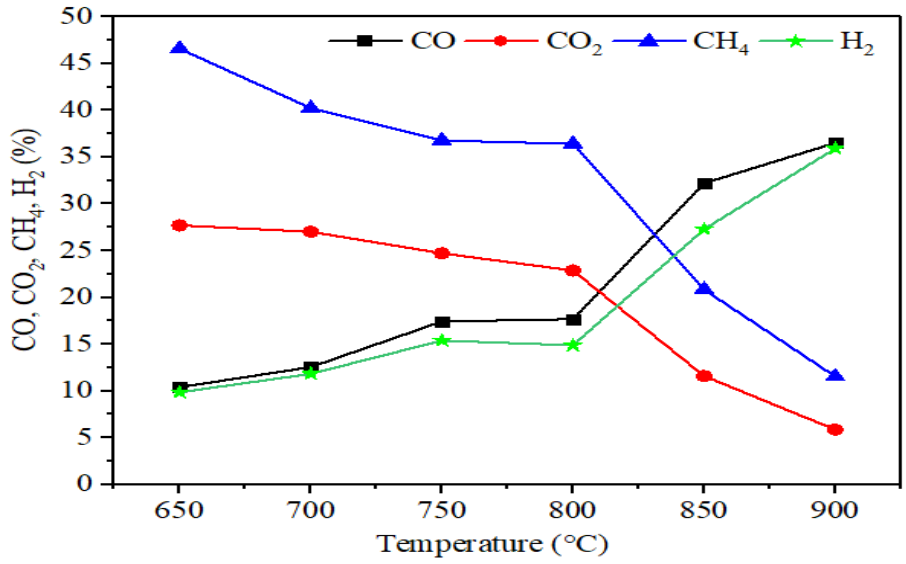

Fig.4.6. Effect of reaction temperature and O_2/CH_4 ratio on concentration of reagents and products profile in dry oxidative reforming at WHSV 40,000 NmL g^{-1} $h^{-1}$and 0.17 O_2/CH_4

4.2.5. Specific energy consumption (SEC)

Fig.4.7 shows the variation in SEC (kJ/NmL-H_2) as a function of temperature for both dry and dry oxidative reforming. It has been observed that the energy share is strongly dependent on the O_2/CH_4 ratio, as well as, the reaction temperature. For instance, at 650°C, the SEC was found to be 26.0 under O_2 free reforming (O_2/CH_4=0), while, oxygen addition with 0.17 O_2/CH_4 ratio, reduced the SEC to 15.2, giving a saving of approximately 41.3%. At higher O_2/CH_4 ratio of 0.37, the SEC steadily increased to 18.3 under the same temperature of 650°C, because the O_2 enriched reforming conditions provided complete combustion of methane produced CO_2 instead of H_2. At 900°C, SEC of 7.3 was observed, which is 71.6%

less compared to O_2 free reforming at 650°C. At 800°C, SEC suddenly increased due to the reduction in H_2 yield. Hence, SEC reduced under low temperatures and high O_2/CH_4 ratios during the reforming process.

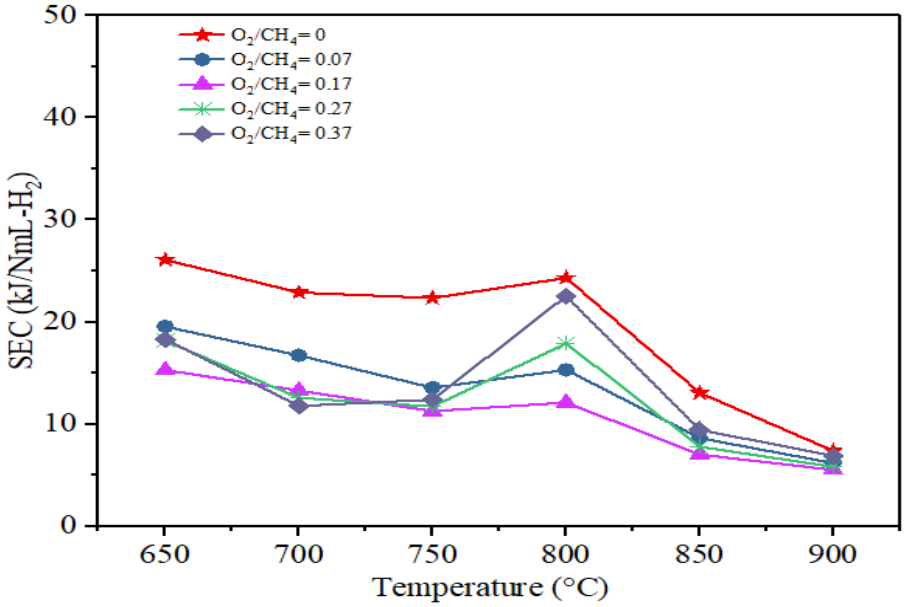

Fig.4.7. Variation in SEC versus reaction temperature in biogas reforming

4.2.6. Stability and carbon deposition tests

Short time stability and carbon deposition tests were performed over pure Ni nanoparticle at the reaction temperature (900°C) and WHSV (20,000 NmL g^{-1} h^{-1}) for dry reforming reaction, while for dry oxidative reforming (40,000 NmL g^{-1} h^{-1}) i.e., under the condition where CH_4 conversion and H_2 enrichment were maximum. Fig. 4.8 illustrates the reactant (CH_4 and CO_2) conversions and product (H_2 and CO) yields of Ni catalyst over 18h of continuous reaction stream for dry reforming. H_2 enrichment of 39.9% with 86.7 and 98.5% CH_4 and CO_2 conversions, respectively, were obtained after 2h of reaction. Thereafter, a small drop (2-3%) in CH_4 and CO_2 conversions was identified over 5h of the reaction period. This reduction indicates that the coke formation starts over the catalyst surface, which reduces the active metal sites as well as blocks the catalyst pores. However, H_2/CO ratio (~0.96) was almost identical over 18h of reaction. Nevertheless, no significant changes in the H_2 and CO formations were observed which indicated the negligible catalyst deactivation. Carbon deposition of 42.7 wt. % was assessed after 18h of the reactant stream. Whereas, in dry oxidative reforming, maximum CH_4 conversion of (80.8%) was observed with 35.9% of H_2 enrichment in biogas after 2h of reaction stream. Thereafter, the catalyst started deactivating

which may be due to oxidation of Ni metal particles. Further; it also indicates that O_2 content leads to oxidize metal particle consequently. The Ni metal deactivated completely after 6h of continuous reaction, and H_2 enrichment reduces to 3.3 %.

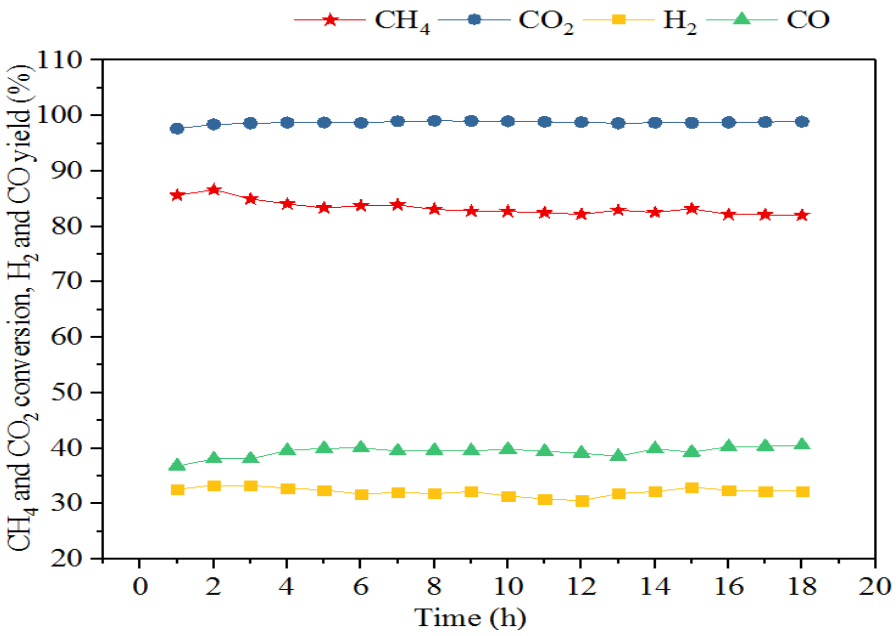

Fig.4.8. Stability test in the dry reforming over Ni at 900°C

4.3. Parametric optimization for H_2 enrichment using response surface methodology

The experiments were conducted to evaluate the influence dry oxidative reforming process parameters on the H_2-enriched biogas production. The 15 experiments run were carried out for optimizing the three independent variables (reaction temperature: X_1, CH_4/CO_2: $X_2$and O_2/CH_4 ratio: X_3). The experimental design and results regards to exit gas concentration, reactants conversion, product selectivity, yield as well as H_2/CO ratio and SEC, are summarized in Table 4.1.

4.3.1. Effect of reaction parameters on dry oxidative reforming of biogas

The results obtained from the dry oxidative reforming of biogas proved that H_2 production significantly increased with increasing all three independent variables. The maximum H_2 enrichment of biogas was found to be 38.7% at conditions of 900°C; 1.5 and 0.1 of CH_4/CO_2 and O_2/CH_4 ratios, respectively. Notable, this enrichment was achieved at 0.1 O_2/CH_4, which is 39.1% less than requires for stoichiometry of the reaction. At 900°C, the increased CH_4/CO_2 and O_2/CH_4 ratios to 2.0 and 0.30, respectively, consequently decreased the reactant

(CH_4 and CO_2) conversions and H_2 production, while a negligible effect on product yield and H_2/CO ratio was observed. It was further examined that, under all experimental tests, the 100 % O_2 conversion was observed, while CO_2 conversion was found to be continuously decreasing upon increasing the O_2/CH_4 ratio as a result of the oxidation of CO to CO_2 with added O_2 (Enger et al., 2008; Liu et al., 2009).

Further, CH_4 combustion occurred to a larger extent at lower temperature ranges, which may be explained on the basis of high CO_2 product selectivity with a higher H_2O production. Meanwhile, the H_2/CO ratio steps up with rising temperature from 800 to 900°C, while under same temperature conditions, the H_2/CO ratio does not show a significant effect relative to CH_4/CO_2 ratios. Djinovic et al., (2012) used the CH_4/CO_2 ratio (>1) and reaction temperature (≥800°C) to minimize the effect of the reverse water gas shift (RWGS) reaction (Eq. 2.2).On the contrary, reduction in the SEC per NmL of H_2 produced was observed corresponding to increasing all of independent variables. Likewise, at 900°C temperature, 1.0 CH_4/CO_2 ratio, and 0.20 O_2/CH_4 ratio, the SEC reduced to 8.45 kJ/NmL of H_2 when compared to 800°C under same reactant conditions. Additionally, this decrement in SEC is because of the increase in H_2 production at same operating conditions.

4.3.2. Statistical Analysis

The regression correlation analysis was performed to correlate dependent and independent variables. Table 4.2 summarizes the experimental matrix that includes three independent factors and the responses based on 15 experimental runs, and finally, the fitted second order polynomial equations for responses, such as products (CO and H_2), reactants conversion (CH_4 and CO_2), H_2/CO ratio, and SEC, were obtained. The positive correlation coefficient represents an increment of a process variable followed by an increase of another variable. On the contrary, if a given increment of a process variable is followed by a decrement of another variable, it indicates a negative correlation coefficient.

From ANOVA (Table 4.3), the response surface quadratic models were formulated for each dependent variable individually. Strategically, if the model *p*-value is <0.05, it indicates that the model terms are significant. Likewise, in the case of CH_4 conversion, the intercept constant, X_1, X_2, X_3, X_1^2 and X_2^2 are significant model terms because they all have a *p*-value less than 0.05. These significant terms suggests that there is a mutual effect between independent variables. Meanwhile, the proportion of O_2/CH_4 ratio (X_2) shows the highest influence on the statistical model with a 673 coefficient value when compared to the reaction

temperature (X_1) and CH_4/CO_2 ratio (X_3), with the coefficient values of 4.90 and 136.3, respectively. Noteworthy, the O_2/CH_4 ratio has a negative influence on the model. The adequacy of a model fit was tested by lack of fit results, whereas the F value for lack of fit shows no statistical significant because the *p*-value is >0.05, and the empirical model could be used for the prediction, because of the insignificant lack of fit. Similarly, Table 4.3 shows significance of the model terms for selective dependent variables.

Apart from that, the goodness of the empirical model was explained by adjusted R^2 values. The adjusted R^2 rises only with the addition of independent factors that are more significant to the dependent factor, and if the non-significant factors are added to the model, the value of adjusted R^2 will significantly decrease. As shown in the Table 4.4, the adjusted R^2 values of CO, H_2, CH_4, and CO_2 conversion were determined as 97.0, 95.89, 98.61, and 94.75, respectively, indicating that only 3.0, 4.11, 1.39, and 5.25% of the total variation in the model was not demonstrated by the input factors. It has been examined that an excellent fit was achieved for all responses, except the H_2/CO ratio, which are further validated by comparing experimental and predicted values (Table 4.2). The predicted and experimental values of CH_4 conversion using equation 4.2 are depicted in Fig. 4.9. From the plot, a more accurate description of the experimental data was examined, becauuse all the distributed points are very close to the line of fit. In addition, the R^2 value of 0.955 indicates a very good agreement good between the predicted values and experimental data mash points.

$$Y_{CH_4} = -2256 + 4.905X_1 + 136.3X_2 - 673X_3 - 0.0720X_1X_2 + 0.565X_1X_3 - 1.5X_2X_3 - 0.002619X_1^2 - 20.22X_2^2 + 282X_3^2 \quad (4.2)$$

The 3D representation of the response surface plot for CH_4 conversion is given in Fig. 4.10. The positive value of process temperature (X_1) and CH_4/CO_2 ratio (X_2) in equation 4.2 reveals that higher the process temperature and CH_4/CO_2 ratio, the higher CH_4 conversion, whereas a negative value of the O_2/CH_4 ratio (X_3) indicates a decline in the O_2/CH_4 ratio leads to a rise in CH_4 conversion. The results showed that CH_4 conversion increased significantly with an increase of process temperature from 800 to 900°C at a constant CH_4/CO_2ratio. However, at higher temperature (900°C), an increase in the O_2/CH_4 ratio from 0.10 to 0.30 significantly decreased the CH_4 conversion. From further analysis of surface response plots, it can be observed that temperature, CH_4/CO_2 ratio, and O_2/CH_4 ratio play a dominant role in CH_4 conversion.

Table 4.1 Experimental data for 3-level-3-factor response surface analysis

DOE			Temp. (°C)	CH_4:CO_2	O_2:CH_4	Product				Conversion		Selectivity		Yield		H_2:CO	SEC
A	B	C	X_1	X_2	X_3	CO	CO_2	CH_4	H_2	CH_4	CO_2	H_2	CO	H_2	CO		
-1	-1	0	800	1	0.2	16.34	25.84	38.68	10.03	14.9	43.2	74.03	61.92	11	18	0.61	23.73
0	0	0	800	1.5	0.2	19.95	25.92	37.72	9.94	29.6	27.4	31.35	77.79	9.3	22.3	0.5	24.64
0	1	-1	850	2	0.1	35.15	8.82	17.08	30.7	72.7	71.8	33.8	51.81	24.6	37.5	0.87	8.31
-1	0	-1	800	1.5	0.1	19.64	20.85	30.27	17.34	46.5	44.7	32.92	45.44	15.3	20.8	0.88	13.3
-1	1	0	800	2	0.2	17.49	22.12	38.94	12.44	33.8	24.8	31.28	64.36	10.6	19.8	0.71	19.15
0	-1	1	850	1	0.3	28.1	15.52	24.78	22.36	43	64.3	59.79	60.23	25.7	32.3	0.8	11.29
0	0	0	850	1.5	0.2	31.7	10.5	20.53	28.36	61.7	70.6	42.92	54.42	26.5	35.5	0.89	8.93
1	0	-1	900	1.5	0.1	38.04	3.47	9.7	38.71	82.9	90.8	41.27	46.86	34.2	40.3	1.02	6.84
1	-1	0	900	1	0.2	34.7	8.95	14.89	31.34	67.2	80.3	51.27	51.74	34.5	38.2	0.9	8.45
0	0	0	850	1.5	0.2	30.16	12.07	21.88	26.64	59.2	66.2	42.03	54.5	24.9	33.8	0.88	9.48
1	0	1	900	1.5	0.3	34.44	8.61	14.1	34.21	72.3	74.6	46.55	55.52	33.6	40.6	0.99	7.87
-1	0	1	800	1.5	0.3	13.55	24.5	38.32	12.03	24.6	27.7	48.01	61.8	11.8	16	0.89	19.24
0	1	1	850	2	0.3	26.92	17.77	24.49	21.96	55.9	36	35.34	65.54	19.8	32.3	0.82	11.55
0	-1	-1	850	1	0.1	32.74	16.02	19.3	21.39	59.5	66.4	37.77	54.64	22.5	34.4	0.65	11.63
1	1	0	900	2	0.2	36.04	7.77	12.44	34.59	78.9	73.6	37.29	52.98	29.4	40.8	0.96	7.74

Table 4.2 DOE and responses for dry oxidative reforming of biogas

DOE			CO		H_2		CH_4 conversion		CO_2 conversion		H_2:CO		SEC	
A	**B**	**C**	**Exp.**	**Predicted**	**Exp.**	**Predicted**	**Exp.**	**Predicted**	**Exp.**	**Predicted**	**Exp.**	**Predicted**	**Exp.**	**Predicted**
-1	-1	0	16.34	16.74	10.03	8.79	14.90	16.83	43.20	39.94	0.61	0.58	23.73	23.48
0	0	0	19.95	17.80	9.94	13.22	29.60	30.77	27.40	35.81	0.50	0.72	24.64	20.10
0	1	-1	35.15	34.64	30.70	30.96	72.70	73.31	71.80	71.99	0.87	0.90	8.31	6.95
-1	0	-1	19.64	20.87	17.34	16.28	46.50	44.64	44.70	44.07	0.88	0.77	13.30	16.05
-1	1	0	17.49	17.57	12.44	12.01	33.80	34.61	24.80	22.09	0.71	0.70	19.15	19.46
0	-1	1	28.10	28.07	22.36	22.92	43.00	42.68	64.30	66.21	0.80	0.82	11.29	11.51
0	0	0	31.70	31.47	28.36	26.68	61.70	60.16	70.60	66.30	0.89	0.83	8.93	10.34
1	0	-1	38.04	38.14	38.71	38.44	82.90	84.66	90.80	90.50	1.02	1.04	6.84	6.24
1	-1	0	34.70	35.16	31.34	30.95	67.20	66.10	80.30	80.91	0.90	0.85	8.45	9.28
0	0	0	30.16	31.47	26.64	26.68	59.20	60.16	66.20	66.30	0.88	0.83	9.48	10.34
1	0	1	34.44	33.75	34.21	34.45	72.30	73.86	74.60	73.13	0.99	1.04	7.87	6.25
-1	0	1	13.55	13.99	12.03	11.48	24.60	22.54	27.70	25.90	0.89	0.81	19.24	20.97
0	1	1	26.92	27.21	21.96	21.71	55.90	56.71	36.00	37.36	0.82	0.82	11.55	11.21
0	-1	-1	32.74	31.92	21.39	22.46	59.50	58.98	66.40	67.14	0.65	0.70	11.63	10.83
1	1	0	36.04	36.18	34.59	35.01	78.90	76.68	73.60	74.76	0.96	0.93	7.74	9.13

Table 4.3 ANOVA for response surface quadratic model of CH_4 conversion

Source	Sum of square	DOF	Mean square	F-Value	P-Value
Model	5974.67	9	663.852	111.28	0.000
X_1	166.54	1	166.537	27.92	0.003
X_2	55.49	1	55.487	9.30	0.028
X_3	57.14	1	57.173	9.58	0.027
X_1X_2	12.96	1	12.960	2.17	0.201
X_1X_3	31.92	1	31.922	5.35	0.069
X_2X_3	0.02	1	0.022	0.00	0.953
X_1^2	138.42	1	138.423	23.20	0.005
X_2^2	88.71	1	88.709	14.87	0.012
X_3^2	27.61	1	27.610	4.63	0.084
Residual	29.83	5	5.966	-	-
Lack of fit	26.70	4	6.676	2.14	0.469
Pure error	3.13	1	3.125	-	-
Significant at $p < 0.05$, Not significant at $p > 0.05$.					

Table 4.4 Coefficients of significant terms for dependent variables

Coefficients	CO	H_2	Conversion		H_2:CO	SEC
			CH_4	CO_2		
Constant	-1386	-	-2256	-2282	-	-
X_1	3.159	-	4.905	5.10	-	-
X_2	-	-	136.3	-	-	-
X_3	-	-	-673	-	-	-
X_1X_2	-0.001766	-	-	-	-	-
X_1X_3	-	-	-	-	-	-
X_2X_3	-	-	-	-1.5	-	-
X_1^2	-	-	-0.002619	-0.002619	-	-
X_2^2	-	-11.28	-20.22	-	-	-
X_3^2	-	-	-	-	-	-
R-Sq(Adj.)	97.00%	95.89%	98.61%	94.75%	20.01%	76.18%

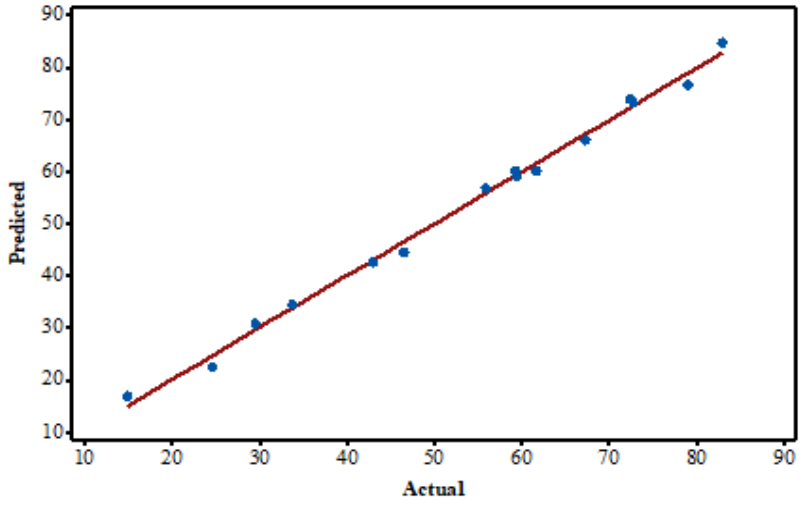

Fig.4.9. Predicted vs. actual value of CH_4 conversion

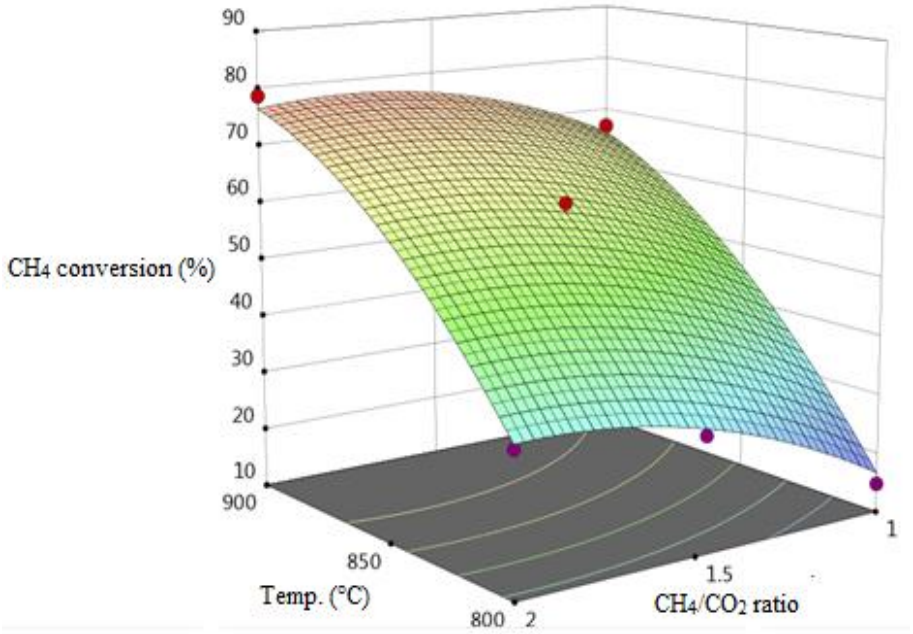

Fig.4.10. Surface plot of CH_4 conversion versus process temperature and CH_4/CO_2 ratio

4.4. Dry reforming with CeO_2 decorated Ni catalyst supported on TiO_2 and Al_2O_3

Catalytic dry reforming of biogas for hydrogen enrichment was studied over CeO_2 promoted Ni catalysts supported on TiO_2 and Al_2O_3. The catalysts were prepared by wet impregnation method and characterized. Their catalytic performance in the biogas dry reforming reaction was studied at temperature ranges from 650 to 850°C, with a CH_4/CO_2 ratio of 1.5:1.

4.4.1. Characterization

Characterization of various synthesized catalysts has been performed with respect to XRD, BET, FE-SEM and H_2-TPR analysis techniques.

4.4.1.1. XRD analysis

Fig.4.11 (a) displays the XRD patterns of the various synthesized catalysts on TiO_2 support. It was observed that the bare TiO_2 support is of rutile structure [JCPDS No: 01-077-0441]. The formation of peak at 2θ=27.3, 36.0, 39.1, 41.1, 54.6, 62.6, 63.9, 68.8, 69.6, 79.6, 82,1, 84.0, 87.2 and 95.0° corresponding to (110), (101), (200), (111), (211), (220), (002), (310), (301), (112), (212), (321), (410) and (411) planes, respectively, indicates TiO_2 phases. Further, the crystalline peaks observed at 2θ= 44.2, 51.5, 75.9, 92.3 and 97.8° were designated to the (111), (200), (220), (311) and (222) planes of the Ni metal, respectively [JCPDS No: 01-071-4653]. The intensified and sharpened NiO peaks were identified at higher Ni loading TiO_2 supported catalysts. This indicates that metal species were not well dispersed on the TiO_2 support. However, the diffraction peak intensity of NiO increased with increasing Ni content, leads to increase the crystalline size (Asencios et al., 2013). The average crystallite sizes of Ni corresponding to the peak (111) in the XRD spectra's were 12.6, 18.9, 35.0 and 39.0 nm respectively, for 7, 11, 15 and 19 wt. % Ni catalysts, respectively (Table. 4.5). As the Ni content increased from 7 to 19 wt. %, the peak intensities corresponding to rutile TiO_2 decreased, leading to a lower degree of crystallinity, and showed partial substitution of Ni into TiO_2 lattice during synthesis. Whereas, NiO phases on the Al_2O_3 and TiO_2supported catalysts exhibited less diffraction intensity when compared to Ni/ TiO_2 (Fig. 4.11 (b)). This indicates higher dispersion and reduced crystalline size in Al_2O_3- TiO_2 supported catalyst. The peak at 36.0° was due to TiO_2 (101) phase, and its intensity broadened with increasing CeO_2 loading, indicate that CeO_2 addition prevented the crystal formation in Ni/ (Al_2O_3-TiO_2) (Kim et al., 2015).

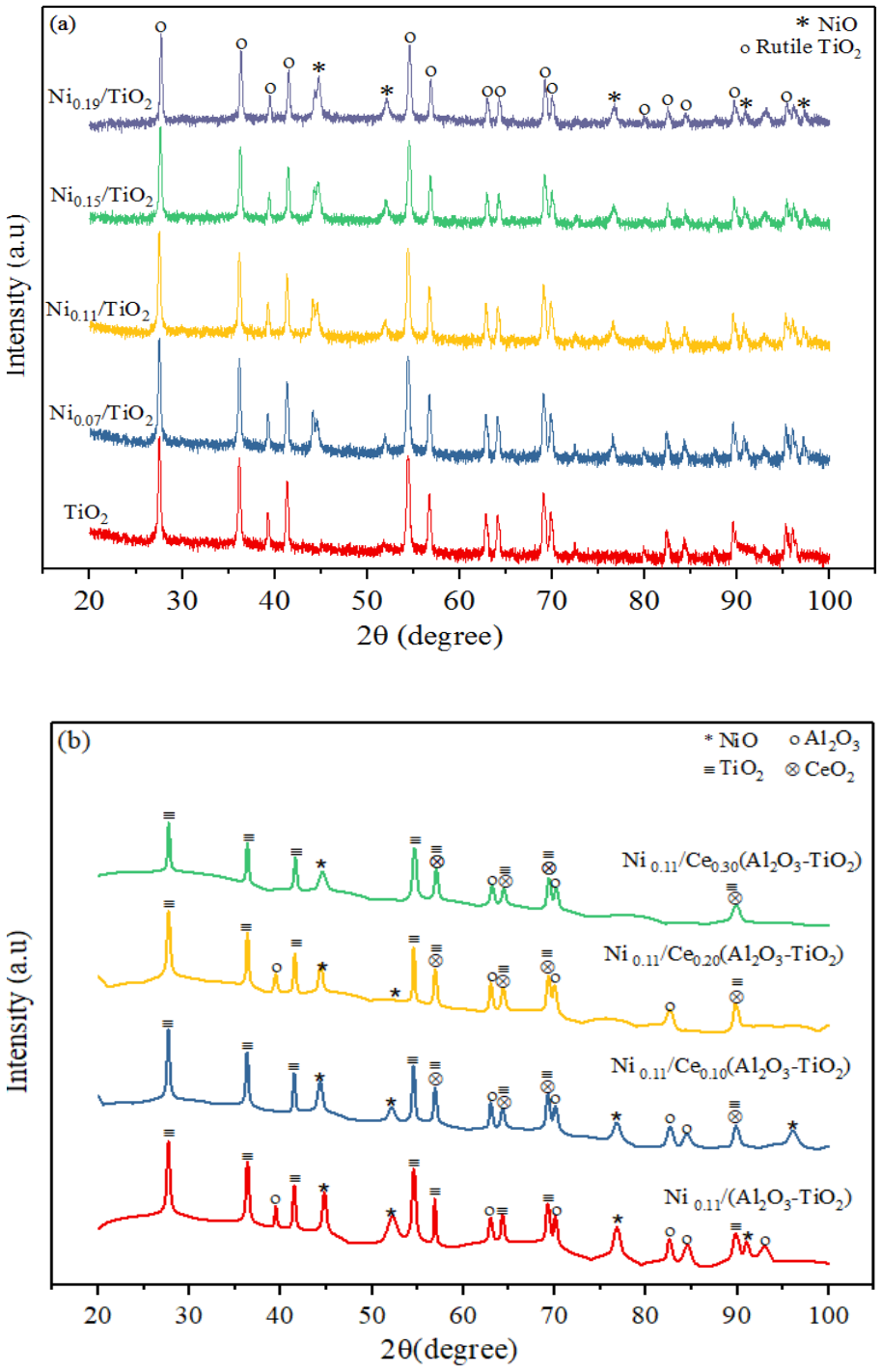

Fig.4.11. XRD patterns of the different catalysts

4.4.1.2. BET analysis

BET surface areas of the different synthesized catalysts are presented in Table 4.5. The N_2 adsorption estimations revealed that the bare TiO_2 support exhibited highest surface area than the synthesized catalysts, whereas after impregnated NiO, Al_2O_3, and CeO_2 it moved to the lower value. For instance, the surface area of $Ni_{0.19}/TiO_2$ reduced to 24.3 m^2 $g^{-1}$when compared to bare TiO_2 (114.8 m^2 g^{-1}). This may be attributed to the presence of large Ni particles that partially block the support pores, and probably due to the preconditioning calcination (at 800°C) of the support before use, that reduced the exposed area (Goula et al., 2015). This result is in consistent with the XRD data, suggesting that increasing Ni content led to increase the Ni peak intensity, resulting in lower surface area. Noteworthy, the catalysts with mixed Al_2O_3 and TiO_2 supports exhibited higher surface area as compared to TiO_2 support. However, after impregnating the CeO_2 in the mixed (Al_2O_3-TiO_2) catalyst, the surface area of the Ni catalyst reduced. The catalyst which was impregnated with 30 wt. % Ce acquired a larger surface area when compared to 10 and 20 wt. % Ce. It was observed that surface area increased with content of Ce, which directly affects the Ni metal dispersion over the catalyst surface. The surface area of 20 and 30 wt. % Ce catalysts were higher in comparison to 10 wt. % showed fine dispersion at higher ceria content.

Table 4.5 Textural properties of different catalyst samples

Catalyst	Surface area, m^2 g^{-1}	Ni particle size(111), nm
TiO_2	114.8	-
$Ni_{0.07}/TiO_2$	84.3	12.6
$Ni_{0.11}/TiO_2$	79.4	18.9
$Ni_{0.15}/TiO_2$	35.9	35.0
$Ni_{0.19}/TiO_2$	24.3	39.0
$Ni_{0.11}/(Al_2O_3$-$TiO_2)$	93.6	10.9
$Ni_{0.11}/Ce_{0.10}$ (Al_2O_3-TiO_2)	62.1	28.3
$Ni_{0.11}/Ce_{0.20}$ (Al_2O_3-TiO_2)	76.1	25.2
$Ni_{0.11}/Ce_{0.30}$ (Al_2O_3-TiO_2)	81.0	14.6

4.4.1.3. FE-SEM analysis

Fig. 4.12 (a), (b), (c) and (d) present the FESEM analysis of $Ni_{0.11}$/ (Al_2O_3-TiO_2), $Ni_{0.11}/Ce_{0.10}$ (Al_2O_3-TiO_2), $Ni_{0.11}/Ce_{0.20}$ (Al_2O_3-TiO_2) and $Ni_{0.11}/Ce_{0.30}$ (Al_2O_3-TiO_2) catalysts, respectively. It can be seen that the formed metal particles in $Ni_{0.11}$/ (Al_2O_3-TiO_2) catalyst were of spherical shape, densely dispersed over the titania and alumina mixed support. In 10 wt. % Ce catalyst, the support surface in the form of sheets, which lead to reduce surface area and increase particle size. With increased ceria contents (>10 wt. %), the improved surface morphology was observed that improves metal dispersion, providing smaller size active metal species. Moreover, the well-dispersed spherical shape metal particles were identified in both 20 and 30 wt. % Ce catalysts.

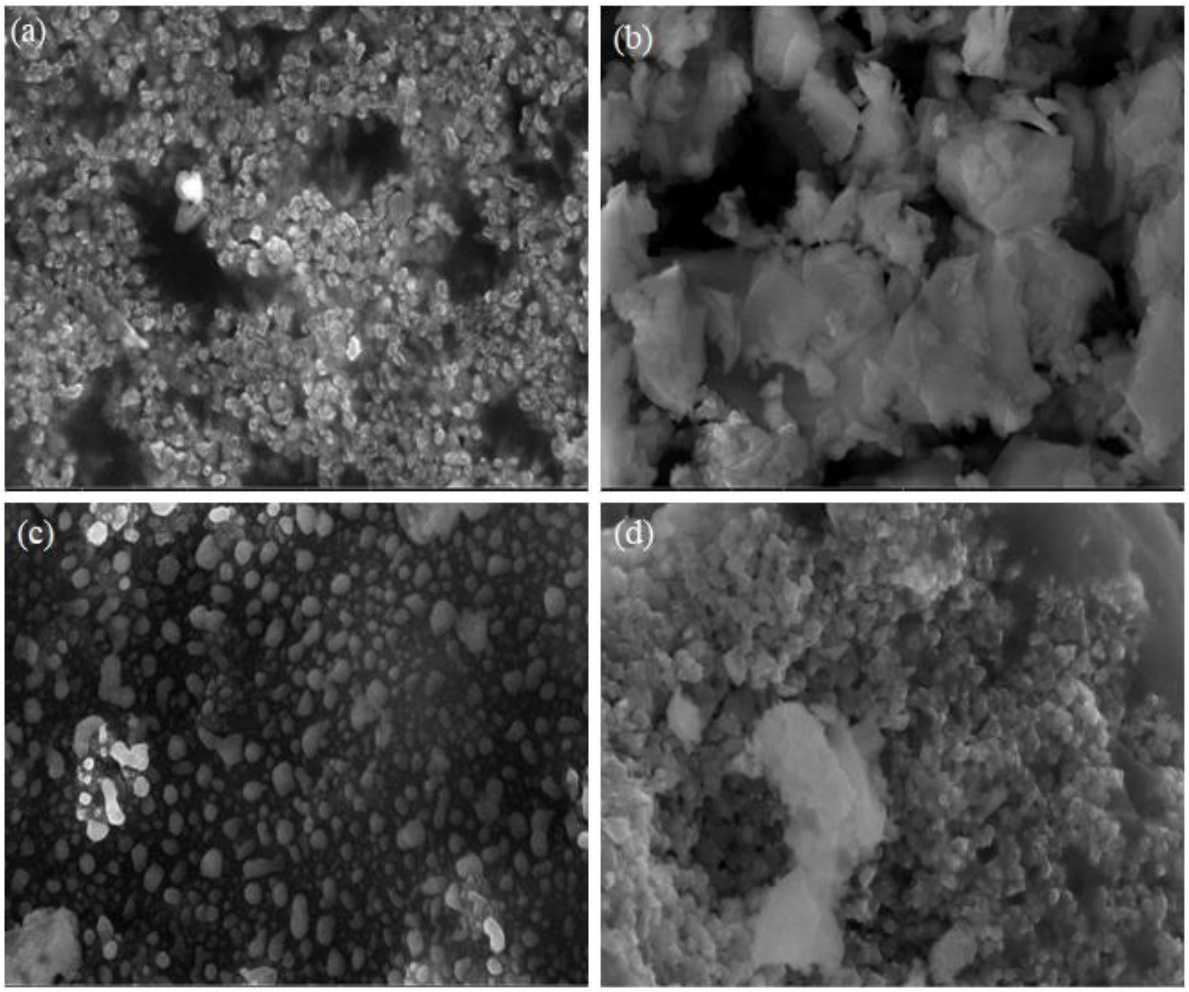

Fig.4.12. FESEM micrographs of catalysts (a) $Ni_{0.11}$/(Al_2O_3-TiO_2); (b) $Ni_{0.11}/Ce_{0.10}$ (Al_2O_3-TiO_2); (c) $Ni_{0.11}/Ce_{0.20}$ (Al_2O_3-TiO_2); (d) $Ni_{0.11}/Ce_{0.30}$ (Al_2O_3-TiO_2)

4.4.1.4. H_2-TPR analysis

Fig.4.13 (a) & (b) depict the H_2-TPR spectrum of the various synthesized Ni based catalysts. The high intensity H_2-TPR reduction peaks exist corresponding to the temperature at which maximum catalyst reduction occurred. There was no reduction peak of NiO appeared in the temperature range between 300-400°C, indicating intense interaction between Ni and support. Meanwhile, all TiO_2 supported catalysts showed only one remarkable reduction peak in the region of 500-650°C. There was relatively sharp reduction peaks appeared at 560, 630, 570 and 520°C for 7, 11, 15 and 19 wt. % Ni catalysts, respectively, as seen in Fig.4.13 (a). Increasing Ni content (11 to 19 wt. %), the reduction peak of NiO shifted towards lower temperature as a result of weak Ni-to-TiO_2 interaction, and suggesting lower dispersion of Ni, as discussed in literature (Zhan et al., 2017). These results are also in consistent with XRD pattern (Fig. 4.11 (a)), in which Ni peak intensities (2θ= 44.5°) decreased when the Ni content reduced to 11 from 19 wt. %. When comparing H_2-TPR patterns together, higher temperature peak was achieved in $Ni_{0.11}/TiO_2$ catalyst, which was attributed to a higher metal dispersion, as well as strong interaction between Ni and TiO_2. Moreover, an addition of Al_2O_3 support shifted reduction peaks toward higher temperature (740°C) when compared to $Ni_{0.11}/ TiO_2$ (570°C), leading large metal-support interaction, seen in Fig.4.13 (b). Meanwhile, three main reduction peaks were observed when CeO_2 was added in $Ni_{0.11}/ (Al_2O_3\text{-}TiO_2)$ catalyst. First, a reduction peak at 336°C, assigned to the reduction of relatively free NiO species, which scarcely interacted with $Al_2O_3\text{-}TiO_2$ support. At 465°C, attributed to the reduction of NiO species those have certain degree of interaction. A higher temperature (740°C) peak, designated to the reduction of complex NiO species which have strong interaction with the support. Additional peaks were observed at 336 and 465°C, which may be attributed to CeO_2 reduction as also documented in the previous study (Tada et al., 2012; Han et al., 2017), moreover; these peaks did not appear in case of $Ni_{0.11}/ Al_2O_3\text{-}TiO_2$ catalyst. The addition of Ce (10 and 30 wt. %) led to a fall in the H_2 consumption rate, indicating less amount of NiO on the catalyst surface, whereas, wide consumption peak in 20 wt. % Ce catalyst indicates a significant amount of NiO present.

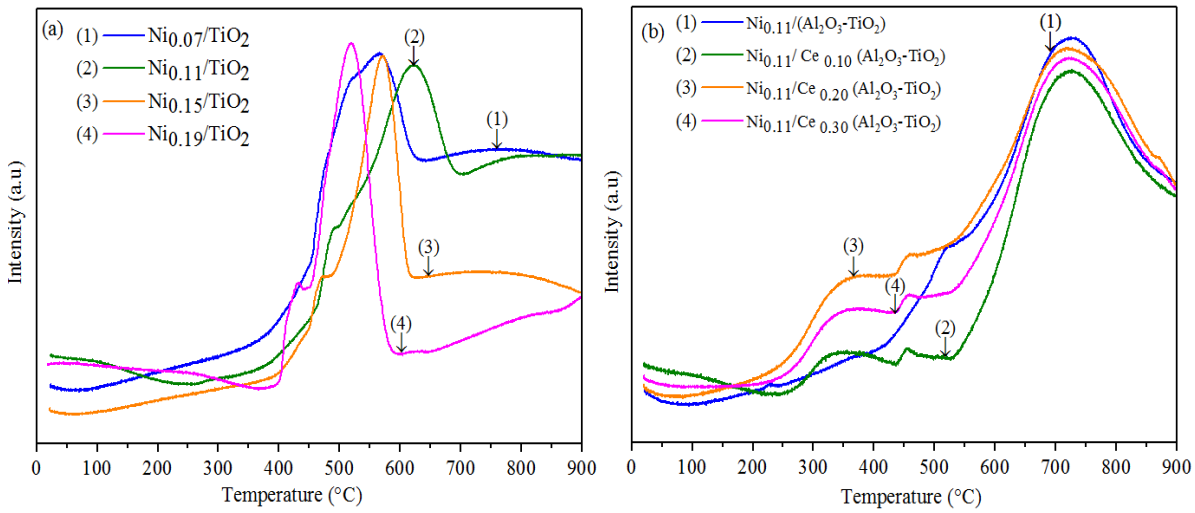

Fig.4.13. H_2-TPR profiles of various synthesized catalysts

4.4.2. Catalytic performance tests

Catalytic performance tests with various synthesized catalysts under dry reforming process were carried out in order to achieve better activity and selectivity of catalyst. First, preliminary tests were carried out to optimize Ni loading on TiO_2 support to maximize H_2 yield. Then, the synergic effect of Al_2O_3 and TiO_2 supported, as well as CeO_2 modified Ni based catalysts was investigated in the dry reforming process.

4.4.2.1. Effect of Ni loading on reactant conversions and product selectivity

The effect of Ni loading on the catalytic performance of TiO_2 supported catalysts was examined at 850°C. The reaction temperature (850°C) was chosen in order to reduce the influence of side reactions, consists of reverse water gas shift (RWGS) reaction (Eq. 2.2), Boudouard (Eq. 2.4) and methane decomposition (Eq. 2.3) reactions (Wang et al., 1996).

Fig.4.14 illustrates the reactant (CH_4 and CO_2) conversions and product (H_2 and CO) formed over the catalysts with Ni loading varying from 7 to 19 wt. %. Experimental observation revealed that the conversions of CH_4 and CO_2 increased with increasing Ni content from 7 to 15 wt. %, due to the presence of more reducible active sites. This result is in consistent with H_2-TPR profile which shows declined reduction temperature corresponding to higher Ni loading. Whereas, an additional increase in Ni (19 wt. %) content decreased CH_4 and CO_2 conversion due to lower dispersion of Ni. According to H_2-TPR results, the 19 wt. % catalyst showed reduction

peak at 520°C, so it was not completely reduced at temperature (≥600°C), which results in reducing the catalyst ability for adsorption and activation of the reactant molecules, and catalytic performance diminished. CH_4 and CO_2 conversion of 83.8 and 92.3%, respectively were obtained with 15 wt. % Ni content, and then reduced to 69.6 and 81.3% with 19 wt. % of Ni. Further, Ni $_{0.11}/TiO_2$ catalyst attained H_2/CO close to stoichiometric (0.89) with 70.5% CH_4 conversion and 89.0% CO_2conversion, which strongly reinforced due to higher Ni dispersion when compared to other catalysts, confirmed by H_2-TPR spectrum (Fig.4.13 (a)). Noteworthy, the higher the metal dispersion over the support leads to a reduction of carbon formation (Zhai et al., 2001; Lau et al., 2011). These results established that 11 wt. % Ni catalysts showed higher metal dispersion over the TiO_2 support. Thus, the 11 wt. % Ni loading was chosen to evaluate the effect of impregnating equal wt. % of Al_2O_3 and TiO_2 support on catalyst activity and selectivity.

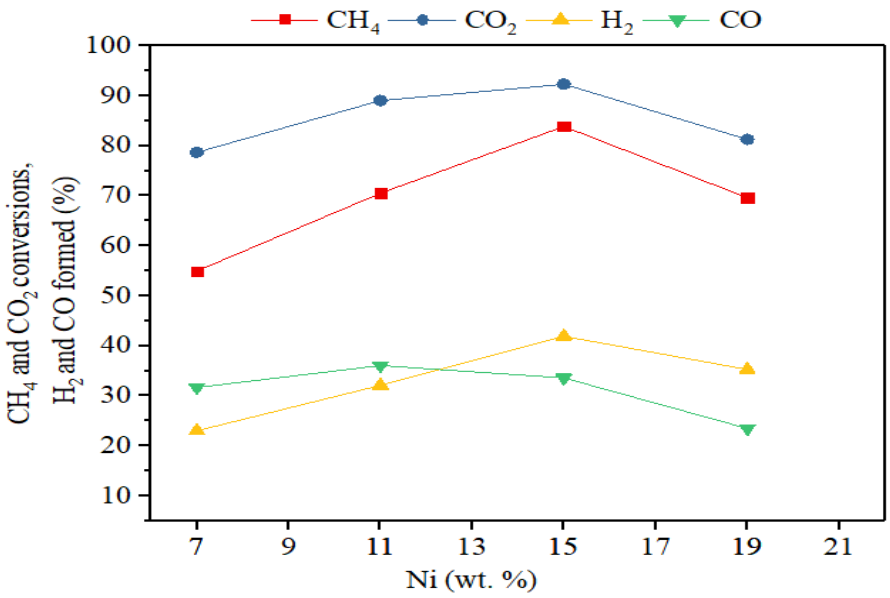

Fig.4.14. Effect of Ni loading on reactant conversions and product selectivity at 850 °C

4.4.2.2. Effect of Al_2O_3 and TiO_2 mixed support

Fig. 4.15 (a) portrays the variation of CH_4 and CO_2 conversions at different reaction temperatures. At 650°C, the $CH_4$and CO_2 conversions of $Ni_{0.11}/TiO_2$ catalyst were 19.2 and 32.9%, respectively, and then conversions increased to 70.5 and 89.0%, respectively, as temperature reached to 850°C. With increased temperature, the upward trends of CH_4 and CO_2 conversions were obviously observed in light of the fact that by increasing temperature, the

equilibrium of endothermic reaction (Eq.4.1) shifts in forward direction and hence the conversions significantly improved. At 650°C, addition of Al_2O_3 in $Ni_{0.11}/TiO_2$ catalyst improved the CH_4 and CO_2 conversions by 16.3 and 16.4%, respectively. Results suggest that the acidic sites on alumina assist the CH_4 activation, which improves conversion rate (Therdthianwong et al., 2008). Rahemi et al., (2013) reported that the addition of reducible oxide to alumina exhibited higher reactant conversion when compared to alumina alone. The higher catalytic activity of $Ni_{0.11}/ (Al_2O_3\text{-}TiO_2)$ catalyst was due to strong metal-support and assemblage of large NiO species when compared to $Ni_{0.11}/TiO_2$, confirmed by TPR results in which reduction peak sifted to higher temperature (740°C), while in $Ni_{0.11}/TiO_2$ (630°C).

Fig.4.15 (b) depicts the trends of H_2 and CO yields at different reaction temperatures. The H_2 and CO yield significantly increased with increasing temperature from 650 to 850°C. At 650°C, 4.6 and 7.9% of H_2 and CO yield, respectively, were obtained in $Ni_{0.11}/TiO_2$catalyst which enhanced to 26.7 and 36.0%, respectively at 850°C. The CO yield values were found to be higher than the H_2 under all temperature ranges, which is a clear indication of the occurrence of RWGS reaction (Eq. 2.2). At 650°C, the H_2 and CO yields improved by 5.3 and 5.9%, respectively, were observed in $Ni_{0.11}/ (Al_2O_3\text{-}TiO_2)$ catalyst as compared to $Ni_{0.11}/TiO_2$. This may be due to smaller Ni crystalline size (10.9 nm) of$Ni_{0.11}/ (Al_2O_3\text{-}TiO_2)$ catalyst when compared to $Ni_{0.11}/TiO_2$ (18.9 nm). The smaller particle size corresponding to larger surface area is important for the effective mass transfer during dry reforming reaction (Davis et al., 2002).

The H_2/CO ratios of the $Ni_{0.11}/TiO_2$ and $Ni_{0.11}/ (Al_2O_3\text{-}TiO_2)$ catalysts are illustrated in Fig. 4.15(c). H_2/CO ratio values varied between 0.69 and 0.98 which is close to the stoichiometry (Eq.4.1). As the reaction temperature increases, the H_2/CO product ratios increased, and it could be noted that these values close to the stoichiometry at elevated temperature. Generally, the H_2/CO ratio largely depends on the parallel side reactions countered in the dry reforming, including Boudouard (Eq. 2.4) and CH_4 decomposition reactions (Eq. 2.3), as well as reverse water gas shift (RWGS) reaction (Eq.2.2). In this study, the dry reforming reaction was initiated at 650°C, and the obtained H_2/CO ratio was 0.69 in $Ni_{0.11}/TiO_2$ catalyst. This ratio increased to 0.89 as the temperature increased from 650 to 850°C. Further, at 850°C, 0.98 H_2/CO ratio was obtained in $Ni_{0.11}/ (Al_2O_3\text{-}TiO_2)$ catalyst which is the clear indication of reduced effect RWGS

reaction when compared to $Ni_{0.11}/TiO_2$ (0.89). This may be due to the better activity of $Ni_{0.11}/(Al_2O_3\text{-}TiO_2)$ catalyst when compared to $Ni_{0.11}/TiO_2$.

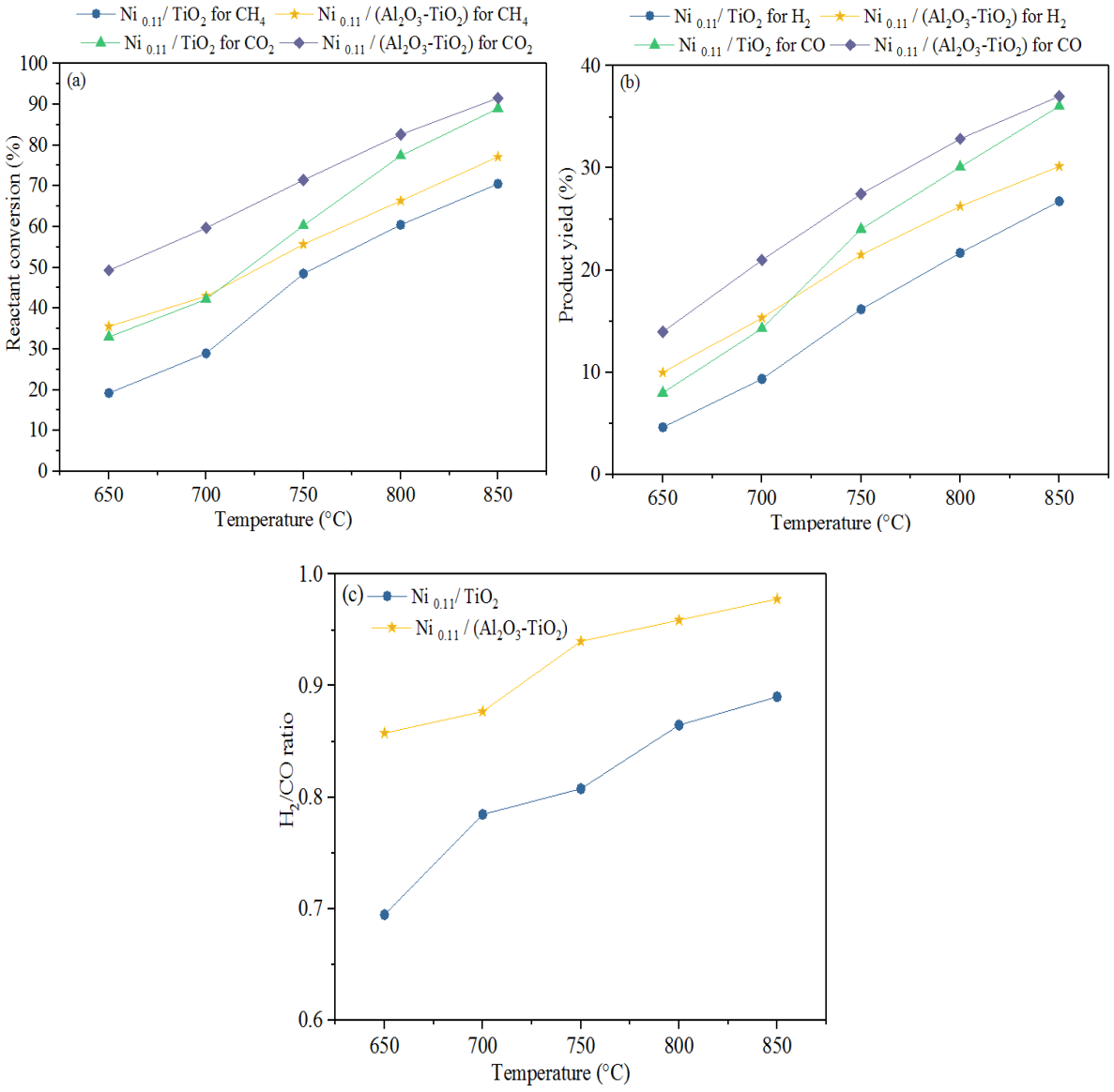

Fig.4.15. Effect of reaction temperatures on (a) Reactant conversions; (b) Product yields; (c) H_2/CO ratios

4.4.2.3. Effect of CeO_2 loading

Effect of CeO_2 addition on the performance of $Ni_{0.11}/(Al_2O_3\text{-}TiO_2)$ catalyst was investigated in the temperature range of 650-850°C, as shown in Fig. 4.16 (a) & (b). The modification of $Al_2O_3\text{-}TiO_2$ mixed support by the addition of CeO_2 resulted in superior O_2 mobility when compared to

Al_2O_3-TiO_2. At 650°C, 20 wt. % Ce doped catalyst yielded enhanced CH_4 and CO_2 conversions of 40.2 and 57.8%, respectively, while only 35.5 and 49.3% of CH_4 and CO_2 conversions, respectively, was achieved with Ni supported on Al_2O_3 and TiO_2. This improved CH_4 conversion can be attributed to the redox properties of ceria i.e. high O_2 storage capacity, which prevents coke formation and improves the performance of catalyst (Atzori et al., 2018). Wang et al., (2000) reported that CeO_2 support provides O_2 to metal, and its addition in reducible support is more beneficial when compared to non-reducible support. In addition, 10 wt. % Ce demonstrated a negative impact in terms of both reactant conversion and product (H_2 and CO) formation throughout temperature ranges compared to the un-promoted catalysts. This may be attributed to reduced metal dispersion with larger metal particle size (28.3 nm) in $Ni_{0.11}$/ $Ce_{0.10}$ (Al_2O_3-TiO_2) catalyst when compared to $Ni_{0.11}$/ (Al_2O_3-TiO_2) of 10.9 nm. At 850°C, 20 wt. % Ce catalyst increased CH_4 and CO_2 conversions to 84.9 and 95.6%, respectively, while, 30 wt. % Ce, CH_4 and CO_2 conversions of 73.7 and 91.7%, respectively, were observed (Fig. 4.16(a)). Increasing the Ce content (>20 wt. %) beyond limit is liable to sintering, especially at higher temperatures (Frontera et al., 2013). Noticeable, at higher temperature ceria loses O_2 storage capacity as it is vulnerable to sintering and hence doesn't show remarkable improvement in catalytic performance (Meshkani et al., 2014).

The H_2/CO ratios of the different ceria modified catalysts are displayed in Fig. 4.16(b). The addition of ceria significantly enhanced H_2/CO ratio value when compared to $Ni_{0.11}$/ (Al_2O_3-TiO_2) catalyst, indicated that the dry reforming reaction was effectively performed, though a low reactant conversion was reported due to the occurrence of side reactions (Eqs. 2.3 & 2.4). In the case of 20 wt. % Ce catalyst, the maximum H_2/CO ratio of 1.06 obtained at 850°C with a 40.6% H_2 enrichment of biogas. On the contrary, almost equal H_2/CO ratio (0.95) was observed in 10 and 30 wt. % Ce catalysts.

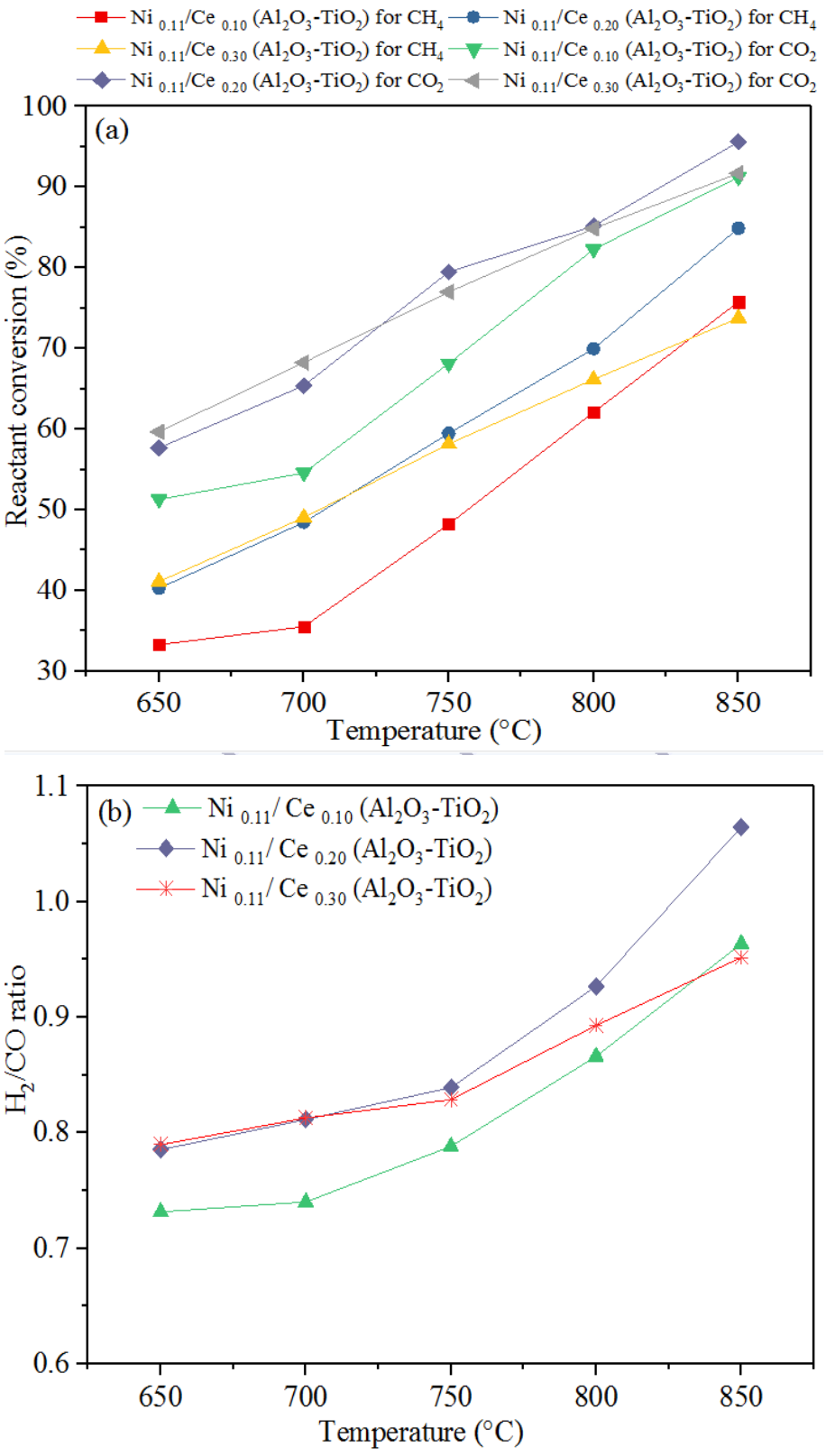

Fig.4.16. Effect of reaction temperatures on (a) Reactant conversions; (b) H_2/CO ratios

4.5. Dry reforming with Ni catalyst supported on ZnO and CeO_2

Dry reforming of biogas with Ni (10 wt. %) catalysts supported on ceria (CeO_2) and Ni catalyst with mixed support of CeO_2 and ZnO. The different catalysts were prepared by wet impregnation method and characterized subsequently. The effect of Zn loading (10 and 20 wt. %) on the catalytic activity was assessed in terms of reactant (CH_4 and CO_2) conversion, product (H_2 and CO) yield and H_2/CO ratio.

4.5.1. Characterization

The different structural and physicochemical properties of laboratory synthesized catalysts were assessed in order to develop a link between these properties with the activity/selectivity of the reforming catalyst, using techniques viz., XRD, H_2-TPR, FESEM and BET.

4.5.1.1. XRD analysis

Fig. 4.17 portrays the XRD analysis of synthesized catalysts. The Ni peak formation was recorded at different 2θ, their miller index is given in parentheses, 44.5° (111), 51.5° (200), 75.9° (220), and 97.8° (222) [JCPDS No: 01-071-4653]. Particularly at 2θ = 44.5° (111), the intensity of Ni diffraction peak varying accordingly with respect to CeO_2 and ZnO supports. The intensity of Ni (111) peak was found to be higher in $Ni_{0.1}/CeO_2$ catalyst, followed by $Ni_{0.10}/ (Zn_{0.2}\text{-}Ce_{0.8})$ and $Ni_{0.10}/ (Zn_{0.1}\text{-}Ce_{0.9})$ catalysts. Results are in consistent with the average Ni particle sizes, obtained using the Scherrer formula (Eq.3.1). Corresponding to phase (111), the average particle sizes of Ni observed were: 37.9, 21.6 and 30.3 nm for $Ni_{0.1}/CeO_2$, $Ni_{0.10}/ (Zn_{0.1}\text{-}Ce_{0.9})$ and $Ni_{0.10}/ (Zn_{0.2}\text{-}Ce_{0.8})$ catalyst, respectively. The particle size of metal is directly related to its diffraction peak intensities; the particle size increases with increasing intensities of diffraction peaks, as depicted in the literature (Movasati et al., 2017). The Ni peak intensity corresponding to Ni phase (111) phase decreased after impregnated ZnO into Ni/CeO_2 catalyst, which demonstrated higher interaction between Ni and CeO_2. After impregnated ZnO into Ni/CeO_2, the broadened peak of CeO_2 corresponding to (111) phase was observed, which indicates that ZnO addition prevented the crystal formation in Ni/CeO_2. Compared to 0 and 20 wt. % Zn catalysts, the more broadened peak of Ni (111) in 10 wt. % Zn indicates higher metal dispersion over ZnO and CeO_2 mixed support composite.

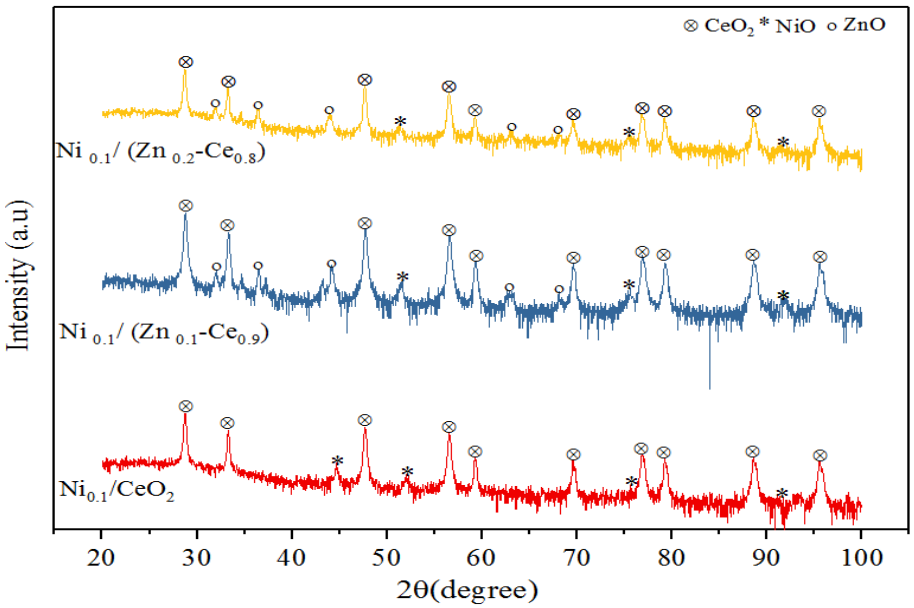

Fig.4.17 XRD patterns of the various synthesized catalysts

4.5.1.2. BET and FE-SEM analysis

The BET analysis revealed that the sole CeO_2 has higher surface area (120 m^2/g), and it starts moving toward lower value after impregnating NiO and ZnO. The BET surface areas of synthesized catalysts are tabulated in Table 4.6. Noteworthy, the 0 wt. % Zn catalyst exhibited higher surface area than 10 and 20 wt. % Zn catalysts. It was observed that Zn loading decreases the surface area, which affects the metal dispersion onto the catalyst surface. Results revealed that the surface area decreases with increasing Zn loading (10 to 20 wt. %), and also affects the dispersion of metal on the catalyst surface. Nematollahi et al., (2011) stated that the catalyst reactivity in dry reforming reaction is not directly related to the catalyst surface area. FESEM analysis of all fabricated catalysts was performed in order to examine the effect of Zn on the surface morphology. The FESEM images of $Ni_{0.1}/CeO_2$, $Ni_{0.10}/ (Zn_{0.1}\text{-}Ce_{0.9})$ and $Ni_{0.10}/ (Zn_{0.2}\text{-}Ce_{0.8})$ catalysts are shown in Fig. 4.18 (b.1), (b.2) and (b.3), respectively. Ni/CeO_2 catalyst showed the presence of metal in the form of flakes with improper (non-uniform) distribution on the surface. In 10 wt. % Zn catalyst, an effectively modified surface morphology found with uniform metal distribution over the entire support surface. Increasing Zn content (>10 wt. %) results Ni agglomeration, leading improper metal dispersion.

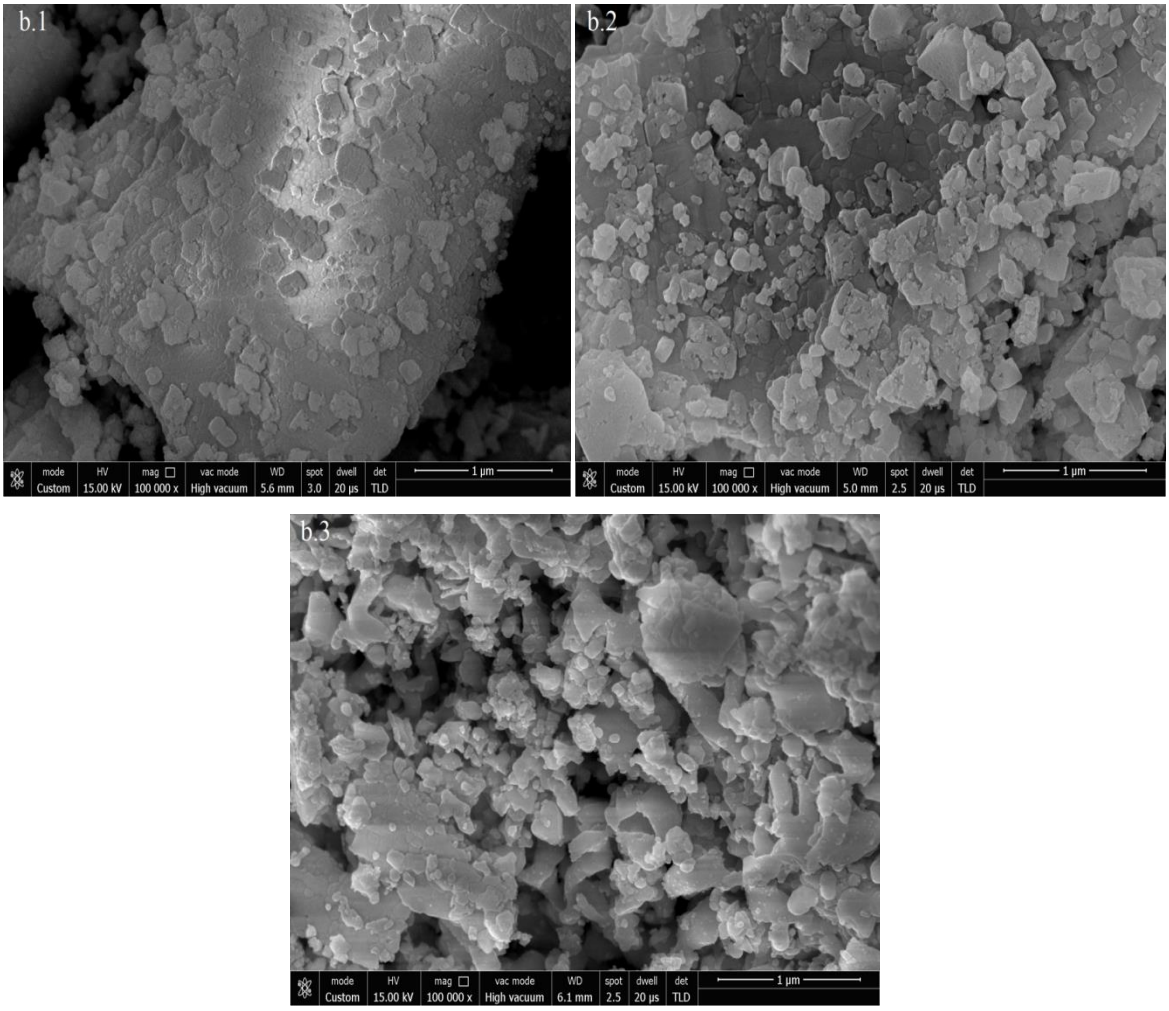

Fig.4.18. FESEM micrographs of catalysts (b.1) $Ni_{0.1}/CeO_2$; (b.2) $Ni_{0.10}/ (Zn_{0.1}\text{-}Ce_{0.9})$; (b.3) $Ni_{0.10}/ (Zn_{0.2}\text{-}Ce_{0.8})$

Table 4.6 Textural properties of different catalyst samples

Catalyst	Surface area, $m^2\ g^{-1}$	Ni particle size (111), nm
TiO_2	120	-
$Ni_{0.1}/CeO_2$	105	37.9
$Ni_{0.10}/ (Zn_{0.1}\text{-}Ce_{0.9})$	90	21.6
$Ni_{0.10}/ (Zn_{0.2}\text{-}Ce_{0.8})$	78	30.3

4.5.1.3. H_2-TPR analysis

The H_2-TPR profiles of synthesized catalysts are shown in Fig. 4.19. H_2-TPR spectra show higher magnitude at the temperature upon which maximum catalyst reduction taking place. The $Ni_{0.1}/CeO_2$ catalyst showed two reduction peaks at around 467 and 550°C, which were designated to NiO reduction, as reported in the literature (Movasati et al., 2017). At 550°C, the peak was designated to moderate interaction between Ni metal and CeO_2 support. H_2-TRP peaks on high temperature ranges indicate larger metal-support interaction. The reducibility of catalyst mainly depends on the NiO aggregation degree; stronger interaction between metal and support prompts fine dispersion of metal (Bengaard et al., 2002). After impregnated ZnO into $Ni0.1/CeO_2$ catalyst, it was observed that the H_2-TPR peaks start shifting toward higher temperature values. This result indicated that the ZnO loading led to enhance the Ni dispersion over the CeO_2 support. In 10 wt. % Zn catalyst, the intensity of reduction peak was found to be higher at 560°C, thereafter, at 635°C, which indicating the existence of two different Ni dispersion phases over catalyst support. Upon increasing Zn content (10 to 20 wt. %), the main reduction peak was seen at 535°C; revealed that the higher ZnO loading brings down the metal dispersion.

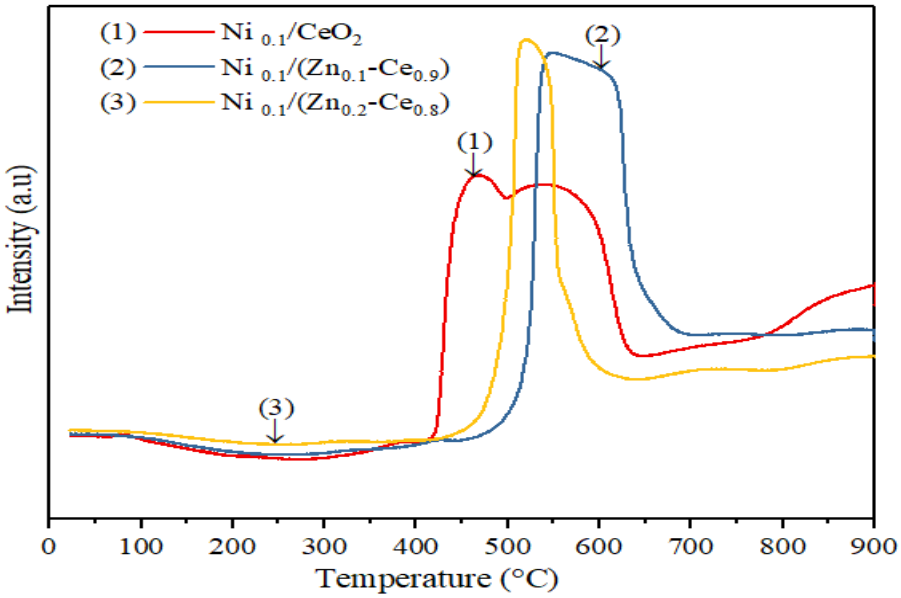

Fig.4.19. H_2-TPR spectra's of synthesized catalysts

4.5.2. Catalytic performance tests

The performance of various synthesized catalysts has been tested in dry reforming reactions of biogas at temperature ranges from 650 to 900°C, with a CH_4/CO_2 ratio of 1.5:1.

4.5.2.1. Effect on CH_4 and CO_2 conversions

CH_4 and CO_2 conversions of $Ni_{0.10}/CeO_2$, $Ni_{0.10}/ (Zn_{0.1}\text{-}Ce_{0.9})$ and $Ni_{0.10}/ (Zn_{0.2}\text{-}Ce_{0.8})$ catalysts are depicted in Fig.4.20 (a) and (b), respectively. With increased reaction temperature, the CH_4 and CO_2 conversions increased, because of the endothermicity of dry reforming reaction (Eq. 4.1) (Rezaei et al., 2006). At 650°C, 18.1% CH_4 conversion was observed in $Ni_{0.10}/CeO_2$ catalyst, and thereafter, it increased to 78.5% at 900°C. The impregnation of Zn into $Ni_{0.10}/CeO_2$ catalyst did not show positive effect on conversion values, especially at low temperature ranges (<800 °C). However, CH_4 conversion reduced by 1.7 and 3.3% respectively, for 10 and 20 wt. % Zn catalysts at 650°C. This reduction in CH_4 conversion may be due to reduced ceria content as a result of ZnO addition in mixed support catalysts. Nematollahi et al., (2011) performed the equilibrium analysis of dry reforming reaction over the temperature range between 450 and 750°C, and reported the equilibrium value (70%) of reactant (CH_4 and CO_2) conversions at 650°C. However, the present study indicates that in case of all synthesized catalysts the reactant conversions are far below from the equilibrium at 650°C, and it approaches to equilibrium conversion with increase in reaction temperature from 650 to 900°C. With increasing temperature (≥800°C), improved CH_4 conversion was observed in 10 wt. % Zn catalyst when compared to 20 wt. %. This was due to higher Ni dispersion, consistency of observation was confirmed by H_2-TPR spectra; in which $Ni_{0.10}/ (Zn_{0.1}\text{-}Ce_{0.9})$ catalyst showed main reduction peak at 635°C, while, in $Ni_{0.10}/ (Zn_{0.2}\text{-}Ce_{0.8})$ catalyst (535°C). At 900°C, reduced CH_4 conversion in 20 wt. % Zn catalyst (69.6 %) was observed when compared to 10 wt. % (83.1%). This could be due to smaller Ni particle size (21.6 nm) of 10 wt. % Zn catalyst in comparison to other catalysts i.e. 37.9 and 30.3 nm for $Ni_{0.10}/CeO_2$ and $Ni_{0.10}/ (Zn_{0.2}\text{-}Ce_{0.8})$ catalysts, respectively.

On the other hand, CH_4 conversion was found to be lower in comparison to CO_2 conversion at all temperature ranges (Fig. 4.20 (b)). It was observed that the biogas dry reforming reaction (Eq.4.1) is thermodynamically more favorable with respect to CH_4 as compared to CO_2. Moreover, the CO_2 producing reactions i.e. boudouard (Eq.2.4) and reverse water gas shift

(RWGS) reaction (Eq.2.2) were more dominant. Apart from that, the endothermic (Eq. 4.1) and CH_4 consuming (Eq. 2.3) reactions move toward forward with increasing temperature. Overall, the CH_4 conversion is higher than CO_2 and largely attributed to the CH_4 decomposition reaction. The 10 wt. % doped Zn catalyst showed higher CO_2 conversion when compared to 20 wt. %. For instance, at 900°C, the CO_2 conversion reduced to 78.9% from 97.0% with the increase in Zn content from 10 to 20 wt. %. This may be probably due to higher metal dispersion in case of $Ni_{0.10}$/ ($Zn_{0.1}$-$Ce_{0.9}$) catalyst when compared to $Ni_{0.10}$/ ($Zn_{0.2}$-$Ce_{0.8}$); observation is in agreement with the previous finding (Balzarotti et al., 2016).

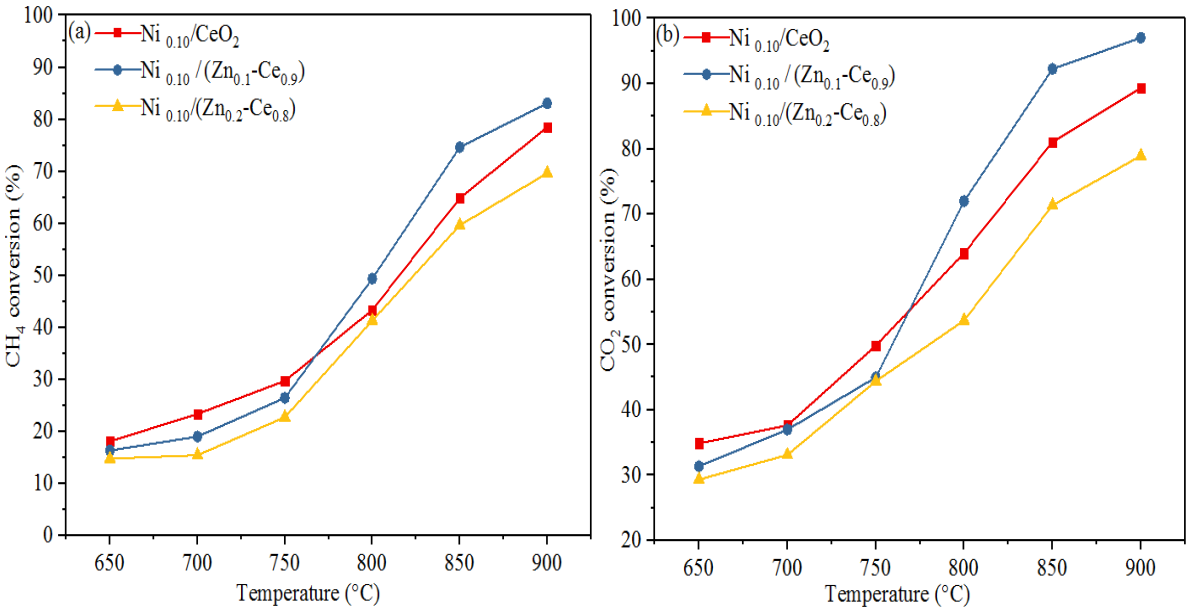

Fig. 4.20. Effect of reaction temperatures on (a) CH_4 conversions; (b) CO_2 conversions

4.5.2.2. Effect on H_2 and CO yields

Fig. 4.21 (a) & (b) portray the variation of H_2 and CO yields in the temperature ranges between 650 and 900°C. With increasing temperature, the increasing trends of product (H_2 and CO) yield were observed same like CH_4 and CO_2 conversions. At 650°C, the H_2 and CO yields in $Ni_{0.10}/CeO_2$ catalyst observed were 4.3 and 8.4%, respectively, thereafter, 29.8% (H_2 yield) and 32.6 % (CO yield) at 900°C. This increment in product yields was due to enhanced reactant conversions with increasing temperature (650 to 900°C). Noteworthy, H_2 yield was observed to be less when compared to CO at all temperature ranges. This difference in product yield values was due to more CO_2 conversion than CH_4 (Kurungot et al., 2004). After impregnated 10% by

wt. of Zn, 3.7 and 6% improvement in H_2 and CO yields, respectively, was observed when compared to 29.8 and 32.6%, respectively, with $Ni_{0.10}/CeO_2$ at 900°C. However, 20 wt. % Zn catalyst showed a reduction in both product yields in comparison to 10 wt. %.

4.5.2.3. Effect on H_2/CO ratio

Fig. 4.21 (c) shows the variation of product (H_2/CO) ratio with temperature. Results demonstrated that with increasing reaction temperature (650 to 900°C), the H_2/CO ratio increases due to increased reactant conversion and product yield. The H_2/CO ratio was found to be less than unity up to temperature (≥850°C), thereafter, it approaches unity at 900°C. The results revealed that the H_2 product selectivity was lower than CO, because of the predominant RWGS reaction at temperatures (≥850°C), as reported in the literature (Shen et al., 2011). At 900°C, the RWGS reaction was dominated over dry reforming which led to enhanced H_2 product selectivity. With $Ni_{0.10}/CeO_2$ catalyst, 0.62 H_2/CO ratio was obtained at 650°C, thereafter, it reached 1.1 at 900°C. However, maximum H_2 enrichment (40.3%) was observed in $Ni_{0.10}/ (Zn_{0.1}\text{-}Ce_{0.9})$ catalyst with 1.04 H_2/CO ratio. It appears that the addition of Zn (10 wt. %) results in H_2/CO of unity (Eq. 4.1); however, 0.83 ratio was attained with 20 wt. % Zn catalyst. This indicates that the 10 wt. % Zn catalyst favored reaching the equilibrium composition.

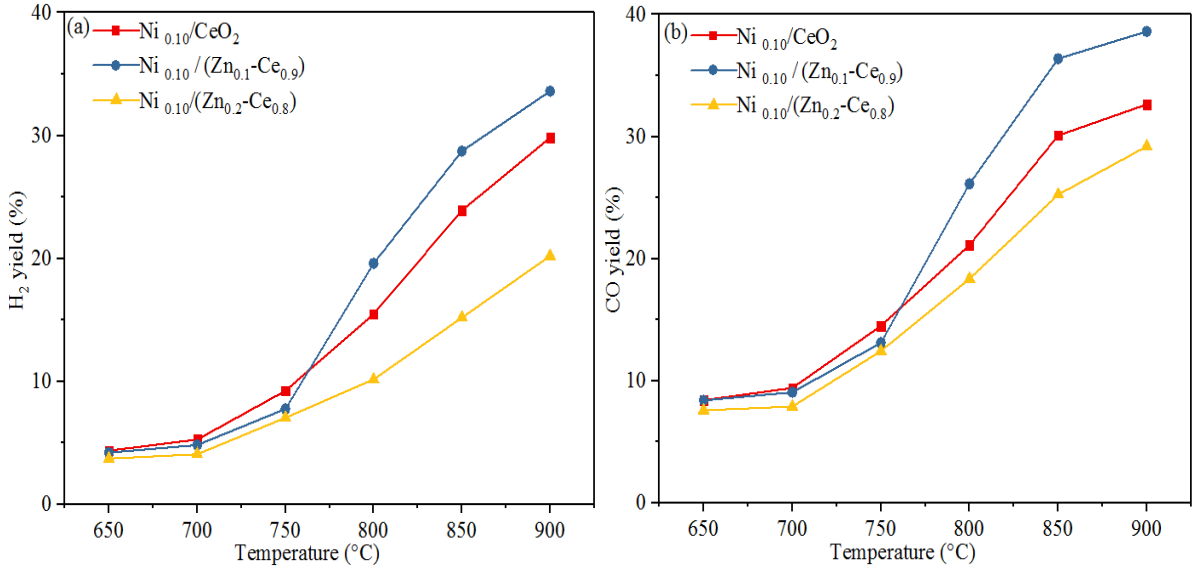

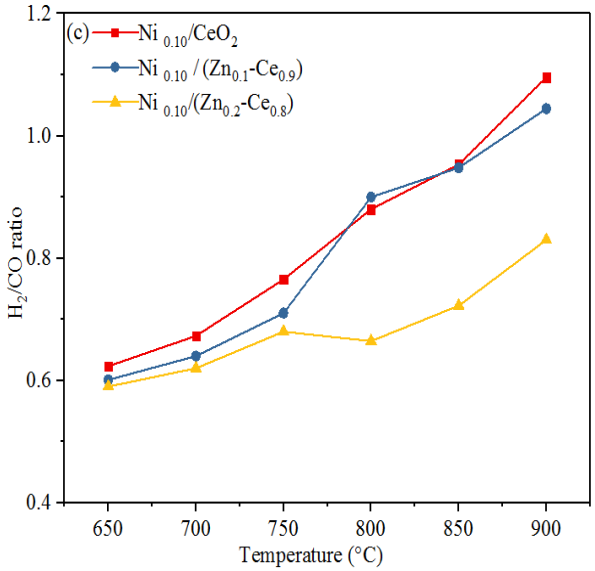

Fig.4.21. Effect of reaction temperatures on (a) H_2 yields; (b) CO yields; (c) H_2/CO ratios

4.6. Effect of O_2 addition over optimized catalysts

The effect of various O_2/CH_4 ratios of feedstock on CH_4 conversion and formed product (H_2/CO) ratio was investigated, as depicted in Fig. 4.22 (a) and (b) for $Ni_{0.11}$/ $Ce_{0.20}$ (Al_2O_3-TiO_2) and $Ni_{0.10}$/ ($Zn_{0.1}$-$Ce_{0.9}$) catalysts, respectively. Since DOR performs well at lower temperature ranges; consequently, lowest temperature used in the dry reforming reactions i.e. 650°C was chosen to study the influence of O_2 along with CH_4 and CO_2 reactants in dry oxidative reforming. The graph (Fig.4.22) emphasizes that the CH_4 conversion and H_2/CO ratio followed upward trend with increasing O_2/CH_4 ratios from 0 to 0.57. CH_4 conversion under dry oxidative reforming was found to be higher than in dry reforming (0.0 O_2/CH_4 ratios), because of two oxidative reactants (O_2 and CO_2) used. Moreover, the H_2/CO ratio values greater than unity was observed at all O_2/CH_4 ratios. This could be due to the increased O_2 content in reactants; however H_2O and CO_2 product formation enhance owing to CH_4 oxidation, leading WGSR consumes more CO and formed more H_2 (Mattos et al., 2003).

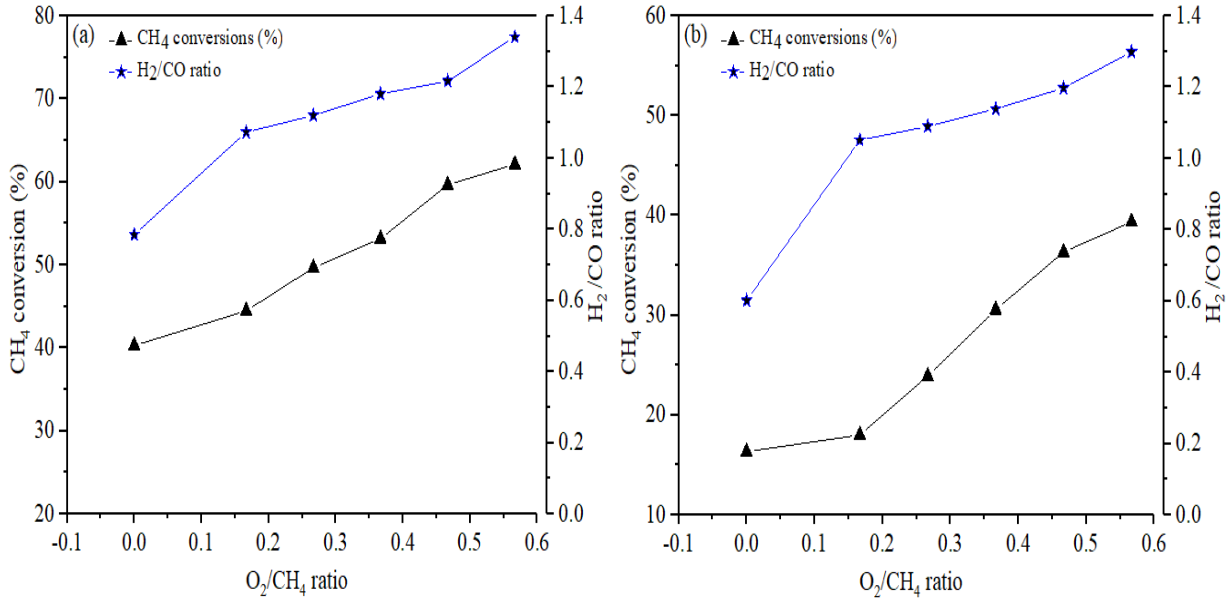

Fig.4.22. Effect of O_2/CH_4 ratios on the CH_4 conversion and H_2/CO ratio at 650°C (a) $Ni_{0.11}$/ $Ce_{0.20}$ (Al_2O_3-TiO_2); (b) $Ni_{0.10}$/ ($Zn_{0.1}$-$Ce_{0.9}$) catalyst

With $Ni_{0.11}$/ $Ce_{0.20}$ (Al_2O_3-TiO_2) catalyst, the CH_4 conversion and H_2/CO ratio with 0.57 O_2/CH_4 ratios significantly increased to 62.1% and 1.34, respectively, whereas, only 40.2% and 0.79, respectively, were obtained with dry reforming (i.e. 0.0 O_2/CH_4 ratios). Whereas, the CH_4 conversion (39.3%) and H_2/CO ratio (1.45) in $Ni_{0.10}$/ ($Zn_{0.1}$-$Ce_{0.9}$) catalyst was identified under same reforming conditions. However, the stoichiometry of dry oxidative reforming reaction (Eq. 2.15) was obtained at 0.47 O_2/CH_4 ratios.

4.7. Stability tests

Stability tests for dry reforming reactions were performed over $Ni_{0.11}/Ce_{0.20}$ (Al_2O_3-TiO_2) catalyst and $Ni_{0.10}$/ ($Zn_{0.1}$-$Ce_{0.9}$) catalysts at 850 and 900°C temperatures, respectively. Fig. 4.23 (a) illustrates the reactant (CH_4 and CO_2) conversions and product (H_2 and CO) yields of $Ni_{0.11}$/ $Ce_{0.20}$ (Al_2O_3-TiO_2) catalyst over 18h of continuous reaction time. Maximum H_2 enrichment of 40.6% with 84.9 and 95.6% CH_4 and CO_2 conversions, respectively, were obtained over $Ni_{0.11}$/ $Ce_{0.20}$ (Al_2O_3-TiO_2) catalyst after 2h of reaction. Whereas, higher CH_4 conversion (83.1%) and H_2 yield (33.6%) were obtained with $Ni_{0.10}$/ ($Zn_{0.1}$-$Ce_{0.9}$) catalyst (Fig. 4.23 (b)). Thereafter, a small drop (2-3%) in CH_4 and CO_2 conversions was identified over 7h of the reaction period.

This reduction indicates that the coke formation starts over the catalyst surface, which reduces the active metal sites as well as blocks the catalyst pores. However, H_2/CO ratio was almost identical in both catalysts i.e. 0.95 after 16h of reaction and remains unchanged thereafter. Nevertheless, no significant changes in the H_2 and CO formations were observed which indicated negligible catalyst deactivation. Carbon depositions of 22.6 wt. % was assessed in $Ni_{0.11}$/ $Ce_{0.20}$ (Al_2O_3-TiO_2) catalyst, while for $Ni_{0.10}$/ ($Zn_{0.1}$-$Ce_{0.9}$), it was 40.2 Wt. % after 18h of the reactant time.

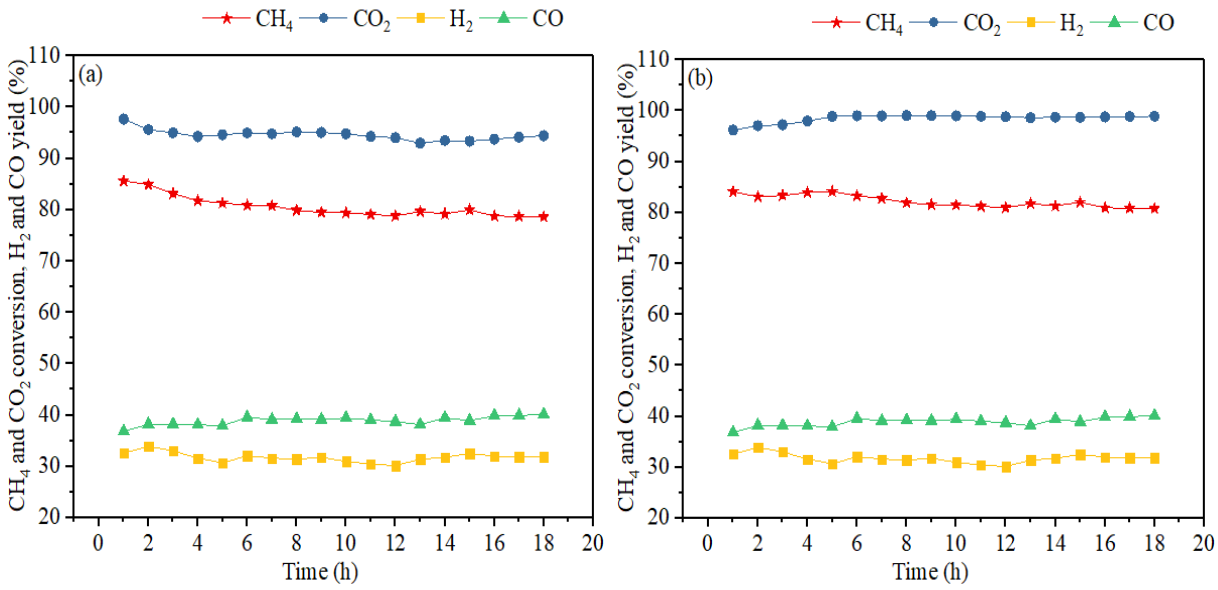

Fig.4.23. Stability test in the dry reforming of biogas over (a) $Ni_{0.11}$/ $Ce_{0.20}$ (Al_2O_3-TiO_2) at 850°C; (b) $Ni_{0.10}$/ ($Zn_{0.1}$-$Ce_{0.9}$) catalyst at 900°C

4.8. Effect of compression ratio on various characteristics of CI engine fueled with palm (B20) biodiesel blend

Literature reveals that B20 is an optimal blend with respect to combustion, performance and emission characteristics of CI engine (Schumacher et al., 1996; Kumar et al., 2015). Consequently, B20 biodiesel blend was chosen in order to evaluate the impact of compression ratios on various engine characteristics of CI engine. Different set of experiments were performed and comparison of results was made between pure diesel at 17:1 CR and B20 over

CRs of 16:1, 17:1 and 18:1. The various physicochemical properties of fuels used are given Table 4.7.

Table 4.7 Diesel and biodiesel fuel properties as per ASTM standards

Fuel properties	Diesel	B100	B20	Limits
Density (kg/m^3)	850	885.8	861	-
Cetane number	48	58	53	>47
Kinematic viscosity (cSt)	2.049	4.60	2.88	1.9-6
Flash Point (ºC)	68	180	79	>130
Fire Point (ºC)	83	194	90	>53
Calorific Value (kJ/kg)	42000	39000	41420	>33000
Cloud Point (ºC)	-1	10	3	-3 to 12
Pour Point (ºC)	-8	6	-5	-15 to 10
FFA %	-	0.12	-	<2.5

4.8.1. Combustion analysis

Fig. 4.24 (a) & (b) portray the variation of ignition delay (ID) and peak cylinder pressure (PCP) with bmep for Diesel and B20 fuels at different CRs. The results revealed that in comparison to diesel the ID period of B20 fuel was lower, whereas, higher values of PCP were also obtained in B20 with increasing CR (16:1 to 18:1). The downward trends of ID period were observed with increasing bmep because, for attaining high power output at higher bmep (engine load) the compressed air pressure and temperature led to increase, which further decreases the ID period (Gumus et al., 2010). At no-load conditions (i.e. 0 bar bmep), the ID periods were observed to be 18.0 and 15.6°CA for diesel and B20, respectively, at CR (17:1). This reduction in ID period was due to higher cetane number (53) of B20 fuel when compared to diesel (48) (Qi et al., 2009). With increased bmep (0 to 3.5 bar), the ID period decreased and corresponding values were 14.0°CA (with diesel) and 11.0 °CA (with B20) on CR of 17:1. Results demonstrated that the ID period continuously decreased with increasing CRs from 16:1 to 18:1 for B20 fuel. For example, the ID decreased from 12.9°CA with CR (16:1) to 11.0 and 10.0°CA with 17:1 and 18:1 CRs, respectively at 3.5 bar bmep. At higher CR (≥17:1), the in-cylinder temperature becomes higher which would reduce the viscosity of fuel and providing better fuel atomization (Ozsezenet al., 2008).The average drop of 8.2% was observed in ID values for B20 with increasing CR (16:1 to

18:1). Whereas, at higher bmep (≥ 2.8 bar), the ID period values were almost identical due to the consistency of combustion and cylinder wall temperature, as also reported in the literature (Datta et al., 2016).

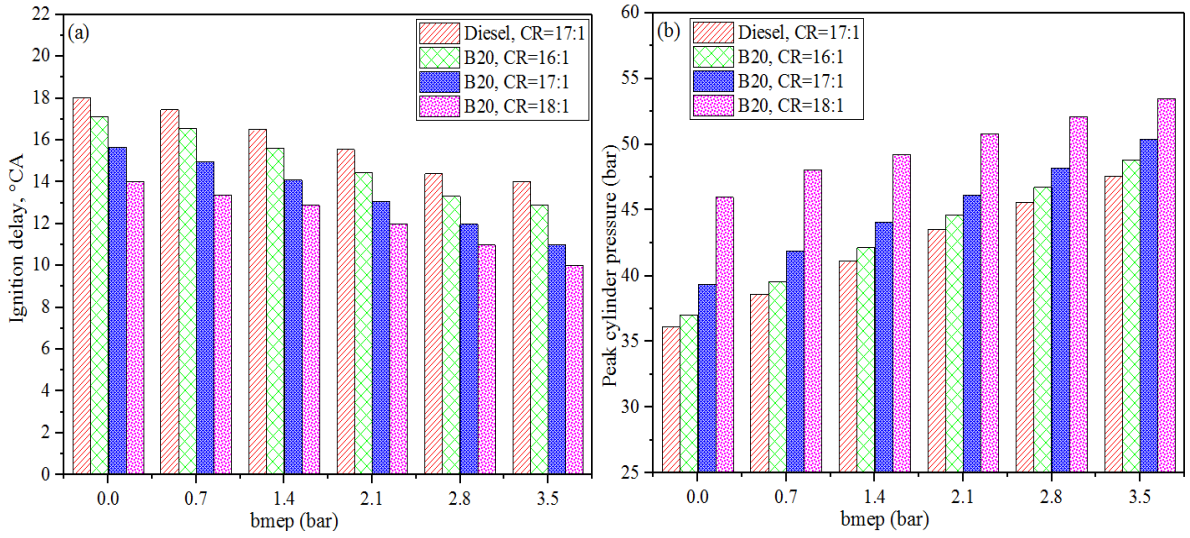

Fig.4.24. Effect of bmep on at different CRs (a) Ignition delay; (b) Peak cylinder pressure

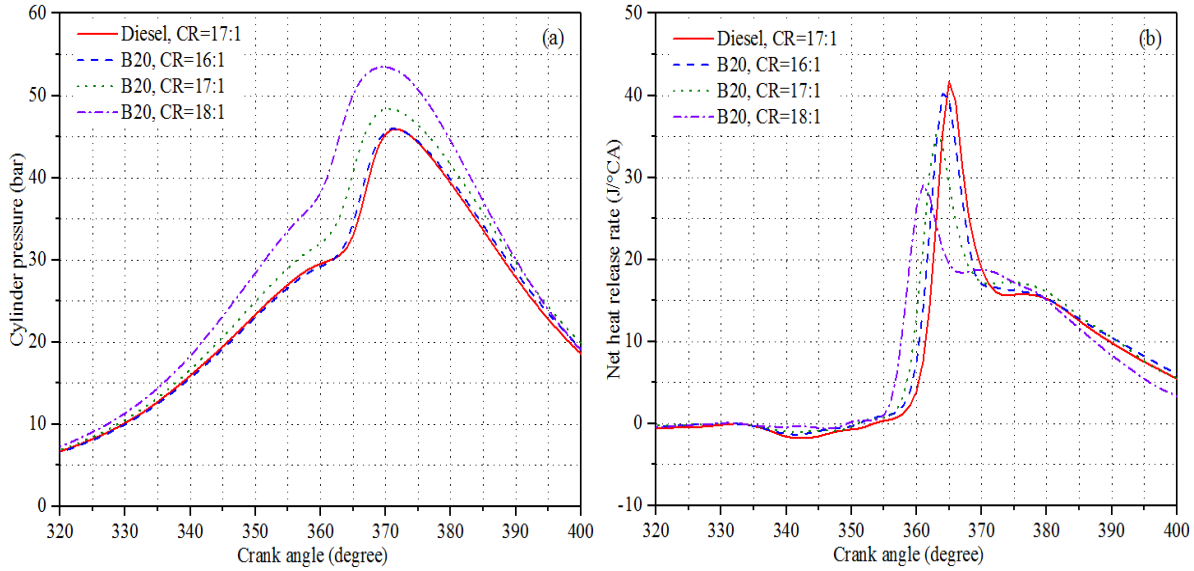

Fig.4.25. Effect of CRs at 3.5 bmep (a) Cylinder pressure; (b) Net heat release rate

The PCP was found to increase with increasing bmep and CR, as seen in Fig. 4.24 (b). This increased PCP at higher bmep was due to more fuel injection, whereas, decreased distance between piston top and cylinder head (i.e. clearance volume) increased PCP at higher CRs.

However, the PCP was found lower for neat diesel operation when compared to B20. This happened due to the reduction in ID period with B20 fuel, which led to advanced combustion process. At higher CR, the fuel-air mixture density becomes larger which leads to provide better charge (B20-air) mixture. The PCP decreases at lower CR, because of weak swirl and poor fuel-air mixture leading to reduce the combustion rate (Raheman et al., 2008).

Fig. 4.25 (a) illustrates the variation of CP with degree crank angles (°CA) for diesel (17:1 CR) and B20 fuels (16:1 to 18:1 CR) at 3.5 bar bmep. It was ascertained from results that the B20 fuel provides higher CP when compared to diesel. The density of B20 fuel (861 kg/m^3) becomes higher than diesel (840 kg/m^3), thereby more quantity of fuel burning in the initial stage of combustion and providing higher CP. With increasing CR (16:1 to 18:1), the increase of in-cylinder pressure and temperature led to increase CP and the combustion process improves subjected to better fuel atomization (Selvan et al., 2009). The lower value of CP was seen at 16:1 CR, which was due to slower premixed combustion phase of B20. The NHRR for both tested (Diesel and B20) fuels is shown in Fig. 4.25 (b). It can be interpreted that in B20 fuel combustion process started earlier in comparison to diesel; more confirmation is obtained with NHRR plots, seen that for B20 fuel the peaks start moving towards left over all CRs. This tendency of early start of combustion may be due to shorter ID and advanced injection of B20 fuel. The magnitude of NHRR peaks was higher in diesel when compared to B20, because of prolonged ID period in diesel led to providing fuel-air premixing for long duration. Moreover, the negative values of NHRR for diesel and B20 fuels were due to vaporization of fuel which was accumulated in ID period. After initiating of combustion, the NHRR becomes positive, and then it rises rapidly. At all crank angles, the decreased in NHRR values was observed with CR increased from 16:1 to 18:1. At CR (17:1), the maximum values of NHRR were: 41.7 J/°CA at 5°ATDC (with diesel) and 35.3 J/°CA at 3°ATDC (with B20). This NHRR value decreased to 29.1 J/°CA at 1 °ATDC with increasing CR (16:1 to 18:1) for B20, whereas, 40.1 J/°CA at 4°ATDC (16:1). At high CR (18:1), the higher in-cylinder pressure and temperature provided better spray formation as well as reduction in fuel viscosity, which become the reason of low values of NHRR (Muralidharnet al., 2011).

4.8.2. Performance analysis

4.8.2.1. Brake power

Fig. 4.26 (a) illustrates the variations in engine BP with bmep for diesel and B20 fuels. The BP increased with increase in bmep from 0 to 3.5 bar for both tested fuels. With increased bmep (0.7 to 3.5 bar) at CR (17:1), the BP increased from 0.5 and 0.4 kW to 2.8 and 2.7 kW, in diesel and B20, respectively. It was due to a large amount of fuel being burnt at higher bmep to meet the power requirements. Nevertheless, the BP of B20 was found to be lower when compared to diesel at all engine loads. The reason for this reduction in BP was due to higher viscosity and lower heating value of B20 fuel than diesel (Table. 4.7). Moreover, the higher values of BP were seen in B20 fuel corresponding to the increased in engine CRs. At 3.5 bar bmep, the BP increased from 2.4 kW with CR (16:1) to 2.7 and 2.9 kW with CR (17:1) and CR (18:1) respectively. At higher CR, the reduced viscosity and density of B20 led to improving combustion process (Rajaket al., 2019).

4.8.2.2. Brake thermal efficiency

BTE is an important parameter used to predict the effectiveness of fuel energy conversion to useful work. Fig. 4.26(b) exhibits the variations in BTE with bmep for diesel and B20 fuels at different CRs. At CR (17:1), the obtained BTEs for neat diesel were: 12.0, 20.0, 27.0, 30.1 and 32.0% corresponding to 0.7, 1.4, 2.1, 2.8 and 3.5 bar bmep, respectively. With increased bmep (0 to 3.5 bar), the BTE improves consequently because increased loads lead to produce more brake power (Muralidharn et al., 2011). In comparison to diesel at 17:1 CR, the lower values of BTE were observed in B20 fuel at all bmep ranges. This reduction in BTE values was due to poor combustion characteristics owing to higher density/viscosity, as well as poor volatility of B20 fuel when compared to diesel. For example, at 0.7 bar bmep and 17:1 CR, the BTE of diesel was 12%, thereafter; it reduced to 11.2% with B20. Moreover, B20 fuel offers high value of BTE at higher CRs, due to enhance in-cylinder temperature and pressure. At 3.5 bar bmep, the BTE in B20 fuel increased from 28.9% with CR (16:1) to 30.8 and 33.8% with CR (17:1) and CR (18:1), respectively.

4.8.2.3. Brake specific fuel consumption

Fig. 4.26 (c) reveals the BSFC decreased sharply with increase in bmep from 0.7 to 3.5barfordiesel and B20 fuels. It occurs because the increment in BP percentage becomes higher than fuel which leads to reducing BSFC at higher bmep (Labecki et al., 2012). At CR (17:1), the observed BSFC values for neat diesel were: 0.73, 0.43, 0.32, 0.29 and 0.27 kg/kWh corresponding to 0.7, 1.4, 2.1, 2.8 and 3.5 bar bmep, respectively. Whereas, the increment in BSFC values in B20 fuel was also observed when compared to diesel because of lower heating value of B20 fuel. For example, at 0.7 bar bmep and 17:1 CR, the BSFC of diesel was 0.73 kg/kWh, thereafter; it reached 0.76 kg/kWh with B20. Also, B20 fuel offers high density (861 kg/m^3) value when compared to diesel (850 kg/m^3), resulting poor B20-air mixing and led to increased BSFC. With increasing CR (16:1 to 18:1) in B20, it was observed that the BSFC values reduce continuously due to improved combustion characteristics at higher CRs when compared to lower CR (Sivaramakrishnan et al., 2014).

4.8.2.4. Exhaust gas temperature

The variation in EGT with bmep at different CRs is presented in Fig. 4.26 (d). Generally, the EGT follows a linear relationship with bmep because more fuel being burnt at higher bmep to meet the power requirements. In pure diesel, at no load condition (i.e. 0 bar bmep), the EGT was assessed as 123°C with CR (16:1), and then it increased to 266°C at 3.5 bar bmep. At 17:1 CR, the higher values of EGT in case of B20 fuel when compared to diesel were also observed. B20 comprise poor volatility constituents that burn in the post combustion phase, resulting higher EGT when compared to diesel. The maximum EGTs observed for diesel and B20 were 266 and 271°C, respectively at 17:1 CR. This result indicated that the combustion of B20 fuel starts earlier than diesel; these results are consistent with NHRR plots. Further, at higher CR, the reduction in EGT was observed; for example, 271 and 261°C with 17:1 and 18:1 CR, respectively, whereas, with 16:1 CR it observed 277°C. Moreover, the higher value of EGT with B20 fuel suggests that the engine becomes thermally overload at lower CRs (Roskillyet al., 2008).

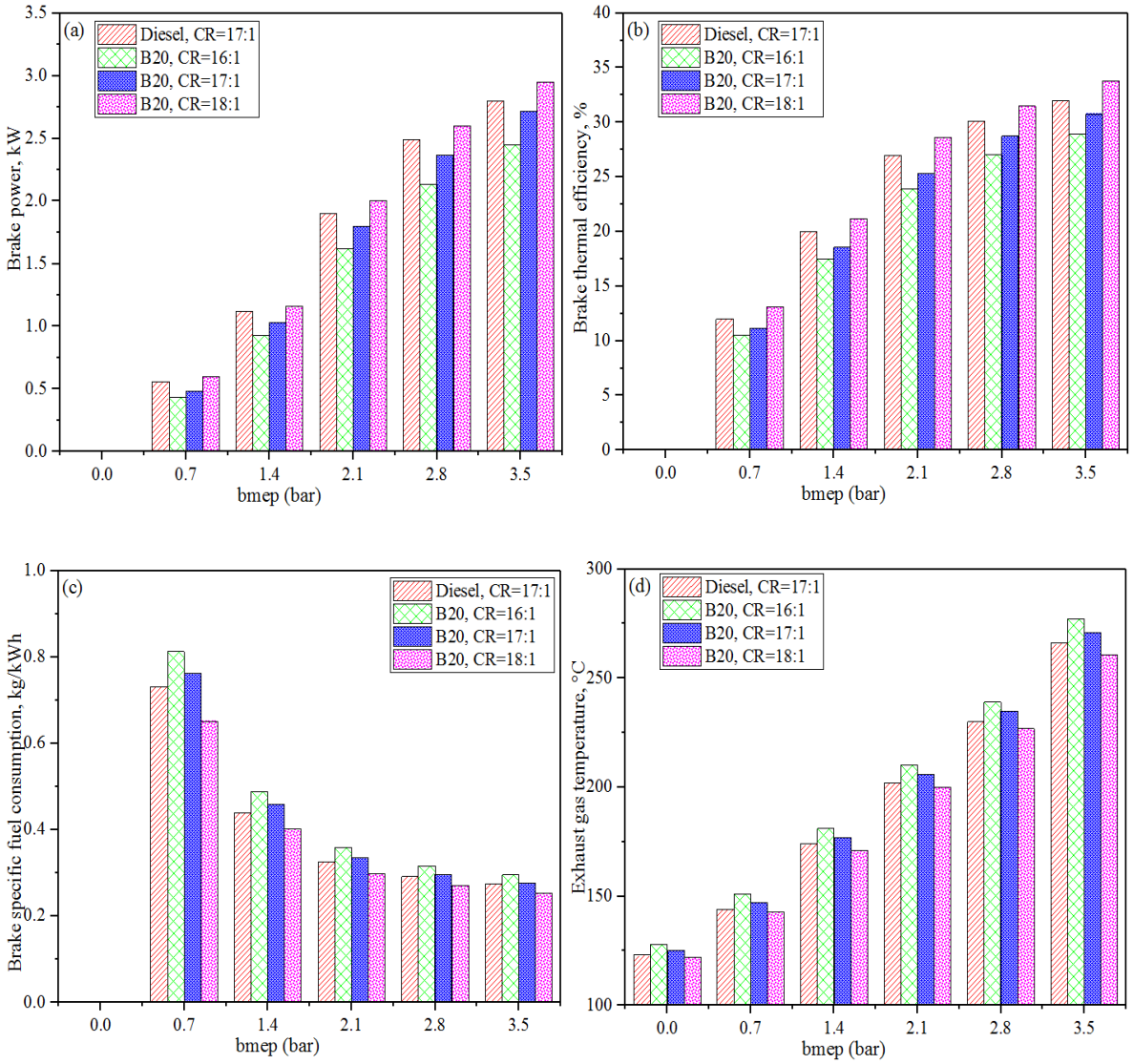

Fig.4.26. Effect of bmep on at different CRs (a) Brake power; (b) Brake thermal efficiency; (c) Brake specific fuel consumption; (d) Exhaust gas temperature

4.8.3. Emission analysis

4.8.3.1. HC emissions

Fig. 4.27 (a) depicts the variation of HC emissions with bmep for diesel and B20 fuels. The results demonstrated that the HC emissions increased with increasing bmep from 0 to 3.5 bar. At CR 17:1 and no-load conditions, for diesel the assessed HC emission was 23 ppm, while, it increased to 42 ppm at 3.5 bar bmep. The increased HC emissions at higher bmep were due to

oxygen deficiency; moreover, leaner combustion offers lower HC emissions. Subsequently, the HC emissions decreased with B20 fuel at all bmep with respect to diesel at CR (17:1). It was happened due to the enhanced oxygen content in B20 fuel which led to providing smother and complete fuel combustion. For example, at 0.7 bar bmep and 17:1 CR, the HC emission of diesel was 25 ppm, thereafter; it reduced to 21 ppm with B20. While, increasing CR (16:1 to 18:1), the HC emissions reduced because higher CRs offer high in-cylinder temperature and pressure which improves fuel combustion. At 3.5 bar bmep, the HC emissions in B20 fuel reduced from 48 ppm with CR (16:1) to 33 and 26 ppm with CR (17:1) and CR (18:1), respectively.

4.8.3.2. NOx emissions

NOx emissions for diesel and B20 fuels with bmep at different CRs are shown in Fig. 4.27 (b). The formation of NOx emissions in CI engines largely depends upon the adiabatic flame temperature, which is closely related to the peak cylinder temperature (Anand et al., 2011). It was observed that the NOx emissions increased with increasing bmep in both tested fuels. This was because of the large amount of fuel burned at higher bmep, led to increased peak cylinder temperature and hence NOx increased. Minimum and maximum values of NOx emissions corresponding to 0 and 3.5 bar bmep were 49 and 285 ppm for diesel and, 70 and 356 ppm for B20 fuel, respectively, at 17:1 CR. Further, the NOx formation was found to be higher in case of B20 fuel when compared to diesel. This increased NOx emission was due to the improved combustion characteristics with B20, which led to offered high combustion temperature inside the engine cylinder (Nagarajan et al., 2014). At 3.5 bar bmep, the NOx emissions in B20 fuel increased from 300 ppm with CR (16:1) to 356 and 370 ppm with CR (17:1) and CR (18:1), respectively.

4.8.3.3. CO emissions

Fig. 4.27 (c) shows the variation of CO emissions with bmep for diesel and B20 fuels. CO emissions occur because of incomplete fuel combustion in CI engines. The CO emissions initially decreased up to 1.4 bmep and then suddenly increased at higher bmep. At bmep ($\leq$1.4 bar), the reduction in CO emissions was due to combustion of leaner fuel-air mixture. At bmep ($\geq$2.1 bar), the excess fuel-air ratio led to produce more smoke, and prevented oxidation of CO to CO_2, as a result, CO emissions increase. The CO emissions observed to be lower in B20 fuel

than neat diesel at all bmep, indicating better fuel combustion (Labeckas et al., 2009). At 3.5 bar bmep and 17:1 CR, the observed CO emissions were: 0.14 and 0.13% for diesel and B20 fuels, respectively. With increasing CR (16:1 to 18:1), the lower values of CO emissions were observed in B20 fuel operations. For example, at 3.5 bar bmep, the CO emissions in B20 fuel reduced from 0.15% with CR (16:1) to 0.13 and 0.12% with CR (17:1) and CR (18:1), respectively.

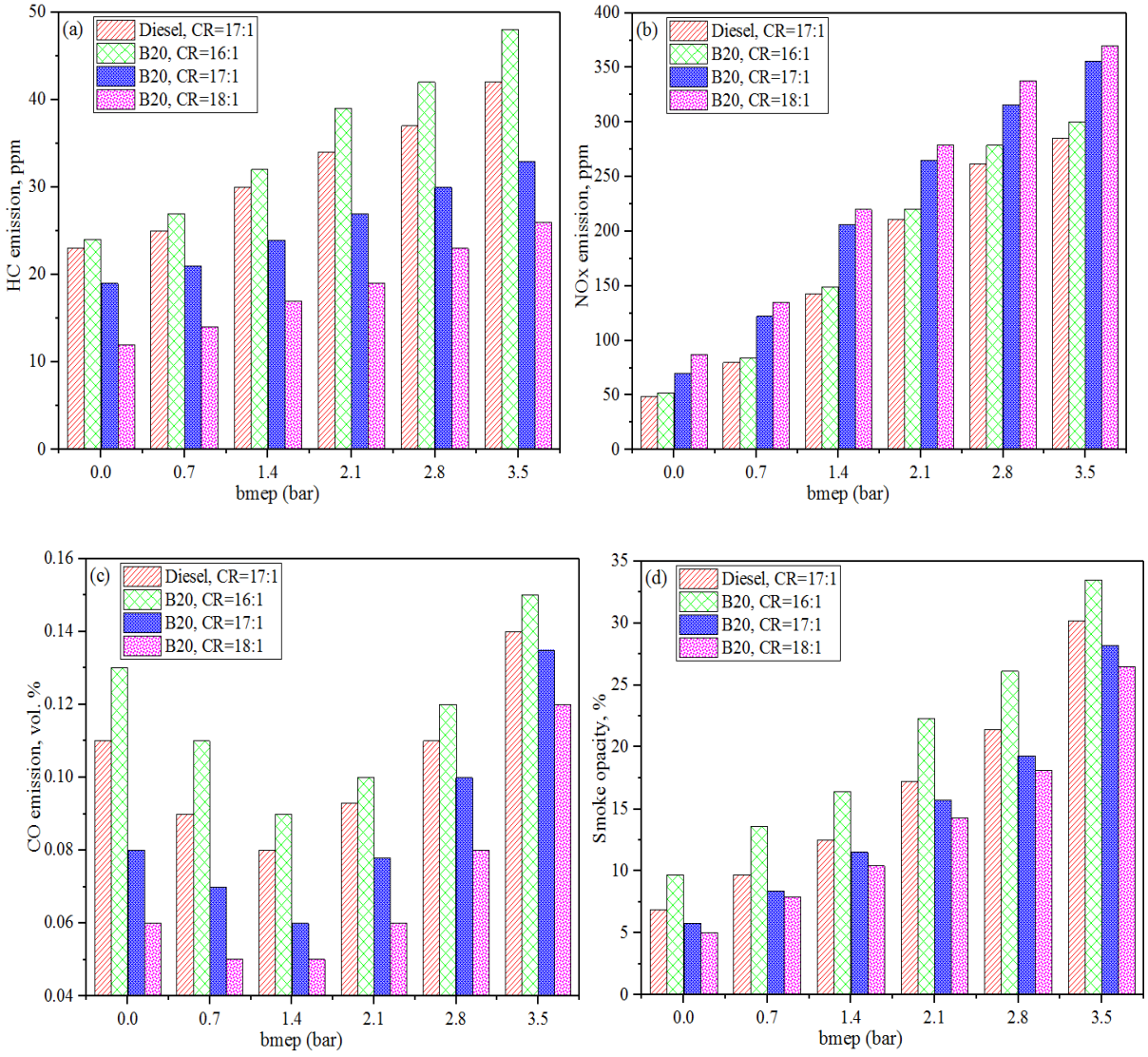

Fig.4.27. Effect of bmep on at different CRs (a) HC emissions ; (b) NOx emissions; (c) CO emissions; (d) Smoke opacity

This reduction in CO emission was due to in-cylinder temperature corresponding to higher CR, which further offers favorable environment for charge oxidation. An adequate amount of heat generated at higher CRs which resulted reduces ID, providing more opportunity to fuel burn in the diffusion mode.

4.8.3.4. Smoke opacity

Smoke opacity is highly dependent on the fuel oxygen content and inlet air during intake stroke of the engine. Smoke opacity from CI engine fueled with neat diesel and B20 is shown in Fig. 4.27 (d). From results, it was observed that smoke level increased with the increase in bmep for both tested fuels. This happened due to the burning of rich fuel-air mixture at higher bmep. As in-cylinder fuel injection increased, more fuel which remains unburnt goes into the exhaust (Qi et al., 2013). At 17:1 CR, the assessed smoke opacities with diesel were: 6.9, 9.7, 12.5, 17.2, 21.4 and 30.2%, and with B20: 5.8, 8.4, 11.5, 15.7, 19.3 and 28.2% at bmep of 0, 0.7, 1.4, 2.1, 2.8 and 3.5 bar, respectively. The smoke opacities decreased with B20 fuel at all bmep with respect to diesel at CR (17:1). This effect may be due to more oxygen content in B20 fuel, which led to oxidize the soot in CI engine and reduces smoke level consequently. At 3.5 bar bmep, the smoke opacities in B20 fuel decreased from 33.5 % with CR (16:1) to 28.2 and 26.5 % with CR (17:1) and CR (18:1), respectively. The reduction in smoke opacity at higher CR was due to enhanced combustion which led to reduce soot formation (Can et al., 2014).

4.8.4. Noise level

Noise level of CI engine fueled with neat diesel and B20 is shown in Fig. 4.28. Results demonstrated that noise level increased with the increase in bmep for both tested fuels. This may be due to enhanced combustion with respect to engine loads in order to produce more power output. At 17:1 CR, the assessed noise levels with diesel were: 89.1, 89.3, 90.1, 91.1, 92.1 and 92.7 dB, and with B20: 89.9, 90.3, 90.7, 91.9, 93.2 and 94.0 dB at bmep of 0, 0.7, 1.4, 2.1, 2.8 and 3.5 bar, respectively. Subsequently, the noise increased continuously with increasing CR (16:1 to 18:1) with B20 fuel. This effect may be due to increased in-cylinder pressure at higher CRs. At 3.5 bar bmep, the noise levels in B20 fuel increased from 93.0 dB with CR (16:1) to 94.0 and 95.8 dB with CR (17:1) and CR (18:1), respectively.

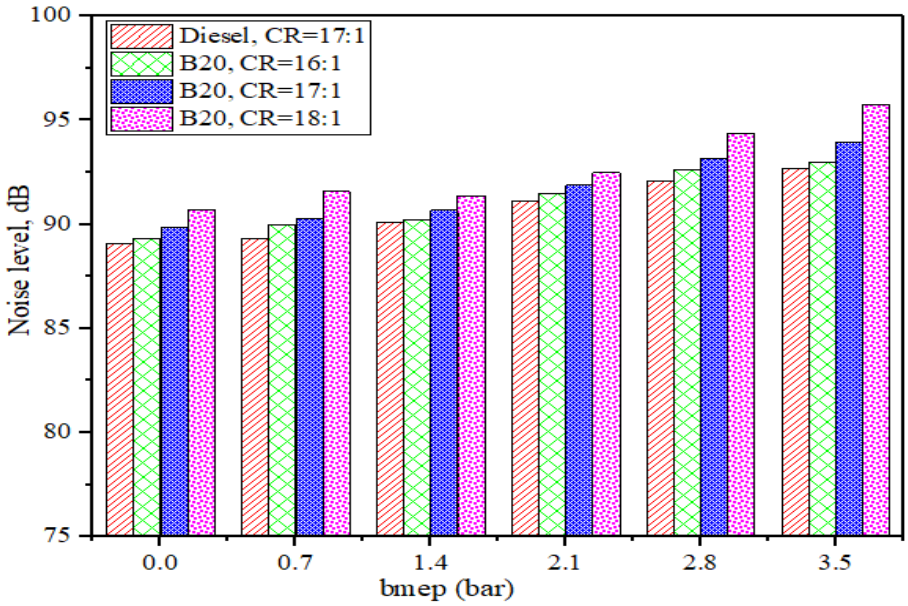

Fig.4.28. Effect of bmep on noise level at different CRs

4.9. Utilization of HEB under dual fuel mode operations with Diesel and B20 pilot fuels

HEB was injected via fumigation technique in the flow rate ranges between 0.1 and 0.5 kg/h in steps of 0.1 kg/h. Moreover, the diesel and B20 were used as pilot fuels in order to initiate combustion inside the engine cylinder. The important properties of HEB were calculated theoretically based on its composition ranges, and are tabulated in Table 4.8.

Table 4.8 H_2-enriched biogas properties

Properties	H_2-enriched biogas
Composition	H_2 : 40%; CO : 40%; CH_4: 10; N_2 : 10% (by vol.)
Calorific Value (kJ/kg)	57000
Density (kg/m^3) at 1 atm, 15°C	0.7164
Maximum flame speed (m/s)	1.2
Stoichiometric A/F ratio (molar)	2.84
Stoichiometric A/F ratio (mass)	5.02
Flammability limits (% by Vol.)	6.5-57.4

4.9.1. Combustion analysis

In dual fuel CI engine, the diesel/B20 spray is surrounded with air-HEB mixture, which significantly affects the diesel ignition. Fig. 4.29 (a) shows the variation of ID period with bmep for diesel and diesel-HEB, and Fig. 4.29 (b) for B20 and B20-HEB fuel modes. Results demonstrated that the ID period decreased with increasing bmep from 0 to 3.5 bar. At no load condition (i.e. 0 bar bmep), the higher air-fuel ratio (AFR) leads to lower the combustion temperature which further led to reduce cylinder wall temperature and hence ID becomes higher (Santosoet al., 2013). With increased bmep (0 to 3.5 bar), the increases in combustion temperature subsequently bring down the ID period. At single fuel mode (diesel), the ID period was observed to be 16.0°CA, and then reduced to 13.0°CA at 3.5 bar bmep. With B20 fuel, the ID period was observed to be 14.6 and 10.5°CA at 0 and 3.5 bar bmep, respectively. The lower values of ID period was observed in case of diesel operations when compared to B20, which was due to higher cetane number (53) of B20 fuel than diesel (48) (Liew et al., 2010). It was further observed that the ID of dual fuel modes become higher when compared to a single mode. At 3.5 bar bmep, the ID period enhanced from 13.0°CA with diesel to 15.8, 16.5, 17.9, 19.3 and 21.0°CA with 0.1, 0.2, 0.3, 0.4 and 0.5 kg/h, respectively. This increased ID may be attributed to the deficiency of fresh air as well as the high auto-ignition temperature of HEB (gaseous fuel). Whereas, the ID period enhanced from 10.5°CA with B20 to 11.2, 11.9, 13.3, 14.7 and 16.4°CA with 0.1, 0.2, 0.3, 0.4 and 0.5 kg/h, respectively, at 3.5 bar bmep. The charge physical properties were also altered by gaseous fuel induction which led to pre-mature ignition due to intermediate compound formation prior to the B20 fuel injection.

Fig. 4.30 (a) shows the variation of PCP with bmep for diesel and diesel-HEB, and Fig. 4.30 (b) for B20 and B20-HEB fuel modes. With increased bmep (0 to 3.5 bar), the PCP increased, because of the earlier combustion led to reduce ID period and hence increases PCP (Liew et al., 2010). At no load condition, 40.6 bar PCP was observed in diesel mode, and then it increased to 52.6 bar at 3.5 bar bmep. While the PCP was found lower for neat diesel operation when compared to B20. With B20 fuel, the PCP was observed to be 43.7and 52.9 bar at 0 and 3.5 bar bmep, respectively. This was due to the reduction in ID period with B20 fuel, which led to an advanced combustion process. Further, the injection of gaseous fuel (HEB) along with fresh air shows a positive effect on PCP values, because of the presence of highly flammable gas (H_2) in

gaseous fuel. At 3.5 bar bmep, the PCP increased to 55.0 bar with HEB flow rate (0.5 kg/h) from 52.6 bar with diesel fuel. Under same loading conditions, the PCP increased to 53.8 bar with HEB flow rate (0.5 kg/h) from 52.9 bar with B20 fuel.

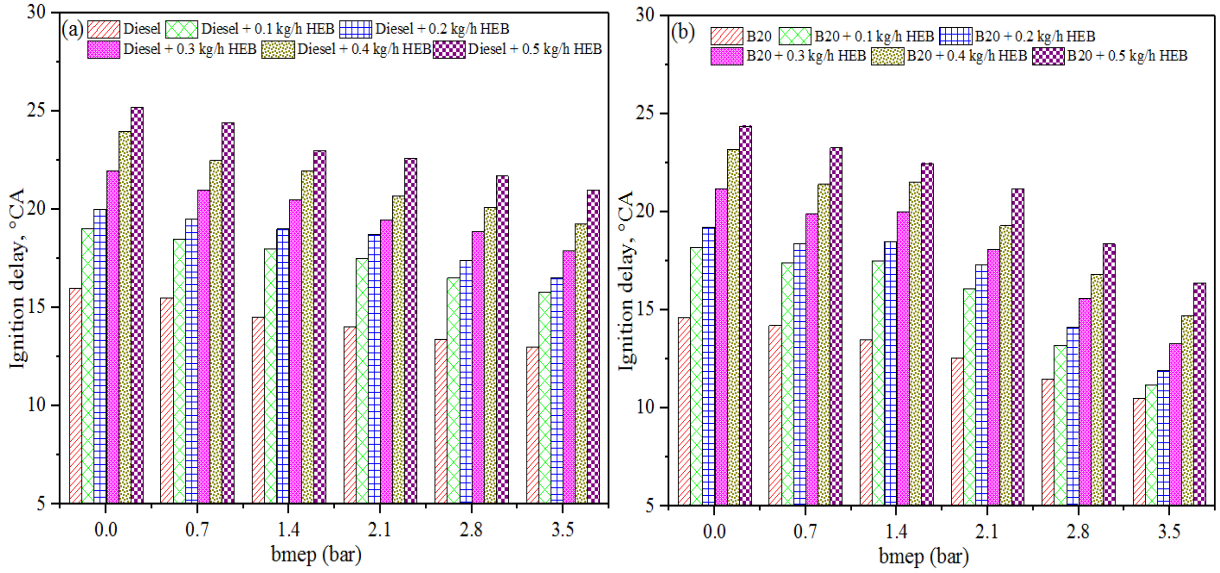

Fig.4.29. Variation of ignition delay with bmep (a) Diesel and Diesel-HEB; (b) B20 and B20-HEB fuel modes

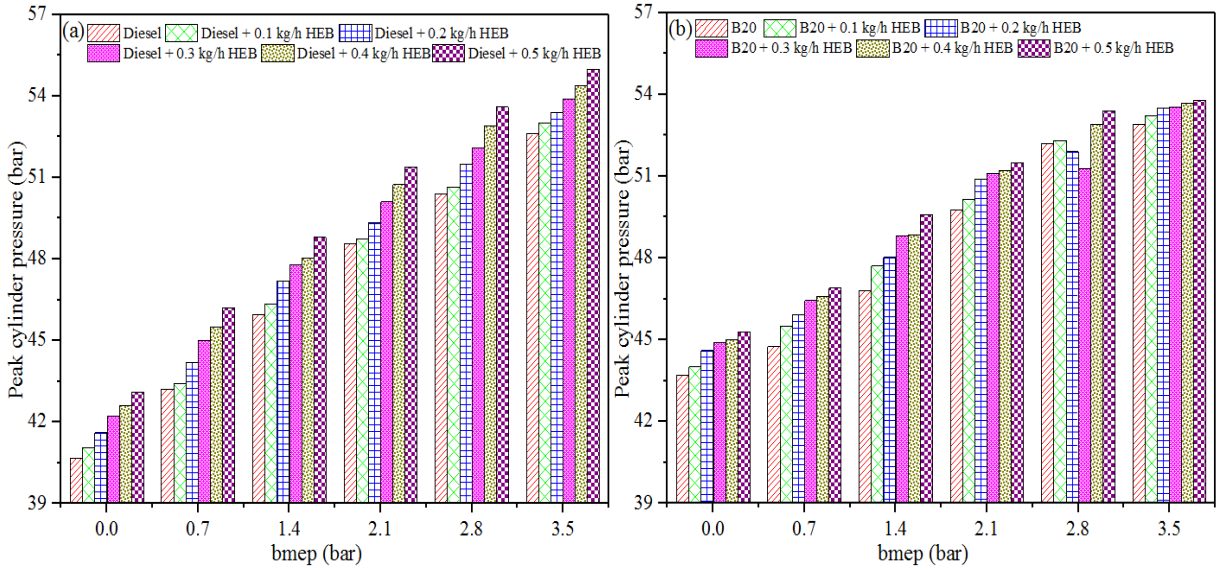

Fig.4.30. Variation of peak cylinder pressure with bmep (a) Diesel and Diesel-HEB; (b) B20 and B20-HEB fuel modes

The CP and NHRR are considered as important parameters to predict the combustion behavior inside the engine cylinder. Fig. 4.31 (a) depicts the change in cylinder pressure with degree crank angles (°CA) at 3.5 bar bmep for diesel and diesel-HEB, and Fig. 4.31 (b) for B20 and B20-HEB fuel modes. Results demonstrated that the B20 fuel provides higher CP when compared to diesel. Since the density of B20 fuel (861 kg/m^3) is higher than diesel (840 kg/m^3), so more quantity of fuel burning takes place in the initial stage of combustion, providing higher CP. It was also observed that dual fuel modes offer high CP and NHRR when compared to single fuel mode. This increment in CP and NHRR was attributed to higher heating value of HEB (57.0 MJ/Kg) when compared to diesel (42.0 MJ/Kg) and B20 (41.4 MJ/Kg). The increased NHRR with increasing CA was clearly evident from Fig. 4.32 (a) & (b). The flame speed of H_2 (292 cm/s) is around eight times higher than diesel (38 cm/s) at ambient conditions (Karim et al., 1980). For this reason, the interval between pilot fuel injection and peak heat release decrease which subsequently increase the PCP and NHRR, closer to top dead centre of engine cylinder (Gunea et al., 1998).

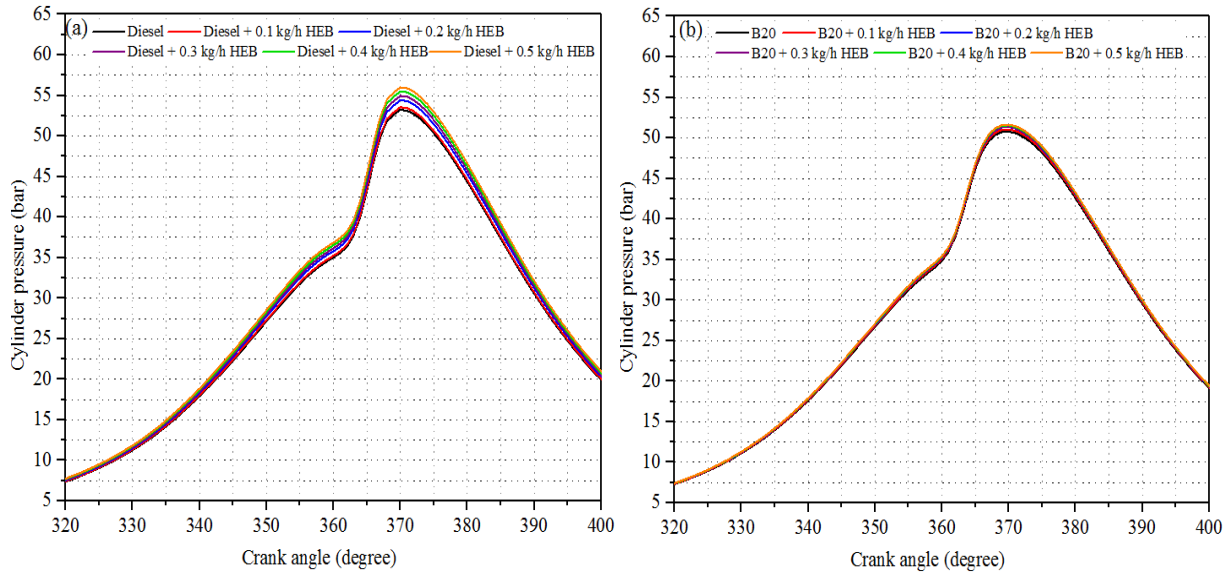

Fig.4.31. Variation of cylinder pressure with crank angle at 3.5 bmep (full load) (a) Diesel-HEB; (b) B20-HEB fuel modes

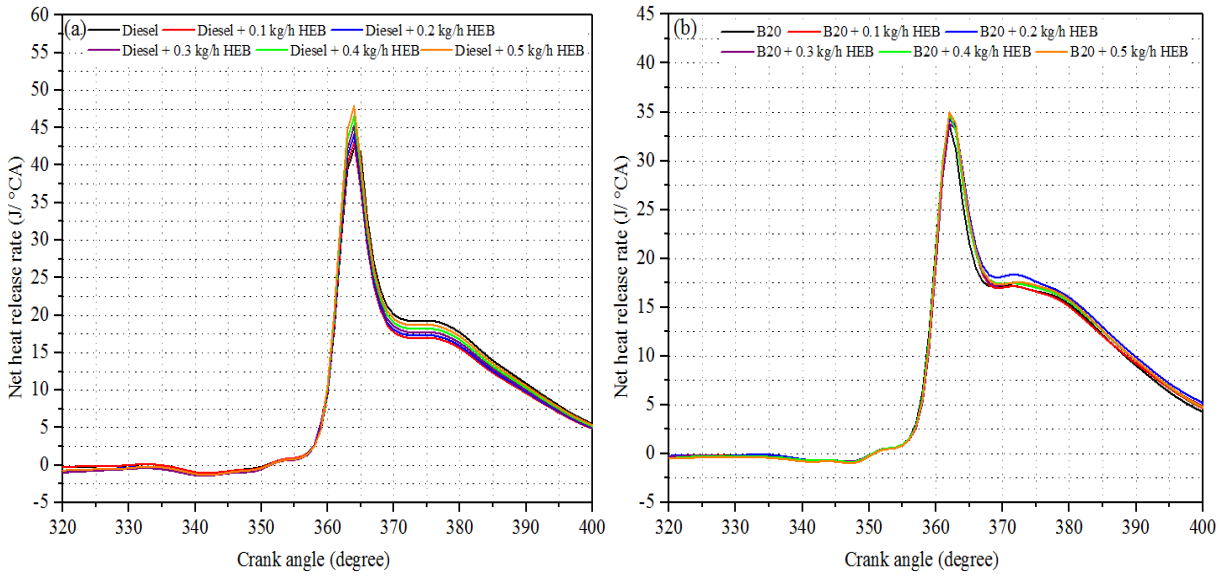

Fig.4.32. Variation of net heat release rate with crank angle at 3.5 bmep (full load) (a) Diesel-HEB; (b) B20 and B20-HEB fuel modes

H_2 is the highly combustible gas present in HEB which significantly affects the combustion under dual fuel modes. Moreover, HEB combusted with diesel fuel becomes leaner and have developed multiple flames at low velocities, led to stoichiometric premixed combustion (Birtas et al., 2011). This led to decreased NHRR after TDC in dual fuel mode of operations. The maximum NHRR for diesel was estimated to be 42.2 J/ °CA when compared to 43.0, 44.1, 45.2, 46.4 and 47.8 J/ °CA for dual fuel mode at 0.1, 0.2, 0.3, 0.4 and 0.5 kg/h, respectively at 3.5 bar bmep. Whereas, the maximum NHRR for B20 was estimated to be 33.6 J/ °CA when compared to 33.8, 34.2, 34.4, 34.8 and 35.4 J/ °CA for dual fuel mode at 0.1, 0.2, 0.3, 0.4 and 0.5 kg/h, respectively at 3.5 bar bmep.

4.9.2. Performance analysis

4.9.2.1. Brake thermal efficiency

BTE is an important parameter used to predict the conversion efficiency of fuel energy into useful work. Fig. 4.33 (a) shows the variation in BTE with bmep for diesel and diesel-HEB, and Fig. 4.33 (b) for B20 and B20-HEB fuel modes. Results showed that BTE increased with increasing bmep (0 to 3.5 bar) for all tested fuel modes. BTE of diesel was found to be 13.5% at 0.7 bar bmep, whereas it enhanced to 31.9% at 3.5 bar bmep, which may be attributed to

increasing power output with respect to load. The BTE of B20 was observed to be 12.7 % at 0.7 bar bmep, and it increased to 33.2% at 3.5 bar bmep. At lower bmep ranges (≤1.4 bar), the lower values of BTE was observed in B20 fuel as compared to diesel.

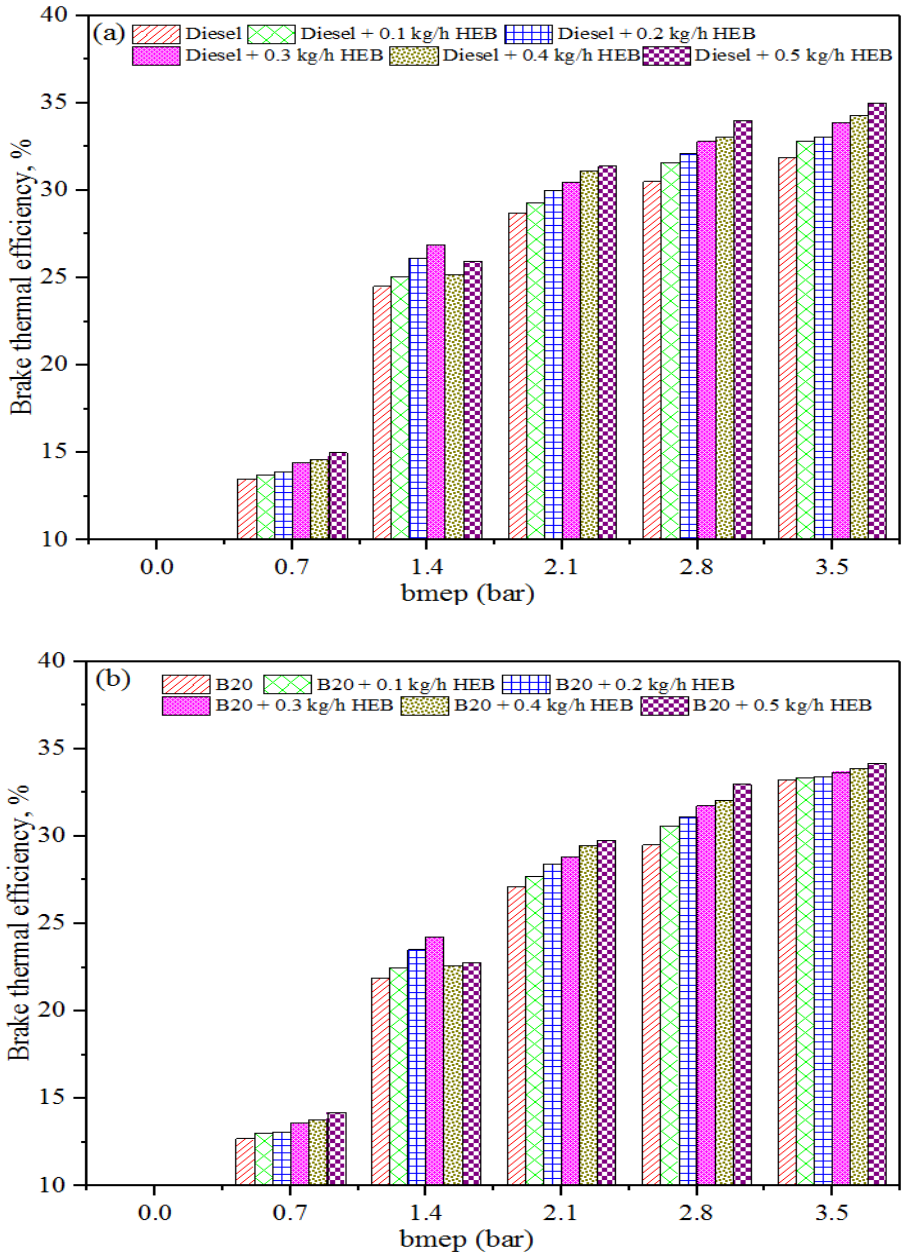

Fig. 4.33. Effect of H_2-enriched biogas on BTE (a) Diesel and Diesel-HEB; (b) B20 and B20-HEB fuel modes

This reduction in BTE values was due to poor combustion characteristics owing to higher density/viscosity, as well as poor volatility of B20 fuel when compared to diesel. The viscosity

and density of B20 started decreasing with increasing bmep which leads to the improvement in BTE (Antunes et al., 2009). The BTE was further increases with dual fuel mode of operations when compared to single mode (diesel/B20) at load conditions. At 2.1 bar bmep, the maximum BTE were observed to be 29.3, 29.9, 30.4, 31.5, and 31.4% with dual fuel mode over 0.1, 0.2, 0.3, 0.4 and 0.5 kg/h flow rate of HEB, respectively, while 28.7% was identified in diesel fuel. This improved BTE with HEB injection under dual fuel mode was due to better fuel combustion owing to the unique characteristics of H_2 presence in HEB gaseous fuel (Sahoo et al., 2011). The BTE increased with HEB induction; consistency of these results was verified with the increase of NHRR by injecting HEB which further reduces the fuel chemical energy and thereby BTE was increased (Hernandez et al., 2016). Moreover, no significant difference in BTE values was observed at higher bmep (3.5 bar). Under same loading conditions, the maximum BTE were observed to be 27.7, 28.3, 28.8, 29.5, and 29.9% with dual fuel mode over 0.1, 0.2, 0.3, 0.4 and 0.5 kg/h flow rate of HEB, respectively, while 27.1% was identified in B20 fuel.

4.9.2.2. Brake specific energy consumption

Fig. 4.34 (a) shows the variation in BSEC with bmep for diesel and diesel-HEB, and Fig. 4.34 (b) for B20 and B20-HEB fuel modes. BSEC values are mainly dependent on BTE; mathematically: BSEC is inversely proportional to BTE. Results illustrated that BSEC decreased with increasing bmep for all tested fuels. BSEC of diesel was calculated to be 26.6 MJ/kW h at 0.7 bar bmep, then it declined to 11.2 MJ/kW h at 3.5 bar bmep. This was due to improved BTE with increasing engine loads; higher BTE values result in lower BSEC. With B20, the BSEC was estimated to be 28.2 MJ/kW h at 0.7 bar bmep, then it declined to 10.8 MJ/kW h at 3.5 bar bmep. Under dual fuel mode of operations, the values of BSEC were found lower than single mode at loading conditions. At 2.1 bar bmep, the attained values of BSEC were: 12.3, 12.0, 11.8, 11.6 and 11.5 MJ/kW h with dual fuel mode over 0.1, 0.2, 0.3, 0.4 and 0.5 kg/h flow rate of HEB, respectively, while 12.5 MJ/kW h was obtained in diesel fuel. The higher BSEC of single (Diesel/B20) fuel indicates larger fuel consumption for obtaining the same power output as compared to dual fuel mode (Wong et al., 1999). The heating value of HEB (57.0 MJ/Kg) is higher than diesel (42.0 MJ/Kg) and B20 (41.4 MJ/Kg), which indicates less amount of fuel (HEB) is required to get the same power output. With increasing HEB flow rates, the decline trends in BSEC were observed in comparison to diesel.

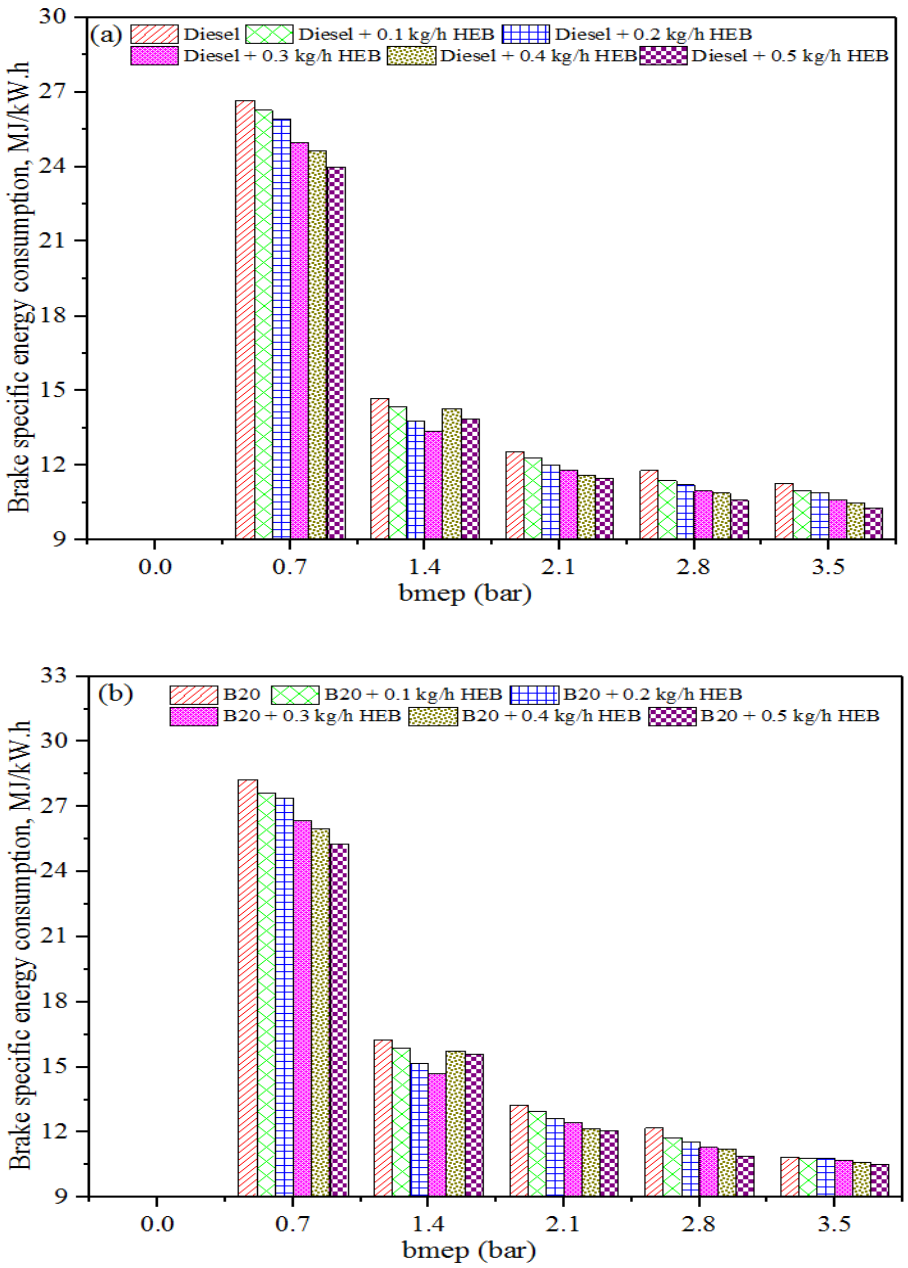

Fig. 4.34. Effect of H_2-enriched biogas on BSEC (a) Diesel and Diesel-HEB; (b) B20 and B20-HEB fuel modes

4.9.2.3. Exhaust gas temperature

Fig. 4.35 (a) shows the variation of EGT with bmep for diesel and diesel-HEB, and Fig. 4.35 (b) for B20 and B20-HEB fuel modes. Result showed that the EGT increased with increasing bmep from 0 to 3.5 bar for all tested fuel modes. At no load condition, the EGT was measured as

126°C for diesel fuel, and it rises (275°C) with increased bmep (3.5 bar). However, the lower values of EGT were observed in diesel when compared to B20 fuel. With B20 fuel, the EGT values were observed to be 128 and 280°C corresponding to 0 and 3.5 bar bmep, respectively. B20 comprise poor volatility constituents that burn in the post-combustion phase, resulting in higher EGT when compared to diesel. Under dual fuel modes, the EGT value becomes higher, which is an indication of more amount of energy released at the end of expansion stroke. Also, it may be due to faster combustion rates over higher HEB flows. In diesel-HEB dual fuel modes, the EGT was about 280, 284, 287, 291, and 295°C under 0.1, 0.2, 0.3, 0.4 and 0.5 kg/h flow rates of HEB, respectively at 3.5 bar bmep. In case of B20-HEB operations, at lower HEB flow ranges (≤ 0.2 kg/h); the EGT value becomes less which is an indication of less amount of energy released at the end of expansion stroke. It then increased at higher flow rates (≥ 0.40 LPM), due to the faster combustion rates over higher HEB flows. EGT was about 289, 293, and 299 °C under 0.3, 0.4 and 0.5 kg/g flow rates of HEB, respectively at 3.5 bar bmep.

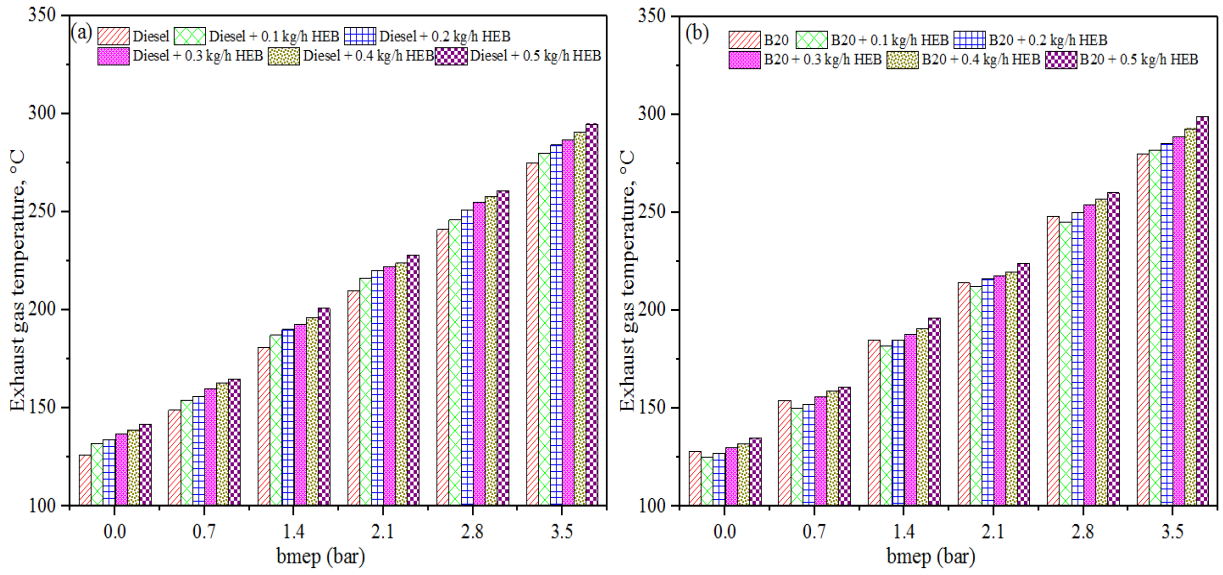

Fig. 4.35. Effect of H_2-enriched biogas on EGT (a) Diesel and Diesel-HEB; (b) B20 and B20-HEB fuel modes

4.9.3. Emission analysis

4.9.3.1. HC emissions

Fig. 4.36 (a) shows the variation in HC emissions with bmep for diesel and diesel-HEB, and Fig. 4.36 (b) for B20 and B20-HEB fuel modes. For all tested fuel modes, HC emissions decrease with an increasing bmep (up to 2.1 bar) and thereafter, it increased at elevated bmep (≥ 2.8 bar). At lower bmep (≤ 2.1 bar), the reduction in HC emissions may be due to increasing in-cylinder wall temperature with increased engine loads. At higher bmep, the increment in HC emissions was due to oxygen deficiency (rich mixture zone).The HC emissions values were measured to be 24, 20, 18, 17, 19 and 26 ppm at 0, 0.7, 1.4, 2.1, 2.8 and 3.5 bar bmep, respectively for diesel fuel. Also, the HC emissions were found less in B20 fuel when compared to diesel. This reduction in HC emissions with B20 fuel was due to the enhanced oxygen content of B20 fuel which led to providing smother and complete fuel combustion. With B20 fuel, the assessed HC emissions were: 23, 18, 17, 16, 19 and 28 ppm at 0, 0.7, 1.4, 2.1, 2.8 and 3.5 bar bmep, respectively. Further, it was observed that injecting HEB (gaseous fuel) in CI under dual fuel mode decreases the HC emission continuously. This reduction in HC emissions could be due to the presence of H_2 gas in HEB, which has high flame speed (2.92 m/s), while, for diesel (0.38 m/s). Under dual fuel mode, this higher flame velocity of H_2 leads quick and complete oxidation of the charge (Diesel-HEB-air) which further declines the HC emissions (Azimov et al., 2011). The recorded HC emissions were: 21, 19, 18, 17 and 16 ppm at 0.1, 0.2, 0.3, 0.4 and 0.5 kg/h flow rates of HEB, respectively at no load conditions. Whereas, at higher bmep; the increment in HC emissions was due to oxygen deficiency (rich mixture zone). At no load conditions, the HC emissions values were measured to be 14, 13, 12, 11 and 10ppmat0.1, 0.2, 0.3, 0.4 and 0.5 kg/h flow rates of HEB, respectively for B20.

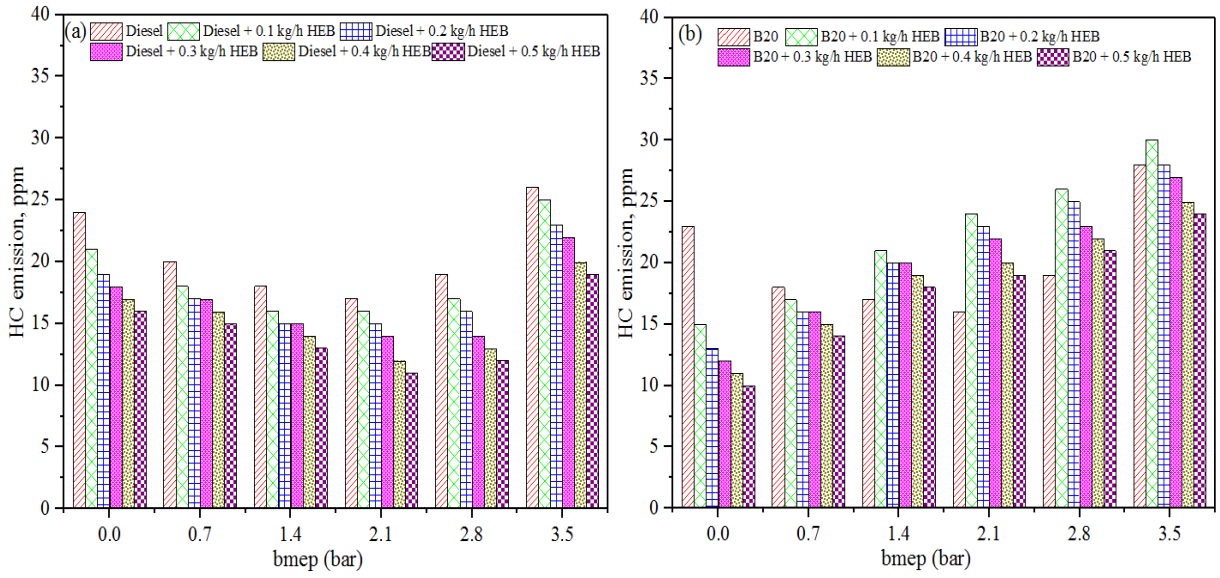

Fig. 4.36. Variation in HC emissions with bmep for (a) Diesel and Diesel-HEB; (b) B20 and B20-HEB fuel modes

4.9.3.2. NOx emissions

Fig. 4.37 (a) shows the variation in NOx emissions with bmep for Diesel and Diesel-HEB, and Fig. 4.37 (b) for B20 and B20-HEB fuel modes. Results demonstrated that the NOx emissions increased with increasing bmep (0 to 3.5 bar). In diesel operations, the NOx emission was found to be 46 ppm at 0 bar bmep, whereas it increased to 199 ppm at 3.5 bar bmep. This increase in NOx emissions was due to enhanced combustion temperature with respect to engine load (Bedoya et al., 2009). The formation of NOx was higher in B20 fuel as compared to diesel. This was due to improved combustion characteristics with B20, which led to enhances in-cylinder combustion temperature (Talibi et al., 2017). With B20 fuel, the NOx emission was observed to be 83 ppm at 0 bar bmep, and it increased to 363 ppm at 3.5 bar bmep. Further, the formation of NOx under dual fuel modes found lower, which may be likely due to the presence of inbuilt CO gas in HEB. The NOx emissions values were assessed to be 190, 183, 181, 170, and 166 ppm under 0.1, 0.2, 0.3, 0.4 and 0.5 kg/h flow rates of HEB, respectively at 3.5 bar bmep. Under same loading conditions, the assessed NOx emissions with B20 (pilot fuel) were: 354, 347, 345, 334, and 330 ppm under 0.1, 0.2, 0.3, 0.4 and 0.5 kg/h flow rates of HEB, respectively. This increased NOx emission was due to the improved combustion characteristics with B20, which led to offered high combustion temperature inside the engine cylinder (Wong et al., 1999).

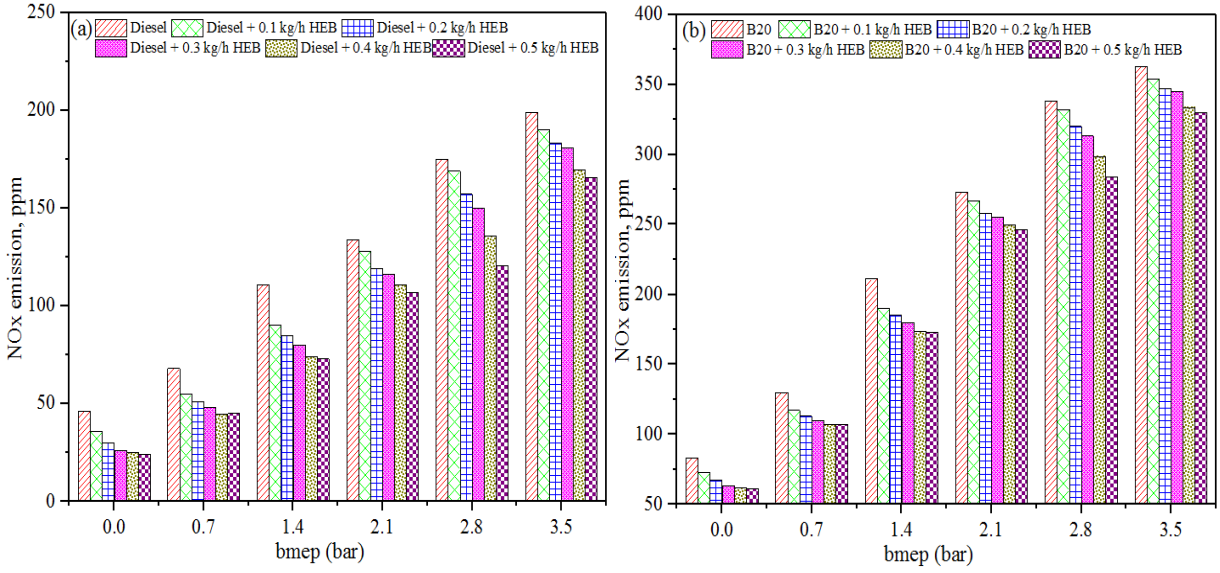

Fig. 4.37. Variation in NOx emissions with bmep for (a) Diesel and Diesel-HEB; (b) B20 and B20-HEB fuel modes

4.9.3.3. CO emissions

Fig. 4.38 (a) provides the variation of CO emissions with bmep for diesel and diesel-HEB, and Fig. 4.38 (b) for B20 and B20-HEB fuel modes. It was observed that the CO emissions decreased up to bmep (≤ 1.4 bar) and then, it increased with increasing bmep (≥ 2.1 bar). At lower bmep (≤ 1.4 bar), the decrease in CO emissions was caused of better fuel combustion which led to more conversion of CO to CO_2. For diesel operations, the assessed CO emissions were: 0.05% (at 0.7 bar bmep); 0.04 (at 1.4 bar bmep), whereas, 0.05, 0.06, and 0.07% CO emissions were observed at 2.1, 2.8, and 3.5 bar bmep, respectively for diesel fuel. With increasing bmep (≥2.1 bar), the excess fuel-air ratio not only led to increase smoke formation, but also prevents the oxidation of CO to CO_2; hence CO formation increased (Talibi et al., 2017). Moreover, the CO emissions found to be lower with B20 fuel than neat diesel at all bmep, indicating better fuel combustion (Saravanan et al., 2009). With B20 fuel, the measured CO emissions were: 0.06% (at 0.7 bar bmep); 0.05 (at 1.4 bar bmep), whereas, 0.06, 0.09, and 0.12 % CO emissions were observed at 2.1, 2.8, and 3.5 bar bmep, respectively. Further, HEB induction leads to increased CO emissions which were due to the presence of CO in HEB. At 3.5 bar bmep, the CO emission value was measured to be 0.11% at 0.5 kg/h flow rate of HEB; it is 0.04% higher when compared to diesel

(0.07 %). Under same loading conditions, the assessed CO emission was: 0.16% at 0.5 kg/h flow rate of HEB, which is 0.04% higher when compared to B20 (0.12%).

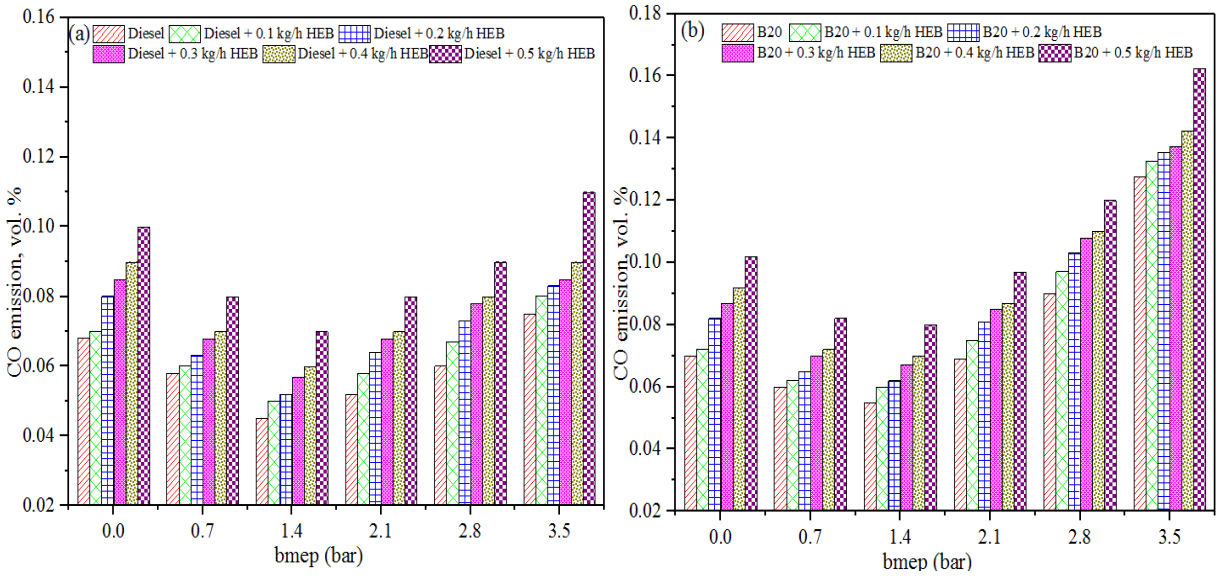

Fig. 4.38. Variation in CO emissions with bmep for (a) Diesel and Diesel-HEB; (b) B20 and B20-HEB fuel modes

4.9.3.4. Smoke opacity

Fig. 4.39 (a) depicts the variation of smoke opacity with bmep for Diesel and Diesel-HEB, and Fig. 4.39 (b) for B20 and B20-HEB fuel modes. Smoke emission occurs mainly in that region where insufficient O_2 is available for fuel combustion. It was inferred from results that smoke level increased with increasing bmep (engine loads). The measured smoke opacities were: 9.3, 13.3, 25.1, 30.8, 38.2, and 54.0% at 0, 0.7, 2.1, 2.8, and 3.5 bar bmep, respectively for Diesel fuel. With increasing bmep, the AFR led to decreased which further increase the smoke opacity at higher bmep (Chintala et al., 2014).Moreover, the smoke opacities decreased with B20 fuel at all bmep with respect to diesel. This effect may be due to more oxygen content in B20 fuel, which led to oxidize the soot in CI engine and reduces smoke level consequently. With B20 fuel, the assessed smoke opacities were: 5.2, 8.1, 10.8, 15.2, 18.5, and 27.6% at 0, 0.7, 2.1, 2.8, and 3.5 bar bmep, respectively. The smoke level values decreased sufficiently with the addition of HEB under dual fuel modes, which may be due to increased homogeneity degree in the charge (air-fuel). At 3.5 bar bmep, the smoke opacities were observed to be 49.0, 44.0, 42.3, 41.1, and 40.0% under 0.1, 0.2, 0.3, 0.4 and 0.5 kg/h flow rates of HEB, respectively in diesel-HEB dual

fuel operations. Under same loading conditions, the measured smoke opacities B20-HEB dual fuel operations were: 25.0, 22.4, 21.6, 20.9, and 20.0% under 0.1, 0.2, 0.3, 0.4 and 0.5 kg/h flow rates of HEB, respectively.

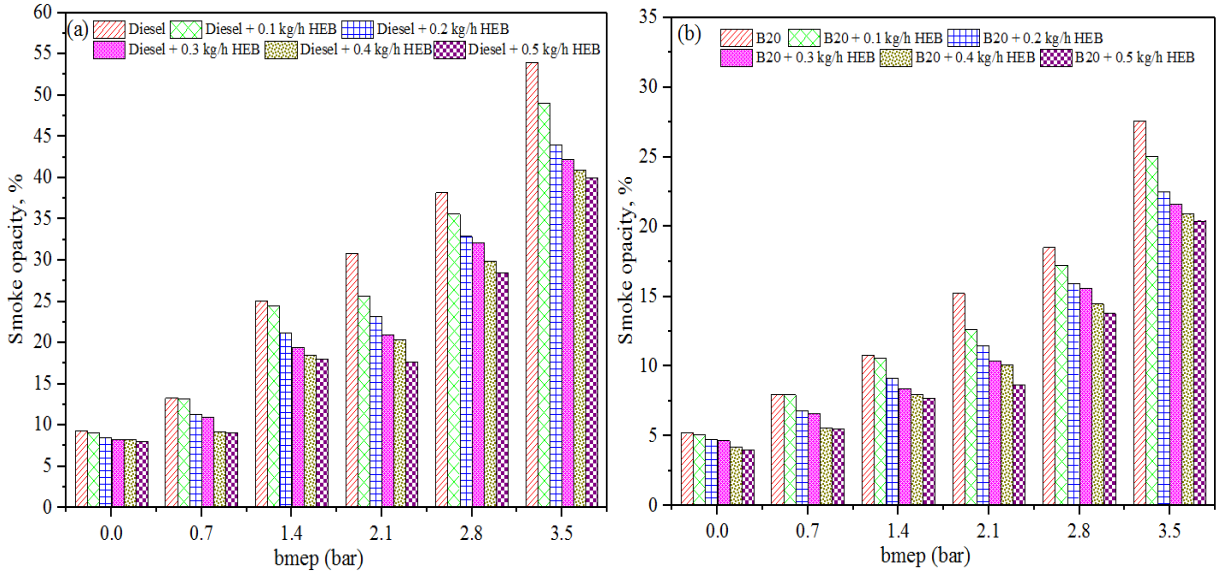

Fig. 4.39. Variation in smoke opacity with bmep for (a) Diesel and Diesel-HEB; (b) B20 and B20-HEB fuel modes

4.9.4. Noise level

Fig. 4.40 (a) illustrates the variation of noise level with bmep for diesel and diesel-HEB, and Fig. 4.40 (b) for B20 and B20-HEB fuel modes. Noise level increased with increasing bmep (engine loads). The assessed noise levels were: 91.2, 94.7, 96.4, 97.3, 98.5 and 99.1 dB at 0, 0.7, 2.1, 2.8, and 3.5 bar bmep, respectively for diesel fuel. The noise levels increased with B20 fuel at all bmep with respect to diesel. With B20 fuel, the observed noise levels were: 93.7, 95.1, 97.1, 97.9, 98.3 and 100 dB at 0, 0.7, 2.1, 2.8, and 3.5 bar bmep, respectively. The noise level values increased sufficiently with the addition of HEB under dual fuel modes when compared to single fuel mode (diesel/B20), which may be due to enhanced combustion inside the engine cylinder. At 3.5 bar bmep, the noise levels were assessed to be 97.2, 97.5, 95.5, 97.7 and 99.3 dB under 0.1, 0.2, 0.3, 0.4 and 0.5 kg/h flow rates of HEB, respectively in diesel-HEB dual fuel operations. Under same loading conditions, the measured smoke opacities B20-HEB dual fuel operations were: 101.5, 101.7, 102.0, 104.0 and 99.7 dB under 0.1, 0.2, 0.3, 0.4 and 0.5 kg/h flow rates of HEB, respectively.

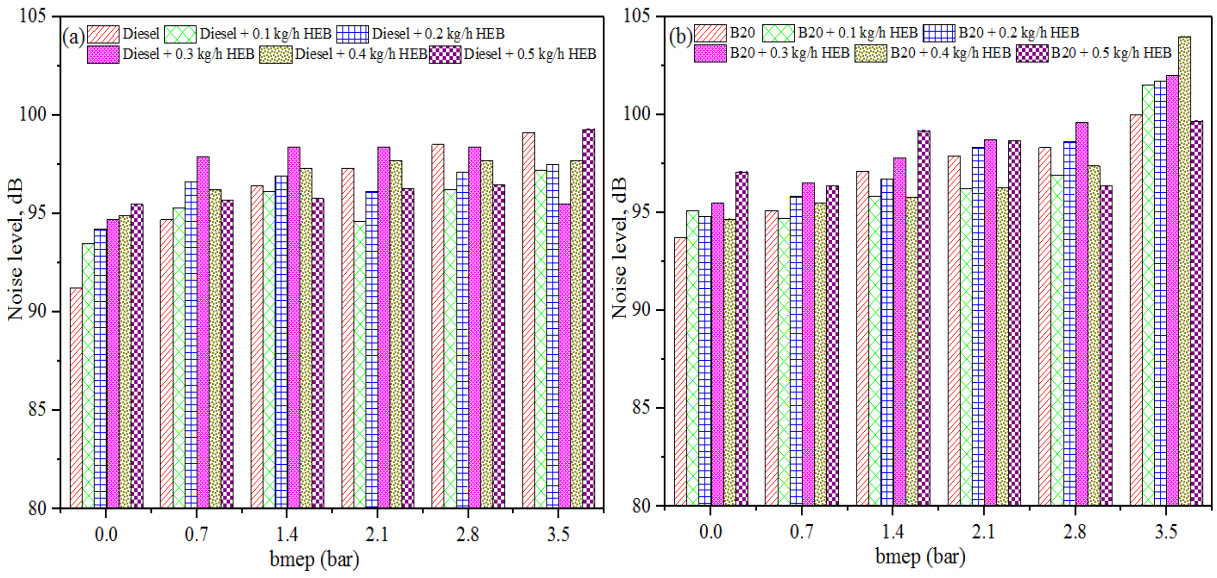

Fig. 4.40. Noise level variations with bmep for (a) Diesel and Diesel-HEB; (b) B20 and B20-HEB fuel modes

4.10. Effects of compression ratio on engine characteristics under Diesel-HEB and B20-HEB dual fuel modes

Previous results revealed that engine performance improves with increasing HEB flow (0.3 to 0.5 kg/h) rates under dual fuel modes with diesel and B20 pilot fuels. Herewith, the effect of compression ratios on the various engine characteristics was examined by choosing higher compression ratios (16:1, 17:1 and 18:1) over 0.5 kg/h HEB flow rate, which are close to standard (17:1) CR of engine.

4.10.1. Combustion analysis

Ignition delay (ID) period is an important parameter that fundamentally influences the combustion of any fuel. Fig. 4.41 (a) depicts the variation of ID period with bmep and CR for diesel-HEB, and Fig. 4.41 (b) for B20-HEB dual fuel modes. It was seen that for both dual (diesel-HEB and B20-HEB) fuel modes the ID period becomes higher at low bmep, thereafter, it starts reducing with increasing bmep from 0 to 3.5 bar. At lower engine loads, the prolonged ID was due to lower combustion temperature inside the engine cylinder, whereas lower ID period at elevated bmep indicates higher gas and cylinder wall temperature (Kumar et al., 2014). At 16:1

CR and 0 bar bmep, the ID period was observed as 26.9°CA, whereas, at 3.5 bar bmep, it becomes decreased to 22.9°CA (Fig. 4.41 (a)). Under same conditions, the ID periods observed were 26.0 and 21.9°CA corresponding to 0 and 3.5 bar bmep for B20-HEB dual fuel mode of operations. The higher cetane number of B20 fuel as compared to diesel could be attributed to providing lower ID values. Thereafter, the ID period decreased continuously with increasing CR from 16:1 to 18:1 in both tested dual fuel modes. For Diesel-HEB dual fuel mode, the ID decreased from 25.1°CA with CR (16:1) to 24.2 and 22.0°CA with 17:1 and 18:1 CRs, respectively at 1.4 bar bmep. Similarly, it decreased from 24.2°CA with CR (16:1) to 23.5 and 21.2°CA with 17:1 and 18:1 CRs, respectively at 1.4 bar bmep under B20-HEB dual fuel modes. This reduction in ID may be due to enhanced in-cylinder pressure and temperature by increasing CR (16:1 to 18:1) which resulted in improving combustion with the efficient oxidation of HEB. The charge physical properties of pilot fuel alter by gaseous fuel induction which led to pre-mature ignition due to intermediate compound formation prior to the pilot fuel injection.

The injection of gaseous fuel (HEB) along with fresh air shows a positive effect on PCP values, because of the presence of highly flammable gas (H_2) in gaseous fuel. The PCP was found to increase with increasing bmep and CR, as seen in Fig. 4.42 (a) and (b) for diesel-HEB and B20-HEB dual fuels, respectively. This increment in PCP could be due to decrease in the distance between piston top and cylinder head (i.e. clearance volume). At no load and diesel-HEB dual fuel mode, 36.0 bar PCP was observed in CR (16:1), and then it increased to 47.1 bar at 3.5 bar bmep. Similarly, the PCP values 36.8 and 48.1 bar corresponding to 0 and 3.5 bar bmep, respectively, were identified under B20-HEB dual fuel modes. Further, the increasing CR (16:1 to 18:1) leads to increase compression pressure which subsequently brings up the PCP during combustion. For example, the PCP increased from 41.6 bar with CR (16:1) to 45.3 and 49.5 bar with 17:1 and 18:1 CRs, respectively at 1.4 bar bmep (Fig. 4.42 (a)). For B20-HEB dual fuel mode, the PCP decreased from 41.7 bar with CR (16:1) to 45.7 and 50.3 bar with 17:1 and 18:1 CRs, respectively at 1.4 bar bmep.

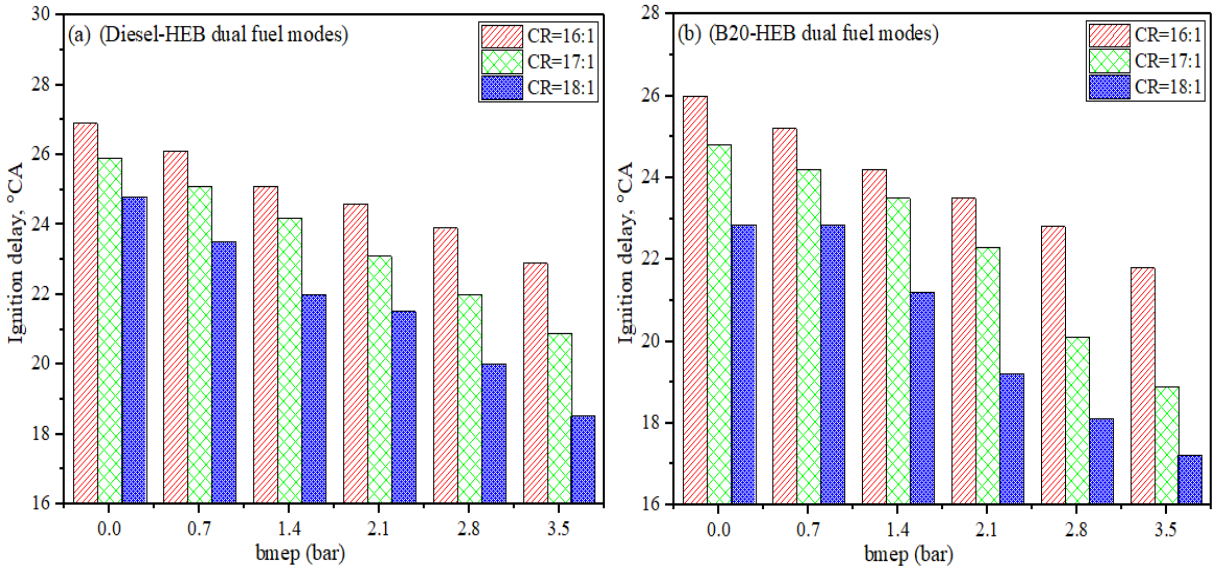

Fig.4.41. Variation of ignition delay with bmep at different CRs (a) Diesel-HEB; (b) B20-HEB fuel modes

Higher peak pressure demonstrates a large amount of fuel burned in the premixed combustion phase. Fig. 4.43 (a) and (b) depict the change in cylinder pressure (CP) for diesel-HEB and B20-HEB dual fuels, respectively related to crank angles (°CA) for CR (16:1 to 18:1) at 3.5 bar bmep. With increasing CR, the CP also increased at each crank angle which can be clearly seen from CP plot. At higher CR (≥17:1), the magnitude of CP peaks was identified greater than lower CR (16:1). The higher CR engines provide compressed HEB-air mixture charge with high density which leads to enhanced fuel atomization and thereby CP increases. Moreover, the increased NHRR with increasing CA was clearly evident from Fig. 4.44 for respective fuel modes. From NHRR plot, it can be clearly seen that the start of combustion (SOC) phase attains earlier at higher CR (18:1) than lower CR (16:1). As the NHRR curve magnitude for 16:1 CR becomes larger in comparison to 17:1 and 18:1 CRs. At 3.5 bar bmep, the maximum NHRR for CR was estimated to be 38.9 J/°CA, while, for 17:1 and 18:1 CR, 42.6 and 45.6 J/°CA, respectively values were identified (Fig. 4.44 (a)). Similarly, 40.1, 38.5 and 33.15 J/°CA values of NHRR were observed with 16:1, 17:1 and 18:1 CR, respectively under B20-HEB dual fuel modes.

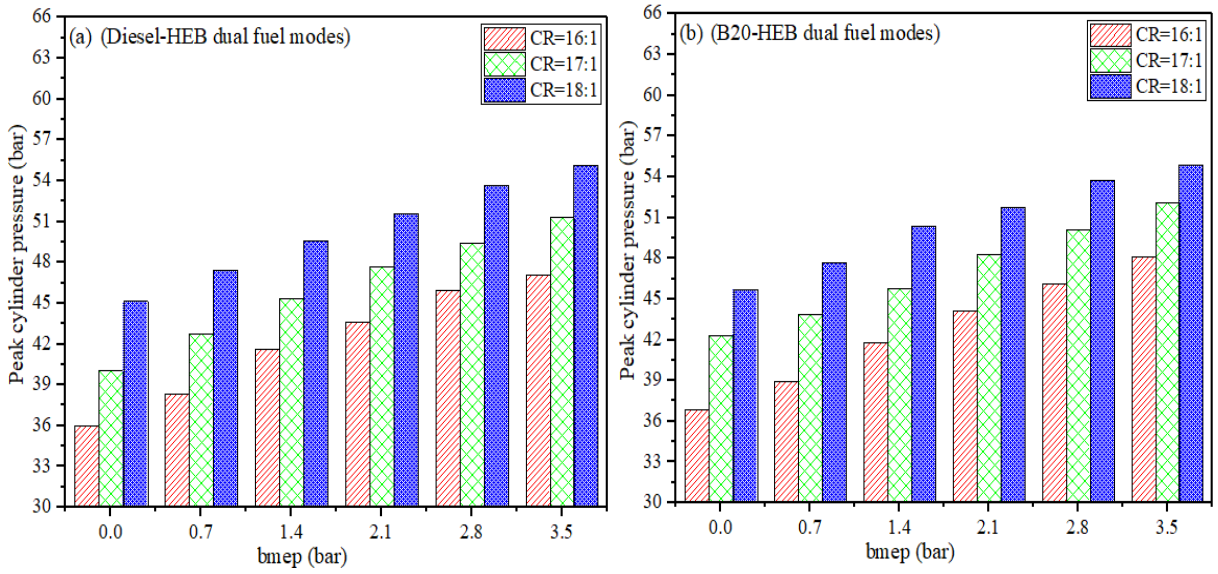

Fig.4.42. Variation of peak cylinder pressure with bmep at different CRs (a) Diesel-HEB; (b) B20-HEB fuel modes

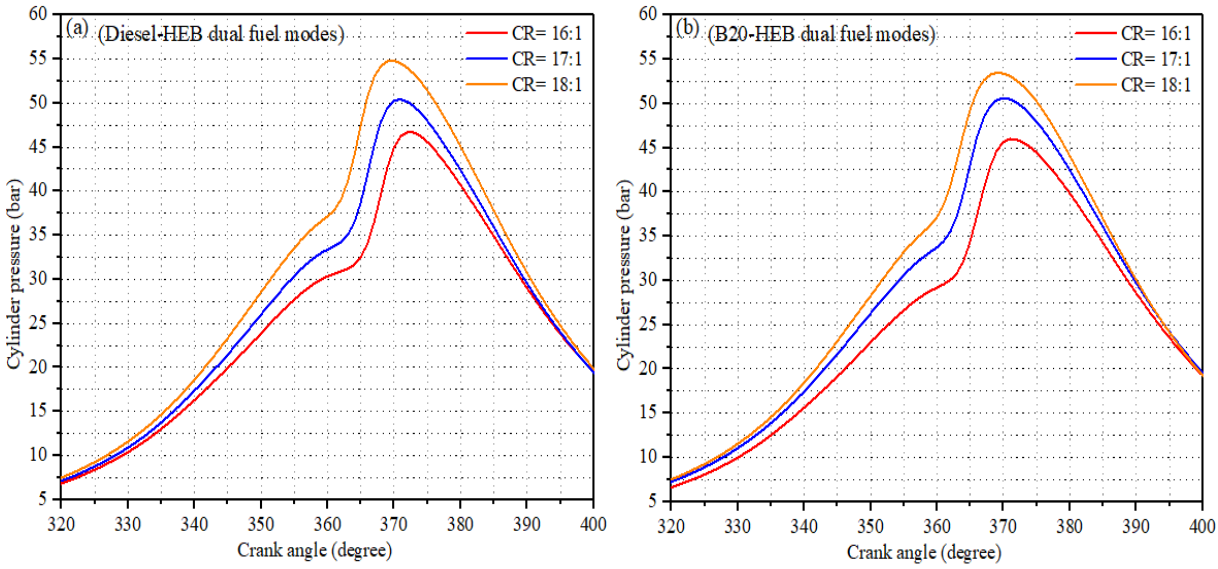

Fig.4.43. Variation of cylinder pressure with crank angle at 3.5 bmep for different CRs (full load) (a) Diesel-HEB; (b) B20-HEB fuel modes

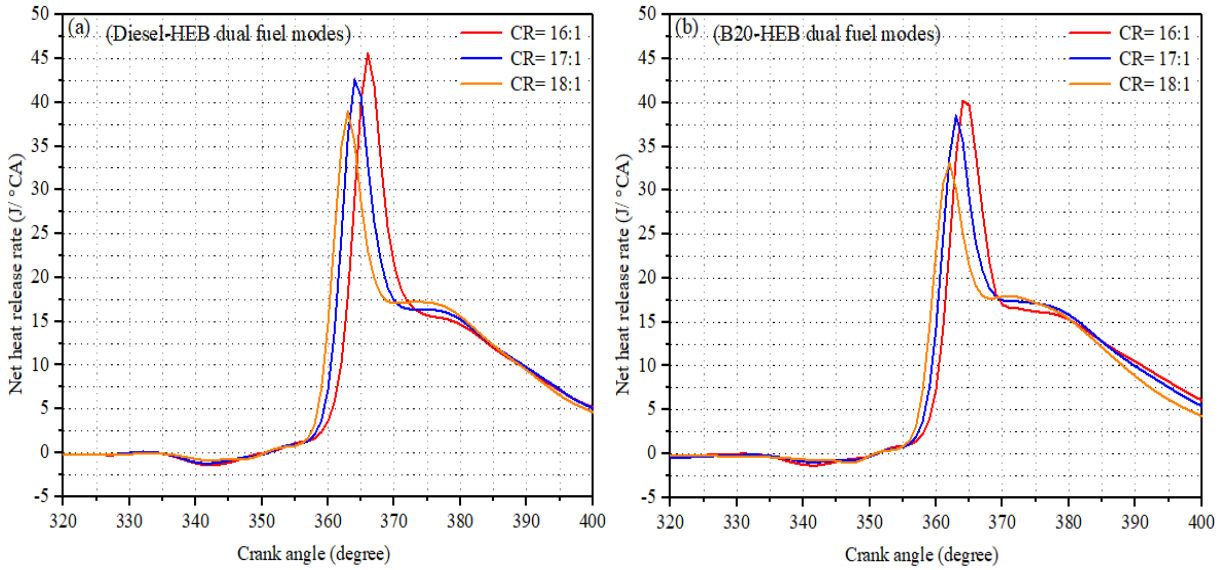

Fig.4.44. Variation of net heat release rate with crank angle at 3.5 bmep for different CRs (full load) (a) Diesel-HEB; (b) B20-HEB fuel modes

4.10.2. Performance analysis

4.10.2.1. Brake thermal efficiency

Fig. 4.45 (a) and (b) illustrate the substantial improvement in BTE with increasing CR (16:1 to 18:1) and bmep (0 to 3.5 bar) for diesel-HEB and B20-HEB dual fuel modes, respectively. With increased bmep (0 to 3.5 bar), the BTE improved consequently because increased loads lead to produce more brake power. At CR (16:1) and diesel-HEB dual fuel modes, the observed BTE values were: 12.1, 22.1, 27.2, 29.1 and 32.0% corresponding to 0.7, 1.4, 2.1, 2.8 and 3.5 bar bmep, respectively. Whereas, 11.2, 18.9, 25.6, 28.1 and 30.8% BTE at 0.7, 1.4, 2.1, 2.8 and 3.5 bar bmep, respectively, were obtained under B20-HEB dual fuel modes over 16:1 CR. The lower values of BTE were found in B20-HEB fuel when compared to diesel-HEB, which may be due to lower heating value of B20 fuel than diesel. Meanwhile, BTE increased further under both tested duel fuel modes, with increasing CR, which was due to better combustion followed by higher temperature and pressure. At 3.5 bar bmep, the BTE found an increase to 36.1 and 34.4% for 17:1 and 18:1 CRs, respectively when compared to 16:1 CR (32.0 %), seen in Fig. 4.45 (a). Rapid mixing behaviour of HEB leads to attaining homogeneous mixture (HEB-air) formation. Moreover, increasing CR enhances the in-cylinder pressure and

temperature, which results in improve engine BTE. Similarly, 30.8, 32.8 and 34.9% values of BTE were obtained with 16:1, 17:1 and 18:1 CR, respectively under B20-HEB dual fuel modes at 3.5 bar bmep.

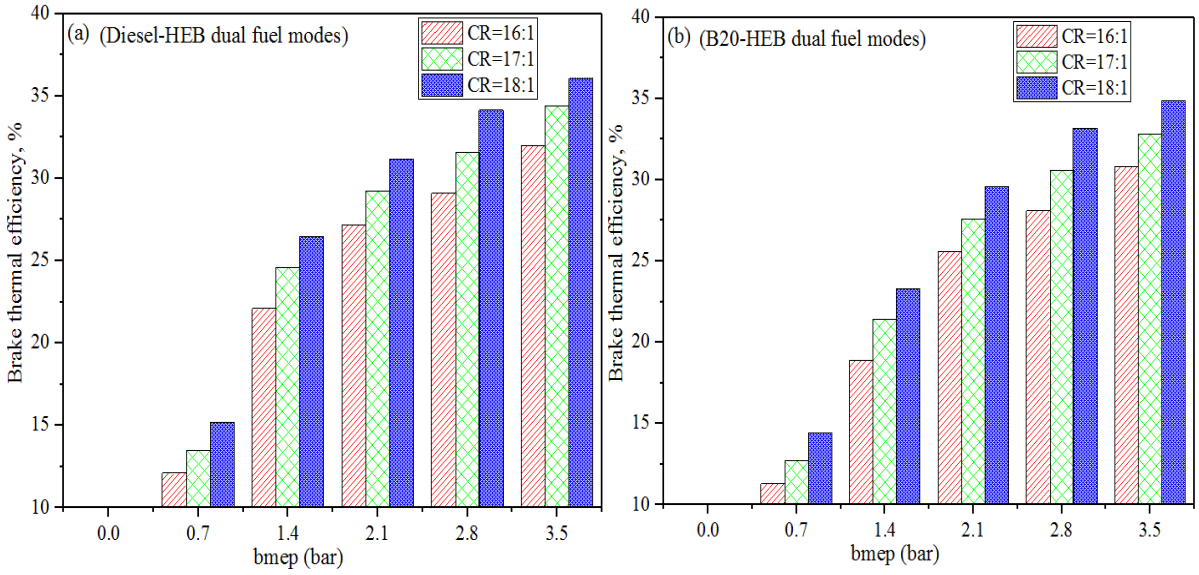

Fig. 4.45. Effect of CRs on BTE (a) Diesel-HEB; (b) B20-HEB fuel modes

4.10.2.2. Brake specific energy consumption

The effect of CR and bmep on BSEC is depicted in Fig. 4.46 (a) and (b) for diesel-HEB and B20-HEB dual fuel modes, respectively, which clearly demonstrates that with increasing CR and bmep reduces BSEC proportionally. For diesel-HEB dual fuel modes at CR (16:1), the BSEC was calculated be 29.7 MJ/kW h at 0.7 bar bmep, then it declined to 11.2 MJ/kW h at 3.5 bar bmep. This was due to improved BTE with increasing engine loads; higher BTE values result in lower BSEC. Similarly, 31.7 (at 0 bar bmep) and 11.7 (at 3.5 bar bmep) MJ/kW h values of BSEC were observed under B20-HEB dual fuel modes at CR (16:1). At higher CRs (≥17:1), the values of BSEC were found to be higher than lower CR (16:1). Specifically, at 1.4 bar bmep, the BSEC decreased from 16.2 MJ/kW h with CR (16:1) to 14.6 and 13.5 MJ/kW h with 17:1 and 18:1 CRs, respectively (Fig. 4.46 (a)). It is inferred from this observation of BSEC that less amount of fuel is required at higher CRs (≥17:1) to obtain same power output when compared to lower CR (16:1). Under B20-HEB dual fuel modes and 1.4 bar bmep; 18.6, 16.5 and 15.2 MJ/kW h of BSEC were attained at 16:1, 17:1 and 18:1 CRs, respectively.

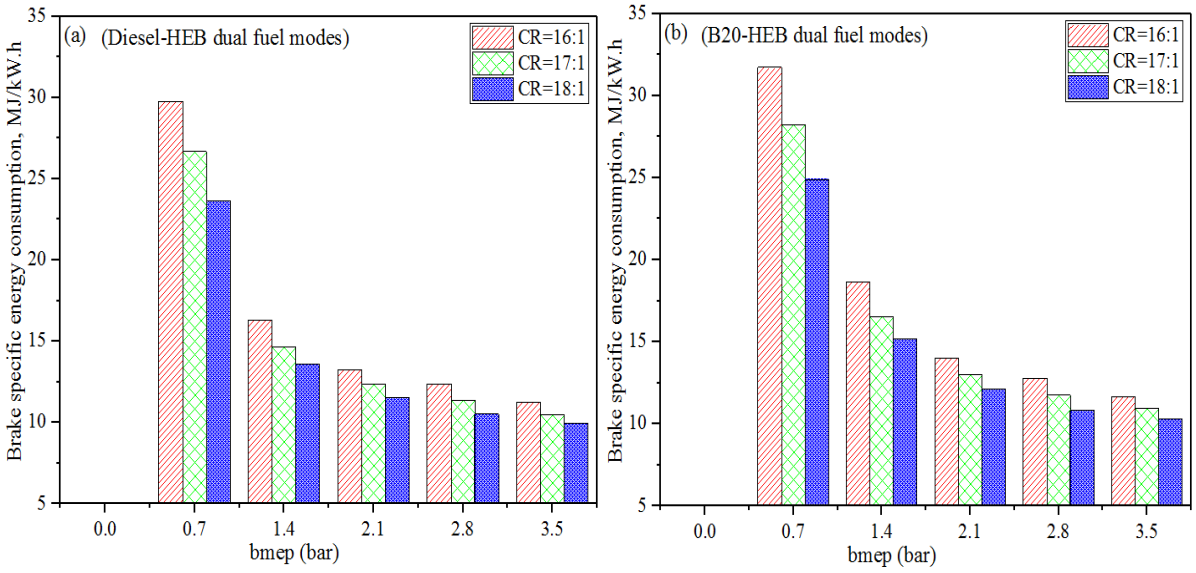

Fig. 4.46. Effect of CRs on BSEC (a) Diesel-HEB; (b) B20-HEB fuel modes

4.10.2.3. Exhaust gas temperature

Fig. 4.47 (a) and (b) illustrate the variation in EGT at different CR and bmep for diesel-HEB and B20-HEB dual fuel modes, respectively. Experimental observation reveals that EGT increases with an increase in bmep from 0 to 3.5 bar, because total energy input increases with increasing loads. For diesel-HEB and 0 bar bmep, the EGT was assessed as 150°C with CR (16:1), and then it increased to 309°C at 3.5 bar bmep. However, the EGT values were found be lower in B20-HEB dual fuel mode of operations as compared to diesel-HEB. For example, at 16:1 CR, 148 and 314°C of EGT were assessed at 0 and 3.5 bar bmep, respectively in B20-HEB dual fuel modes. With respect to bmep over all CRs i.e. 16:1, 17:1 and 18:1, the EGT follows the same trends for both tested dual fuel modes. Further, at higher CR, the reduction in EGT was observed; at 3.5 bar bmep, 300 and 280°C with 17:1 and 18:1 CR, respectively, whereas, with 16:1 CR it observed 309°C (Fig. 4.47 (a)). This reduction in EGT at higher CRs was due to reduced ID period, which shifts the combustion process towards expansion stroke; thereby EGT reduces. Under B20-HEB dual fuel modes and 3.5 bar bmep; 314, 305 and 285°C of EGT were measured at 16:1, 17:1 and 18:1 CRs, respectively.

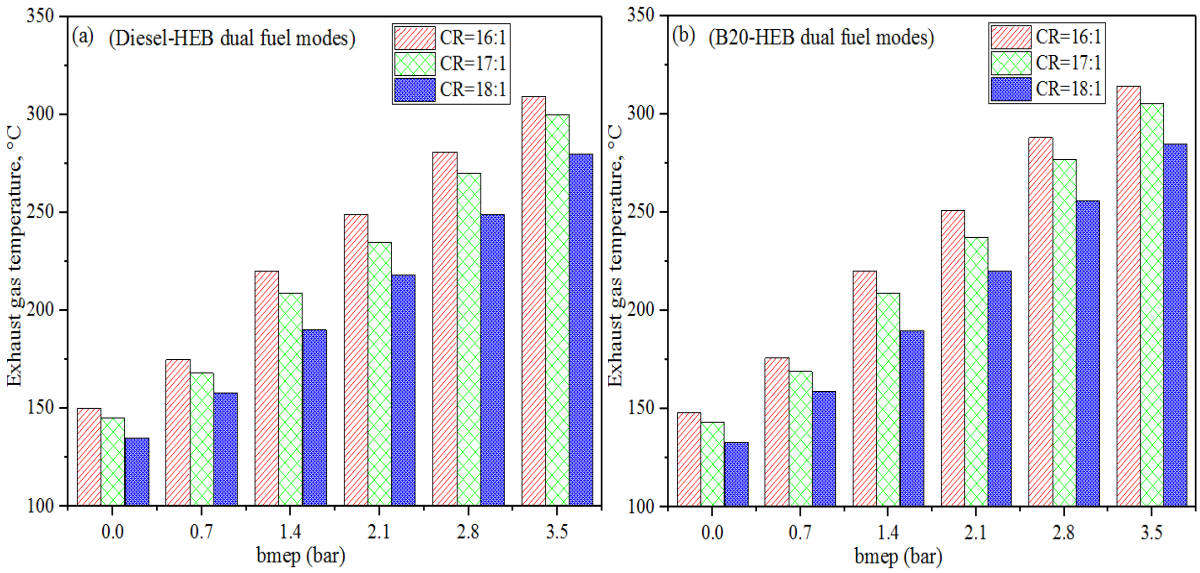

Fig. 4.47. Effect of CRs on EGT (a) Diesel-HEB; (b) B20-HEB fuel modes

4.10.3. Emission analysis

4.10.3.1. HC emissions

Fig. 4.48 (a) and (b) depict the variation of HC emissions with bmep and CR for diesel-HEB and B20-HEB dual fuel modes, respectively. Results demonstrated that the HC emissions decreased with increasing bmep up to 2.1 bar and after that, a steady rise was seen at higher bmep (≥ 2.8 bar). This reduction in HC emission was due to improved oxidation of fuel at elevated bmep; higher HC emission after particular engine load or certain extent of bmep was due to the deficiency of oxygen inside the engine cylinder (Koten et al., 2018). The recorded HC emissions were: 32, 27, 23, 22, 23 and 26 ppm at 0.7, 1.4, 2.1, 2.8 and 3.5 bar bmep, respectively at 16:1 CR (Fig. 4.48 (a)). Similarly, the assessed HC emissions for B20-HEB dual fuel modes were: 29, 25, 22, 20, 22 and 24 ppm at 0.7, 1.4, 2.1, 2.8 and 3.5 bar bmep, respectively at 16:1 CR. Meanwhile, the HC emissions were found to be lower in B20-HEB when compared to diesel-HEB dual fuel mode of operations. This may be due to enhanced oxygen content in B20 fuel in comparison to diesel. Further, the HC emissions decrease continuously with rising CR (16:1 to 18:1) in both tested dual fuel modes. Under diesel-HEB dual fuel modes and 1.4 bar bmep, 23, 20 and 18 ppm HC emissions were assessed at 16:1, 17:1 and 18:1 CR, respectively. With increased CR, the decreases in HC emission due to improved combustion process followed by

increased cylinder temperature. At 1.4 bar bmep, HC emissions reduced to 17 and 16 ppm with 17:1 and 18:1 CR, respectively, whereas, with 16:1 CR (22 ppm) (Fig. 4.48 (b)).

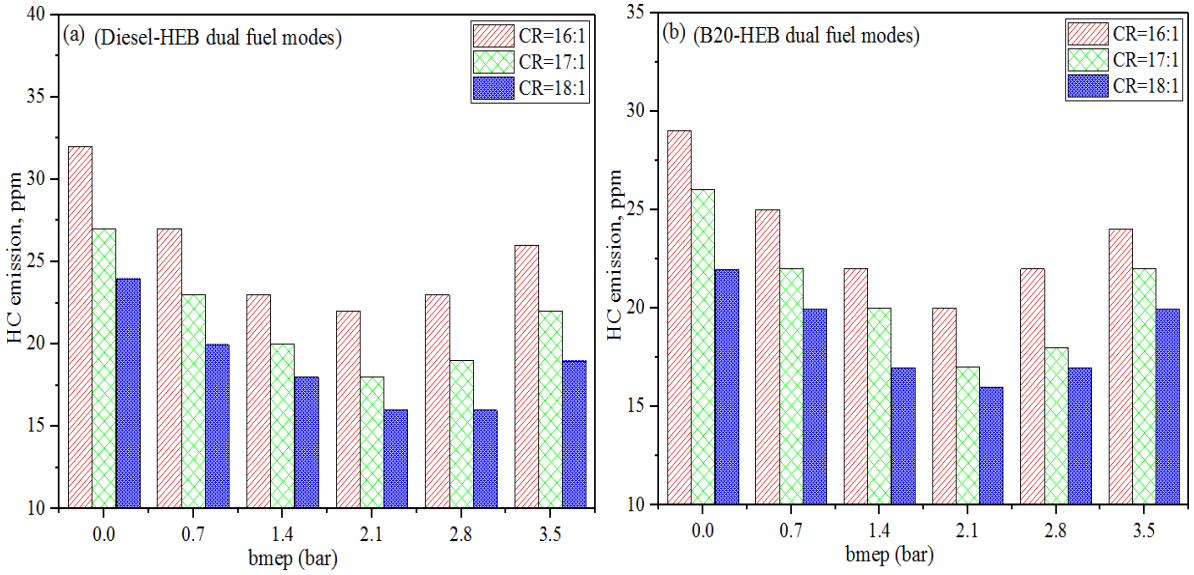

Fig. 4.48. HC emission variations at different CRs and bmep (a) Diesel-HEB; (b) B20-HEB fuel modes

4.10.3.2. NOx emissions

Fig. 4.49 (a) and (b) illustrate the variation in NOx emissions with bmep and CR for diesel-HEB and B20-HEB dual fuel modes, respectively. Result reveals that with increasing bmep, the NOx formation continuously increased. As NO_x formation mainly depend upon temperature and nitrogen availability in air during combustion (Bora et al., 2016). NOx emission increased with the rising bmep owing to high combustion temperature at elevated engine loads. The assessed NOx emissions were: 15, 36, 65, 91, 155 and 184 ppm at 0.7, 1.4, 2.1, 2.8 and 3.5 bar bmep, respectively at 16:1 CR (Fig. 4.49 (a)). The NOx formation was found to be higher in case of B20-HEB dual fuel operations than with diesel-HEB. Under B20-HEB dual fuel modes, the NOx emissions were observed to be 27, 40, 70, 101, 167 and 207 at 0.7, 1.4, 2.1, 2.8 and 3.5 bar bmep, respectively at 16:1 CR. Thereafter, the NOx emissions continuously increase with increasing CR from 16:1 to 18:1. This may be attributed to enlarged combustion temperature and pressure result from the reduced clearance volume at higher CR. At 3.5 bar bmep and diesel-HEB dual fuel modes, the NOx emissions measured were: 195 and 212 ppm for CR 17:1 and 18:1, respectively, while, 184 ppm was measured for 16:1 CR. At 3.5 bar bmep, NOx emissions

increased to 277 and 310 ppm with 17:1 and 18:1 CR, respectively, whereas, with 16:1 CR (207 ppm) in B20-HEB dual fuel modes.

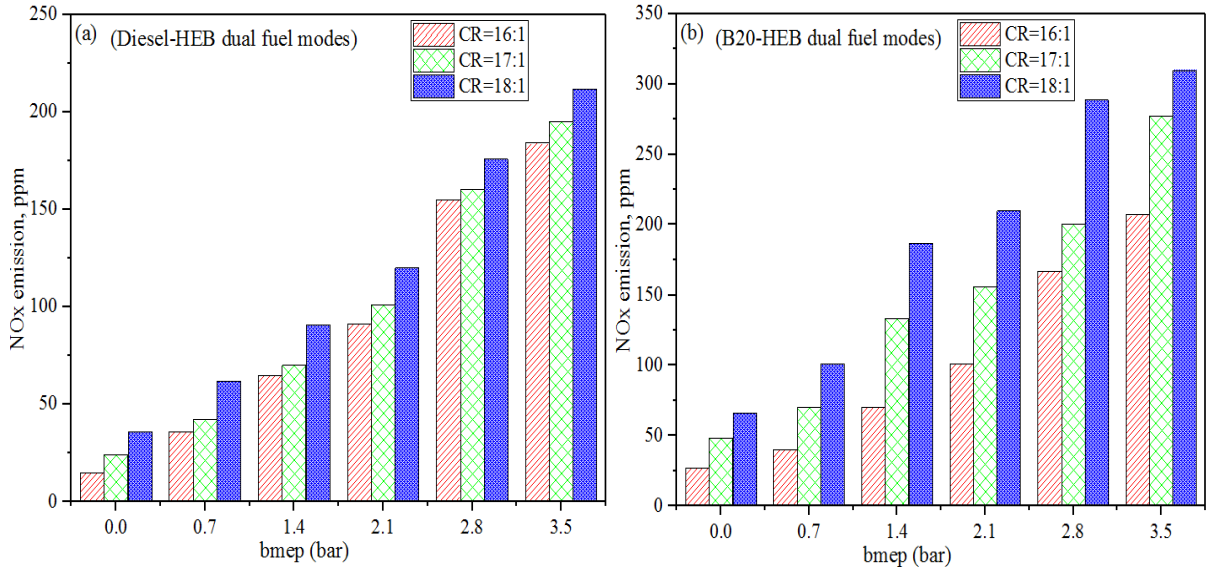

Fig. 4.49. NOx emission variations at different CRs and bmep (a) Diesel-HEB; (b) B20-HEB fuel modes

*4.10.3.3.*CO emissions

The CO emission results obtained at different bmep and CR for diesel-HEB and B20-HEB dual fuel modes were plotted in Fig. 4.50 (a) and (b), respectively. Results revealed that CO emissions continuously decrease with increasing bmep (up to 2.1 bar), thereafter, it rises up continually at higher bmep (≥ 2.8 bar). The CO emissions decreased to 0.10 from 0.12 % with increased bmep from 0 to 2.8 bar, while, it increased 0.13 % with 3.5 bar bmep (Fig. 4.50 (a)). This reduction in CO emissions due to improved combustion and lean air-fuel charge mixture, whereas, enhanced CO emissions observed at higher bmep owing to insufficient oxygen present inside the engine cylinder (Bora et al., 2017; Lal et al., 2017). Under B20-HEB dual fuel modes, the CO emissions were observed to be 0.13, 0.10, 0.08, 0.09, 0.14 and 0.18% at 0, 0.7, 1.4, 2.1, 2.8 and 3.5 bar bmep, respectively at 16:1 CR. Thereafter, the CO emissions declined further with increase in CR 18:1 when compared to 16:1 CR. At 3.5 bar bmep, the assessed CO emissions were: 0.11 and 0.09% with CR 17:1 and 18:1, respectively, whereas, 0.13 % was observed with 16:1 CR under diesel-HEB dual fuel modes. With increased CR (16:1 to 18:1), the in-cylinder combustion improved owing to enlarged combustion temperature and pressure, which further led to enhance

oxidation of carbon molecules present in the hydrocarbon fuel. Similarly, CO emissions decreased to 0.16 and 0.14 % with 17:1 and 18:1 CR, respectively, whereas, with 16:1 CR (0.18 %) under B20-HEB dual fuel modes.

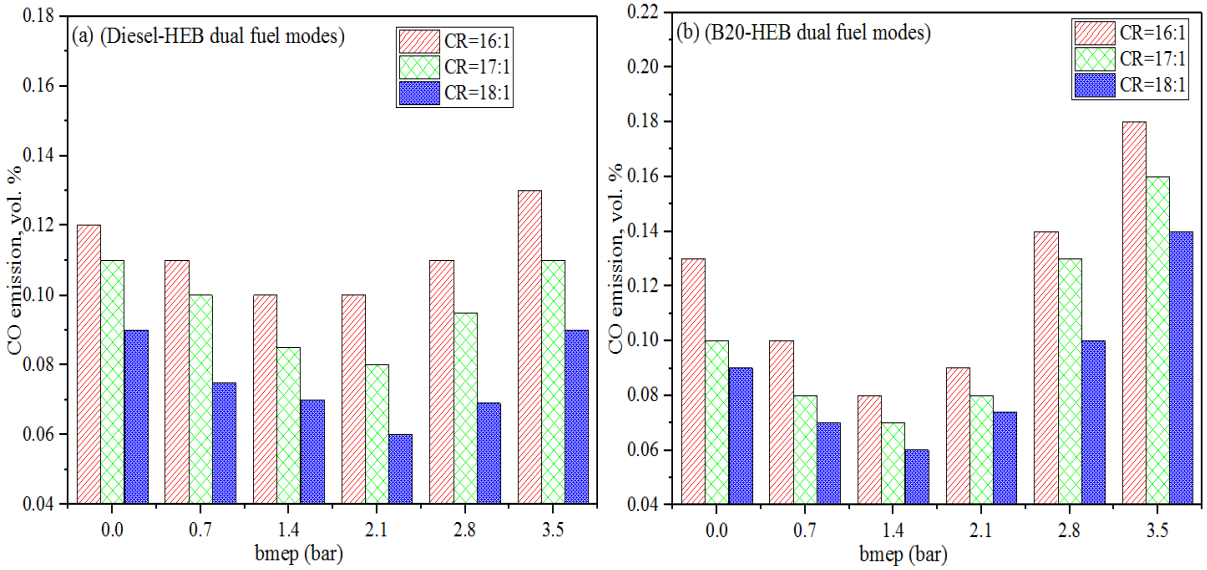

Fig. 4.50. CO emission variations at different CRs and bmep (a) Diesel-HEB; (b) B20-HEB fuel modes

4.10.3.4. Smoke opacity

Fig. 4.51 (a) and (b) depict the changes in smoke opacity with bmep and CR for diesel-HEB and B20-HEB dual fuel modes, respectively. Results demonstrated that the smoke opacity increases with increasing bmep from 0 to 3.5 bar. The smoke opacities observed were: 10.1, 12.2, 19.6, 23.8, 31.5 and 42.2% at 0.7, 1.4, 2.1, 2.8 and 3.5 bar bmep, respectively with CR (16:1) under diesel-HEB dual fuel modes. With increasing engine loads, the AFR decreased which further increase the smoke opacity at higher bmep. Similarly, the smoke opacities were observed to be 9.8, 11.5, 18.3, 21.1, 29.0 and 40.1% at 0, 0.7, 1.4, 2.1, 2.8 and 3.5 bar bmep, respectively at 16:1 CR (Fig. 4.51 (b)). This effect may be due to more oxygen content in B20 fuel, which led to oxidize the soot in CI engine and reduces smoke level consequently. With increased CR (16:1 to 18:1), the decline trends in smoke opacity were observed throughout the load spectrum in both tested dual fuel modes. At 3.5 bar bmep, the smoke opacities measured were 40 and 37% with CR 17:1 and 18:1, respectively, while, with CR (16:1) it was observed 42.2% (Fig. 4.51 (a)). The heat of compressed charge (HEB-air) increased with an increase in CR (16:1 to 18:1), which

further led to promote better fuel oxidation and subsequently reduce the smoke levels. Similarly, smoke opacities decreased to 38.1 and 26.0% with 17:1 and 18:1 CR, respectively, whereas, with 16:1 CR (40.1%) under B20-HEB dual fuel modes.

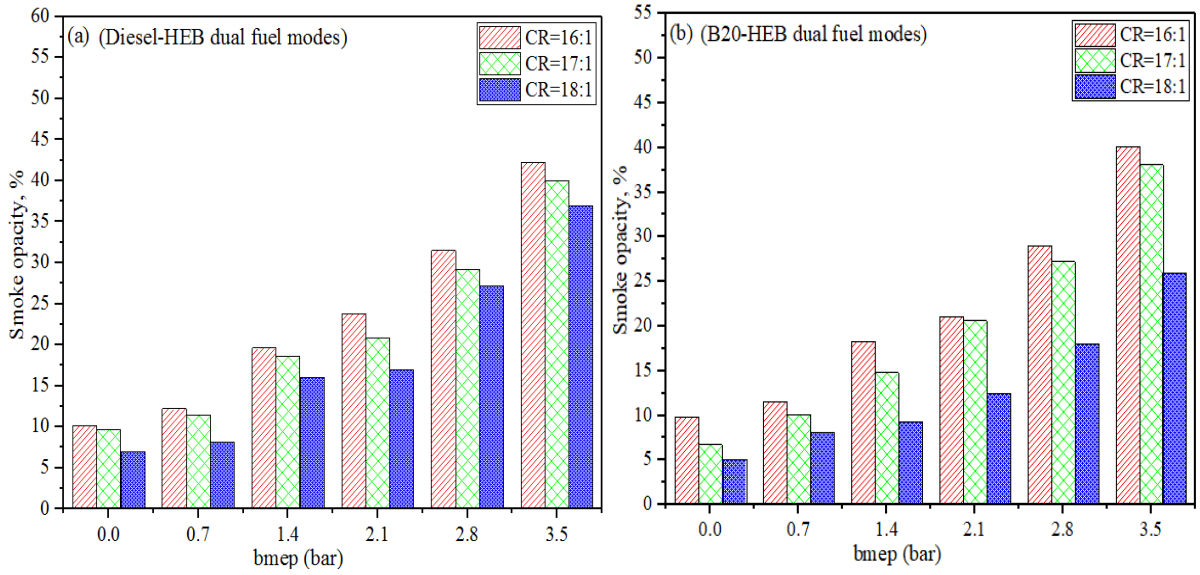

Fig. 4.51. Smoke opacity variations at different CRs and bmep (a) Diesel-HEB; (b) B20-HEB fuel modes

4.10.4. Noise level

Fig. 4.52 (a) and (b) illustrate the variations in noise level with bmep and CR for diesel-HEB and B20-HEB dual fuel modes, respectively. It can be seen from results that the noise level increased with increasing bmep from 0 to 3.5 bar. The noise levels assessed were: 94.1, 93.7, 95.3, 96.6, 96.8 and 96.1 dB at 0.7, 1.4, 2.1, 2.8 and 3.5 bar bmep, respectively with CR (16:1) under diesel-HEB dual fuel modes. Similarly, the noise levels were observed to be 93.0, 95.40, 96.3, 96.9, 97.4 and 98.0 dB at 0, 0.7, 1.4, 2.1, 2.8 and 3.5 bar bmep, respectively at 16:1 CR (Fig. 4.52 (b)). This effect may be due to more oxygen content in B20 fuel, which led to oxidize more fuel in CI engine and increases noise level consequently. With increased CR (16:1 to 17:1), the increment in noise level was observed throughout the load spectrum in both tested dual fuel modes. At 3.5 bar bmep, the noise levels measured were 96.3 and 96.2 dB with CR 17:1 and 18:1, respectively, while, with CR (16:1) it was observed 96.1 dB (Fig. 4.52 (a)). Similarly, noise levels increased to 99.3 and 99.2 dB with 17:1 and 18:1 CR, respectively, whereas, with 16:1 CR (98.0 dB) under B20-HEB dual fuel modes.

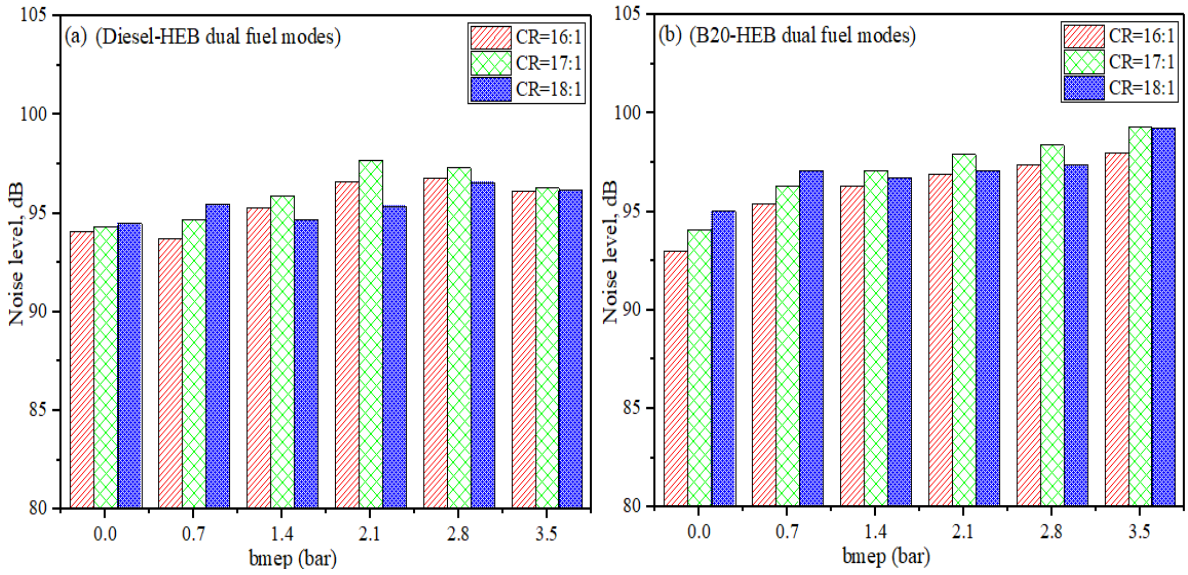

Fig. 4.52. Noise level variations at different CRs and bmep (a) Diesel-HEB; (b) B20-HEB fuel modes

Chapter-5

CONCLUSIONS

The present study dealt in two phases; initially with H_2 enrichment of synthetic biogas using DR and DOR with commercial (Ni) and synthesized catalysts. Thereafter, the produced H_2-enriched biogas (gaseous fuel) was utilized in dual fuel CI engine with Diesel and B20 pilot fuels.

- Ni nanopowder used as catalyst showed good H_2 enrichment in reforming process, but, higher activity was observed in DOR process due to the synergistic effect of reaction temperature and O_2 induction.
- Influence of reaction temperature was found strong on H_2/CO ratio in both (DR and DOR) reforming processes, whereas, WHSV showed variation in products yields. In DR, better catalytic performance was observed at high temperature and low WHSV.
- In DOR, the CH_4 conversion is largely depends on O_2/CH_4 ratio. DOR exhibited higher H_2 enrichment of biogas when compared to DR at high WHSV, with the added advantage of low SEC and carbon deposition values.
- As Ni content was increased from 11 to 19 wt. % on TiO_2 support. At 850°C, $Ni_{0.11}/TiO_2$ catalyst exhibited maximum CH_4 conversion of 70.5% with 32.0% H_2 enrichment in DR.
- CeO_2 addition into $Ni_{0.11}/ (Al_2O_3\text{-}TiO_2)$ catalyst not only enhanced the catalytic activity but also reduced the carbon deposition. Result ascertained that 20 and 30 wt. % Ce promoted catalysts offered same catalytic performance, but declined performance was observed in 30 wt. % at (≥750°C). It is concluded that the catalytic performance of Ni catalyst was effectively improved by adding of 20 wt. % Ce into $Al_2O_3\text{-}TiO_2$ support, with the additional advantage of low carbon deposition in the DR reactions.
- ZnO addition showed positive outcomes in increasing the activity and selectivity of reforming catalysts. The $Ni_{0.10}/ (Zn_{0.1}\text{-}Ce_{0.9})$ catalyst attained 83.1 and 97.0 % of maximum CH_4 and CO_2 conversion, respectively, with 40.3 % H_2 enrichment in DR reactions at 900°C. However, the reduced activity and performance was observed with increase in $Ni_{0.10}/ (Zn_{0.2}\text{-}Ce_{0.8})$ catalyst when compared to $Ni_{0.10}/ (Zn_{0.1}\text{-}Ce_{0.9})$ catalyst.

- B20 fuel has a high cetane number (53) when compared to diesel (48) which led to declined ID period at 17:1 CR. Higher CR (≥17:1) provides better fuel atomization which further reduced ID period in B20 fuel.
- Combustion started earlier with increased engine CR (16:1 to 18:1) in B20 fuel, which was due to enhanced in-cylinder temperature and pressure corresponding to higher CRs. At higher CR (18:1), the in-cylinder pressure and temperature became higher leading to earlier start of combustion; moreover, it also lowers the NHRR. With increasing CRs, the peak NHRR decreased, and the maximum values were: 40.1, 35.3 and 29.1 J/°CA for CRs 16:1, 17:1 and 18:1, respectively, while, 41.7 J/°CA for diesel (17:1 CR).
- PCP was found to be higher in case of B20 fuel when compared to neat diesel operation at CR (17:1). The PCP increased further with increasing CR (16:1 to 18:1) owing to the improved BTE at higher CRs. At 3.5 bar bmep, the PCP increased by 9.8 %, whereas, 14.9 % in BTE, by increasing CR from 16:1 to 18:1.
- The increment in BSFC values with B20 fuel was observed in comparison to diesel because of lower the heating value of B20 fuel. Also, B20 fuel offers high density (861 kg/m^3) value when compared to diesel (850 kg/m^3), resulting in poor B20-air mixing that leads to increased BSFC. With increasing CR (16:1 to 18:1) in B20, it was observed that the BSFC values reduced continuously due to improved combustion characteristics at higher CRs when compared to lower CR.
- HC, CO and smoke emissions reduced notably with B20 fuel when compared to neat diesel. This was due to enhanced oxygen content in B20 fuel which further led to providing smother and complete fuel combustion.
- NOx formation was found to be higher in case of B20 fuel in comparison to diesel due to higher combustion temperature. It further increased with increasing CR (16:1 to 18:1) which may be attributed to the enhancement in adiabatic flame temperature with increasing CR.
- ID period and PCP were found to be higher in HEB assisted dual fuel CI engine when compared to single (diesel and B20) mode.
- Under dual fuel mode (0.5 kg/h), at 3.5 bar bmep, higher value of BTE was obtained when compared to single mode, which may be attributed to higher NHRR, because of the higher diffusivity of HEB led to faster chemical reaction between fuels.

- Under various loading conditions, the HC and NOx emissions found to decrease continuously with increasing HEB (0.1 to 0.5 kg/h), however, CO emissions increased due to the presence of CO (40 %) in HEB.
- Smoke emissions decreased sufficiently with the addition of HEB under dual fuel modes which may be due to improved homogeneity degree in the charge with HEB injection.
- Injection of gaseous fuel (HEB) along with fresh air shows positive effect on PCP values, because of the presence of highly flammable gas (H_2) in gaseous fuel. At higher CR (≥17:1), the magnitude of CP peaks was identified greater than lower CR (16:1).
- With increasing CR, the combustion temperature and pressure increased which led to improved BTE. Reduction of harmful emissions (HC, CO, and smoke emissions) was observed with increasing CR (16:1 to 18:1).
- NOx formation was found higher with increasing CR, which was due to enlarged combustion temperature and pressure result from the reduced clearance volume at higher CR.

Future recommendations:

The present study highlighted the exploitation of biogas to produce H_2-enriched biogas, followed by its utilization in CI engine under dual fuel mode, but there are certain allied areas which need further attention:

- The catalytic performance of Ni catalyst was effectively improved by supporting metal oxides (CeO_2, Al_2O_3, TiO_2, and ZnO), with the additional advantage of low carbon deposition in the both reforming reactions. Thus, it is suggested that the optimized catalyst may be assessed for its activity & selectivity in reforming of real biogas to study the impact of catalyst poisoning gas like H_2S.
- Synthesis of catalysts using another techniques viz., wet impregnation and sol-gel methods, should be made, because dispersion of active sites is greatly influenced by the synthesis method. Moreover, a study by varying the variables (temperature, ramp rate, reduction temperature and stirring speed) involved in catalyst synthesis needs to done.
- Reaction repetitions can be performed by reactivating the deactivated catalysts to assess the activity recoverable after reactivation of catalyst.
- H_2 energy, additionally to hydro, biomass and solar, is also one of the long term renewable fuel. Nevertheless, the technologies for H_2 production at an affordable cost and safe storage are the great challenges for the utilization of H_2 in CI engines. Moreover, the transportation of H_2 needs standards related to safety aspects like safety distance for in/outdoor operations, refuelling rate, leakage sensing, etc. which needs to be formulated and notified to the public.
- The combustion characteristics of the engine powered with gaseous fuel will depends upon the injection duration and timing, therefore, their impact on combustion uniqueness of dual fuel CI engines need to be further explored.
- H_2 has faster burning rate which results in increase of in-cylinder temperature earlier during the power stroke and injected the pilot fuel towards the end of the injection stroke, so, alternative technology needs to be assessed and identified to overcome this issue.
- The detailed numerical and experimental studies with varying HEB compositions (by varying H_2 content) in CI engines and engine parameters need to be further evaluated.

References

1. 100% biogas for urban transport in Linkoping. Sweden biogas in buses, cars and trains. Biogas in the society Information from IEA bioenergy task 37 energy from biogas and landfill gas, http://www.iea-biogas.net/files/daten-redaktion/download/linkoping_final.pdf [Accessed 21.05.17].
2. A report of trends in global CO_2 emissions. PBL Netherlands environmental assessment agency, http://edgar.jrc.ec.europa.eu/news_docs/jrc-2015-trends-in-global-co2-emissions-2015-report-98184.pdf; 2015 [Assessed 23.07.16].
3. Abd Alla GH, Soliman HA, Badr OA, Abd Rabbo MF. Effect of pilot fuel quantity on the performance of a dual fuel engine. Energy Conversion and Management 2000;41:559-572.
4. Abd Alla GH, Soliman HA, Badr OA, Abd Rabbo MF. Effects of diluent admissions and intake air temperature in exhaust gas recirculation on the emissions of an indirect injection dual fuel engine. Energy Conversion and Management 2001;42:1033-1045.
5. Abdelaal MM, Rabee BA, Hegab AH. Effect of adding oxygen to the intake air on a dual-fuel engine performance, emissions, and knock tendency. Energy 2013;61:612-620.
6. Abu-Jrai A, Tsolakis A, Megaritis A. The influence of H_2 and CO on diesel engine combustion characteristics, exhaust gas emissions, and after-treatment selective catalytic NOx reduction. International Journal of Hydrogen Energy 2007;32:3565-3571.
7. Ahmad M. Abu-Jrai, Ala'a H. Al-Muhtaseb, Ahmad O. Hasan. Combustion, performance, and selective catalytic reduction of NOx for a diesel engine operated with combined tri fuel (H_2, CH_4, and conventional diesel). Energy 2016;119:901-910.
8. Akash Deep, Sandhu SS, Chander S. Experimental Investigations on the Influence of Fuel Injection Timing and Pressure on Single Cylinder CI Engine Fueled With 20% Blend of Castor Biodiesel in Diesel. Fuel 2017;210:15-22.
9. Akash Deep, Sandhu SS, Chander S. Experimental Investigations on Castor Biodiesel as an Alternative Fuel for Single Cylinder Compression Ignition Engine. Environmental Progress & Sustainable Energy 2017;36 (4):1139-1150.
10. Al-Fatesh A, Singh SK, Kanade GS, Atia H, Fakeeha AH, Ibrahim AA, El-Toni AM, Labhasetwar NK. Rh promoted and ZrO_2/Al_2O_3 supported Ni/Co based catalysts: High

activity for CO_2 reforming, steam-CO_2 reforming and oxy-CO_2 reforming of CH_4. International Journal of Hydrogen Energy2018;43:12069-12080.

11. Alkabbashi AN, Alam MZ, Mirghani MES, Al-Fusaiel AMA. Biodiesel production from crude palm oil by transesterification process. Journal of Applied Science 2009;9(17):3166-3170.
12. Amin NAS, Yaw TC. Thermodynamic equilibrium analysis of combined carbon dioxide reforming with partial oxidation of methane to syngas. International Journal of Hydrogen Energy 2007;32(12):1789-1798.
13. An H, Yang WM, Maghbouli A, Li J, Chou SK, Chua KJ. A numerical study on a hydrogen assisted diesel engine. International Journal of Hydrogen Energy 2013;38:2919-2928.
14. Anand K, Sharma RP, Mehla PS. Experimental investigation on combustion, performance and emission characteristics of neat karanji biodiesel and its methanol blend in a diesel engine. Biomass and Bioenergy 2011;35:533-541.
15. Anjaneyulu C, Costa LO da, Ribeiro MC, Rabelo-Neto RC, Mattos LV, Venugopal A, Noronha FB. Effect of Zn addition on the performance of Ni/Al_2O_3 catalyst for steam reforming of ethanol. Applied Catalysis A: General 2016;519:85-98.
16. Annual Energy outlook 2015 with projection to 2040. International Energy Agency (IEA), https://www.iea.org/Textbase/npsum/WEO2015SUM.pdf; 2015 [Accessed 28.07.16].
17. Antunes JMG, Mikalsen R, Roskilly AP. An experimental study of a direct injection compression ignition hydrogen engine. International Journal of Hydrogen Energy 2009; 34:6516-6522.
18. Antunes JMG, Mikalsen R, Roskilly AP. An investigation of hydrogen-fuelled HCCI engine performance and operation. International Journal of Hydrogen Energy 2008;33:5823-5828.
19. Arbag H. Effect of impregnation sequence of Mg on performance of mesoporous alumina supported Ni catalyst in dry reforming of methane. International Journal of Hydrogen Energy 2018;43:6561-6574.

20. Asencios YJO, Assa EM. Combination of dry reforming and partial oxidation of methane on NiO–MgO–ZrO_2 catalyst: Effect of nickel content. Fuel Processing Technology2013;106:247-252.
21. Atzori L, Cutrufello MG, Meloni D, Cannas C, Gazzoli D, Monaci R, Sini MF, Rombi E. Highly active NiO-CeO_2 catalysts for synthetic natural gas production by CO_2 methanation. Catalyst Today2018;229:183-192.
22. Avila-Neto CN, Dantas SC, Silva FA, Franco TV, Romanielo LL, Hori CE, Assis AJ. Hydrogen production from methane reforming: Thermodynamic assessment and autothermal reactor design. Journal of Natural Gas Science and Engineering 2009;1:205-215.
23. Azimov U, Tomita E, Kawahara N, Harada Y. Effect of syngas composition on combustion and exhaust emission characteristics in a pilot-ignited dual-fuel engine operated in PREMIER combustion mode. International Journal of Hydrogen Energy 2011;36:11985-11996.
24. Balat M, Balat H. Progress in biodiesel processing. Applied Energy 2010;87(6):1815-1835.
25. Balzarotti R, Italiano C, Pino L, Cristiani C, Vita A. Ni/CeO_2-thin ceramic layer depositions on ceramic monoliths for syngas production by Oxy Steam Reforming of biogas. Fuel Processing Technology2016;149:40-48.
26. Barelli L, Ottaviano A. Solid oxide fuel cell technology coupled with methane dry reforming: A viable option for high efficiency plant with reduced CO_2 emissions. Energy 2014;71:118-129.
27. Bari S. Effect of carbon dioxide on the performance of biogas/diesel dual-fuel engine. Renewable Energy 1996;9:1007-1010.
28. Barik D, Murugan S, Sivaram N.M, Baburaj E, Shanmuga Sundaram P, Experimental investigation on the behavior of a direct injection diesel engine fueled with Karanja methyl ester-biogas dual fuel at different injection timings. Energy 2017;118:127-138.
29. Barik D, Murugan S. Experimental investigation on the behavior of a DI diesel engine fueled with raw biogas-diesel dual fuel at different injection timing. Journal of Energy Institute 2015;1-16.

30. Barik D, Murugan S. Investigation on combustion performance and emission characteristics of a DI (direct injection) diesel engine fueled with biogas–diesel in dual fuel mode. Energy 2014;72:760-771.
31. Barik D, Sivalingam M. Investigation on Performance and Exhaust Emissions Characteristics of a DI Diesel Engine Fueled with Karanja Methyl Ester and Biogas in Dual Fuel Mode. SAE Int 2014. SAE no. 2014-01-1311.
32. Barik D, Sivalingam M. Performance and Emission Characteristics of a Biogas Fueled DI Diesel Engine. SAE Int 2013, SAE no. 2013-01-2507.
33. Basha JS, Anand R B. An experimental study in a CI engine using nanoadditive blended water–diesel emulsion fuel. International Journal of Green Energy 2011; 8: 332-348.
34. Bedoya ID, Arrieta AA, Cadavid FJ. Effects of mixing system and pilot fuel quality on diesel-biogas dual fuel engine performance. Bioresource Technology 2009;100:6624-6629.
35. Bekeketidou OA, Goula MA. Biogas reforming for syngas production over nickel supported on ceria–alumina catalysts. Catalyst Today 2012;195:93-100.
36. Bengaard HS, Norskov JK, Sehested BS, Clausen BS, Nielsen LP, Molenbroek AM, Rostrup-Nielsen JR. Steam Reforming and Graphite Formation on Ni Catalysts. Journal of Catalysis 2002;209:365-384.
37. Birtas A, Voicu I, Petcu C, Chiriac R, Apostolescu N. The effect of HRG gas addition on diesel engine combustion characteristics and exhaust emissions. International Journal of Hydrogen Energy 2011;36(18):12007-12014.
38. Bohacik T, Maria D, Saman WY. Constant-volume adiabatic combustion of stoichiometric hydrogen-oxygen mixtures. Renewable Energy 1996;9(1-4):1254-1257.
39. Bora BJ, Saha UK, Chatterjee S, Veer V. Effect of compression ratio on performance, combustion and emission characteristics of a dual fuel diesel engine run on raw biogas. Energy Conversion Management2014;87:1000-1009.
40. Bora BJ, Saha UK. Comparative assessment of a biogas run dual fuel diesel engine with rice bran oil methyl ester, pongamia oil methyl ester and palm oil methyl ester as pilot fuels. Renewable Energy 2015;81:490-498.
41. Bora BJ, Saha UK. Experimental evaluation of a rice bran biodiesel e biogas run dual fuel diesel engine at varying compression ratios. Renewable Energy 2016;87:782-790.

42. Bora BJ, Saha UK. Improving the Performance of a Biogas Powered Dual Fuel Diesel Engine Using Emulsified Rice Bran Biodiesel as Pilot Fuel Through Adjustment of Compression Ratio and Injection Timing. Journal of Engineering Gas Turbines Power 2015;137:91505-91514.
43. Bora BJ, Saha UK. On the attainment of optimum injection timing of pilot fuel in a Dual fuel diesel engine run on biogas. ASME 2014.
44. Boretti A. Advantages of the direct injection of both diesel and hydrogen in dual fuel H_2 ICE. International Journal of Hydrogen Energy 2011;36:9321-9317.
45. Boyano A, Blanco-Marigorta AM, Morosuk T, Tsatsaronis G. Exergo environmental analysis of a steam methane reforming process for hydrogen production. Energy 2011;36:2202-2214.
46. Bradford MCJ, Vannice MA. Catalytic reforming of methane with carbon dioxide over nickel catalysts I. Catalyst characterization and activity. Applied Catalyst A General 1996;142:73-96.
47. Bradford MCJ, Vannice MA. Catalytic reforming of methane with carbon dioxide over nickel catalysts II. Reaction kinetics. Applied Catalyst A 1996;142(1):97-122.
48. Cacua K, Amell A, Cadavid F. Effects of oxygen enriched air on the operation and performance of a diesel-biogas dual fuel engine. Biomass and Bio-energy 2012;45:159-167.
49. Cacua K, Olmos-Villalba L, Herrera B, Gallego A. Experimental evaluation of a diesel-biogas dual fuel engine operated on micro-trigeneration system for power, drying and cooling. Applied Thermal Engineering2016;100:762-767.
50. Can O. Combustion characteristics, performance and exhaust emissions of a diesel engine fueled with a waste cooking oil biodiesel mixture. Energy Conversion Management 2014;87:676-686.
51. Chanphavong L, Zainal ZA. Characterization and challenge of development of producer gas fuel combustor: A review. Journal of the Energy Institute 2018;1-14.
52. Chauhan BS, Singh RK, Cho HM, Lim HC. Practice of diesel fuel blends using alternative fuels: A review. Renewable and Sustainable Energy Reviews 2016; 59 (6): 1358-1368.

53. Che Mat S, Idroas MF, Hamida MF, Zainal ZA. Performance and emissions of straight vegetable oils and its blends as a fuel in diesel engine: A review. Renewable and Sustainable Energy Reviews 2018;82:808-823.
54. Chen L, Zhu Q, Hao Z, Zhang T, Xie Z. Development of a Co-Ni bimetallic aerogel catalyst for hydrogen production via methane oxidative CO_2 reforming in a magnetic assisted fluidized bed. International Journal of Hydrogen Energy 2010;35:8494-502.
55. Chen MN, Zhang DY, Thompson LT, Ma ZF. Catalytic properties of Ag promoted ZnO/Al2O_3 catalysts for hydrogen production by steam reforming of ethanol. International Journal of Hydrogen Energy2011;36:7516-7522.
56. Chen WH, Lin MR, Lu JJ, Chao Y, Leu TS. Thermodynamic analysis of hydrogen production from methane via autothermal reforming and partial oxidation followed by water gas shift reaction. International Journal of Hydrogen Energy2010;35:11787-11797.
57. Chen WH, Shen CT, Lin BJ, Liu SC. Hydrogen production from methanol partial oxidation over Pt/Al_2O_3 catalyst with low Pt content. Energy 2015;88: 399-407.
58. Chintala V, Subramanian KA. An effort to enhance hydrogen energy share in a compression ignition engine under dual-fuel mode using low temperature combustion strategies. Applied Energy 2015;146:174-183.
59. Chintala V, Subramanian KA. Experimental investigation on effect of enhanced premixed charge on combustion characteristics of a direct injection diesel engine.International Journal of Advances in Engineering Sciences and Applied Mathematics 2014;6(1-2):3-16.
60. Chintala V, Subramanian KA. Experimental investigations on effect of different compression ratios on enhancement of maximum hydrogen energy share in a compression ignition engine under dual-fuel mode. Energy 2015;1-15.
61. Crisafulli C, Scire S, Maggiore R, Minico S, Galvagno S. CO_2 reforming of methane over Ni–Ru and Ni–Pd bimetallic catalysts. Catalysis Letters. 1999;59:21-26.
62. Crookes RJ. Comparative bio-fuel performance in internal combustion engines. Biomass and Bioenergy 2006;30:461-68.
63. Danilova MM, Fedorova ZA, Zaikovskii VI, Porsin AV, Kirillov VA, Krieger TA. Porous nickel-based catalysts for combined steam and carbon dioxide reforming of methane. Applied Catalyst B Environment 2014;147:858-863.

64. Das LM. Hydrogen engine: A view of the past and a look into the future. International Journal of Hydrogen Energy1990;15:425-443.
65. Datta A, Mandal BK. A comprehensive review of biodiesel as an alternative fuel for compression ignition engine. Renewable and Sustainable Energy Reviews2016;57:799-721.
66. Davis ME. Ordered porous materials for emerging applications. Nature 2002;417:813-821.
67. Debnath BK, Saha UK, Sahoo N. Effect of hydrogen-diesel quantity variation on BTE of a dual fuelled diesel engine. Journal of Power Technologies 2012;92(1);55-67.
68. Deepanraj B, Dhanesh C, Senthil R, Kannan M, Santhosh kumar A, Lawrence P. Use of Palm oil Biodiesel Blends as a Fuel for Compression Ignition Engine. American Journal of Applied Sciences2011;8(11):1154-1158.
69. Derk AR, Moore GM, Sharma S, McFarland EW, Metiu H. Catalytic Dry Reforming of Methane on Ruthenium-Doped Ceria and Ruthenium Supported on Ceria. TopicsinCatalysis2013;57:118-124.
70. Devan PK, Mahalakshmi NV. Study of the performance, emission and combustion characteristics of a diesel engine using poon oil-based fuels. Fuel Processing Technology 2009;90:513-519.
71. Dhariwal HC. Control of blow by emissions and lubricating oil consumption in I.C. engines. Energy Conversion and Management1997;38:1267-1274.
72. Djinovic P, Osojnik Crnivec IG, Erjavec B, Pintar A. Influence of active metal loading and oxygen mobility on coke-free dry reforming of Ni–Co bimetallic catalysts. Applied Catalyst B Environment 2012;125:259-270.
73. Duc PM, Wattanavichien K. Study on biogas premixed charge diesel dual fuelled engine. Energy Conversion and Management 2007;48:2286-2308.
74. Edwin Geo V, Nagarajan G, Nagalingam B. Studies on dual fuel operation of rubber seed oil and its bio-diesel with hydrogen as the inducted fuel. International Journal of Hydrogen Energy 2008;33(21):6357-6367.
75. ELKassaby M, Nemitallah MA. Studying the effect of compression ratio on an engine fueled with waste oil produced biodiesel diesel fuel. Alexandria Engineering Journal2013;52:1-11.

76. Enger BC, Lodeng R, Holmen A. A review of catalytic partial oxidation of methane to synthesis gas with emphasis on reaction mechanisms over transition metal catalysts. Applied Catalyst A: General2008;346:1-27.
77. Escobar JC, Lora ES, Venture OJ, Yonez EG, Castillo EF, Almazan O. Biofuels. Environment, technology and food security. Renewable and Sustainable Energy Reviews 2009;13(6-7):1275-1287.
78. Faiz A, Weaver CS, Walsh PW. Air pollution from motor vehicles: standards and texhnologies for controlling emissions. The World Bank, Washington 1996.
79. Farrukh J, Lamya AH, Ala'a H. Al-Muhtaseb, Mohab AH, Mahad B, Umer R, Mohammad NMA. Current Scenario of Catalysts for Biodiesel Production: A Critical Review. Reviews in Chemical Engineering 2018;34:267-297.
80. Ferguson CR. Internal Combustion Engines (Applied Thermo Sciences). New York: Wiley;1986.
81. Fidalgo B, Arenillas A, Menéndez JA. Synergetic effect of a mixture of activated carbon+Ni/Al_2O_3 used as catalysts for the CO_2 reforming of CH_4. Applied Catalysis A: General 2010; 390(1-2): 78-83.
82. Fischer F, Tropsch H. Conversion of methane into hydrogen and carbon monoxide. Brennst Chem. 1928;3(9):39-46.
83. Frontera P, Macario A, Aloise A, Antonucci PL, Giordano G, Nagy JB. Effect of support surface on methane dry-reforming catalyst preparation. Catalyst Today2013;218:18-29.
84. Gaddalla AM, Sommer ME. Carbon dioxide reforming of methane on nickel catalysts. Chemical Engineering Science 1989; 44(12): 2825-2829.
85. Gatts T, Li H, Liew C, Liu S, Spencer T, Wayne S, Clark N. An experimental investigation of H_2 emissions of a 2004 heavy-duty diesel engine supplemented with H_2. International Journal of Hydrogen Energy2010;35:11349-11356.
86. Gautam R, Kumar N. Performance emission and combustion studies of diesel engine on Jatropha ethyl ester and its higher alcohol blends. International Journal of Global Warming 2018;14:159-169.
87. Geo VE, Nagarajan G, Nagalingam B. Studies on dual fuel operation of rubber seed oil and its bio-diesel with hydrogen as the inducted fuel. International Journal of Hydrogen Energy 2008;33:6357-6367.

88. Ghazal OH. Performance and combustion characteristic of CI engine fueled with hydrogen enriched diesel. International Journal of Hydrogen Energy 2013;38:15469-15476.
89. Gopal G, Rao PS, Gopalkrishnan KV, Murthly BS. Use of hydrogen in dual fuel engine. International Journal of Hydrogen Energy 1982;7(3):267-272.
90. Goula MA, Charisiou ND, Papageridis KN, Delimitis A, Pachatouridou E, Iliopoulou EF. Nickel on alumina catalysts for the production of hydrogen rich mixtures via the biogas dry reforming reaction: influence of the synthesis method. International Journal of Hydrogen Energy 2015;40:9183-9200.
91. Goula MA, Charisiou Nd, Siakavelas G, Tzounis L, Tsiaoussis I, Panagiotopoulou P, Goula G, Yentekakis IV. Syngas production via the biogas dry reforming reaction over Ni supported on zirconia modified with CeO_2 or La_2O_3 catalysts. International Journal of Hydrogen Energy2017;42:13724-13740.
92. Gumus M. Comprehensive experimental investigation of combustion and heat release characteristics of a biodiesel (hazelnut kernel oil methyl ester) fueled direct injection compression ignition engine. Fuel 2010;89(10):2802-2814.
93. Gunea C, Razavi MRM, Karim GA. The effects of pilot fuel quality on dual fuel engine ignition delay. SAE Int 1998. SAE no. 982453.
94. Gupta HK, Agrawal GD, Mathur J. An experimental investigation of a low temperature Al2O3-H2O nanofluid based direct absorption solar collector. Solar Energy 2015;118:390-396.
95. Gustavsson L, Borjesson P, Johansson B, Svenningsson P. Reducing CO_2 emission by substituting biomass for fossil fuels. Energy 1995;20:1097-1113.
96. Hadian N, Rezaei M. Combination of dry reforming and partial oxidation of methane over Ni catalysts supported on nanocrystalline $MgAl_2O_4$. Fuel. 2013;113:571-579.
97. Hamdan MO, Selim MYE. Performance of CI engine operating with hydrogen supplement co-combustion with jojoba methyl ester. International Journal of Hydrogen Energy 2016;41:10255-10264.
98. Han X, Wang Y, Zhang Y, Yu Y, He H. Hydrogen production from oxidative steam reforming of ethanol over Ir catalysts supported on Ce–La solid solution. International Journal of Hydrogen Energy 2017;42:11177-11186.

99. Haragopala Rao B. Hydrogen for dual fuel engine operation. International Journal of Hydrogen Energy 1983;8(5):833-842.
100. Hauserman WB. High-yield hydrogen production by catalytic gasification of coal or biomass. International Journal of Hydrogen Energy 1994;19:413-419.
101. Hekkert MP, Hendriks FHJF, Faaij APC, Neelis ML. Natural gas as an alternative to crude oil in automotive fuel chains well-to-wheel analysis and transition strategy development. Energy Policy 2005; 33:579-594.
102. Henham A, Makkar M. Combustion of simulated biogas in a dual-fuel diesel engine. Energy Conversion and Management 1998;39(16-18):2001-2009.
103. Hernandez JJ, Lapuerta M, Barba J. Separate effect of H_2, CH_4 and CO on diesel engine performance and emissions under partial diesel fuel replacement. Fuel 2016;165:173-184.
104. Heywood JB. Internal combustion engines fundamentals. New York: McGraw-Hill, Inc.; 1988.
105. Hiroyuki Y, Misawa K, Suzuki D, Tanaka K, Matsumoto J, Fujii M, Tanaka K. Detailed analysis of diesel vehicle exhaust emissions: nitrogen oxides, hydrocarbons and particulate size distributions. Proceedings of the Combustion Institute2011;33:2895-2902.
106. Hoffmann P. The fuel forever, the story of hydrogen. West view press, Boulder, Colorado, USA; 1981.
107. Homan HS, Reynolds RK, De Boar PCT, McLean WJ. Hydrogen-fueled diesel engine without timed ignition. International Journal of Hydrogen Energy 1979;4(4):315-325.
108. Hori CE, Permana H, Simon Ng KV, Brenner A, More K, Rahmoeller KM, Belton D. Thermal stability of oxygen storage properties in a mixed CeO_2-ZrO_2 system. Catalysis B: Environmental 1998;16:105-117.
109. Hu YH, Ruckenstein E. Catalytic Conversion of Methane to Synthesis Gas by Partial Oxidation and CO_2 Reforming. Advances in Catalysis 2004;48:297-345.
110. Ikegami M, Miwa K, Shioji T. A study of H_2fueled diesel combustion. Japan Society of Mechanical Engineers1980;23:1187-1193.
111. Iranmanesh M, Subrahmanyam JP, Babu MKG. Potential of Diethyl ether as supplementary fuel to improve combustion and emission characteristics of diesel engines. SAE Int 2008. SAE no. 2008-28-0044.

112. Iranmanesh M. Combustion Analysis and Study on Smoke and NOX Emissions of Diesel and Biodiesel Fueled CI Engines With Ethanol Blends. The American Society of Mechanical Engineers 2011:1069-1077.
113. Italiano C, Balzarotti R, Vita A, Latorrata S, Fabiano C, Pino L, Cristiani C. Preparation of structured catalysts with Ni and Ni-Rh/CeO_2 catalytic layers for syngas production by biogas reforming processes. Catalysis Today 2016;273:3-11.
114. Ji G, Zhao M, Wang G. Computational fluid dynamic simulation of a sorption-enhanced palladium membrane reactor for enhancing hydrogen production from methane steam reforming. Energy 2018;147:884-895.
115. Jiang CQ, Liu TW, Zhong JL. A study on compressed biogas and its application to the compression ignition dual-fuel engine. Biomass 1989;20:53-59.
116. Jiang Z, Li R, Li A, Ji C. Runoff forecast uncertainty considered load adjustment model of cascade hydropower stations and its application. Energy 2018;158:693-708.
117. Jimmy U, Mohamedali M, Ibrahim H. Thermodynamic Analysis of Autothermal Reforming of Synthetic Crude Glycerol (SCG) for Hydrogen Production. ChemEngineering 2017;1(1):4.
118. Jindal S, Nandwana BP, Rathore NS, Manistha V. Experimental Investigation of the effect of compression ratio and injection pressure in a direct injection diesel engine running on Jatropha methyl ester. Applied Thermal Engineering 2010; 30(5):442-448.
119. Jing QS, Zheng XM. Combined catalytic partial oxidation and CO_2 reforming of methane over ZrO_2-modified Ni/SiO_2 catalysts using fluidized-bed reactor. Energy 2006;31:2184-2192.
120. Jingura RM, Matengaifa R. Optimization of biogas production by anaerobic digestion for sustainable energy development in Zimbabwe. Renewable and Sustainable Energy Reviews 2009;13(5):1116-1120.
121. Kadota T, Yamasaki H. Recent advances in the combustion of water fuel emulsion. Progress in Energy and Combustion Science 2002;28(5):385-404.
122. Kalsi SS, Subramanian KA. Effect of simulated biogas on performance, combustion and emissions characteristics of a bio-diesel fueled diesel engine. Renewable Energy 2017;106:78-90.

123. Kampa M, Castanas E. Human health effects of air pollution. Environmental Pollution2008;151:362-367.
124. Kannah RY, Kavitha S, Sivashanmugham P, Kumar GK, Nguyen DD, Chang SW, Rajesh BJ. Biohydrogen production from rice straw: Effect of combinative pretreatment, modelling assessment and energy balance consideration. International Journal of Hydrogen Energy 2019;44(4):2203-2215.
125. Karagoz Y, Guler I, Sandalci T, Yuksek L, Dalkilic AS. Effect of hydrogen enrichment on combustion characteristics, emissions and performance of a diesel engine. International Journal of Hydrogen Energy 2016;41:656-665.
126. Karagoz Y, Sandalci T, Yuksek L, Dalkilic AS. Engine performance and emission effects of diesel burns enriched by hydrogenon different engine loads. International Journal of Hydrogen Energy 2015;1-12.
127. Karim G. Hydrogen as a spark ignition engine fuel. International Journal of Hydrogen Energy 2003;28(5):569-577.
128. Karim GA. A review of combustion processes in the dual fuel engine-the gas diesel engine. Progress in Energy and Combustion Science 1980;6(3):277-285.
129. Karim GA. Combustion in gas fueled compression ignition engines of the dual fuel type. Journal of Engineering for Gas Turbines and Power - ASME2003;125(3):827-836.
130. Khin T, Annachhatre AP. Nitrogen removal in a fluidized bed bioreactor by using mixed culture under oxygen-limited conditions. Water Science and Technology 2004;50(6):313-320.
131. Kim H, Kim C, Lim HC, Song. Spray Formation of a Liquid Carbon Dioxide-Water Mixture at Elevated Pressures. Energies 2016;9.
132. Kim SS, Lee SM, Won JM, Yang HJ, Hong SC. Effect of Ce/Ti ratio on the catalytic activity and stability of Ni/CeO_2-TiO_2 catalyst for dry reforming of methane. Chemical Engineering Journal2015;280:433-440.
133. Kodama T, Shimizu T, Satoh T, Shimizu KI. Stepwise production of CO-rich syngas and hydrogen via methane reforming by a WO_3-redox catalyst. Energy 2003;28:1055-1068.
134. Kong SC, Reitz RD. Use of detailed chemical kinetics to study HCCI engine combustion with consideration of turbulent mixing effects. Journal of Engineering for Gas Turbines and Power - ASME2002;124:702-712.

135. Kose H, Ciniviz M. An experimental investigation of effect on diesel engine performance and exhaust emissions of addition at dual fuel mode of hydrogen. Fuel Processing Technology2013;114:26-34.
136. Koten H. Hydrogen effects on the diesel engine performance and emissions. International Journal of Hydrogen Energy 2018;43:10511-10519.
137. Kovacs VB, Torok A. Investigation on transport related biogas utilization. Transport 2010;25(1):77-80.
138. Kumar BSP, Reddy VK, Rao BN. Effect of CNG flow rate on the performance and emissions of a mullite coated diesel engine under dual fuel mode. International Journal of Technology and Engineering Studies2014;6:29-42.
139. Kumar MS, Ramesh A, Nagalingam B. Use of hydrogen to enhance the performance of a vegetable oil fuelled compression ignition engine. International Journal of Hydrogen Energy 2003;28:1143-1154.
140. Kumar N, Tomar M. Influence of nano additives on ignition characteristics of Kusum (Schleichera oleosa) biodiesel. International Journal of Energy Research 2019;1-14.
141. Kumar RS, Loganathan M, Gunasekaran EJ. Performance, emission and combustion characteristics of CI engine fuelled with diesel and hydrogen. Frontiers in Energy 2015;9(4):486-494.
142. Kumar SS, Sivakumar G, Manoharan S. Investigation of palm methyl ester biodiesel with additive on performance and emission characteristics of a diesel engine under 8 mode testing cycle. Alexandria Engineering Journal 2015;54 (3):423-428.
143. Kurungot S, Yamaguchi T. Stability improvement of Rh/γ-Al_2O_3 catalyst layer by ceria doping for steam reforming in an integrated catalytic membrane reactor system. Catalysis Letters 2004;92:181-187.
144. Labeckas G, Slavinskas S. Study of exhaust emissions of direct injection diesel engine operating on ethanol, petrol and rapeseed oil blends. Energy Conversion and Management 2009;50:802-812.
145. Labecki L, Cairns A, Xia J, Megaritis A, Zhao HL, Ganippa LC. Combustion and emission of rapeseed oil blends in diesel engine. Applied Energy 2012;3:139-146.

146. Lal S, Mohapatra SK. The effect of compression ratio on the performance and emission characteristics of a dual fuel diesel engine using biomass derived producer gas. Applied Thermal Engineering 2017;119:63-72.
147. Laosiripojana N, Assabumrungrat S. Methane steam reforming over Ni/Ce–ZrO_2 catalyst: Influences of Ce-ZrO_2 support on reactivity, resistance toward carbon formation, and intrinsic reaction kinetics. Applied Catalysis A: General 2005;290:200-211.
148. Laosiripojana N, Chadwick D, Assabumrungrat S. Effect of high surface area CeO_2 and Ce-ZrO_2 supports over Ni catalyst on CH_4 reforming with H_2O in the presence of O_2, H_2, and CO_2. Chemical Engineering Journal 2008;138:264-273.
149. Larimi AS, Alavi SM. Ceria-zirconia supported Ni catalysts for partial oxidation of methane to synthesis gas. Fuel 2012;102:366-371.
150. Lashof DA, Aujla DR. Relative contributions of greenhouse gas emissions to global warming. Nature 1990;344:529-531.
151. Lata DB, Misra A, Medhekar S. Investigations on the combustion parameters of a dual fuel diesel engine with H_2 and LPG as secondary fuels. International Journal of Hydrogen Energy 2011;36:13808-13819.
152. Lata DB, Misra A. Analysis of ignition delay period of a dual fuel diesel engine with hydrogen and LPG as secondary fuels. International Journal of Hydrogen Energy 2011;36(5):3746-3756.
153. Lau CS, Tsolakis A, Wyszynski ML. Biogas upgrade to syn-gas (H_2-CO) via dry and oxidative reforming. International Journal of Hydrogen Energy 2011;36:397-404.
154. Li D, Nishida K, Zhan Y, Shishido T, Oumi Y, Sano T, Takehira K. Sustainable Ru-doped Ni catalyst derived from hydrotalcite in propane reforming. Applied Clay Science 2009;43:49-56.
155. Li Rongbo, Jiang Z, Ji C, Li A, Yu S. An improved risk-benefit collaborative grey target decision model and its application in the decision making of load adjustment schemes. Energy 2018;156:387-400.
156. Liew C, Li H, Nuszkowski J, Liu S, Gatts T, Atkinson R, Clark N. An experimental investigation of the combustion process of a heavy-duty diesel engine enriched with hydrogen. International Journal of Hydrogen Energy 2010;35:11357-11365.

157. Lilik GK, Zhang H, Herreros JM, Haworth DC, Boehman AL. Hydrogen assisted diesel combustion. International Journal of Hydrogen Energy 2010;35:4382-4398.
158. Lin KH, Chang HF, Chang AC. Biogas reforming for hydrogen production over mesoporous $Ni_{2x}Ce_1L_xO_2$ catalysts. International Journal of Hydrogen Energy 2012;37:15696-15703.
159. Liu D, Quek XY, Wah HHA, Zeng G, Li Y, Yang Y. Carbon dioxide reforming of methane over nickel-grafted SBA-15 and MCM-41 catalysts. Catalysis Today 2009; 148 (3-4): 243-250.
160. Lohan SK, Dixit J, Kumar R, Pandey Y, Khan J, Ishaq M, et al. Biogas: A boon for sustainable energy development in India's cold climate. Renewable and Sustainable Energy Reviews 2015;43:95-101.
161. Lounici MS, Loubar K, Tazerout M, Balistrou M, Tarabet L. Experimental investigation on the performance and exhaust emission of biogas-diesel dual fuel combustion in a CI engine. SAE Int 2014. SAE no. 2014-01-2689.
162. Lucredio AF, Assaf EA. Cobalt catalysts prepared from hydrotalcite precursors and tested in methane steam reforming. JournalofPower Sources 2006;159:667-672.
163. Luijten CCM, Kerkhof E. Jatropha oil and biogas in a dual fuel CI engine for rural electrification. Energy Conversion and Management 2011;52:1426-1438.
164. Mahla SK, Dhir A, Gill KJS, Cho HM, Lim HC, Chauhan BS. Influence of EGR on the simultaneous reduction of NOx-smoke emissions trade-off under CNG-biodiesel dual fuel engine. Energy 2018;152:303-312.
165. Makareviciene V, Sendzikiene E, Pukalskas S, Rimkus A, Vegneris R. Performance and emission characteristics of biogas used in diesel engine operation. Energy Conversion and Management 2013;75:224-233.
166. Mandal T, Kiran BA, Mandal NK. Determination of the quality of biogas by flame temperature measurement. Energy Conversion and Management 1999;40:1225-28.
167. Maricq MM. Chemical characterization of particulate emissions from diesel engines: a review. Journal of Aerosol Science 2007;38:1079-1118.
168. Marwaha A, Rosha P, Mohapatra SK, Mahla SK, Dhir A. Waste materials as potential catalysts for biodiesel production: Current state and future scope. Fuel Processing Technology 2018;181:175-86.

169. Masood M, Mehdi SN, Ram Reddy P. Experimental investigations on a hydrogen diesel dual fuel engine at different compression ratios. Journal of Engineering for Gas Turbines and Power - ASME2007;129(2):572-78.
170. Mathur HB, Das LM, Patro TN. Hydrogen-fuelled diesel engine: Performance improvement through charge dilution technique. International Journal of Hydrogen Energy 1993;18(5):421-31.
171. Mathur J, Das LM, Patro TN. Hydrogen fuel utilization in a CI engine powered and utility systems. International Journal of Hydrogen Energy 1992;17(5):369-374.
172. Mattos LV, Rodino E, Resasco DE, Passos FB, Noronha FB. Partial oxidation and CO_2 reforming of methane on Pt/Al_2O_3, Pt/ZrO_2, and $Pt/Ce\text{-}ZrO_2$ catalysts. Fuel Processing Technology 2003;83:147-161.
173. McWilliam L, Megaritis T, Zhao H. Experimental investigation of the effects of combined hydrogen and diesel combustion on the emissions of a HSDI diesel engine. SAE Int 2008. SAE no. 2008-01-1787.
174. Meshkani F, Rezaei M, Andache M. Investigation of the catalytic performance of Ni/MgO catalysts in partial oxidation, dry reforming and combined reforming of methane. Journal of Industrial Engineering and Chemical Research 2014;20:1251-1260.
175. Mesrar F, Kacimi M, Liotta LF, Puleo F, Ziyad M. Syngas production from dry reforming of methane over ni/perlite catalysts: Effect of zirconia and ceria impregnation. International Journal of Hydrogen Energy 2018;43:17142-17155.
176. Midilli A, Dincer I. Hydrogen as a renewable and sustainable solution in reducing global fossil fuel consumption. International Journal of Hydrogen Energy 2008; 33:4209-4222.
177. Mitzlaff KV. Engines for biogas: theory, modification, economic operation. Vieweg; 1988.
178. Miyamoto T, Hasegawa H, Mikami M, Kojima N, Kabashima H, Urata Y. Effect of hydrogen addition to intake gas on combustion and exhaust emission characteristics of a diesel engine. International Journal of Hydrogen Energy 2011;36:13138-13149.
179. Miyamoto T, Mikami M, Kojima N, Kabashima H, Urata Y. Effect of hydrogen fraction in intake mixture on combustion and exhaust emission characteristics of a diesel engine. SAE Int 2009. SAE no. 2009-24-0086.

180. Moffat RJ. Contributions to the theory of single-sample uncertainly analysis. ASME Journal of fluid engineering 1982;104:250-260.
181. Mohamedali M, Henni A, Ibrahim H. Recent Advances in Supported Metal Catalysts for Syngas Production from Methane. ChemEngineering 2018;2(1):9.
182. Moradi GR, Rahmanzadeh M, Khosravian F. The effects of partial substitution of Ni by Zn in $LaNiO_3$ perovskite catalyst for methane dry reforming. Journal of CO_2 Utilization 2014;6: 7-11.
183. Movasati A, Alavi SM, Mazloom G. CO_2 reforming of methane over $Ni/ZnAl_2O_4$ catalysts: Influence of Ce addition on activity and stability. International Journal of Hydrogen Energy 2017;42:16436-16448.
184. Muralidharn K, Vasudevan D. Performance, emission and combustion characteristics of a variable compression ratio engine using esters of waste cooking oil and diesel blends. Applied Energy 2011;88:3959-3968.
185. MuralidharnK,Vasudevan D, Sheeba KN. Performance, emission and combustion characteristics of a variable compression ratio engine. Energy 2011;36:5385-5393.
186. Naber J. Hydrogen combustion under diesel engine conditions. International Journal of Hydrogen Energy 1998;23(5):363-371.
187. Nagaki H, Furutani H, Takahashi S. Acceptability of premixed hydrogen in hydrogen diesel engine. SAE Int 1999. SAE no 1999-01-2521.
188. Nagarajan S, Ilangkumaran M, Gaikwad A. Comparative analysis of performance, emission and combustion parameters of diesel engine fueled with ethyl ester of fish oil and its diesel blends. Fuel 2014;132:116-124.
189. Nakagawa K, Ikenaga N, Kobayashi T, Suzuki T. Transient response of catalyst bed temperature in the pulsed reaction of partial oxidation of methane to synthesis gas over supported group VIII metal catalysts. Catalyst Today. 2001;64:31-41.
190. Nandor N, Peter B, Rozsenberszki T, Kumar GK, Kook L, Kelemen G, Kim S, Belafi-Bako K. Assessment via the modified gompertz-model reveals new insights concerning the effects of ionic liquids on biohydrogen production. International Journal of Hydrogen Energy 2018;43:18918-18924.

191. Nataj SMM, Alavi SM, Mazloom G. Catalytic performance of Ni supported on ZnO-Al_2O_3 composites with different Zn content in methane dry reforming. Journal of chemical technology and biotechnology 2019;94:1305-1314.
192. Nathan SS, Mallikarjuna JM, Ramesh A. An experimental study of the biogas–diesel HCCI mode of engine operation. Energy Conversion and Management 2010;51:1347-1353.
193. National Hydrogen Energy Road Map - 2006 (Abridged Version, 2007). National hydrogen energy board, Ministry of New and Renewable Energy Government of India. 2007.
194. Nematollahi B, Rezaei M, Khajenoori M. Combined dry reforming and partial oxidation of methane to synthesis gas on noble metal catalysts. International Journal of Hydrogen Energy 2011;36: 2969-2978.
195. Nematollahi B, Rezaei M, Lay EN, Khajenoor M. Thermodynamic analysis of combined reforming process using Gibbs energy minimization method: In view of solid carbon formation. Journal of Natural Gas Chemistry 2012;21:694-702.
196. Nwafor OMI. Effect of advanced injection timing on emission characteristic of diesel engine running on natural gas. Renewable Energy 2007;32:2361-2368.
197. Ocsachoque M, Pompeo F, Gonzalez G. Rh–Ni/CeO_2–Al_2O_3 catalysts for methane dry reforming. Catalyst Today 2011;172:226-231.
198. Ozsezen AN, Canakci M, Sayin C. Effects of biodiesel from used frying palm oil on the performance, injection and combustion characteristics of an indirect injection diesel engine. Energy & Fuel 2008;22:1297-1305.
199. Pakhare D, Spivey J. A review of dry (CO_2) reforming of methane over noble metal catalysts. Chemical Society Reviews 2014;43:7813-37.
200. Park JH, Yeo S, Kang TJ, Shin HR, Heo I, Chang TS. Effect of Zn promoter on catalytic activity and stability of Co/ZrO_2 catalyst for dry reforming of CH_4. Journal of CO_2 Utilization 2018;23:10-19.
201. Patel PD, Lakdawala A, Chourasia S, Patel RN. Bio fuels for compression ignition engine: A review on engine performance, emission and life cycle analysis. Renewable and Sustainable Energy Reviews 2016;65:24-43.

202. Pattanaik BP, Nayak C, Nanda BK. Investigation on utilization of biogas & Karanja oil biodiesel in dual fuel mode in a single cylinder DI diesel engine. International Journal of Energy and Environment 2013;4:279-290.
203. Pecharaply A, Parkpian P, Annachhatre AP, Jugsujinda A. Influence of anaerobic co-digestion of sewage and brewery sludges on biogas production and sludge quality. Journal of Environmental Science and Health, Part A 2007;42(7):911-923.
204. Perego C, Villa P. Catalyst preparation methods. Catalysis Today 1997;34:281-305.
205. Petkov T, Veziroglu TN, Sheffield JW. An outlook of hydrogen as an alternative fuel. International Journal of Hydrogen Energy 1989;14:449-474.
206. Poonia P, Ramesh A, Gaur RR. Experimental Investigation of the Factors Affecting the Performance of a LPG Diesel Dual Fuel Engine. SAE Int 1999, SAE no.1999-01-1123.
207. Pramanik K. Properties and use of jatropha curcas oil and diesel fuel blends in compression ignition engine. Renewable Energy 2003;28:239-248.
208. Qi D, Bae C, Feng Y, Jia C. Preparation, characterization, engine combustion and emission characteristics of rapeseed oil based hybrid fuels. Renewable Energy 2013;60:98-106.
209. Qi DH, Geng LM, Chen H, Bian YZH, Liu J, Ren XCH. Combustion and performance evaluation of a diesel engine fueled with biodiesel produced from soybean crude oil. Renewable Energy 2009;34:2706-2713.
210. Raheman H, Ghadge S. Performance of diesel engine with biodiesel at varying compression ratio and ignition timing. Fuel 2008;87:2659-2666.
211. Rahemi N, Haghighi M, Babaluo AA, Jafari MF, Estifaee P. Synthesis and physicochemical characterizations of Ni/Al_2O_3-ZrO_2nano catalyst prepared via impregnation method and treated with non-thermal plasma for CO_2 reforming of CH_4. Journal of Industrial Engineering Chemistry 2013;19:1566-1576.
212. Rajak U, Nashine P, Verma TN. Assessment of diesel engine performance using *spirulina* microalgae biodiesel. Energy 2019;166:1025-1036.
213. Rajbongshi BM, Ramchiary A, Samdarshi SK. Influence of N-doping on photocatalytic activity of ZnO nanoparticles under visible light irradiation. Materials Letters 2014;134:111-114.

214. Rajbongshi BM, Samdarshi SK. Cobalt-doped zincblende–wurtzite mixed-phase ZnO photocatalyst nanoparticles with high activity in visible spectrum. Applied Catalysis B: Environmental 2014;144:435-441.
215. Rajkumari K, Govindarajan P. Experimental investigation of oxygen air intake on combustion parameters on single cylinder diesel engine. International Journal of Engineering Science and Technology 2010;2(8):3621-3627.
216. Ramadhas AS, Muraleedharan C, Jayaraj S. Performance and emission evaluation of a diesel engine fueled with methyl esters of rubber seed oil. Renewable and Sustainable Energy Reviews 2005:30(12):1789-1800.
217. Ramesha DK, Bangaria AS, Chirag P. Rathoda, Chaitanya R S. Combustion, performance and emissions characteristics of a biogas fuelled diesel engine with fish biodiesel as pilot fuel. Biofuels 2015.
218. Ramesha DK, Bangaria AS, Chirag P. Rathoda, Chaitanya R S. Experimental investigation of biogas-biodiesel dual fuel combustion in a diesel engine. Journal of Middle European Construction and Design of Cars 2015;13:12-20.
219. Ramesohl S, Merten F. Energy system aspects of hydrogen as an alternative fuel in transport. Energy Policy 2006;34:1251-1259.
220. Ranjbar A, Rezaei M. Dry reforming reaction over nickel catalysts supported on nanocrystalline calcium aluminates with different CaO/Al_2O_3 ratios. Journal of Natural Gas Chemistry 2012; 21(2): 178-183.
221. Raub JA. Health effects of exposure to ambient carbon monoxide. Chemosphere: global change. Science 1 1999:331-351.
222. Reitmeier RE, Atwood Kenton, Bennett H, Baugh H. Production of Synthetic Gas - Reaction of Light Hydrocarbons with Steam and Carbon Dioxide. Industrial and Engineering Chemistry Research. 1948; 40 (4):620-626.
223. Reşitoğlu İA, Altinişik K, Keskin A. The pollutant emissions from diesel-engine vehicles and exhaust after treatment systems. Clean Technologies and Environmental Policy 2015; 17(1): 15-27.
224. Rezaei M, Alavi SM, Sahebdelfar S, Yan ZF. Syngas production by methane reforming with carbon dioxide on noble metal catalysts. Journal of Natural Gas Chemistry 2006;15:327-34.

225. Rezaei M, Alavi SM, Sahebdelfar S. Z.F Yan, A highly stable catalyst in methane reforming with carbon dioxide. Scripta Materialia 2009;61:173-176.
226. Rinaldini CA, Allesina GA, Pedrazzi S, Mattarelli E, Savioli T, Morselli N, Puglia M, Tartarini P. Experimental investigation on a Common Rail Diesel engine partially fuelled by syngas. Energy Conversion and Management 2017;138:526-537.
227. Roskilly AP, Nanda SK, Wang YD, Chirkowski J. The performance and the gaseous emissions of two small marine craft diesel engines fuelled with biodiesel. Applied Thermal Engineering 2008;28:872-880.
228. Rostrup NJ. Process for the production of a reforming catalyst. US Patent 3791993A;1974.
229. Roy MM, Tomita E, Kawahara N, Harada Y, Sakane A. An experimental investigation on engine performance and emissions of a supercharged hydrogen-diesel dual-fuel engine. International Journal of Hydrogen Energy 2010;35:844-853.
230. Ruckenstein E, Hang HuY. Methane partial oxidation over NiO/MgO solid solution catalysts. Applied Catalyst A: General 1999;183:85-92.
231. Ruckenstein E, Hu YH. Carbon dioxide reforming of methane over nickel/alkaline earth metal oxide catalysts. Applied Catalyst A: General 1995;133:149-161.
232. Ruckenstein E, Wang HY. Combined catalytic partial oxidation and CO_2 reforming of methane over supported cobalt catalysts. Catalysis Letters 2001;73:99-105.
233. Sahoo BB, Saha UK, Sahoo N. Theoretical performance limits of a syngas-diesel fueled compression ignition engine from second law analysis. Energy 2011;36:760-769.
234. Sahoo BB, Sahoo N, Saha UK. Effect of engine parameters and type of gaseous fuels on the performance of dual-fuel gas diesel engines-a critical review. Renewable and Sustainable Energy Reviews2009;13:1151-84.
235. Sahoo BB, Sahoo N, Saha UK. Effect of H_2:CO ratio in syngas on the performance of a dual fuel diesel engine operation. Applied Thermal Engineering 2012;49:139-146.
236. Sajjadi SM, Haghighi M, Rahmani F. Sol-gel synthesis of $NiCo/Al_2O_3$-MgO-ZrO_2nanocatalyst used in hydrogen production via reforming of CH_4/CO_2greenhouse gases. Journal of Natural Gas Science and Engineering 2015;22: 9-21.

237. Sandalci T, Karagoz Y. Experimental investigation of the combustion characteristics, emissions and performance of hydrogen port fuel injection in a diesel engine. International Journal of Hydrogen Energy 2014;39:18480-18489.
238. Santoso WB, Bakar RA, Nur A. Combustion characteristics of diesel-hydrogen dual fuel engine at low load. Energy Procedia 2013;32:3-10.
239. Saravanan N, Nagarajan G, Dhanasekaran C, Kalaiselvan KM. Experimental investigation of hydrogen port fuel injection in DI diesel engine. International Journal of Hydrogen Energy 2007;32:4071-80.
240. Saravanan N, Nagarajan G. An experimental investigation on manifold-injected hydrogen as a dual fuel for diesel engine system with different injection duration. International Journal Energy Research 2009;33:1352-1366.
241. Schumacher LG, Borgelt SC, Fosseen D, Goetz W, Hires WG. Heavy-duty diesel engine exhaust emission tests using methyl ester soybean oil/diesel fuel blends. Bio-resource Technology 1996;57:31-36.
242. Selim MYE. Effect on exhaust gas recirculation on some combustion characteristics of dual fuel engine. Energy Conversion and Management 2003;44:707-721.
243. Selim MYE. Sensitivity of dual fuel engine combustion and knocking limits to gaseous fuel composition. Energy Conversion and Management 2004;45(3):411-425.
244. Selvan VAM, Anand RB, Udayakumar K. Combustion characteristics of Diesohol using biodiesel as an additive in a direct injection ignition engine under various compression ratio. Energy & Fuels 2009;23:5413-5422.
245. Seo HO, Sim JK, Kim KD, Kim YD, Lim HC, Kim SH. Carbon dioxide reforming of methane to synthesis gas over a TiO_2-Ni inverse catalyst. Applied Catalysis A: General 2013;451:43-49.
246. Sepehria S, Rezae M. Ce promoting effect on the activity and coke formation of Ni catalysts supported on mesoporous nanocrystalline g-Al_2O_3 in autothermal reforming of methane. International Journal of Hydrogen Energy 2017;42:11130-11138.
247. Shao J, Zeng G, Li Y. Effect of Zn substitution to a $LaNiO_{3-\delta}$ perovskite structured catalyst in ethanol steam reforming. International Journal of Hydrogen Energy 2017;42:17362-17375.

248. Sharma A, Murugan S. Potential for using a tyre pyrolysis oil-biodiesel blend in a diesel engine at different compression ratios. Energy Conversion and Management 2015;93:289-297.
249. Sharma M, Agarwal AK, Bharathi KV. Characterization of exhaust particulates from diesel engine. Atmospheric Environment 2005;39:3023-3028.
250. Shen W, Momoi H, Komatsubara K, Saito T, Yoshida A, Naito S. Marked role of mesopores for the prevention of sintering and carbon deposition in dry reforming of methane over ordered mesoporous Ni-Mg-Al oxides. Catalyst Today 2011;171:150-155.
251. Shinde VM, Madras G. Catalytic performance of highly dispersed Ni/TiO_2 for dry and steam reforming of methane. RSC Advances 2014;4:4817-4826.
252. Shirk MG, McGuire TP, Neal GL, Haworth DC. Investigation of a hydrogen-assisted combustion system for a light-duty diesel vehicle. International Journal of Hydrogen Energy 2008;33:7237-7244.
253. Sivaramakrishnan K, Ravikumar P. Optimization of operational parameters on performance and emissions of a diesel engine using biodiesel. International Journal ofEnvironmentalScience and Technology 2014;11(4):949-958.
254. Sokolov S, Radnik J, Schneider M, Rodemerck U. Low-temperature CO_2 reforming of methane over Ni supported on ZnAl mixed metal oxides. International Journal Hydrogen Energy 2017;42:9831-9839.
255. Solymosi F, Erdohelyi A, Cserenyi J. A comparative study on the activation and reactions of CH, on supported metals. Catalysis Letters 1992;16:399-405.
256. Sousa FF de, Sousa HAS de, Oliveira AC, Junior MCC, Ayala AP, Barros EB, Viana BC, Filho JM, Oliveira AC. Nanostructured Ni-containing spinel oxides for the dry reforming of methane: Effect of the presence of cobalt and nickel on the deactivation behaviour of catalysts. International Journal of Hydrogen Energy 2012; 37(4): 3201-3212.
257. Souza Mariana MVM, Schmal M. Combination of carbon dioxide reforming and partial oxidation of methane over supported platinum catalysts. Applied catalyst A: General 2003;225:83-92.
258. Spath PL, Dayton DC. Preliminary Screening-Technical and Economic Assessment of Synthesis Gas to Fuels and Chemicals with Emphasis on the Potential for Biomass-Derived Syngas. NREL 2003; Report no. TP-510-34929.

259. Stanmore BR, Brilhac JF, Gilot P. The oxidation of soot: a review of experiments, mechanisms and models. Carbon 2001;39:2247-2268.
260. Subramanian KAA. A comparison of water–diesel emulsion and timed injection of water into the intake manifold of a diesel engine simultaneous control of NO and smoke emissions. Energy Conversion and Management 2011;52:849-857.
261. Suelves I, Lazaro MJ, Moliner R, Corbella BM, Palacios JM. Hydrogen production by thermo catalytic decomposition of methane on Ni-based catalysts: influence of operating conditions on catalyst deactivation and carbon characteristics. International Journal of Hydrogen Energy 2005;30:1555-1567.
262. Sukumar P, Saravanan N, Nagarajan G, Vedaraman N. Effect of biodiesel unsaturated fatty acid on combustion characteristics of a DI compression ignition engine. Biomass and Bioenergy 2010;34:1079-88.
263. Szwaja S, Rogalinski KG. Hydrogen combustion in a compression ignition diesel engine. International Journal of Hydrogen Energy2009;34:4413-4421.
264. Tada S, Shimizu T, kameyama H, Haneda T, Kikuchi R. Ni/CeO_2 catalysts with high CO_2 methanation activity and high CH_4 selectivity at low temperatures. International Journal of Hydrogen Energy 2012;37:5527-5531.
265. Talibi M, Hellier P, Balachandran R, Ladommatos. Effect of hydrogen-diesel fuel co-combustion on exhaust emissions with verification using an in-cylinder gas sampling technique. International Journal of Hydrogen Energy2014;39:15088-15102.
266. Talibi M, Hellier P, Ladommatos N. Combustion and exhaust emission characteristics, and in-cylinder gas composition, of hydrogen enriched biogas mixtures in a diesel engine. Energy 2017;124:397-412.
267. Therdthianwong S, Therdthianwong A, Siangchin C, Yongprapat S. Synthesis gas production from dry reforming of methane over Ni/Al_2O_3 stabilized by ZrO_2. International Journal of Hydrogen Energy 2008;33:991-999.
268. Tippayawong N, Promwungkwa A, Rerkkriangkrai P. Long-term operation of a small biogas/diesel dual-fuel engine for on-farm electricity generation. Biosystems Engineer 2007;98:26-32.

269. U.S. Department of Energy. Just the basics: diesel engine, https://www1.eere.energy.gov/vehiclesandfuels/pdfs/basics/jtb_diesel_engine.pdf; 2003 [Accessed 28.07.16].
270. Varde KS, Frame GA. Hydrogen aspiration in a direct injection diesel engine-its effects on smoke and other engine parameters. International Journal of Hydrogen Energy 1983;8(7):549-555.
271. Vernon PDF, Green MLH. Partial oxidation of methane to synthesis gas, and carbon dioxide as an oxidising agent for methane conversion. Catalysis Today 1992;13:417-426.
272. Waheed QMK, Williams PT. Hydrogen Production from High Temperature Pyrolysis/Steam Reforming of Waste Biomass: Rice Husk, Sugar Cane Bagasse, and Wheat Straw. Energy & Fuels. 2013;27:6695-704.
273. Walsh MP. Mobile source related air pollution: effects on health and the environment. Encyclopedia of Environ Health 2011;3:803-809
274. Wang HY, Ruckenstein E. Carbon dioxide reforming of methane to synthesis gas over supported rhodium catalysts: the effect of support. Applied Catalyst A: General 2000;204:143-152.
275. Wang S, Lu GQ. Carbon dioxide reforming of methane to produce synthesis gas over metal-supported catalysts: state of the art. Energy & Fuels 1996;10:896-904.
276. Wong JKS. Compression ignition of hydrogen in a direct injection diesel engine modified to operate as a low heat rejection engine. International Journal of Hydrogen Energy 1990;15(7):507-514.
277. Wong YK, Karim GA. A kinetic examination of the effects of the presence of some gaseous fuels and preignition reaction products with hydrogen in engines. International Journal of Hydrogen Energy 1999;24(5):473-478.
278. Wong YK, Karim GA. An Analytical Examination of the Effects of Exhaust Gas Recirculation on the Compression Ignition Process of Engines Fuelled with Gaseous Fuels. SAE Int 1996, SAE no.961936.
279. Xu J, Zhou W, Li Z, Wang J, Ma J. Biogas reforming for hydrogen production over nickel and cobalt bimetallic catalysts. International Journal of Hydrogen Energy 2009;34:6646-6654.

280. Xue J, Grift TE, Hansen AC. Effect of biodiesel on engine performances and emissions. Renewable and Sustainable Energy Reviews 2011;15:1098-1016.
281. Yadav VS, Soni SL, Sharma D. Engine performance of optimized hydrogen-fueled direct injection engine. Energy 2014;65:116-122.
282. Yan QG, Weng WZ, Wan HL, Toghiani H, Toghiani RK, Pittman Jr, CU. Activation of methane to syngas over a Ni/TiO_2 catalyst. Applied Catalyst A: General 2003;239:43-58.
283. Yang Y, Liu J, Shen W, Li J, Chien IL. High-efficiency utilization of CO_2 in the methanol production by a novel parallel-series system combining steam and dry methane reforming. Energy 2018;158:820-29.
284. Yilmaz IT, Demir A, Gumus M. Effects of hydrogen enrichment on combustion characteristics of a CI engine. International Journal of Hydrogen Energy 2017;42:10536-10546.
285. Yoon SH, Lee CK. Experimental investigation on the combustion and exhaust emission characteristics of biogas–biodiesel dual-fuel combustion in a CI engine. Fuel Processing Technology 2011;92:992-1000.
286. Yoon SH, Lee CS. Effect of biofuels combustion on the nanoparticle and emission characteristics of a common-rail DI diesel engine. Fuel 2011;90:3071-3077.
287. Zhai X, Ding S, Liu Z, Jin Y, Cheng Y. Catalytic performance of Ni catalysts for steam reforming of methane at high space velocity. International Journal of Hydrogen Energy 2001;36:482-489.
288. Zhan Y, Han J, Bao Z, Cao B, Li Y, Street J, Yu F. Biogas reforming of carbon dioxide to syngas production over Ni-Mg-Al catalysts. Molecular Catalysis 2017;436:248-258.
289. Zhou JH, Cheung CS, Leung CW. Combustion, performance, regulated and unregulated emissions of a diesel engine with hydrogen addition. Applied Energy 2014;126:1-12.
290. https://www.dieselnet.com/standards/eu/hd.php [Accessed 20.06.16].
291. https://www.transportpolicy.net/standard/india-fuels-diesel-and-gasoline[Accessed 11.04.17].

SCI-PUBLICATIONS

1. P. Rosha, A. Dhir, S.K. Mohapatra. Influence of gaseous fuel induction on the various engine characteristics of a dual fuel compression ignition engine: A review. *Renewable & Sustainable Energy Reviews* 2018;82:3333-3349. ***(IF.:10.556)***
2. P. Rosha, S.K. Mohapatra, S.K. Mahla, A. Dhir. Biogas reforming for hydrogen enrichment by ceria decorated over nickel catalyst supported on titania and alumina. *International Journal of Hydrogen Energy* 2018;43:21246-21255. ***(I.F.:4.084)***
3. P. Rosha, S.K. Mohapatra, S.K. Mahla, A. Dhir. Hydrogen enrichment of biogas via dry and autothermal-dry reforming with pure nickel (Ni) nanoparticle. *Energy* 2019;172: 733-739. ***(I.F.:5.537)***
4. P. Rosha, S.K. Mohapatra, S.K. Mahla, A. Dhir. Catalytic reforming of biogas for hydrogen enrichment over Ni supported on ZnO-CeO_2 mixed catalyst. *Biomass and Bioenergy* 2019;125:70-78. ***(I.F.:3.537)***
5. P. Rosha, R. Singh, S.K. Mohapatra, S.K. Mahla, A. Dhir. Optimization of hydrogen enriched biogas by dry oxidative reforming with nickel nanopowder using response surface methodology. *Energy & Fuels* 2018;32:6995-7001. ***(I.F.:3.021)***
6. P. Rosha, S.K. Mohapatra, S.K. Mahla, A. Dhir, H.M Cho, B.S. Chauhan. Effect of compression ratio on combustion, performance, and emission characteristics of compression ignition engine fueled with palm (B20) biodiesel blend. Energy 2019; 178:676-684. ***(I.F.:5.537)***